KTH Electrical Engineering

Modeling and Design of Wireless Protocols for Networked Control Applications

PIERGIUSEPPE DI MARCO

Doctoral Thesis
Stockholm, Sweden 2012

KTH School of Electrical Engineering
Automatic Control Lab
SE-100 44 Stockholm
SWEDEN

TRITA-EE 2012:067
ISSN 1653-5146
ISBN 978-91-7501-602-3

Akademisk avhandling som med tillstånd av Kungliga Tekniska högskolan framlägges till offentlig granskning för avläggande av teknologie doktorsexamen i telekommunikation onsdagen den 16 Januari 2013 klockan 10.15 i sal F3, Kungliga Tekniska högskolan, Lindstedtsvägen 26, Stockholm.

Tryck: Universitetsservice US AB

Abstract

Wireless networking offers great potentials for the development of new applications in real-time monitoring and control. However, current design processes do not simultaneously consider energy efficiency, system requirements, and standards compatibility. Modeling, optimization, and integration of communication and control protocols are essential to achieve efficient overall operations. We propose a holistic design framework, which includes physical channels, medium access control (MAC), multi-hop routing, and control applications. Accordingly, we provide the following contributions.

First, we investigate the performance of the IEEE 802.15.4 MAC through an accurate Markov chain model and its simplified representation. The effects of traffic load, number of devices, and MAC parameters on reliability, delay, and energy consumption are determined analytically and experimentally. We show that the delay distribution is different with respect to commonly used models in networked control systems design. Moreover, we introduce an adaptive mechanism to minimize the energy consumption while fulfilling reliability and delay constraints.

Second, we extend the analysis to multi-hop networks, including heterogeneous traffic distribution and limited carrier sensing range. Due to the contention-based channel access, routing decisions based on reliability or delay typically direct traffic toward nodes with high packet generation rates, leading to unbalanced performance and higher energy consumption. A load balancing metric is proposed for the IETF routing protocol for low-power and lossy networks. Furthermore, a mechanism to optimally select routes and MAC parameters is implemented.

Third, we include a realistic channel model in the analysis. Multi-path and shadowing are modeled by a Nakagami-lognormal distribution. A moment matching approximation is used to derive the statistics of aggregate signals. The impact of fading on MAC and routing is determined for various traffic regimes, distances among devices, and signal-to-(interference plus noise)-ratio settings. The results show that a certain level of fading actually improves the network performance.

Fourth, we propose TREnD, a cross-layer protocol that takes into account tunable application requirements. Duty cycling, data aggregation, and power control are employed to provide energy efficiency and an optimization problem is solved to select the protocol parameters adaptively. TREnD is implemented on a test-bed and it is compared to existing protocols. Experimental results show load balancing and adaptation for static and dynamic scenarios.

Finally, the analytical models developed in the thesis are formalized into a contract-based design framework. We consider a building automation example with a feedback control system over a heterogeneous network. We include the effects of delays and losses in the controller synthesis and we compare various robust control strategies. The use of contracts allows for a compositional design that handles performance, heterogeneity, and reconfigurability in a systematic and efficient way.

Acknowledgements

There are several people I would like to acknowledge for their great support and contribution in the realization of this thesis. First, I would like to thank my main supervisor Prof. Karl Henrik Johansson for accepting me as a PhD student, for leading my research with constructive advices and feedbacks, and for truly inspiring motivation and enthusiasm. My co-supervisor, Prof. Carlo Fischione, deserves all my gratitude for the precious technical contribution in my research, for the continuous assistance, and for the invaluable support over the years. I would like to thank my advisor at the University of L'Aquila, Prof. Fortunato Santucci, for his guidance since I was an undergraduate student.

I am grateful to the other people that contributed in the works included in this thesis: Dr. George Athanasiou, Dr. Corentin Briat, Dr. Pierluigi Nuzzo, Dr. Pablo Soldati, Prof. Emmanuel Witrant, but especially Dr. Pangun Park for the fruitful collaboration and for holding my hand when I was moving the first steps in the research. I want to thank also Euhanna Ghadimi, Dr. Jeffrey Larson, Tekn. Lic. Chithrupa Ramesh, and Sadegh Talebi for proofreading various parts of this thesis. For any mistake that may remain, of course, the responsibility is entirely my own.

My gratitude goes to the Swedish Foundation for Strategic Research, the Swedish Research Council, the Swedish Governmental Agency for Innovation Systems, and the EU projects FeedNetBack, Hycon2, and Hydrobionets for providing financial support to my research.

The Automatic Control lab at KTH is a wonderful workplace. I would like to thank all professors, lab administrators, and colleagues for providing a stimulating, interesting, and fun working environment. Among the others, I would like to mention Euhanna, my reliable friend and flat mate, then also Alessandra, Alireza, André, Antonio, Assad, Burak, Chithrupa, Christian, Damiano, Davide, Dimitri, Erik, Farhad, Jeff, José, Kuo-Yun, Mariette, Martin J., Martin A., Olle, Oscar, Pato, Winston, and I want to wish good luck to the freshmen Afrooz, Demia, Sadegh, and Valerio. Lower in the food chain, I would like to thank also the master students Antonio, Dario, Elisabetta, Francesca, Giada, Marco, Silvia, and Umberto. I had a great time with Gabriel and Pablo, who visited the department for a short but joyful period in 2011, and I miss the time Iman, Jim, Pablo, Pan, Phoebus, and Ubaldo were also here. It has been a great pleasure to work, discuss, and spend time with all of you.

I would like to express my gratitude to Prof. Alberto Sangiovanni-Vincentelli for hosting my pleasant visit at UC Berkeley. I had interesting collaborations and discussions with Alberto P., Chung-Wei, John, Mehdi, Mostafiz, and Pierluigi. I had the fortune to meet an exceptional person, Henrik Ohlsson; a special old friend, Pangun Park; and many nice people with whom I share a lot of good memories of Berkeley.

Many people deserve to be acknowledged for the wonderful time in Stockholm. I met very good friends in five years and I would like to mention Alberto, Ane, Cata & Diogo, Edurne, Irina, Jana, Keren, Marco & Elena, Marco, Nacho, Nastia, Nok, Pilar, Rafa, Salome, and Sandra.

I would like to thank all my friends and my family in Italy. In particular, I would like to express my gratitude to my parents Rosalba and Marco for their love and support in all the important moments of my life. My sister(-in-law) Martina deserves to be thanked for taking a good care of Alessandra, when I could not.

Finally, I would like to thank my wife Alessandra, because without her love, and also her complains, I would have not made it through here. Thanks for making my life fantastic and for carrying with you the nicest gift I could ever expect for my PhD graduation (...and I am not talking about the iPad).

Piergiuseppe Di Marco
Stockholm, December 2012.

Contents

Chapter 1

Introduction

"A great piece of art is composed not just of what is in the final piece, but equally important, what is not. It is the discipline to discard what does not fit, to cut out what might have already cost days or even years of effort, that distinguishes the truly exceptional artist and marks the ideal piece of work, be it a symphony, a novel, a painting, a company or, most important of all, a life."

Jim Collins, 2003.

Wireless technology enables the seamless integration of communication, control, and computation. Distributed sensing and processing are achieved efficiently by pervasive interconnection of wireless devices. Thanks to the flexibility and low installation cost, the development of wireless solutions for control applications has been growing in the last decade. IDTechEx [1] predicts a continuous growth from $0.45 billion USD in 2011 to $2 billion USD in 2021 for this market. It corresponds to both an increase of the number of devices and the number of heterogeneous applications that protocols need to support. For this reason, standards organizations such as the IEEE and the IETF are currently working on wireless protocol enhancements to support this demand.

Energy efficient operations, adaptability to heterogeneous requirements, and interoperability represent challenging aspects that are not addressed satisfactorily in the technical literature and in the current protocol design processes. The increase in functionalities of wireless devices comes at the cost of higher energy expenditure, which is critical in many applications. Wireless sensor networks (WSNs) are often used in areas where recharging or replacing power units is difficult. In smartphones, recharge is possible and not expensive but a short battery lifetime limits the usability. A higher number of wireless devices increases the interference, which imposes a constraint to the transmitted energy. Moreover, in control systems, real-time operations and reliable information delivery are necessary to guarantee stability and good performance. Applications often share the same communication infrastructure, so the wireless protocol needs to adapt dynamically to requirements ranging from monitoring to safety critical applications. However, most proposed protocols

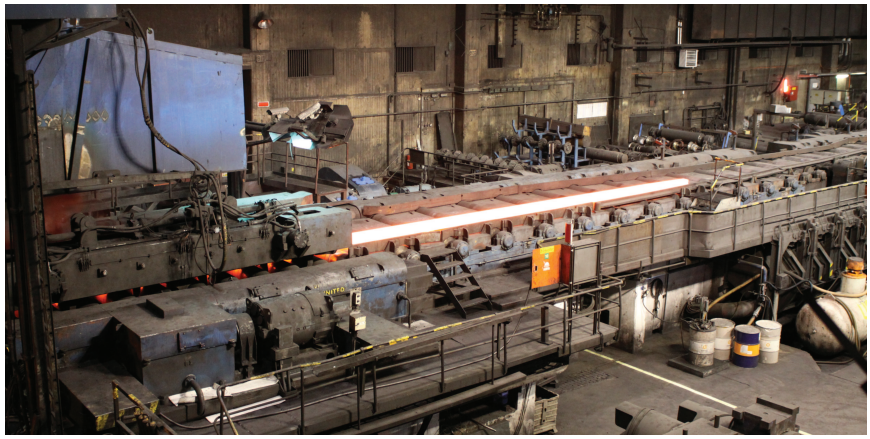

Figure 1.1: Wireless networks offer flexible and easy installation in industrial environments. The picture shows a steel manufacturing plant (courtesy of Sandvik AB).

are designed and optimized for specific implementation platforms and system requirements and they may not be scalable or interoperable with existing standards. Current standards often guarantee a certain performance as stand-alone solutions, but may not be efficient when patched together.

Understanding the basic interactions between communication technologies and control applications is essential to obtain efficient overall operations. The design of wireless protocols for networked control systems can benefit from analysis, optimization, and opportune composition of protocol mechanisms. In the rest of this chapter, we introduce the main challenges in modeling and designing heterogeneous communication protocols for control applications. Furthermore, we describe our design framework and outline the main contributions of this thesis.

1.1 Motivating Applications

There are many emerging applications in which wireless networks are used to achieve remote connection and flexibility. Here, we focus on three examples showing how system heterogeneity, communication protocols interaction, and energy efficient operations pose critical design challenges. We consider industrial automation, future mobility systems, and intelligent green buildings.

1.1.1 Industrial Automation

Wireless integration in process automation is an active research area [2]. The emphasis of industrial automation has shifted from intensifying productivity and reducing costs, to increasing quality and flexibility. With the introduction of wireless

networks, in combination with self-tuning, self-diagnosing, and optimizing features, it is possible to make process routines easy and efficient. According to a study by Frost & Sullivan [3] there is a 27% annual growth rate for revenues on the adoption of wireless solutions in process industries. Many wireless standards have been proposed and commercialized specifically for industrial automation, e.g., WISA [4], WirelessHART [5], and ISA SP100 [6]. Process control over wireless is achievable in various application scenarios. A wireless control system based on the IEEE 802.15.4 standard [7] has been implemented for the froth flotation process at Boliden, and also developed for the steel manufacturing process at Sandvik AB, within the VINNOVA project WiComPI [8] (see Figure 1.1). The design of a wireless bioMEM sensor and actuator network for autonomous control of large-scale water treatment plants is targeted within the EU project Hydrobionets [9].

Wireless device compatibility is a major obstacle to the development of wireless solutions in automation and control. Standards such as WirelessHART and ISA SP100 rank very low in adoption level among industries, while Zigbee, Bluetooth, Wi-Fi, and other unlicensed technologies are widely adopted [3]. On the other side, the fundamental limits and achievable performance of these unlicensed standards are not clear, since they are not specifically designed for industrial control applications. We model and characterize the achievable performance of existing standards for medium access control (MAC), routing, and their interactions in Chapters 3 and 4 of this thesis.

The harsh propagation environment is an important factor to include in the analysis of wireless protocols. Manufacturing process are characterized by complex physical structures with metal obstacles (see Figure 1.1). Measurement campaigns at Boliden [8] have shown that the channel quality varies considerably depending on the deployment and is far from ideal conditions. In Chapter 5, we consider explicitly channel fading in our performance analysis.

Both the environment and the requirements may vary dynamically in process control. ISA SP100 [6] identifies six classes of application in industrial automation, according to the level of hazard. Wireless protocols need to be able to switch from monitoring and periodic maintenance (non critical) to real-time supervisory control and emergency actions (critical). If packet delivery and latency constraints are not met, the correct execution of control actions can be severely compromised [10]. For each class of operation, a tradeoff between packet delivery ratio and delay can be exploited to minimize the energy consumption. In Chapter 6, we propose a cross-layer protocol solution for industrial automation, which guarantees energy efficient operation under tunable constraints.

1.1.2 Future Mobility

Intelligent transportation systems automate the interactions among vehicles and infrastructure to achieve high levels of security, comfort, and efficiency. It is estimated that by 2050 the cost for urban mobility will be around $1 trillion USD per year across the globe, more than four times higher than in 1990 [11]. A per-

Figure 1.2: Wireless communications are able to support intelligent real-time fleet control and management systems. The illustration shows a platooning demonstration (courtesy of SCANIA AB).

vasive use of wireless sensors is provisioned inside vehicles and along roads. The number of sensing nodes deployed in urban environments is expected to be up to to millions [12]. The IEEE has developed a specific system architecture to provide wireless access in vehicular environments (WAVE) [13]. A showcase of hundreds of magnetic wireless sensors on highway stretches is proposed for traffic monitoring and control, within the EU project HYCON2 [14].

The vehicular communication requirements may vary widely, ranging from low-overhead delay-tolerant infotainment applications to safety critical applications such as collision avoidance and traffic management [15]. In Figure 1.2 we show an example of intelligent real-time fleet control and management systems for heavy duty vehicle platooning promoted by SCANIA within the IQfleet project [16]. Vehicles traveling close to each other reduce fuel consumption and exhaust emissions. The integration of communication among vehicles and adaptive cruise control is critical and time constraints are on the order of milliseconds to avoid collisions.

Vehicular and urban networks present a challenging environment due to their potentially large scale and high degree of dynamism. Multi-hop communications are often required under severe wireless propagation environments. We investigate the effects of multi-path fading channel on multi-hop networks in Chapter 5 of this thesis.

1.1.3 Intelligent Green Buildings

Buildings currently account for about 40% of the worldwide energy demand with 33% coming from commercial buildings and 67% from residential buildings. Build-

Figure 1.3: Wireless control is an important enabling technology for intelligent green buildings. The illustration shows a design project for the Stockholm Royal Seaport (courtesy of Folkhem & Wingårdh Architects).

ing automation systems and building energy management systems are designed to provide centralized oversight and remote control over heating, ventilation, and air conditioning (HVAC) systems, lighting and other building systems. Improved energy efficiency as well as improved convenience are some goals of intelligent green buildings, for which currently wired systems like BACnet, LonWorks, or KNX are under development or already deployed [17]. The concept of intelligent green operations can be extended to urban districts to form smart grids as in the Stockholm Royal Seaport [18] project involving ABB, Fortum, and Ericsson among others (see Figure 1.3). The project is developed within the global Climate Positive Development Program, launched in May 2009 by the Clinton Climate Initiative and the US Green Building Council. An intelligent electricity grid will reduce annual energy consumption up to 55 KWh per square meter. The fully automated system, currently being developed, will fine-tune heating and ventilation systems to run when electricity prices are low.

The flexibility and low cost of installation offered by wireless networks are attractive incentives for building automation systems. However, a major challenge is the complexity of the system, composed by many different applications sharing the same infrastructure. A systematic integration of building automation with the communication technology is therefore critical.

Design strategies that take into account heterogeneous requirements from both the communication network and the control application can provide efficient and scalable solutions for intelligent green buildings. In Chapter 7, we illustrate a design methodology for wireless protocol and control synthesis applied to an under-floor air distribution (UFAD) system. An indoor climate regulation process is set with

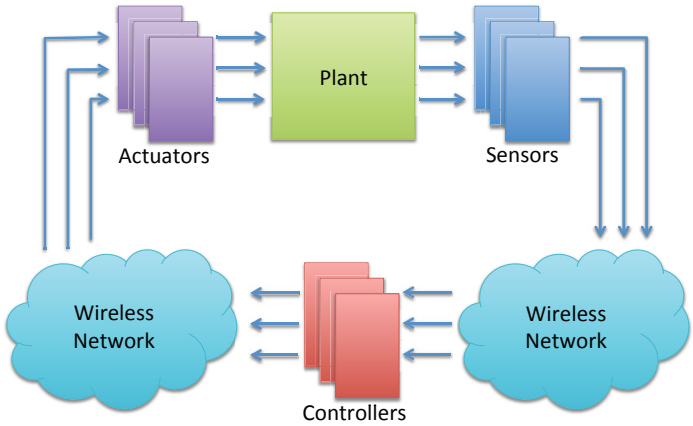

Figure 1.4: Networked control system architecture. The state of a plant is sampled by sensors and controlled over a wireless network.

the injection of a fresh airflow from the floor and an exhaust located at the ceiling. Feedback regulation is a key element for an optimized system operation and it can be achieved thanks to actuated diffusers and distributed measurements provided by a WSN deployed in the ventilated area. Time-triggered metering applications on electrical appliances may share the same communication infrastructure. The challenge is the composition of communication protocols and the effective mapping of requirements from the UFAD control system.

1.2 Illustrative Examples

In this section, we present two simple examples that highlight the challenges and show the importance of a careful design of wireless protocols for control applications. The setup is illustrated in Figure 1.4, where we show the main components of a typical networked control system, namely, plant, sensors, controllers, and actuators, interconnected by one or more wireless networks.

We consider a plant given by a double integrator system, which is a typical illustrative example in control, such as a robotic arm in a manufacturing process [19]. A wireless network of 10 sensors is deployed to measure the plant state and report it to a feedback controller periodically using the contention-based channel access of the IEEE 802.15.4 standard. As we describe later in the thesis, nodes contend the shared access to the wireless channel by selecting a random time to start the transmission within a backoff window.

In the first example, we illustrate the effects of the sampling period on the performance of the control system.

Example 1.1
We assume that the controller is fixed, so that the only design variable is the sampling period T in the range $10-40$ ms, and the default parameters of the IEEE 802.15.4 standard [7] are used. Shorter sampling periods are desired from a control perspective to increase the amount of information available at the controller and the frequency of actuation to stabilize the system. In our example, a controller design would select $T = 10$ ms. However, each transmission consumes energy and increases the level of contention. From a communication perspective, it is preferable to maximize the sampling period and, therefore, to select $T = 40$ ms.

In Figure 1.5(a), we compare the step response of the system with different sampling periods $T = 10, 20, 30, 40$ ms to the ideal step response when delay and packet losses are ignored. The system is highly oscillating for $T = 40$ ms, as the control acts less frequently. However, the system has a long settling time also for $T = 10$ ms, since the level of contention is too high and many samples are lost in the wireless transmission. The system with $T = 20$ ms achieves performance close to the ideal step response, by using half of the transmissions with respect to $T = 10$ ms. A tradeoff in the choice of the sampling period exists in the design of wireless networked control systems.

In the second example, we consider the effects of protocol parameter selection on the stability of the control system.

Example 1.2
We assume that the sampling period is fixed to $T = 20$ ms so that the only design variable is the length of the initial contention window $W_0 = 2^{m_0}$ time units, where m_0 is in the range $2 - 8$. As we explain later, nodes contend the shared channel by choosing a random access time within the contention window. Given a fixed traffic generation period, a pure communication-oriented approach would select the network parameter that maximizes the amount of delivered data (reliability). This is obtained, in our case, by selecting the largest contention window $m_0 = 8$, thus minimizing the probability that two transmitters select the same transmission time and collide. On the other side, a pure control-oriented approach would ask the network to minimize the contention time such that the variance of the delay for delivered packets is minimized. This is obtained in our case by selecting the smallest contention window $m_0 = 2$.

In Figure 1.5(b), we compare the step response of the system with different protocol parameters $m_0 = 2, 4, 6, 8$, compared with the ideal step response when delay and packet losses are ignored. We notice that the system is unstable with $m_0 = 8$, due to the large variability of the delay. However, the step response also oscillates widely for $m_0 = 2$ due to the high number of collisions. The intermediate value $m_0 = 4$ gives instead satisfactory performance in terms of rise time, overshoot, and settling time.

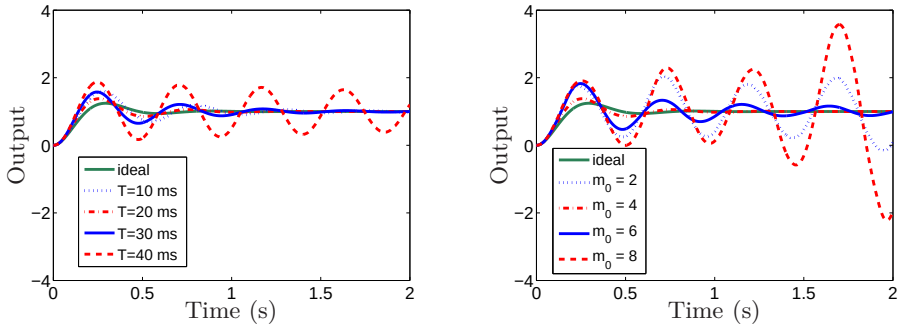

(a) A tradeoff in the selection of the sampling period T

(b) A tradeoff in the selection of the backoff exponent m_0

Figure 1.5: Effect of delay and packet losses on a state feedback wireless networked control system. We consider 10 sensors that measure the plant state and transmit periodically using the contention-based CSMA/CA MAC of the IEEE 802.15.4 standard.

The examples illustrate the influence of the traffic and communication protocol parameters for a very simple control system by using a homogenous single-hop network operating under ideal channel conditions. In this thesis, we develop a framework to explore tradeoffs between communication and control for more complex systems, with multi-hop networks over time-varying channels.

1.3 Problem Formulation

The aim of this thesis is to provide a framework to model and design wireless networks with applications in industrial, vehicular, and building automation systems. As illustrated in our motivating examples, the complexity and heterogeneity of systems and communication environments involved, the need of energy efficient operations, and the compliance with existing wireless standards introduce additional design challenges and determine different constraints with respect to traditional communication system engineering.

We formulate the problem as follows. Given a set of system requirements, we want to design communication and control strategies by a proper composition of protocol components. There are several questions that need to be addressed in order to solve the problem:

- What is the achievable performance of each protocol component?
- How to model the interactions in the communication protocol stack?
- How to tune communication protocol parameters to guarantee system requirements?

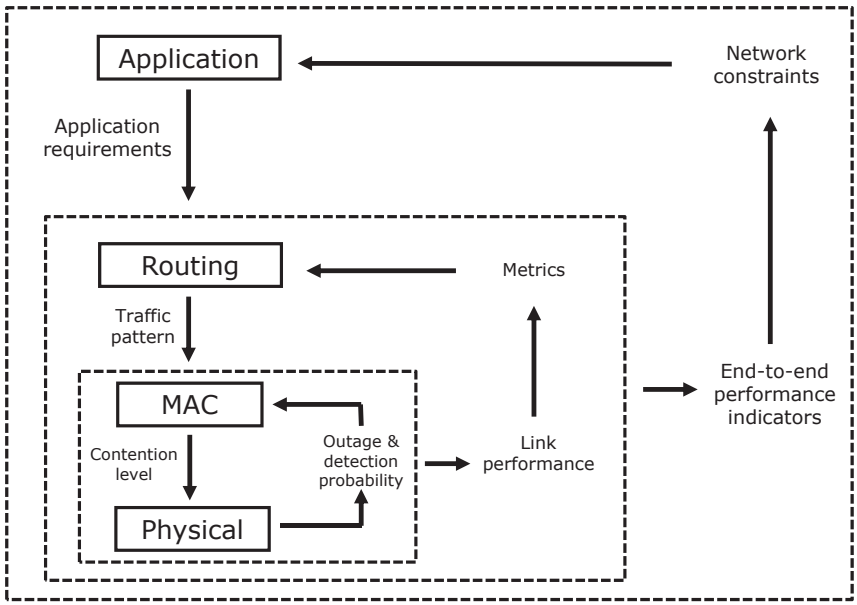

Figure 1.6: Interaction of layers for modeling and design.

- How to integrate communication protocols and control applications?

The essence of the presented problem can be visualized by the block diagram in Figure 1.6, in which we synthesize the main components and the mutual interaction between the layers of interest in the protocol stack. We abstract the complex interaction among layers by using a triple feedback structure. The **application** sets its requirements for the underlying communication infrastructure. They can be a traffic generation rate for each node in the network, derived from the required sampling time of the sensing operation in case of WSNs, or a generic data generation rate of the application. The application layer translates performance objectives (e.g., stability, robustness) into requirements for the lower protocol layers (e.g., minimum data delivery rate and maximum packet delay feasible for the controller). The **routing** layer combines topological information with the application requirements in a network communication graph. Based on specific metrics, the routing protocol takes appropriate decisions to distribute the end-to-end traffic flow in the network. The outcome is a different traffic load in each link of the network. The **MAC** layer describes policies for accessing the wireless resource, generating a certain level of contention (e.g., number of concurrent transmissions or time slot allocations) that affects the physical transmission over the channel. As an output of the transmission at the **physical** layer we obtain a certain outage and detection probability at the receiver. The effects of outages and channel losses influence the behavior and

the performance of the MAC layer, indicated in Figure 1.6 as a loop at link level between MAC and physical layer. The link performance indicators such as energy consumption, reliability, or delay can influence the routing metric directly, closing a second loop between link layers and routing layer. The combination of physical, MAC, and routing layers determines end-to-end performance indicators, which can be fed back to the control application as network constraints so that a third loop is closed between the communication layers and the application.

To apply the proposed design framework, analytical models of the performance indicators need to be embedded in the design methodology. An optimization problem can be posed to select design components and protocol parameters in the following form:

$$\begin{aligned} \underset{\mathbf{u}}{\text{minimize}} \quad & f(\mathbf{u}) \\ \text{subject to} \quad & \mathbf{u} \in \mathcal{C}\,, \end{aligned}$$

where the decision variables being $\mathbf{u}$ are selected to minimize a cost function $f(\mathbf{u})$, subject to a set of constraints $\mathcal{C}$ being fulfilled.

The cost function f can be expressed as the number of component, the design cost, or the cost during the operation. The set of constraints $\mathcal{C}$ is expressed in terms of requirements for the system and for each design component. The system requirements for control applications are typically given in terms of stability, time response, and robustness. For the communication protocol design, these requirements are mapped into quality of service indicators. Throughout the thesis, we consider three major indicators, namely energy efficiency, reliability, and delay:

- Energy efficiency: a long network lifetime is a major challenge for battery-equipped devices. Therefore, the energy consumption of the devices can be used as the cost function.
- Reliability: at the network layer, reliability is measured as the packet delivery ratio from each transmitter to the destination. A maximization of the reliability can require a large packet overhead and many retransmissions, thus increasing the energy consumption. Controllers can usually tolerate a certain degree of losses without an impact on the overall performance [20], therefore, a design strategy in which reliability is a tunable constraint is desirable.
- End-to-end delay: at the network layer, delay is computed for successfully received packets to the destination. Minimizing the delay determines high duty cycles, thus requiring high energy expenditure. Similarly to the reliability, controllers can compensate for average delays with low jitter [19]. Therefore the delay can be used as a tunable constraint.

The decision variables $\mathbf{u}$ are the parameters of the design. In Chapter 3, we consider the IEEE 802.15.4 standard, and we show how the contention windows and the maximum number of channel access attempts can be tuned to minimize the energy consumption, subject to reliability and delay requirements. In Chapter 6, we

propose a cross-layer protocol called TREnD, based on a semi-random routing and a hybrid MAC with duty cycling. An optimization problem is posed to select the slot duration, the wake-up probability in transmission, and the wake-up probability in reception.

1.4 Thesis Outline and Contributions

In this section, we outline the contents of the thesis and the major contributions. In Chapter 2, we illustrate the background on communication protocol models and design for networked control systems and the related literature. The original contribution of the thesis is presented in four chapters, and the material is outlined as follows. In Chapter 3, we describe a Markov chain model of the contention-based channel access mechanism of the IEEE 802.15.4 MAC. Chapter 4 extends the analysis of the Markov chain to include the effect of routing over multi-hop networks. In Chapter 5, we model the effects of channel fading on MAC and routing. In Chapter 6, we consider the effects of tunable application requirements on the design of routing and MAC protocols for control and actuation. We propose a design framework for communication and control in building automation systems in Chapter 7. Finally, Chapter 8 concludes the thesis and prospects our future work. Note that a list of the main symbols and acronyms used in the thesis is reported in Appendix F. In the following, we discuss the details of the contributions.

Markov Chain Modeling of Contention-based MAC Protocols

In Chapter 3, we introduce a generalized Markov chain model of the carrier sensing multiple access mechanism of the IEEE 802.15.4 MAC for single-hop star networks. In contrast to previous works, the presence of retransmission limits, acknowledgments, unsaturated traffic, packet size, and packet copying delay due to hardware limitations is accounted for. We devise an accurate model and a simplified, effective method that drastically reduces the computation complexity while ensuring a satisfactory accuracy. The model is then used to derive a distributed adaptive algorithm for minimizing the energy consumption while guaranteeing a given successful packet reception probability and delay constraints in the packet transmission. The algorithm does not require any modification of the IEEE 802.15.4 medium access control and can be easily implemented on network devices. Moreover, the probability distribution of the delay for successfully received packets is characterized. The analysis uses a moment generating function method and gives an accurate, explicit expression of the probability distribution of the network delay as a function of the traffic load, number of nodes, and parameters of the communication protocol. We show that the probability distribution of the delay is different from existing network models used for networked control system design. The model and the tuning algorithm have been experimentally validated and evaluated on a test-bed with off-the-shelf wireless sensor devices. The material presented in this chapter is based mainly on the journal publication

- P. Park, P. Di Marco, C. Fischione, and K. H. Johansson: Modeling and Optimization of the IEEE 802.15.4 Protocol for Reliable and Timely Communications. *IEEE Transactions on Parallel and Distributed Systems*. 2013. To appear.

The Markov chain model was originally presented in

- P. Park, P. Di Marco, P. Soldati, C. Fischione, and K. H. Johansson: A Generalized Markov Chain Model for Effective Analysis of Slotted IEEE 802.15.4. *IEEE International Conference on Mobile Ad Hoc and Sensor Systems*, (Best paper award). Macau SAR. October 2009.

An extensive analysis of the packet delay distribution appears in

- P. Park, P. Di Marco, C. Fischione, and K. H. Johansson: Delay Distribution Analysis of Wireless Personal Area Networks. *IEEE Conference on Decision and Control*. Maui, Hawaii. December 2012.

Modeling the MAC and Routing Interactions

In Chapter 4, we describe the proposed model for multi-hop IEEE 802.15.4 networks. The design loop interaction between routing and MAC protocols is investigated. Link performance at the MAC layer are studied by a Markov chain model that includes all the features of the unslotted mechanism of the IEEE 802.15.4 MAC, in heterogeneous traffic regimes and with limited carrier sensing range of nodes. We extend this model to multi-hop networks by considering the specifications of the IETF routing protocol for low-power and lossy networks [12]. For various network configurations, conditions under which routing decisions based on packet loss probability or delay lead to an unbalanced distribution of the traffic load across multi-hop paths are studied. Analytical and experimental results show that the behavior of the MAC protocol can hurt the performance of the routing protocol and vice versa. It is shown that routing decisions based on packet loss probability or delay tend to direct traffic toward nodes with high packet generation rates, with potential catastrophic effects for the energy consumption. A metric that guides the interaction between MAC and routing is presented and compared to existing metrics. Moreover, a protocol selection mechanism is implemented to optimally select the routing metric and MAC parameters given specific performance requirements. The material presented in this chapter is mainly based on the journal publication

- P. Di Marco, P. Park, C. Fischione, and K. H. Johansson: Analytical Modeling of Multi-hop IEEE 802.15.4 Networks. *IEEE Transactions on Vehicular Technology*, 61(7):3191–3208. September 2012.

The analytical model was originally presented in

- P. Di Marco, P. Park, C. Fischione, and K. H. Johansson: Analytical Modeling of IEEE 802.15.4 for Multi-hop Networks with Heterogeneous Traffic

and Hidden Terminals. *IEEE Global Communications Conference*. Miami, Florida. December 2010.

The routing metrics and the protocol selection mechanism are included instead in the conference submission

- P. Di Marco, C. Fischione, and G. Athanasiou: MAC and Routing Interactions in Low Power and Lossy Networks. *IEEE International Conference on Sensing, Communication, and Networking*. 2013. Submitted.

Modeling the Effects of Fading in Multi-hop Networks

In Chapter 5, we include realistic channel models in the analysis and determine the impact of fading conditions on the MAC and routing performance, under various settings for traffic, distances, carrier sensing range, and signal-to-(interference plus noise)-ratio (SINR). The analysis considers simultaneously composite channel fading, interference generated by multiple terminals, the effects induced by hidden terminals, and the MAC reduced carrier sensing capabilities. New results on the routing-MAC-physical layer interactions are derived and validated for single-hop and multi-hop topologies. It is shown that performance indicators of the IEEE 802.15.4 protocol over fading channels are often far from those derived under ideal channel assumptions. Moreover, it is established to what extent fading can be beneficial for the overall network performance and how these results can be used to drive joint optimization of the communication parameters. The material presented in this chapter is submitted for journal publication in

- P. Di Marco, C. Fischione, F. Santucci, and K. H. Johansson: Modeling IEEE 802.15.4 Networks over Fading Channels. *IEEE Transactions on Vehicular Technology*. 2013. Submitted.

A simplified model of the fading is described and validated in

- P. Di Marco, C. Fischione, F. Santucci, and K. H. Johansson: Effects of Rayleigh-lognormal fading on IEEE 802.15.4 Networks. *IEEE International Conference on Communications*. 2013. Submitted.

Cross-layer Communication Protocol Design

In Chapter 6, we broaden the perspective by considering the effects of dynamic application requirements on the design of routing and MAC protocols for industrial control. We introduce a novel cross-layer protocol solution called TREnD that efficiently integrates routing algorithm, a hybrid MAC, data aggregation, duty cycling, and radio power control. The protocol parameters are adapted by an optimization problem, whose objective function is the network energy consumption, and the constraints are the reliability and packet delay. TREnD is implemented on a test-bed and compared to existing protocols for industrial automation. Experimental results

show good performance in terms of reliability, latency, low duty-cycle, and load balancing for both static and time-varying scenarios. The material in this chapter is based on the conference publication

- P. Di Marco, P. Park, C. Fischione, and K. H. Johansson: TREnD: a Timely, Reliable, Energy-efficient Dynamic WSN Protocol for Control Application. *IEEE International Conference on Communications*. Capetown, South Africa. May 2010.

A preliminary experimental validation was presented in

- P. Di Marco, P. Park, C. Fischione, and K. H. Johansson: A Dynamic Energy-efficient Protocol for Reliable and Timely Communications for Wireless Sensor Networks in Control and Automation. *IEEE Conference on Sensor, Mesh and Ad Hoc Communications and Networks - Workshops*. Rome, Italy. June 2009.

The material appears also as a part of the book chapter

- C. Fischione, P. Park, P. Di Marco, and K. H. Johansson: Design Principles of Wireless Sensor Networks Protocols for Control Applications. In Sudip K. Mazumder ed. *Wireless Networking Based Control*, pp. 203–238. Springer New York, 2011.

Wireless Networked Control Systems Design

In Chapter 7, we close the loop between application layer and communication protocol. A design methodology is illustrated by using contracts for the synthesis of a heterogeneous wireless network with applications in building automation. The analytical models developed in the previous chapters are formalized into simple contracts and used to drive the design of communication and control. We consider the effects of communication delays and packet losses explicitly in the controller and we compare various robust control strategies based on a mixed sensitivity H_∞ synthesis. We observe that the implementation of contracts on the communication delay in the controller synthesis significantly affects the overall system performance. The material in this chapter related to the contract-based design methodology is included in

- P. Di Marco, P. Nuzzo, C. Fischione, and K. H. Johansson: Wireless Networked Control System Design using Contracts. Manuscript in preparation.

Limitations and performances of the robust controllers are discussed in the journal publication

- E. Witrant, P. Di Marco, P. Park, and C. Briat: Limitations and Performances of Robust Control over WSN: UFAD Control in Intelligent Buildings. *IMA Journal of Mathematical Control and Information*, 27(4):527–543, November 2010.

Other Publications

The following publications are not covered in this thesis but they inspired some of the contents.

- C. W. Lin, A. Puggelli, P. Di Marco, and A. Sangiovanni-Vincentelli: VMS Communication Modeling and Architecture. *MuSyC Workshop on Distributed Sense and Control Systems*. Berkeley, CA. April 2012.
- B. Tahla, P. Di Marco, and M. Kaveh: Application of an Integrated PHY and MAC Layer Model for Half-Duplex IEEE 802.15.4 Networks to Smart Grids. *ACM International Symposium on Applied Sciences in Biomedical and Communication Technologies*. Barcelona, Spain. October 2011.
- S. C. Ergen, P. Di Marco, and C. Fischione: MAC Protocol Engine for Sensor Networks. *IEEE Global Communications Conference*. Honolulu, Hawaii. December 2009.
- P. Di Marco, C. Rinaldi, F. Santucci, K. H. Johansson, and N. Moller: Performance Analysis and Optimization of TCP over Adaptive Wireless Links. *IEEE International Symposium on Personal, Indoor and Mobile Radio Communications*. Helsinki, Finland. September 2006.

Contributions by the Author

The order of authors' names reflects the workload, where the first author had the most important contribution. In all the publications, the thesis author participated actively both in the development of the theory and the implementation, as well as in the paper writing.

Chapter 2

Background

In this chapter, we provide an overview of the background for the topics in the following chapters and we briefly summarize the related works. In Section 2.1, the contract-based design paradigm is presented. Section 2.2 focuses on the design and challenges in networked control systems. Eventually, Section 2.3 introduces a survey of recent MAC and routing protocols for control applications.

2.1 Contract-based Design

The concept of contract has been used extensively for a long time as verification mean for the design of software [37]. The design by contracts refers to formal, precise, and verifiable interface specifications for software components, which extend the definition of abstract data types with assumptions, guarantees, and invariants. These specifications are referred to as contracts in accordance with a conceptual metaphor with the conditions and obligations of business contracts. Inspired by recent results on assume-guarantee frameworks and compositional reasoning in the context of hybrid systems [38], and mixed-signal integrated circuits [39, 40], the methodology has been recently proposed for the application to cyber-physical systems [41]. In this context, contracts mimic the thought process of a designer, who aims at guaranteeing certain performance figures for the design under specific assumptions on its environment. The essence of contracts is, therefore, a compositional approach, where design and verification complexity is reduced by decomposing system-level tasks into more manageable subproblems at the component level, under a set of assumptions. System properties can then be inferred or proved based on component properties. In this respect, contract-based design can be a rigorous and effective paradigm while dealing with the complexity of modern system design.

2.1.1 Theory of Contracts

We summarize the main concepts behind contract-based design starting with the notion of component. A component x can be seen as an abstraction, a hierarchical

entity representing an element of a design. Components can be connected together by sharing interfaces and agreeing on the values of certain variables. A component may be associated with both implementations and contracts. An implementation X is an instantiation of a component x and consists of a set of variables and of a set of behaviors. Behaviors are generic, and could be continuous functions that result from solving differential equations, or sequences of values or events recognized by an automata model. A contract $\mathcal{C}$ for a component x is a pair of assertions (A, G), which express its assumptions and guarantees. An assertion B represents a specific set of behaviors over variables. Operations on assertions and contracts are set operations. An implementation X satisfies an assertion B whenever X and B are defined over the same set of variables and all the behaviors of X satisfy the assertion, i.e., when $X \subseteq B$. An implementation of a component satisfies a contract whenever it satisfies its promise, subject to the assumptions. Formally, $X \cap A \subseteq G$, where X and $\mathcal{C}$ have the same variables. We denote such a satisfaction relation by writing $X \models \mathcal{C}$. A contract is in canonical form when $G \supseteq \neg A$. Any contract can be turned into an equivalent one, i.e., having identical set of satisfying implementations, which is in canonical form. Contracts related to different components can be combined according to rules. Similar to parallel composition of components, parallel composition of contracts can be used to construct complex contracts out of simpler ones. A survey review of the mathematical theory underpinning the use of contracts, composition, abstraction, and refinement under the assume-guarantee paradigm is presented in [42].

2.1.2 Composition of Contracts

The theory of contracts is particularly fit in the context of system-level design [43], a paradigm that allows reasoning about design in a structured way. Design progresses in precisely defined abstraction levels. At each level, functionality (what the system is supposed to do) is strictly separated from architecture (how the functionality can be implemented). System-level design consists of a meet-in-the-middle approach where successive top-down refinements of high-level specifications across design layers are mapped onto bottom-up abstractions and characterizations of potential implementations. Each layer is defined by a design platform, which is a collection of components, models, representing functionality and performance of the components, and composition rules. In this context, contracts can play a fundamental role in determining the correct composition rules so that when the architecture space is explored, only compatible compositions of available components are taken into consideration (see Figure 2.1). Since compatibility is assessed among components at the same abstraction layer, these contracts are denoted as horizontal contracts. If an environment violates a horizontal contract, it cannot host any of its implementations. However, checking horizontal contracts is not sufficient, in general, to guarantee correct implementations. When analyzing the behavior of complex networked control systems, simplified macro-models can be used to capture the relevant behavior of the components at higher levels of abstraction. Therefore,

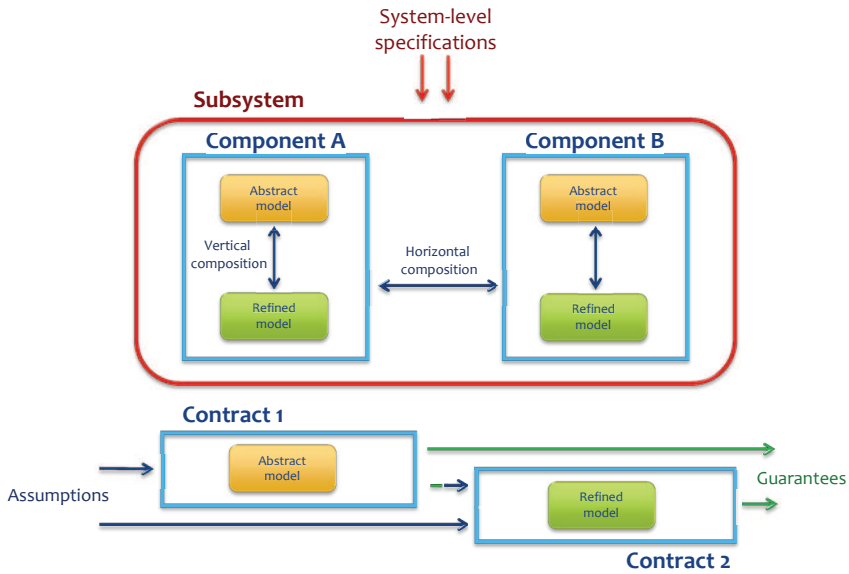

Figure 2.1: Contracts for the composition of components. Each component carries models at different levels of abstraction. Contracts can be defined both for horizontal and vertical composition, by opportunely mapping system-level specifications into sets of assumptions and guarantees.

guarantees should also be provided on the accuracy of the macro-models with respect to models at lower levels of abstraction. These guarantees are captured via bottom-up vertical contracts. On the other hand, vertical contracts can be used, for instance, to encode top-down requirements that system architects introduce to craft the behavior of a chosen architecture according to the desired functionality. The above set of constraints can be expressed using top-down vertical contracts. To ensure that an implementation is correct by construction, we need to check that the architecture platform is indeed a refinement of the specification platform. In our design flow, mapping of the specifications onto an architecture is cast as an optimization problem. Therefore, checking (enforcing) vertical contracts translates into constraining the optimization space with both system and component assumptions.

2.2 Networked Control Systems

Control over wireless networks is an active research area [2]. In this field, we refer to wireless networked control systems, namely, control systems in which actuators, sensors, and controllers are connected and communicate over a wireless network.

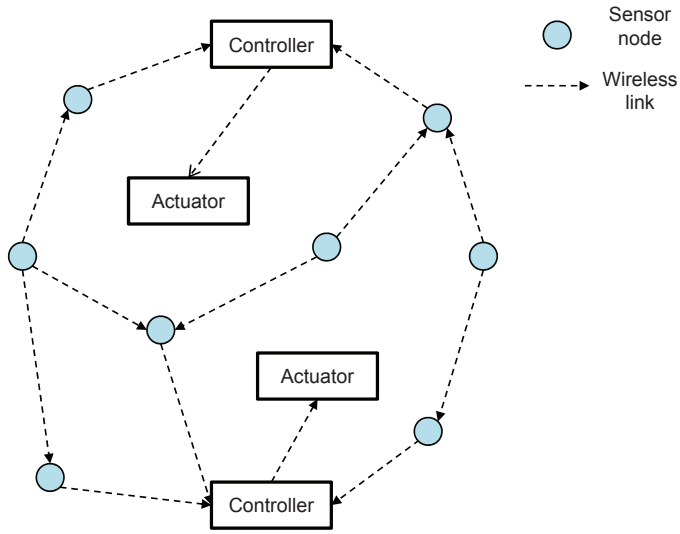

Figure 2.2: Multi-hop wireless networked control system scheme.

The network can involve multi-hop communications. The need of interaction between control and communication was raised in [44, 45]. A cross-layer framework for the joint design of wireless networks and distributed controller is in [46], although undesirable interactions should be taken into account [47]. Furthermore, extensive research on the impact of communication performance on the stability of the network can be found in [19, 48].

In the following, we summarize the important network quality measures for networked control systems and related works.

- Bandwidth: when multiple devices share a common network resource, the rate at which they can transmit data over the network is limited by the resource bandwidth. This limitation imposes constraints on the achievable performance. An overview of feedback control under bandwidth constraints and the derivation of the minimum bit rate to stabilize a linear system are given in [49, 50]. The data rate of a network must be considered together with the packet size and overhead since data are encapsulated into packets. Notice that the size of the headers depends on the protocol design of the communication network.

- Delay: we refer to delay of data on the network as the total time between the data being available at the source node (e.g., sampling at the sensor) and being available at the sink node (e.g., reception at the controller). The over-

all delay between sampling and receiving can be highly variable. In fact, the medium access delay (i.e., the time it takes for a shared network to accept data), the network delay (i.e., the time for relay nodes in multi-hop networks to forward data), and the transmission delays (i.e., the time during which data are in transit in the medium) depend on highly variable network conditions such as routing, congestion, and link quality. In some control systems, the data transmitted are time-stamped, which means that the receiver may have an estimate of the delay duration and can take appropriate corrective actions. Many research results have characterized upper bounds on the sampling interval for which stability can be guaranteed (e.g., [51]). These results implicitly attempt to minimize the packet rate that is needed to stabilize a system through feedback. Furthermore, the jitter of the delay is critical since it can be more difficult to compensate for, especially if the variability is large.

- Packet losses: overflows in communication buffers, transmission errors in the physical layer, and collisions cause packet losses, which affect the performance of the controller [52]. Different techniques have been developed to compensate for packet losses in wireless networks. A common approach to model losses is to assume that packet losses are independent and identically distributed (i.i.d.) according to a Bernoulli distribution, as in [20].

The possibility to compensate a certain degree of delay and packet losses [19] suggest that a different network design approach is beneficial with respect to traditional wireless network applications. When wireless sensors are used for communications, the network energy consumption is fundamental. A trade-off between delay, packet losses, and stability requirements for the benefit of the energy consumption has been advocated by [53].

Control applications are usually designed from a protocol stack point of view by a top-down approach, whereby most of the essential aspects of the network and sensing infrastructure that has to be deployed to support control applications are ignored. Here, packet losses and delays introduced by the communication network are considered as uncertainties and the controllers are tuned to cope with them without having any influence on them. The top-down approach is limited for two reasons: i) it does not consider the aspect of energy efficiency of the wireless network [2]; ii) it can be quite conservative and therefore inefficient, because the controllers are built by presuming worst case wireless channel conditions that may be rarely experienced in the reality. On the other side, protocols for wireless networks are traditionally designed to maximize the reliability and minimize the delay. This is a bottom-up approach, where controller specifications are not explicitly considered even though the protocols are used for control. This approach is energy inefficient because high reliability and low delay may demand significant energy consumption [54].

In conclusion, a well designed wireless networked control system must include both communication and control aspects and consider their complex interaction. For this scope, contract-based design represents a promising methodology.

2.3 Wireless Protocols for Control Applications

In this section, we introduce some wireless protocols that have been proposed in the recent years for the applications of interest in this thesis. We first discuss relevant MAC protocols, routing protocols, and cross-layer solutions. Then, we focus on the specifications of standard solutions for low-power networks, with emphasis on the IEEE 802.15.4 MAC protocol and the IETF routing protocol for low-power and lossy networks (RPL), which are analyzed throughout the thesis.

In Table 2.3, we report relevant protocols for control applications by evidencing different performance indicators (energy consumption, reliability, and delay), the communication layer involved, and the availability of analytical models of the performance indicators. An extensive survey of wireless protocols for control applications is also reported in [55].

2.3.1 MAC Protocols

The MAC layer is responsible for managing access to a channel shared by several nodes. The principles of MAC layer design for low-power wireless networks differ from those of traditional wireless networks mainly in two aspects: (i) energy conservation is a design concern, and (ii) distributed mechanisms are often required [75].

Idle listening is considered as one of the dominant components of energy waste in many traditional MAC protocols. Since a node does not know a priori when it can receive a message from a neighbor, its radio must be on to listen to the medium. However, the channel may be idle for most of the time. To save energy, many MAC proposals keep the radio in sleep mode (i.e., switched off) during some periods of time, trading off energy conservation for latency. Furthermore, collisions contribute to energy inefficiency, since energy is consumed for the transmission of a data unit that is not received successfully. In addition, control overhead must be kept reasonably low. Finally, because a multi-hop path requires the transmission of a data unit in several links, nodes must be appropriately organized to achieve good performance in terms of end-to-end reliability, latency, and network energy consumption.

In the following, we categorize MAC solutions in contention-based, scheduled-based and hybrid solutions.

Contention-based MAC

In contention-based MAC protocols, nodes compete for the medium and coordinate in a probabilistic way. Packet collisions can occur and reliability may be strongly reduced for high traffic, but packet delay is usually low and a strict synchronization is not needed.

The basic mechanism to handle channel contentions is the carrier sense multiple access (CSMA). A transmitting node tries to detect the presence of an encoded signal from another node before attempting to transmit. If a carrier is sensed, the

Table 2.3: Protocol Comparison - The letters **E**, **R**, and **D** denote energy, reliability, and delay. The circle denotes that a protocol is designed by considering the indication of the column, but it has not been validated experimentally. The circle with plus denotes that the protocol is designed by considering the indication and experimentally validated. The dot denotes that the protocol design does not include the indication and hence cannot control it, but simulation or experiment results include it. Medium access control and routing layers are denoted by MAC and ROU, respectively.

Protocol	**E**	**R**	**D**	**Layers**
BMAC [56]	⊕	·	·	MAC
XMAC [57]	⊕	·	·	MAC
RI-MAC [58]	⊕	·	·	MAC
TRAMA [59]	⊕	·	·	MAC
PEDAMACS [60]	◯		◯	MAC
TSMP [61]	⊕	⊕	·	MAC
SMAC [62]	⊕	·	·	MAC
TMAC [63]	⊕			MAC
ZMAC [64]	⊕	⊕	·	MAC
LEACH [65]	◯			ROU
CTP [66]	◯	◯		ROU
BCP [67]	·	⊕	⊕	ROU
MMSPEED [68]		◯	◯	ROU
GAF [69]	◯	·	·	ROU
SPAN [70]	◯	·	·	MAC, ROU
GERAF [71]	◯		◯	MAC, ROU
Dozer [72]	⊕	⊕		MAC, ROU
XLP [73]	◯	◯	◯	MAC, ROU
SERAN [53]	◯		◯	MAC, ROU
Breath [74]	⊕	⊕	⊕	MAC, ROU
TREnD [29]	⊕	⊕	⊕	MAC, ROU

node keeps on sensing the channel with probability p (p-persistent CSMA) or delays its transmission for a random number of time units (CSMA with collision avoidance CSMA/CA).

Relevant contention-based MAC solutions for energy efficient operations in sensor networks are BMAC [56] and XMAC [57], which are based on preamble sampling. In these MACs, the receiver wakes up periodically to check whether there

is a transmission and the sender, instead of coordinating the wake-up times of neighbors, sends a preamble that is long enough to ensure the receiver wakes up. A low-power listening (LPL) scheme [76] where a node cycles between awake and sleep cycles is employed. While awake, the node listens for a long enough preamble to assess if it needs to stay awake or can return to sleep mode.

The cycled receiver [77] is the reverse approach to LPL, which shifts communication initiation from the transmitter side to the receiver side. When the receiver is ready to receive messages, then it sends out beacons at a regular interval instead of listening periodically. To send a data frame, the transmitter stays awake and monitors the channel waiting for a beacon from the receiver. Once the transmitter receives the beacon, it transmits the data frame and waits for an ACK to end the session. This avoids sending a long wake-up preamble of LPL and shortens transmission times considerably. The cycled receiver achieves high energy savings for unicast and anycast communications. Receiver-Initiated (RI) MAC [58] is based on a similar mechanism. However, cycled receiver approaches cannot be used for broadcast and multicast communications. Furthermore, the beacons from receivers adds interference to the data traffic.

Sift [78] is a MAC protocol proposed for very low latency event-driven sensor network environments. Sift uses a non-uniform probability distribution function of picking a slot within a slotted contention window. If no node starts to transmit in the first slot of the window, then each node increases its transmission probability exponentially for the next slot assuming that the number of competing nodes is small. Energy consumption increases as overhearing and idle-listening are not negligible.

Scheduling-based MAC

Scheduling-based MAC protocols use dedicated resources for packet transmissions. The protocol selects specific time intervals for the transmission of each node in time division multiple access (TDMA) fashion. This approach assumes that nodes are synchronized, which can be performed by using time-stamps or even GPS. Since nodes do not compete for the medium and have reserved resources, scheduling-based MAC protocols are collision-free.

The traffic-adaptive medium access protocol (TRAMA) [59] is a conflict-free, scheduling-based MAC protocol designed for energy efficiency. This feature is achieved by transmission schedules and by allowing nodes to switch the radio to a low-power mode when they are not involved in communications. TRAMA uses a single and time-slotted channel for data and signaling transmissions.

The power efficient and delay aware medium access control protocol for sensor networks (PEDAMACS) [60] is also based on centralized scheduling. The sink gathers information about traffic and topology during the setup phase. Then it calculates a global scheduling and sends it to the entire network. Note that the protocol assumes that the sink can reach all nodes when it transmits. The uplink communications follows a TDMA scheme established by the sink. The method is

limited to converge-cast traffic patterns (many different sources to a single sink). In addition, the assumption that the sink reaches all nodes is not always satisfied.

Time synchronized mesh protocol (TSMP) [61] is a protocol developed by Dust Networks, which provides services with the aim of contributing to end-to-end reliability particularly for industrial automation networks. TSMP, is based on a TDMA approach and frequency hopping spread spectrum (FHSS). Hence, consecutive transmissions between two nodes take place in different frequencies as well as in different time slots. A node can participate in different frames (which comprise a number of time-slots) of different sizes to perform different tasks at once.

Hybrid MAC

Hybrid solutions are interesting for industrial and building applications, because of the possibility to obtain a trade-off between advantages of contention-based and collision-free mechanisms with low energy consumption.

Sensor-MAC (SMAC) [62] is based on locally managed synchronization and periodic sleep-listen schedules. Basically built in a contention-based fashion, SMAC strives to retain the flexibility of contention-based protocols while improving energy efficiency in multi-hop networks. SMAC includes approaches to reduce energy consumption from all the major sources of energy waste: idle listening, collision, overhearing, and control overhead. Neighboring nodes form virtual clusters to set up a common sleep schedule.

Timeout-MAC (TMAC) [63] is proposed to enhance the poor results of the SMAC protocol under variable traffic loads. Indeed, the static sleep-listen periods of SMAC result in high latency and lower throughput. In TMAC, the listen period ends when no activation event has occurred for a time threshold. The main drawback of this protocol is the early sleeping problem.

ZMAC [64] is a hybrid MAC scheme for sensor networks that combines the strengths of TDMA and CSMA while offsetting their weaknesses. The main feature of ZMAC is its adaptability to the level of contention in the network so that under low contention, it behaves like CSMA, and under high contention, like TDMA. By mixing CSMA and TDMA, ZMAC becomes more robust to timing failures, time-varying channel conditions, slot assignment failures and topology changes than a stand-alone TDMA. In ZMAC, a time slot assignment is performed at the time of deployment and higher overhead is incurred at the beginning.

2.3.2 Routing Protocols

One way to classify routing protocols is based on link state and distance vector. In the first case, each node uses topological information to map routing tables, while distance vector algorithms exchange routing information among neighbors. Routers using distance vector protocol do not have knowledge of the entire path to a destination. While link state protocols typically present higher convergence speed and less overhead, distance vector protocols are simpler, require less computational

capability and have smaller storage requirements. Open shortest path first (OSPF) and optimized link state routing (OLSR) are link state protocols, while ad-hoc on-demand distance vector (AODV) and dynamic source routing (DSR) are examples of distance vector protocols for mobile ad hoc networks (MANETs), all of them proposed by the internet engineering task force (IETF) [79]. AODV is part of the ZigBee Alliance [80] protocol stack. The routing solution adopted by AODV uses an on-demand approach for finding routes, which are established only when it is required by a source node for transmitting data packets. It employs destination sequence numbers to identify the most recent path.

Low energy adaptive clustering hierarchy (LEACH) [65] is a cluster-based protocol that includes distributed cluster formation and a hierarchical clustering algorithm. LEACH randomly selects a few sensor nodes as cluster heads (CHs) and rotates this role to evenly distribute the energy load among the sensors in the network. In LEACH, the CH nodes compress data arriving from nodes that belong to the respective cluster, and send an aggregated packet to the network coordinator in order to reduce the amount of information that must be transmitted. LEACH uses TDMA MAC protocol to avoid intra-cluster collisions and code-division multiple access (CDMA) to reduce inter-cluster interference. However, data collection is centralized and performed periodically.

Other relevant studies include collection protocols. They provide best-effort, unreliable packet delivery to one of the data sinks in the network. Having a robust, highly reliable, and efficient collection protocol benefits almost every sensor network application today, as well as the many transport, routing, overlay, and application protocols that sit on top of collection trees. A relevant example is the collection tree protocol (CTP) [66]. CTP uses link quality estimations for parent selection. However, this approach may incur a load balancing problem because the node with good quality link will be selected as the preferred parent and consumes more energy. Furthermore, CTP uses a very aggressive retransmission policy, i.e., the default value of the maximum number of retransmissions is 32, which can create contention problems at MAC layer. The back-pressure collection protocol (BCP) [67] introduces dynamic back-pressure routing for wireless networks. In BCP, the routing and forwarding decisions are made on a per-packet basis by computing a back-pressure weight of each outgoing link that is a function of localized queue and link state information. Therefore, the overhead due to the back-pressure algorithm depends on all possible forwarding nodes of the next hop. Furthermore, the back-pressure algorithm does not prevent loops of the routing and may incur in large delay.

In location-based routing protocols, each node knows its own position and the position of its neighbors. The location information is needed to calculate the distance between two particular nodes so that energy consumption can be estimated. The GAF [69] and SPAN [70] protocols mainly consider the energy efficiency as an objective. Only a fraction of the nodes are activated in a certain area at any given time. Geographic Random Forwarding (GeRaF) [71] provides a complete solution combining the routing and CSMA/CA mechanism as MAC layer. The forwarding

node is chosen among nodes that are awake at the time of the transmission request. Hence, the routing consumes more power and increases the latency of the network. The dependency on the exact location information can be reduced by opportune algorithms [81].

Reliable end-to-end performance is guaranteed by protocol solutions such as MMSPEED [68] and RMST [82]. MMSPEED satisfies high reliability constraint by using duplicated packets. However, duplicated packets increase the traffic load with negative effect on the stability and energy efficiency. RMST guarantee the eventual delivery of packets by using an end-to-end acknowledgement mechanism that affects the latency and the energy efficiency. Dozer [72] specifies MAC and routing layers to minimize the energy consumption while guaranteeing a reliability constraint, but without considering an analytical study.

Analytical studies and parameter tuning are present in XLP [73], but no experimental validation is available. Example of cross-layer protocols that consider energy efficiency, tunable parameters, and experimental implementation are SERAN [53], Breath [74], and TREnD [29], which we will discuss in Chapter 6.

2.3.3 IEEE 802.15.4 Standard

Many standard proposals and existing commercial systems for low-power and low-rate personal area networks are based on the IEEE 802.15.4 standard [7]. This standard plays a key role in industrial and building automation [2, 83].

To achieve low average power consumption, IEEE 802.15.4 assumes that the amount of data transmitted is short and that it is transmitted infrequently in order to keep a low duty-cycle. The IEEE 802.15.4 MAC operation is based on CSMA/CA and it allows for beacon-enabled and beacon-less functionalities.

In slotted (beacon-enabled) mode, communication is controlled by a network coordinator, which transmits regular beacons for synchronization and association procedures. A superframe structure is imposed with active and optional inactive periods as shown in Figure 2.4. The active period of a superframe consists of a contention access period (CAP) and a contention-free period (CFP). Channel access in the CAP is in the form of slotted CSMA, while the coordinator allots guaranteed time slots (GTSs) in the CFP for low latency applications. Coordinator and nodes can communicate during the active period and enter a low-power mode during the inactive period. The structure of the superframe is defined by two parameters, the beacon order and the superframe order, which determine the length of the superframe and its active period. In addition, the superframe is divided into 16 equally sized superframe slots of length $aBaseSlotDuration$.

In unslotted (beacon-less) mode there are no regular beacons, but the coordinator may unicast beacons to a soliciting device. Communication among devices in the beacon-less mode uses unslotted CSMA/CA for decentralized access.

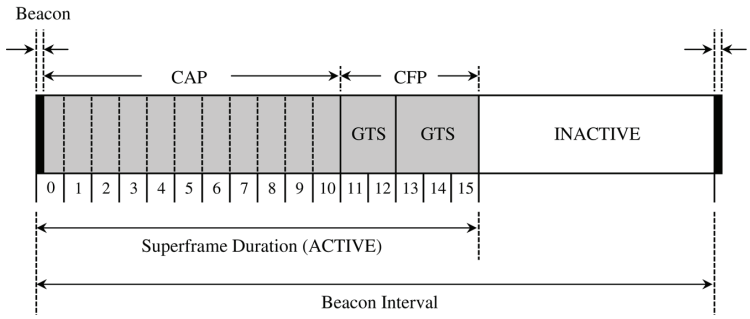

Figure 2.4: Superframe structure of slotted IEEE 802.15.4 MAC.

CSMA/CA with Binary Exponential Backoff (BEB)

Let us consider a node in transmission. In the slotted CSMA/CA of IEEE 802.15.4, first the MAC protocol initializes three variables given by the number of backoffs NB, backoff exponent BE, and retransmission times RT. The default initialization is NB=0, BE=*macMinBE* and RT=0.

The node delays for a random number of complete backoff periods in the range $[0, 2^{\mathrm{BE}} - 1]$ units *aUnitBackoffPeriod*. When the backoff period is zero, the node performs the first clear channel assessment (CCA). If two consecutive CCAs are idle, then the node commences the packet transmission. If either of the CCA fails due to busy channel, the protocol increases the value of both NB and BE by one up to maximum values *macMaxCSMABackoffs* and *macMaxBE*, respectively. Hence, the values of NB and BE depend on the number of CCA failures of a packet. Once BE reaches *macMaxBE*, it remains at the value of *macMaxBE* until it is reset. If NB exceeds *macMaxCSMABackoffs*, then the packet is discarded due to channel access failure. Otherwise the CSMA/CA algorithm generates a random number of complete backoff periods and repeat the process. The variable *macMaxCSMABackoffs* is the maximum number of times the CSMA/CA algorithm is required to backoff. If channel access is successful, the node starts transmitting packets and waits for an ACK. The reception of the corresponding ACK is interpreted as successful packet transmission. If the node fails to receive the ACK, the variable RT is increased by one up to *macMaxFrameRetries*. If RT is less than *macMaxFrameRetries*, the MAC protocol initializes BE=*macMinBE* and follows the CSMA/CA mechanism to re-access the channel. Otherwise the packet is discarded due to the retry limit.

The unslotted CSMA/CA is implemented similarly, with the difference of having only a single CCA for each transmission attempt.

In the rest of the thesis, we denote the IEEE 802.15.4 MAC parameters by $W_0 = 2^{macMinBE}$, $m_0 = macMinBE$, $m_b = macMaxBE$, $m = macMaxCSMABackoffs$, $n = macMaxFrameRetries$, and $S_b = aUnitBackoffPeriod$.

2.3.4 Routing over Low-Power and Lossy Networks

The IETF routing over low-power and lossy networks (ROLL) working group [12] was created in 2007 with the aim of analyzing and eventually developing solutions for IP-based low-power and lossy networks (LLNs). LLNs are made largely of constrained nodes (with limited processing power, memory, and energy when they are battery operated). These nodes are interconnected by lossy links, typically supporting only low data rates, that are usually unstable with relatively low packet delivery rates. Another characteristic of such networks is that the traffic patterns are not simply unicast, but in many cases point-to-multipoint or multipoint-to-point. Furthermore, such networks may potentially comprise up to thousands of nodes.

The working group first elaborated a list of requirements for a routing protocol on top of LLNs in each of the following application domains: home automation, commercial building automation, industrial automation, and urban automation. Based on these requirements, the working group carried out an analysis of existing routing protocols within the IP domain with regard to their applicability to LLNs. The general requirements are as follows:

- The routing state of a node must not increase linearly with the number of nodes in the network or in the neighborhood. A routing state that depends linearly on the number of unique destination is acceptable.

- Local events, such as the failure of a link between two nodes, must not lead to flooding broadcast messages to the whole network.

- The rate at which the routing messages are sent or received must be bounded by the rate of data packets.

According to the analysis, none of the existing IP routing protocols would fulfill all the criteria without modification. In consequence, the working group started to work on the specification of a new routing protocol suitable for LLNs. This routing protocol is called IPv6 routing protocol for low-power and lossy networks (RPL).

The feature of RPL is the construction of destination-oriented directed acyclic graphs (DODAGs) over the network, according to optimization objectives based on metrics along the paths. In the RPL context, all edges are contained in paths oriented toward and terminating at one or more root nodes. One or more DODAGs that share the same performance criteria and constraints represent a RPL instance. A network may run multiple instances concurrently.

Each node inside a DODAG is identified by the rank, a scalar value that represents the relative position of the node with respect to other nodes and the root. The rank does not have a physical unit, it increases in a strictly monotonic fashion from the root to the leaf nodes and can be used to validate a progression from or towards the root. The exact calculation of the rank depends of an objective function (OF) but it does not represent necessarily a path cost. For rank comparisons,

RPL uses only the integer part of the rank, computed by the DAGrank() macro, which scales the rank by the maximum number of hops in the network.

The fundamental use of the rank is to avoid and detect loops. Loop avoidance is implemented by letting nodes of the network select their parents only among nodes with lower rank. However, loops may occur when nodes detaches from the DODAG and reattaches to a node in its prior sub-DOGAG. This effect is mitigated by loop detection mechanisms implemented locally.

RPL nodes build and maintain DODAGs by multicasting DODAG information object (DIO) messages to their neighbors periodically. The DIO message includes the rank of a node, among other fields. In order to join a DODAG, a node listens to the DIO messages sent by its neighbors and selects a subset of these nodes as their parents in the DODAG. A node may also identify siblings, which are neighbors having the same rank (but do not necessarily share a common parent with this node). This allows path diversity to be increased, as a node can decide to forward a packet to a sibling. However, communications between siblings is limited to one hop to avoid loops.

A node can select one preferred parent. The rank of the node would then be computed as the rank of the preferred parent plus an increment that depends on the cost of the link between the node and the preferred parent. Although the rank is computed by using link costs, in principle, topology building and maintenance mechanisms are independent of packet forwarding procedures.

There are various metrics and constraints that can be used for path calculation and packet forwarding in RPL. The protocol supports both static and dynamic metrics. Link reliability, packet delay, and node energy consumption are measurements that can be used both as metric and constraints. Expected transmissions count (ETX) is a reliability metric that provides the number of transmissions a node expects to make to a destination in order to successfully deliver a packet. In addition, more metrics can be embedded in the same DODAG metric container.

2.4 Summary

In this chapter, we introduced the contract-based design methodology and the challenges in networked control systems. We reviewed communication protocols that can be used in the design of networked control applications, by giving emphasis to the IEEE 802.15.4 MAC and RPL routing, which we analyze in the next chapters.

Chapter 3

Markov Chain Modeling of Contention-based MAC Protocols

In this chapter, we present a framework for modeling and optimization of CSMA/CA mechanisms, with particular reference to the specifications of the IEEE 802.15.4 MAC protocol. Recalling the general flow diagram in Figure 3.1, we restrict the attention to the performance of the MAC on a single-hop network, where the wireless channel is ideal. We propose a generalized Markov chain model of the exponential backoff process with retry limits, acknowledgments, unsaturated traffic, packet size, and packet copying delay due to hardware limitations. The model is used to derive accurate and approximate equations to characterize the performance in terms of successful packet reception probability, delay for successfully received packets, and network energy consumption. Moreover, we derive a distributed adaptive algorithm for the protocol parameters selection. Results are validated through experiments for various combinations of MAC parameters, traffic regime, and number of nodes.

The chapter starts by introducing the related literature in Section 3.1. Then, we describe the accurate model and the approximate model in Section 3.2, and derive reliability, delay, and energy consumption in Section 3.3. The adaptive algorithm operation is illustrated in Section 3.4, and the results validated experimentally in Section 3.5. The chapter concludes with a brief summary. The limitations of the Markov chain model are discussed in Appendix C. A list of symbols and acronyms is reported in Appendix F.

3.1 Related Work

The CSMA/CA is the basic mechanism for wireless contention-based MACs and has been implemented with some modifications in many standards (e.g., IEEE 802.11, IEEE 802.15.4). Bianchi's model has been the first model to describe the basic functionalities of the IEEE 802.11 MAC through a Markov chain under saturated traffic condition [84]. The core contribution of the model is the analytical evaluation of the saturation throughput, in the assumption of ideal channel conditions

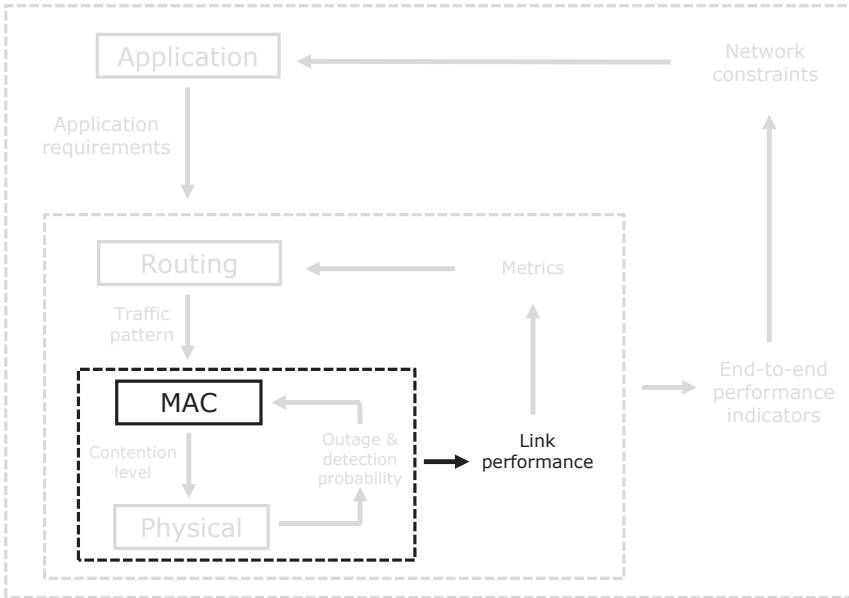

Figure 3.1: Interaction of layers for modeling and design: performance analysis of the MAC.

(i.e., no hidden terminals and capture). In the analysis, a fixed number of devices is assumed, with each device always having a packet available for transmission. The analysis is divided into two distinct parts. First, the behavior of a single device is studied by a Markov model to obtain the stationary probability that the device transmits a packet in a generic (i.e., randomly chosen) slot. This probability does not depend on the access mechanism employed. Then, by studying the events that can occur within a generic slot time, the throughput is expressed as a function of the computed value. The key approximation that enables Bianchi's model is the assumption of constant and independent collision probability of a packet transmitted by each device, regardless of the number of retransmissions already suffered. As proven by comparison with simulation, this assumption leads to very accurate results. Extensions of this model have been used to analyze the packet reception rate [85], the delay [86, 87], the service time [88, 89], and the throughput [90, 91] of IEEE 802.11. A simple and effective delay distribution analysis of IEEE 802.11 is studied in [92].

The analysis of the packet delay, throughput, and power consumption of IEEE 802.15.4 has been the focus of the simulations-based study in [93], and some more recent analytical works, e.g., [94] – [98]. Inspired by Bianchi's work, a Markov model for IEEE 802.15.4 has been introduced in [94]. An extension of the model with ACK mechanism has been proposed in [95]. In [96], a throughput analysis

has been performed, by including the superframe structure and the retransmission mechanism. However, the proposed Markov chain does not model the length of data and ACK packets, which is crucial to analyze the performance metrics for IEEE 802.15.4 networks with low-data rate. A modified Markov model including retransmissions with finite retry limits has been studied in [97]. The basic assumptions of Bianchi's model are discussed and the accuracy in the calculation of different performance indicators is determined. In [98], a query-based approach has been considered to analyze the throughput, reliability, and delay of the network. Although this approach is interesting, the ACK mechanism and the retransmission mechanism have not been accounted for.

We remark here that the analytical models available from the literature use numerical methods to solve non-linear equations [94] – [98], which is a major drawback for in-network processing [99]. Practical hardware limitations are not accurately considered. Furthermore, despite the theoretical promises of the analytical models for analyzing the IEEE 802.15.4 MAC using Monte Carlo simulations, these theoretical results have not been validated by experiments.

Due to the availability of analytical models for the protocol characterization, various algorithms to tune the MAC parameters of IEEE 802.11 and IEEE 802.15.4 protocols have been proposed. The algorithms can be grouped in those based on the use of physical layer measurements, and those based on the use of link-layer information. Adaptive tuning based on physical layer measurements have been investigated in [100] – [102], where a p-persistent IEEE 802.11 protocol has been considered to optimize the average backoff window size. This algorithm and its scalability to the network size have been studied also for IEEE 802.15.4 [102]. However, the channel sensing mechanism, the optional ACK, and retransmission mechanisms therein proposed are hard to be approximated by a p-persistent MAC. Furthermore, in [101] and [102] a saturated traffic regime has been assumed, which is a scenario of reduced interest for typical sensor network applications. In [103], a cross-layer MAC design has been proposed by estimating both the MAC queue dynamics of each traffic class and the overall network contention level to meet the requirement of delay sensitive applications. However, this approach is not energy efficient because each device requires to monitor the queue dynamics and contention level. Link-based optimizations for IEEE 802.11 have been investigated in [104, 105], where simple window adjustment mechanisms that are based on ACK transmissions have been considered. In these papers, the algorithms adapt the contention window size depending on the successful packet transmission, packet collision, and channel sensing state, but the algorithms are not grounded on an analytical study. In [106], the authors have proposed an algorithm to tune the contenting window based on the multivariable control theory. Unfortunately, an IEEE 802.15.4 enhancement based on the use of link-layer information has the drawback of requiring a modification of the standard, and of a costly ACK mechanism since it introduces large overhead for small packets.

3.2 Markov Chain Model of the IEEE 802.15.4 MAC

We consider a network with N devices transmitting with single-hop communication toward a personal area network (PAN) coordinator. We assume that the devices use the slotted CSMA/CA modality described in Section 2.3.3. The use of this MAC modality is suggested by the single-hop topology, where superframe synchronization can be achieved easily. The model can be extended to include the features of the unslotted MAC modality, as illustrated in the next chapter.

The parameters of the CSMA/CA algorithm that influence reliability, delay, and energy consumption are the minimum value of the backoff exponent m_0, the maximum value of the backoff exponent m_b, the number of backoffs allowed before declaring a channel access failure m, and the maximum number of retries allowed after a transmission failure n.

Throughout this chapter, we consider applications where devices asynchronously generate traffic with probability $1-\eta$ when a device sends a packet[1] successfully or discard a packet or the sampling interval is expired. Otherwise, with probability η, the device stays for a time $L_0 S_b$ without generating packets, where L_0 is an integer and S_b is the time unit *aUnitBackoffPeriod* (corresponding to 20 symbols). This traffic generation model allows for an easy computation of the model equations and it is practical to model control applications with time-variant sampling periods [107]. However, more general traffic generation models can be included in the Markov chain, as we show in the extensions of the model in the following chapters.

We consider the following assumptions.

- The probability to sense the channel busy during the clear channel assessments (CCAs) does not depend on the backoff stage where the corresponding CCA is performed.
- The probability to sense the channel busy during the CCAs does not depend on the number of attempts the current packet has gone through.
- The probability of sensing the channel busy during a CCA does not depend on the random backoff value drawn in the backoff stage preceding the CCA.
- The probability that, at a given time, a given device starts sensing the channel is independent of what other devices in the network are doing at the same time.

These assumptions are used, wherever applicable, in all previous models [94] – [96], leading to accurate and computationally convenient derivations.

Let $s(t), c(t)$ and $r(t)$ be the stochastic processes representing the backoff stage, the state of the backoff counter and the state of retransmission counter at time t experienced by a device to transmit a packet. The triple $(s(t), c(t), r(t))$ is represented by the three-dimensional Markov chain in Figure 3.2, where we use (i, k, j) to denote a particular state.

[1] We refer to packets as the MAC protocol data units.

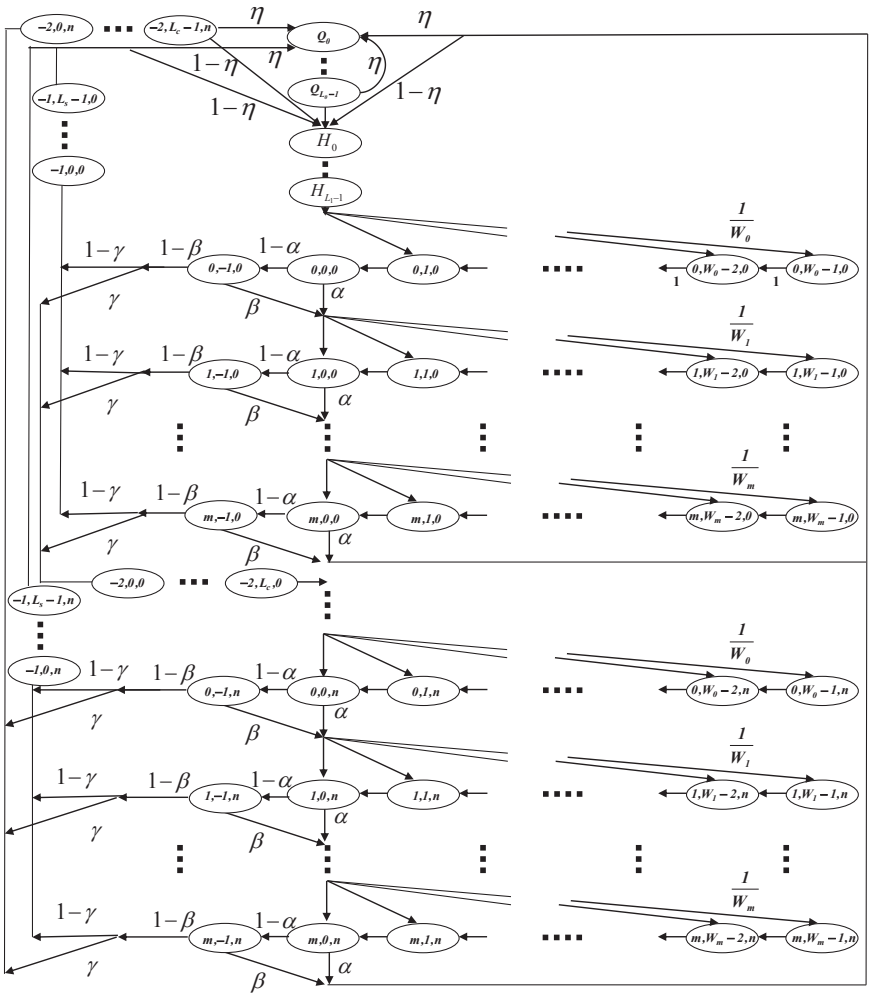

Figure 3.2: Markov chain model for the slotted CSMA/CA of IEEE 802.15.4.

The Markov chain consists of five main parts corresponding to the idle-queue states, packet copying states, backoff states, CCA states, and packet transmission states. The states $(Q_0, \ldots, Q_{L_0-1})$ correspond to the idle-queue states when the packet queue is empty and the device is waiting for the next packet generation time. Hence, the device sets its radio to sleep mode during the idle-queue states. The states $(H_0, \ldots, H_{L_1-1})$ represent the packet copying delay between the microcon-

troller and the radio transceiver, where

$$L_1 = \left\lceil \frac{L}{\nu S_b} \right\rceil ,$$

with L being the total length of a packet including overhead and payload and ν is the serial peripheral interface (SPI) bus speed. Note that before sending a packet, the microcontroller copies the packet data into the transmit buffer of the radio transceiver over the SPI bus [7]. In [108], the authors show that packet copying is a critical issue when forwarding a packet. The states from $(i, W_m - 1, j)$ to $(i, W_0 - 1, j)$ represent the backoff states. The radio circuits of the device are set to idle mode or to sleep mode during the backoff period. The states $(i, 0, j)$ and $(i, -1, j)$ represent first CCA (CCA_1) and second CCA (CCA_2), respectively. Let α be the probability that CCA_1 is busy, β the probability that CCA_2 is busy, and γ the collision probability. The states $(-1, k, j)$ and $(-2, k, j)$ correspond to the successful transmission and packet collision, respectively. By knowing the duration of an ACK frame, ACK timeout, inter-frame spacing (IFS), data packet length, and header duration, we define the packet successful transmission time L_s and the packet collision time L_c as

$$\begin{aligned} L_s &= L + t_{\text{ack}} + L_{\text{ack}} + IFS\,, \\ L_c &= L + t_{\text{m,ack}}, \end{aligned} \tag{3.1}$$

where t_{ack} is ACK waiting time, L_{ack} is the length of ACK frame, and $t_{\text{m,ack}}$ is the timeout of the ACK, see details in [7].

The state transition probabilities associated with the Markov chain in Figure 3.2 are

$$P(i, k, j | i, k+1, j) = 1, \text{ for } k \geq 0\,, \tag{3.2}$$

$$P(i, k, j | i-1, 0, j) = \frac{\alpha + (1-\alpha)\beta}{W_i}, \text{ for } i \leq m\,, \tag{3.3}$$

$$P(0, k, j | i, 0, j-1) = \frac{(1-\alpha)(1-\beta)\gamma}{W_0}, \text{ for } j \leq n\,, \tag{3.4}$$

$$P(Q_0 | m, 0, j) = \eta\,(\alpha + (1-\alpha)\beta), \text{ for } j < n\,, \tag{3.5}$$

$$P(Q_0 | i, 0, n) = \eta\,(1-\alpha)(1-\beta), \text{ for } i < m\,, \tag{3.6}$$

$$P(Q_0 | m, 0, n) = \eta, \tag{3.7}$$

$$P(0, k, 0 | Q_0) = \frac{1-\eta}{W_0}, \text{ for } k \leq W_0 - 1\,. \tag{3.8}$$

Equation (3.2) is the decrement of the backoff counter, which happens with probability 1. Equation (3.3) represents the probability of finding busy channel in CCA_1 or CCA_2 and selecting a state in the next backoff stage. Equation (3.4) gives the unsuccessful transmission probability after finding an idle channel in both CCA_1 and CCA_2, and selecting a state in the next retransmission stage. Equation (3.5)

and (3.6) represent the probability of going back to the idle-queue stage due to channel access failure and retry limits, respectively. Equation (3.7) accounts for the traffic regime and is the probability of going back to the idle-queue stage at backoff counter m and retransmission stage n. Equation (3.8) models the probability of going back to the first backoff stage from the idle-queue stage.

Let the stationary probability of the Markov chain in Figure 3.2 be

$$b_{i,k,j} = \lim_{t\to\infty} \Pr(s(t) = i, c(t) = k, r(t) = j),$$

where $i \in (-2, m), k \in (-1, \max(W_i - 1, L_s - 1, L_c - 1)), j \in (0, n)$. Owing to the chain regularities and Equations (3.2)–(3.8), we have

$$b_{i,k,j} = \frac{W_i - k}{W_i} b_{i,0,j}\,, \tag{3.9}$$

where

$$W_i = \begin{cases} 2^i W_0, & i \le m_b - m_0\,, \\ 2^{m_b}, & i > m_b - m_0\,. \end{cases}$$

From Equation (3.3), for $i \le m$ we obtain

$$b_{i,0,j} = (\alpha + (1-\alpha)\beta)^i b_{0,0,j}. \tag{3.10}$$

From Equation (3.4), $b_{0,0,j}$ is rewritten as follows

$$b_{0,0,j} = \left((1-\alpha)(1-\beta)\gamma \sum_{i=0}^{m} (\alpha + (1-\alpha)\beta)^i \right)^j b_{0,0,0}\,. \tag{3.11}$$

Moreover,

$$b_{-1,k,j} = (1-\alpha)(1-\beta)(1-\gamma) \sum_{i=1}^{m} b_{i,0,j}\,, \quad 0 \le k \le L_s - 1\,, \tag{3.12}$$

and

$$b_{-2,k,j} = (1-\alpha)(1-\beta)\gamma \sum_{i=1}^{m} b_{i,0,j}\,, \quad 0 \le k \le L_c - 1\,. \tag{3.13}$$

By the normalization condition, we know that

$$\sum_{i=0}^{m} \sum_{k=0}^{W_i-1} \sum_{j=0}^{n} b_{i,k,j} + \sum_{i=0}^{m} \sum_{j=0}^{n} b_{i,-1,j} + \sum_{j=0}^{n} \left(\sum_{k=0}^{L_s-1} b_{-1,k,j} + \sum_{k=0}^{L_c-1} b_{-2,k,j} \right) + \sum_{l=0}^{L_0-1} Q_l + \sum_{l=0}^{L_1-1} H_l = 1\,. \tag{3.14}$$

We next derive the expressions of each term in Equation (3.14). From Equations (3.9) and (3.10), we have

$$\sum_{i=0}^{m}\sum_{k=0}^{W_i-1}\sum_{j=0}^{n} b_{i,k,j} = \sum_{i=0}^{m}\sum_{j=0}^{n} \frac{W_i+1}{2}(\alpha+(1-\alpha)\beta)^i\, b_{0,0,j}$$
$$= \begin{cases} \frac{b_{0,0,0}}{2}\left(\frac{1-(2x)^{m+1}}{1-2x}W_0 + \frac{1-x^{m+1}}{1-x}\right)\frac{1-y^{n+1}}{1-y} \\ \quad \text{if } m \le m_b - m_0 \\ \frac{b_{0,0,0}}{2}\left(\frac{1-(2x)^{m_b-m_0+1}}{1-2x}W_0 + \frac{1-x^{m_b-m_0+1}}{1-x} + \right. \\ \left.(2^{m_b}+1)x^{m_b-m_0+1}\frac{1-x^{m-m_b+m_0}}{1-x}\right)\frac{1-y^{n+1}}{1-y} \\ \quad \text{otherwise,} \end{cases} \tag{3.15}$$

where $x = \alpha + (1-\alpha)\beta$ and $y = \gamma(1-x^{m+1})$. Similarly,

$$\sum_{i=0}^{m}\sum_{j=0}^{n} b_{i,-1,j} = (1-\alpha)\frac{1-x^{m+1}}{1-x}\,\frac{1-y^{n+1}}{1-y}\, b_{0,0,0}\,, \tag{3.16}$$

and

$$\sum_{j=0}^{n}\left(\sum_{k=0}^{L_s-1} b_{-1,k,j} + \sum_{k=0}^{L_c-1} b_{-2,k,j}\right) = (L_s(1-\gamma)+L_c\gamma)(1-x^{m+1})\frac{1-y^{n+1}}{1-y}\, b_{0,0,0}\,. \tag{3.17}$$

By considering that the successful transmission and the failure events are due to the limited number of backoff stages m and the retry limit n, the idle state probability is

$$\begin{aligned} Q_0 =& \eta\, Q_{L_0-1} + \eta\left(\sum_{j=0}^{n}(\alpha+(1-\alpha)\beta)\; b_{m,0,j} + \sum_{i=0}^{m}\gamma(1-\beta)\, b_{i,-1,n}\right. \\ &\left. + \sum_{i=0}^{m}\sum_{j=0}^{n}(1-\gamma)\,(1-\beta)\, b_{i,-1,j}\right) \\ =& \frac{\eta}{1-\eta}\left(\frac{x^{m+1}(1-y^{n+1})}{1-y} + \gamma(1-x^{m+1})y^n\right. \\ &\left. + (1-\gamma)\frac{(1-x^{m+1})(1-y^{n+1})}{1-y}\right) b_{0,0,0}\,, \end{aligned} \tag{3.18}$$

where L_0 is the idle state length without generating packets and $\sum_{l=0}^{L_0-1} Q_l = L_0 Q_0$.

Similarly, the packet copying state is

$$\sum_{l=0}^{L_1-1} H_l = L_1 H_0 = \frac{L_1(1-\eta)}{\eta} Q_0 \,, \tag{3.19}$$

where L_1 is the packet copying delay between the microcontroller and the radio transceiver. Note that Equations (3.15)–(3.19) give the state values $b_{i,k,j}$ as a function of $b_{0,0,0}$. By replacing Equations (3.15)–(3.19) in the normalization condition given by Equation (3.14), we obtain the expression for the stationary probability $b_{0,0,0}$.

$$b_{0,0,0} = \begin{cases} \left[\frac{1}{2}\left(\frac{1-(2x)^{m+1}}{1-2x}W_0 + \frac{1-x^{m+1}}{1-x}\right) y_\Sigma + (1-\alpha)C_1 \right. \\ \left. +(L_s(1-\gamma)+L_c\gamma)C_2 + \left(\frac{L_0\eta}{1-\eta}+L_1\right)C_3\right]^{-1} \\ \qquad\qquad\qquad\qquad \text{if} \quad m \le m_b - m_0 \\ \left[\frac{1}{2}\left(\frac{1-(2x)^{m_b-m_0+1}}{1-2x}W_0 + \frac{1-x^{m_b-m_0+1}}{1-x} + (2^{m_b}+1)\right.\right. \\ \left.\left. \times x^{m_b-m_0+1}\frac{1-x^{m-m_b+m_0}}{1-x}\right) y_\Sigma + (1-\alpha)C_1 \right. \\ \left. +(L_s(1-\gamma)+L_c\gamma)C_2 + \left(\frac{L_0\eta}{1-\eta}+L_1\right)C_3\right]^{-1} \\ \qquad\qquad\qquad\qquad \text{otherwise,} \end{cases} \tag{3.20}$$

where $C_1 = (1-x^{m+1})/(1-x)y_\Sigma$, $C_2 = (1-x^{m+1})y_\Sigma$, $C_3 = ((1-\gamma)(1-x^{m+1}) + x^{m+1})y_\Sigma + \gamma(1-x^{m+1})y^n$, $y_\Sigma = (1-y^{n+1})/(1-y)$, $y = \gamma(1-x^{m+1})$, and γ is the collision probability.

We remark here that the term $b_{0,0,0}$, which plays a key role in the analysis, is different from the corresponding term given in [94] – [98] due to our accurate modeling of the retransmissions, ACK, unsaturated traffic, packet size, and packet copying delay.

We derive the stationary channel access probability τ, namely the probability that a device attempts CCA_1 in a randomly chosen time slot as

$$\tau = \sum_{i=0}^{m}\sum_{j=0}^{n} b_{i,0,j} = \frac{1-x^{m+1}}{1-x}\frac{1-y^{n+1}}{1-y} b_{0,0,0}. \tag{3.21}$$

where $x = \alpha + (1-\alpha)\beta$ and $y = \gamma(1-x^{m+1})$. This probability depends on the probability γ that a transmitted packet encounters a collision, and the busy channel probabilities α and β. These probabilities are derived in the following.

The term γ is the probability that at least one of the $N-1$ remaining devices transmits in the same time slot. If all devices transmit with probability τ, γ is

$$\gamma = 1 - (1-\tau)^{N-1} \,,$$

where N is the number of devices. Similarly to [95], we derive the busy channel probabilities α and β as follows:

$$\alpha = \alpha_{\text{pkt}} + \alpha_{\text{ack}} \,, \tag{3.22}$$

where α_{pkt} is the probability of finding the channel busy during CCA_1 due to data transmission, namely,

$$\alpha_{\text{pkt}} = L(1-(1-\tau)^{N-1})(1-\alpha)(1-\beta) \,,$$

and α_{ack} is the probability of finding the channel busy during CCA_1 due to ACK transmission, which is

$$\alpha_{\text{ack}} = L_{\text{ack}} \frac{N\tau(1-\tau)^{N-1}}{1-(1-\tau)^N}(1-(1-\tau)^{N-1})(1-\alpha)(1-\beta) \,,$$

where L_{ack} is the length of the ACK. By a similar argument, the probability of finding the channel busy during CCA_2 is

$$\beta = \frac{1-(1-\tau)^{N-1}+N\tau(1-\tau)^{N-1}}{2-(1-\tau)^N+N\tau(1-\tau)^{N-1}} \,. \tag{3.23}$$

The carrier sensing probability τ in Equation (3.21) and the busy channel probabilities α in Equation (3.22) and β in Equation (3.23) form a system of non-linear equations, whose solution provides us with the operating point of the Markov chain. From these probabilities then we can derive expressions of the performance indicators. The drawback of such an approach is that there is no closed form expression for these probabilities, and the system of equations that gives τ, α and β must be solved by numerical methods [109]. This can be computationally demanding and in some cases not practical for simple sensor devices. However, sensor devices can estimate the busy channel probabilities α and β and the channel sensing probability τ, by exploiting local measurements rather than solving nonlinear equations. In the following, we present accurate and approximate analytical expressions of the performance indicators. The approximate model is used in combination with estimates of α, β, and τ to optimize the IEEE 802.15.4 MAC parameters by an in-network processing of the nodes.

3.3 Performance Indicators

In this section, we derive precise and approximate expressions of the protocol performance indicators, namely reliability, delay for successful packet delivery, and energy consumption.

3.3.1 Reliability

In the slotted CSMA/CA, packets are unsuccessfully received due to two reasons: channel access failure and retry limits. Channel access failure happens when a

packet fails to obtain idle channel in two consecutive CCAs within $m+1$ backoffs. Furthermore, a packet is discarded if the transmission fails due to repeated collisions after $n+1$ attempts. Following the Markov chain in Figure 3.2, the probability that the packet is discarded due to channel access failure is

$$p_{cf} = x^{m+1} \sum_{j=0}^{n} y^j = x^{m+1} \frac{1-y^{n+1}}{1-y} \,. \tag{3.24}$$

The probability of a packet being discarded due to retry limits is

$$p_{cr} = y^{n+1} \,. \tag{3.25}$$

Therefore, the reliability is

$$R = 1 - x^{m+1} \frac{1-y^{n+1}}{1-y} - y^{n+1} \,, \tag{3.26}$$

where $x = \alpha + (1-\alpha)\beta$ and $y = \gamma(1-x^{m+1})$. An approximate expression of the reliability is provided in the following.

Approximation 3.3.1. *Assume $x, y \ll 1$. The reliability can be approximated by*

$$\widetilde{R} = 1 - x^{m+1}(1+\widetilde{y}) - \widetilde{y}^{n+1} \tag{3.27}$$

where

$$\begin{aligned}
\widetilde{y} =& (1-(1-(1+x)(1+\hat{y})\widetilde{b}_{0,0,0})^{N-1})(1-x^2) \,, \\
\widetilde{b}_{0,0,0} =& 2[(W_0(1+2x)(1+\hat{y}) + 2L_s(1-x^2)(1+\hat{y}) \\
& + (L_0\eta/(1-\eta) + L_1)\,(1+\hat{y}^2+\hat{y}^{n+1})]^{-1} \,, \\
\hat{y} =& (1-(1-\tau)^{N-1})(1-x^2) \,.
\end{aligned}$$

Derivation: The key idea is to consider a first-order approximation

$$\sum_{i=0}^{m+1} z^i \approx 1+z \,, \qquad \text{if} \quad z \ll 1 \,.$$

and apply it to the terms in Equations (3.15)–(3.19). A step-by-step derivation is reported in Appendix A.1. □

We remark that $\widetilde{R}$ is a function of the measurable busy channel probabilities α and β, the channel access probability τ and the MAC parameters m_0, m_b, m, n.

3.3.2 Delay

We compute average delay and delay distribution for successfully received packets. Note that we do not consider queueing delay because a packet is generated only

after the previous packet is successfully received or discarded. In Chapter 4, we compute the MAC queueing delay for a different traffic generation pattern. The delay for a successfully received packet is defined as the time interval from the instant the packet is ready to be transmitted, until an ACK for such a packet is received. If a packet is dropped due to either the limited backoffs m or the finite retry limit n, its delay is not included into the average delay.

Let D_j be the random time associated with the successful transmission of a packet at the j-th backoff stage. Denote with $\mathscr{C}_j$ the event of a successful transmission at time $j+1$ after j events of unsuccessful transmission. Let $\mathscr{C}$ be the event of successful transmission within the total attempts n. Then, the delay for a successful transmission after j unsuccessful attempts is

$$D = \sum_{j=0}^{n} \mathbb{1}_{\mathscr{C}_j|\mathscr{C}}\, D_j\,,$$

where $\mathbb{1}_{\mathscr{C}_j|\mathscr{C}}$ is 1 if $\mathscr{C}_j|\mathscr{C}$ holds, and 0 otherwise and $D_j = T_s + j\,T_c + \sum_{h=0}^{j} t_h$, with t_h being the backoff stage delay, $T_s = L_s S_b$ is the packet successful transmission time, and $T_c = L_c S_b$ is the packet collision transmission time. Recall that L_s and L_c are defined in Equation (3.1), and S_b is the time unit *aUnitBackoffPeriod*.

A transmission is successful with probability $1-\gamma$, or collide with probability γ. Then, the probability of the event $\mathscr{C}_j|\mathscr{C}$ is

$$\Pr(\mathscr{C}_j|\mathscr{C}) = \frac{\gamma^j(1-x^{m+1})^j}{\sum\limits_{k=0}^{n}\left(\gamma(1-x^{m+1})\right)^k} = \frac{(1-y)\,y^j}{1-y^{n+1}}\,. \tag{3.28}$$

where the normalization comes by considering all the possible events of successful attempts $\mathscr{C}$. Note that $(1-x^{m+1})$ is the probability of successful channel access within the maximum number of m backoff stages. By following a similar approach as the one for the characterization of D, we see that the total backoff delay t_h is modeled by

$$t_h = \sum_{i=0}^{m} \mathbb{1}_{\mathscr{D}_i|\mathscr{D}}\, t_{h,i}\,,$$

where

$$t_{h,i} = 2\,t_{sc} + \sum_{k=1}^{i} t_{h,k}^{sc} + \sum_{k=0}^{i} t_{h,k}^{b}\,, \tag{3.29}$$

and where $2t_{sc}$ is the successful sensing time, $\sum_{k=1}^{i} t_{h,k}^{sc}$ is the unsuccessful sensing time due to busy channel during CCA, and $\sum_{k=0}^{i} t_{h,k}^{b}$ is the backoff time. The event $\mathscr{D}_i$ denotes the occurrence of a busy channel for i-th times, and then of idle channel at the $i+1$th time. By considering all the possibilities of busy channel

during two CCAs, the probability of $\mathscr{D}_i$ is conditioned on the successful sensing event within m attempts $\mathscr{D}$, given that the node senses an idle channel in CCA. It follows that

$$\Pr(\mathscr{D}_i|\mathscr{D}) = \frac{\sum_{k=1}^{2^i} C_{\alpha\beta}^k(i)}{\sum_{k=0}^{m} C_{\alpha\beta}(k)},$$

where $C_{\alpha\beta}(i)$ gives all possibilities of choosing i elements from a set of busy channel probabilities $\{\alpha, (1-\alpha)\beta\}$ and $C_{\alpha\beta}^k(i)$ is one of the elements in the set $C_{\alpha\beta}(i)$. Hence, the total number of combinations for i elements is equal to 2^i and $C_{\alpha\beta}^k(i)$ returns one combination out of 2^i. The unsuccessful sensing time $\sum_{k=1}^{i} t_{h,k}^{sc}$ in Equation (3.29) is related to the selection of i elements in the set $C_{\alpha\beta}(i)$. For instance, the combination (α, α) returns the unsuccessful sensing delay $t_{sc} + t_{sc}$ and the combination $(\alpha, (1-\alpha)\beta)$ gives the unsuccessful sensing delay $t_{sc} + 2t_{sc}$. Furthermore, the backoff time $t_{h,k}^b$ of k unsuccessful sensing tries is uniformly distributed in $[0, W_k - 1]$.

Therefore we can derive the expected value of the delay as

$$\mathbb{E}[D] = \sum_{j=0}^{n} \Pr[\mathscr{C}_j|\mathscr{C}] \left(T_s + j\, T_c + \sum_{h=0}^{j} \mathbb{E}[t_h] \right), \tag{3.30}$$

where

$$\begin{aligned}\mathbb{E}[t_h] =& 2t_{sc} + \sum_{k=0}^{m} \Pr(\mathscr{D}_i|\mathscr{D}) \sum_{k=0}^{i} \frac{W_k - 1}{2} S_b \\ &+ \frac{t_{sc}}{\sum_{k=0}^{m} C_{\alpha\beta}(k)} \sum_{i=0}^{m} \sum_{k=1}^{2^i} C_{\alpha\beta}^k(i)(N_\alpha^k(i) + 2\, N_{\hat{\beta}}^k(i)),\end{aligned}$$

and $N_\alpha^k(i)$, $N_{\hat{\beta}}^k(i)$ return the number of α and $(1-\alpha)\beta$ of the combination $C_{\alpha\beta}^k(i)$, respectively.

The probability distribution of the delay can be derived from the Markov chain by using the probability generating function (PGF) $D(Z)$, as we summarize in the following.

Proposition 3.3.2. *The PGF of the packet delay for successfully received packet $D(Z)$ is*

$$D(Z) = Z^{T_s} \sum_{j=0}^{n} \Pr(\mathcal{C}_j|\mathcal{C}) Z^{jT_c + 2(j+1)} \left(\sum_{i=0}^{m} \frac{G_i(Z) H_i(Z)}{\sum_{k=0}^{m} C_{\alpha\beta}(k)} \right)^{j+1}, \tag{3.31}$$

where

$$G_i(Z) = \sum_{k=1}^{2^i} C_{\alpha\beta}^k(i) Z^{N_\alpha^k(i)+2N_\beta^k(i)} \tag{3.32}$$

$$H_i(Z) = \prod_{k=0}^{i} \begin{cases} \frac{1-Z^{2^i W_0}}{2^i W_0(1-Z)} & \text{if } i \leq m_b - m_0 \\ \frac{1-Z^{2^{m_b}}}{2^{m_b}(1-Z)} & \text{otherwise} \end{cases} .$$

Proof. The PGF is derived by considering the generalized state transition diagram related to the Markov chain, in which the transition time is expressed as an exponent of a Z variable in each branch. A detailed derivation is reported in Appendix A.2 □

We recall that the moments of any order and degree can be obtained by the derivation of $D(Z)$. For example, the mean and variance of D are

$$\mathbb{E}[D] = D^{'}(1) \tag{3.33}$$

$$\mathbb{E}[(D - \mathbb{E}[D])^2] = D^{''}(1) + D^{'}(1) - \{D^{'}(1)\}^2 , \tag{3.34}$$

where $'$ indicates the derivative with respect to Z.

In the following, we derive an approximation of the average delay.

Approximation 3.3.3. *The average delay for successfully received packets is approximated by*

$$\widetilde{D} = T_s + \mathbb{E}[\widetilde{t}_h] + \left(\frac{y}{1-y} - \frac{(n+1)y^{n+1}}{1-y^{n+1}} \right) (T_c + \mathbb{E}[\widetilde{t}_h]) , \tag{3.35}$$

where

$$\mathbb{E}[\widetilde{t}_h] = 2S_b \left(1 + \frac{1}{4} \left(\frac{1-\xi}{1-\xi^{m+1}} \left(2W_0 \frac{1-(2\xi)^{m+1}}{1-2\xi} - \frac{3(m+1)\xi^{m+1}}{1-\xi} \right) + \frac{3\xi}{1-\xi} - (W_0+1) \right) \right) ,$$

and $\xi = \max(\alpha, (1-\alpha)\beta)$.

Derivation: The derivation is reported in Appendix A.3. □

3.3.3 Energy Consumption

Here, we derive the energy consumption of the devices in the network. We consider two operational modes depending on the radio state during the backoff mechanism. Let us denote by *I-mode* and *S-mode* the situations where the radio during the

backoff period is set to idle mode or to sleep mode, respectively. By considering the Markov chain model given in Figure 3.2, the average energy consumption is given as follow

$$\begin{aligned} E_{\text{tot}} =& P_b \sum_{i=0}^{m} \sum_{k=1}^{W_i-1} \sum_{j=0}^{n} b_{i,k,j} + P_{sc} \sum_{i=0}^{m} \sum_{j=0}^{n} (b_{i,0,j} + b_{i,-1,j}) + P_t \sum_{j=0}^{n} \sum_{k=0}^{L-1} (b_{-1,k,j} \\ &+ b_{-2,k,j}) + P_i \sum_{j=0}^{n} (b_{-1,L,j} + b_{-2,L,j}) + \sum_{j=0}^{n} \sum_{k=L+1}^{L+L_{\text{ack}}+1} (P_r\, b_{-1,k,j} \\ &+ P_i\, b_{-2,k,j}) + P_{sp} \sum_{l=0}^{L_0-1} Q_l + P_{sp} \sum_{l=0}^{L_1-2} H_l + P_w H_{L_1-1}\,, \end{aligned} \tag{3.36}$$

where $P_b, P_{sc}, P_t, P_r, P_w$ and P_{sp} are the average energy consumption in backoff, channel sensing, transmit, receive, wake-up, and sleep states, respectively. In Equation (3.36), the first term takes into account the energy consumption during backoff state. The second term takes into account the energy consumption during the channel sensing state. The third, fourth and fifth terms consider the energy consumption of packet transmission stage. The sixth and seventh term represent the energy consumption of idle stage and packet copying stage. The last term consider wake-up consumption after packet generation. By substituting Equations (3.15)–(3.19) to Equation (3.36), we obtain the average energy consumption in closed form. In the derivation, we replace $P_b = P_i$ in *I-mode* and $P_b = P_s$ in *S-mode*. Then, the following approximate expressions hold.

Approximation 3.3.4. *The energy consumption of the I-mode is approximated by*

$$\begin{aligned} \widetilde{E}_{\text{tot},i} =& \frac{P_i \tau}{2} \left[\frac{(1-x)(1-(2x)^{m+1})}{(1-2x)(1-x^{m+1})} W_0 - 1 \right] + P_{sc}(2-\alpha)\tau + C_4 \\ &+ P_w \left(x^{m+1}(1+y) \; + (\gamma y^n + (1-\gamma)(1+y))(1-x^2) \right) \widetilde{b}_{0,0,0} \end{aligned} \tag{3.37}$$

and of the S-mode is approximated by

$$\begin{aligned} \widetilde{E}_{\text{tot},s} =& P_w \left(\tau - \frac{\widetilde{b}_{0,0,0}(1-(0.5x)^{m+1})}{W_0(1-0.5x)} \frac{1-y^{n+1}}{1-y} \right) + P_{sc}(2-\alpha)\tau \\ &+ (1-\alpha)(1-\beta)\tau \left(P_t L + P_i + L_{\text{ack}} \left(P_r(1-\gamma) + P_i \gamma \right) \right). \end{aligned} \tag{3.38}$$

Derivation: See Appendix A.4. □

3.4 IEEE 802.15.4 Optimization

In this section, we propose an adaptive tuning algorithm of the IEEE 802.15.4 MAC parameters for reliable and timely communication while minimizing the energy

consumption. The protocol is adjusted dynamically by a constrained optimization problem that each device of the network solves. The constrained optimization problem for a generic transmitting device in the network is formulated as

$$\underset{\mathbf{V}}{\text{minimize}} \quad \widetilde{E}_{\text{tot}}(\mathbf{V}) \tag{3.39a}$$

$$\text{subject to} \quad \widetilde{R}(\mathbf{V}) \geq R_{\min}\,, \tag{3.39b}$$

$$\widetilde{D}(\mathbf{V}) \leq D_{\max}\,, \tag{3.39c}$$

$$\mathbf{V}_0 \leq \mathbf{V} \leq \mathbf{V}_m\,. \tag{3.39d}$$

The objective function is the energy consumption $\widetilde{E}_{\text{tot}}$ derived in Equation (3.37) for the *I-mode* and Equation (3.37) for the *S-mode*, $\widetilde{R}(\mathbf{V})$ is the reliability evaluated in Equation (3.27), and $R_{\min}$ is the minimum desired probability for successful packet delivery. $\widetilde{D}(\mathbf{V})$ is the average delay for a successfully received packet in Equation (3.35) , and $D_{\max}$ is the desired maximum average delay. The decision variables are $\mathbf{V} = (m_0, m, n)$, where m_0 is the minimum value of the backoff exponent, m is the number of backoffs allowed before declaring a channel access failure, and n is the maximum number of retries allowed after a transmission failure. The constraint $\mathbf{V}_0 \leq \mathbf{V} \leq \mathbf{V}_m$ captures the limited range of the MAC parameters. The solution of the optimization problem gives the optimal MAC parameter (m_0, m, n) that each device uses to minimize its energy expenditure, subject to reliability and delay constraints. The problem is combinatorial because the decision variables take on discrete values.

In a practical implementation, the optimal solution (m_0, m, n) of Problem (3.39) can be computed off-line and stored in a look-up table as a function of the busy channel probabilities α and β and the channel access probability τ. The table can be thought of as a matrix with the set of values of α, β, τ. Each device can estimate α, β, τ, and read from the look-up table the entries of the solutions at location α, β, τ closer to the estimated values. Then, the device uses (m_0, m, n) corresponding to the entry of the look-up table. Note that the size of the matrix can be significantly reduced by using a lossless data compression [110].

We have seen by the Approximations 3.3.1, 3.3.3 and 3.3.4 that the performance metrics are function of the busy channel probabilities α and β and the channel access probability τ. Once these probabilities are known at a device, the optimal MAC parameters can be computed readily. In the algorithm, the number of devices and packet generation rates are assumed to be known, whereas the busy channel probability and channel access probability are periodically estimated in each device during the sensing states of the MAC layer, and they do not require an ACK mechanism, as we describe the details in the following.

The average busy channel probabilities α and β are estimated at each device while sending a data packet to the coordinator. These probabilities are initialized at the beginning of the device's operation. The estimations of the busy channel probabilities and the channel access probability use a sliding window. When the

device senses the channel at CCA_1 or CCA_2, these probabilities are updated by $\alpha = r\alpha + (1-r)\hat{\alpha}, \beta = r\beta + (1-r)\hat{\beta}$ for some $r \in (0,1)$, respectively. Note that $\hat{\alpha}$ and $\hat{\beta}$ are the busy channel probability of CCA_1 and CCA_2 of the current sliding window, respectively. Therefore, a device does not require any extra communication and sensing state to estimate these probabilities compared to the IEEE 802.15.4 standard. By contrast, the estimation algorithms for IEEE 802.11 proposed in [100] and [91] are not energy efficient since a device needs to sense the channel state during the backoff stage. This allows one to estimate the average length of idle period. Hence, these schemes are implementable only in *I-mode*. By contrast, our scheme is applied in both *I-mode* and *S-mode* and does not require any computation load during the backoff stage. During an initialization phase of the algorithm, a device communicates with the initial MAC parameters $m_0 = 3, m_b = 8, m = 4, n = 1$. Then, the busy channel probabilities α and β and the channel access probability τ are estimated in each device during the channel sensing state of IEEE 802.15.4 without any extra state. The application requirements are communicated by the coordinator to the device if there are changes. It is also possible that each device makes a decision of application requirements depending on the data type e.g., strict delay requirement for alarm message. The robustness of the algorithm to possible errors in the estimation of the number of devices and traffic load is investigated in [21].

3.5 Experimental Evaluation

In the following, we present an extensive set of real-world experiments and Monte Carlo simulations to validate the model and show the implementation of the adaptive algorithm for tuning the MAC parameters. The IEEE 802.15.4 protocol was implemented on a test-bed using the TelosB platform [111] running the Contiki OS [112] based on the specifications of the IEEE 802.15.4 [7]. The IEEE 802.15.4 defines one backoff as 20 symbols that correspond to $320\,\mu s$ for 2.45 GHz. Since the hardware timer available for TelosB is based on a 32768 Hz clock, we use a backoff with duration of $305\,\mu s$ instead of $320\,\mu s$.

3.5.1 Model Validation

We have implemented the IEEE 802.15.4 protocol to assess our analysis of the approximated model of the reliability by experimental results, which are reported in Figure 3.3. Figure 3.3 compares the reliability given by Equation (3.27), the analytical model in [95], and experimental results as a function of the traffic regime, through the idle probabilities $\eta = 0.3, 0.5, 0.7$ with $N = 10$ devices and different MAC parameters m_0, m, n. The vertical bars indicate the standard deviation as obtained out of 5 experimental runs of 2×10^5 time slots each. In the figure, note that "Pollin" refers to the reliability model derived in [95]. Our analytical expression matches quite well the experimental results. Note that the percentage error of the

reliability given by Equation (3.27) is 0.993%. The expression is closer to experimental results under low traffic regime $\eta = 0.5, 0.7$ than high traffic regime $\eta = 0.3$ because the approximation given by Equation (A.1) holds if $x = \alpha + (1-\alpha)\beta \ll 1$, but x increases as the traffic and the number of devices increase. The reliability approaches 1 under very low traffic regime $\eta = 0.7$. In Figure 3.3(a), 3.3(b), the reliability increases as MAC parameters m_0, m increase, respectively. In Figure 3.3(c), we observe that the improvement of reliability is small as the retry limits n increases for $n \geq 3$. Notice that the reliability saturates to 0.92 for traffic regime $\eta = 0.3$ for $n \geq 3$. Hence, the retransmissions are necessary but not sufficient to obtain high reliability under high traffic regimes.

Figure 3.4 shows the average delay as obtained by Equation (3.35) as a function of different idle probabilities $\eta = 0.3, 0.5, 0.7$ with a given number of devices $N = 10$ and different MAC parameters m_0, m, n. The vertical bars indicate the standard deviation as obtained out of 5 experimental runs of 2×10^5 time slots each. The analytical model predicts well the experimental results. Note that the percentage error of the average delay given by Equation (3.35) is 3.155%. The accuracy is reduced under high traffic regime $\eta = 0.3$ due to the approximation given by Equation (A.1). Observe that the average delay increases as traffic regime increases due to high busy channel probability and collision probability. Figure 3.4(a) shows that the average delay increases exponentially as m_0 increases. Hence, we conclude that m_0 is the key parameter affecting the average delay when compared to m, n.

Figure 3.5 shows the probability distribution of the delay D as a function of different number of nodes $N = 10, 30$ and $m_b = 5, 8$ with given $m_0 = 3$, $m = 4$, $n = 3$ and a fixed length of packet $L = 70$ bytes. We observe that the analytical probability distribution predicts well the experimental results. The low traffic $\eta = 0.9$ gives a distribution similar to a deterministic one. This is due to that the collision probability is lower as traffic decreases and most of packets are successfully transmitted at the first backoff stage without channel sensing fails or retransmissions. The saturated traffic $\eta = 0$ results in a heavy tail of the delay distribution due to the high interference in the network. Figures 3.5(a), 3.5(b) show the effect of the number of nodes in terms of the delay. It is interesting to observe that as the number of nodes increases the side lobe increases. This is due to that as the traffic and number of nodes increase, the busy channel probability α, β and the collision probability γ are also increasing.

By comparing Figures 3.5(a), 3.5(b) to 3.5(c), 3.5(d), we observe that $m_b = 8$ gives a longer tail than $m_b = 5$. The probability of delay larger than 50 ms is almost zero for $m_b = 5$ while the probability of delay larger than 50 ms is still nonzero for $m_b = 8$. Hence, the tail for $m_b = 8$ is much longer than the distribution for $m_b = 5$. The random backoff time increases as increasing m_b. As the traffic, number of nodes and m_b increase, the probability distribution has a longer tail, i.e., a higher average and variance. We remark that the probability distribution of the delay is significantly different from the existing network models used for networked control system design such as Poisson distribution and exponential distribution [48, 113].

Figure 3.6 compares our proposed analytical model and experimental results for

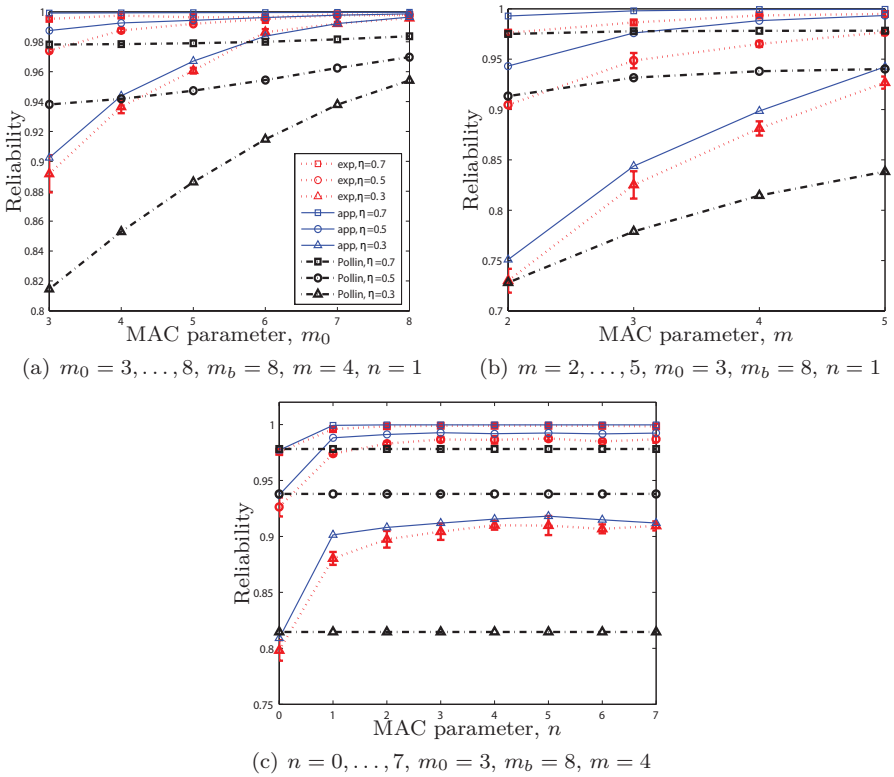

(a) $m_0 = 3, \ldots, 8$, $m_b = 8$, $m = 4$, $n = 1$

(b) $m = 2, \ldots, 5$, $m_0 = 3$, $m_b = 8$, $n = 1$

(c) $n = 0, \ldots, 7$, $m_0 = 3$, $m_b = 8$, $m = 4$

Figure 3.3: Reliability as a function of the idle probabilities $\eta = 0.3, 0.5, 0.7$, and MAC parameters $m_0 = 3, \ldots, 8$, $m_b = 8$, $m = 2, \ldots, 5$, $n = 0, \ldots, 7$ as obtained by our proposed analysis, experimental implementation, and with Pollin's Markov chain model [95]. The length of the packet is $L = 5$ and the number of devices is $N = 10$. The vertical bars indicate the standard deviation as obtained out of 5 experimental runs of 2×10^5 time slots each. The percentage error of the analytical model for the reliability is 0.993%.

the power consumption for both *I-mode* and *S-mode* as a function of different idle probabilities $\eta = 0.3, 0.5, 0.7$ with a number of devices $N = 10$ and different MAC parameters m_0, m, n. The vertical bars indicate the standard deviation as obtained out of 5 experimental runs of 2×10^5 time slots each. The percentage errors of the average power consumption for *I-mode* given by Equation (3.37) and *S-mode* given by Equation (3.38) are 0.193% and 0.175%, respectively. The power consumption of *S-mode* and *I-mode* decreases as m_0 increases because of sleep mode and idle mode during the backoff time for high traffic regime $\eta = 0.3, 0.5$. The main component of the average power consumption is the transmit or receiving power rather than power

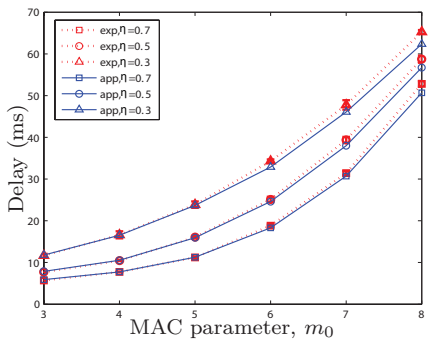

(a) $m_0 = 3, \ldots, 8$, $m_b = 8$, $m = 4$, $n = 1$

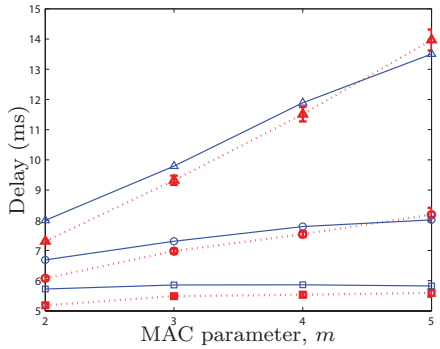

(b) $m = 2, \ldots, 5$, $m_0 = 3$, $m_b = 8$, $n = 1$

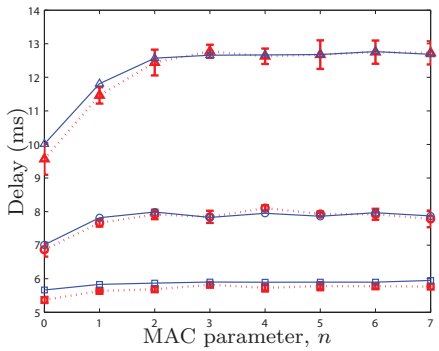

(c) $n = 0, \ldots, 7$, $m_0 = 3$, $m_b = 8$, $m = 4$

Figure 3.4: Average delay as a function of the idle probabilities $\eta = 0.3, 0.5, 0.7$ and MAC parameters $m_0 = 3, \ldots, 8$, $m_b = 8$, $m = 2, \ldots, 5$, $n = 0, \ldots, 7$ as obtained by our proposed analysis and experimental implementation. The length of the packet is $L = 5$ and the number of devices is $N = 10$. The percentage error of the analytical model for the average delay is 3.155%.

consumption during backoff time for high traffic regime. However, the power consumption of *I-mode* increases as the MAC parameters (m_0, m, n) increase under low traffic regime $\eta = 0.7$. Since the device needs to stay more time in idle sleep stage without packet generation, the main component of average power consumption is the idle backoff time rather than transmit or receiving power consumption under low traffic regime $\eta = 0.7$. It is interesting to observe that the power consumption has a weaker dependence on m and n than on m_0.

3.5.2 IEEE 802.15.4 MAC Adaptation

Figure 3.7 compares the experimental results for the reliability, average delay, and power gain values of the IEEE 802.15.4 MAC protocol as obtained by our algorithm

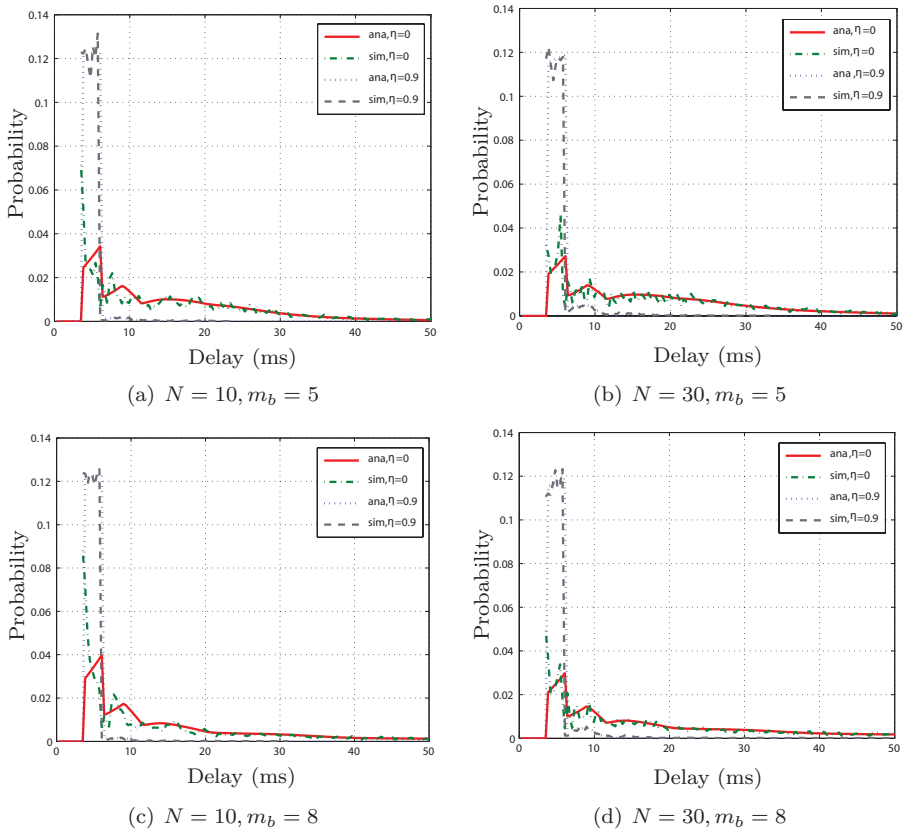

Figure 3.5: Probability distribution of the delay for successfully received packets as a function of different number of nodes $N = 10, 30$ and $m_b = 5, 8$ with given $m_0 = 3$, $m = 4$, $n = 3$ and $L = 7$.

and with default MAC parameters. The vertical bars indicate the standard deviation as obtained out of 5 experimental runs of 5×10^5 time slots each. Both the *I-mode* and *S-mode* for various traffic configurations and requirements are considered. The requirements for both the *I-mode* and *S-mode* are $R_{\min} = 0.9, 0.95, D_{\max} = 50$ and $R_{\min} = 0.95, D_{\max} = 20, 100\,\text{ms}$, respectively. Figure 3.7(a) shows that both *I-mode* and *S-mode* satisfy the reliability constraint for different traffic regime. We observe a strong dependence of the reliability of default MAC on different traffic regime. At the high traffic regime $\eta = 0.2$, the reliability of default MAC is 0.89. In Figure 3.7(b), the delay constraint is fulfilled both *I-mode* and *S-mode*. Observe that average delay of *I-mode* decreases when traffic regime is low, $\eta \geq 0.4$. This is due to that the optimal MAC parameters at higher traffic regime increase more than the ones at lower traffic regime to satisfy the reliability constraint.

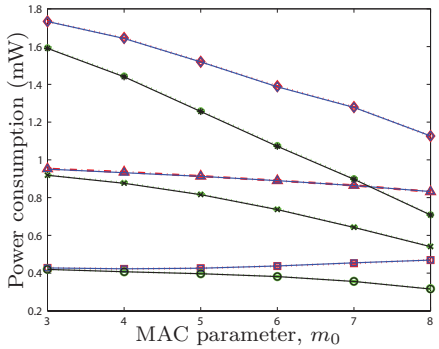

(a) $m_0 = 3, \ldots, 8$, $m_b = 8$, $m = 4$, $n = 1$

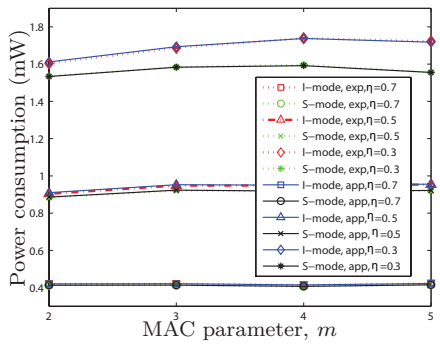

(b) $m = 2, \ldots, 5$, $m_0 = 3$, $m_b = 8$, $n = 1$

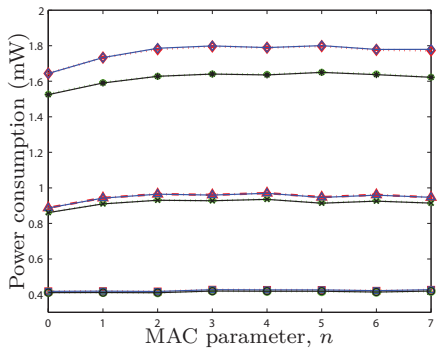

(c) $n = 0, \ldots, 7$, $m_0 = 3$, $m_b = 8$, $m = 4$

Figure 3.6: Average power consumption of *I-mode* and *S-mode* as a function of the idle probabilities $\eta = 0.3, 0.5, 0.7$ and MAC parameters $m_0 = 3, \ldots, 8$, $m_b = 8$, $m = 2, \ldots, 5$, $n = 0, \ldots, 7$ as obtained by our analysis and experimental implementation. The length of the packet is $L = 5$ and the number of devices is $N = 10$. The percentage errors of the analytical model for the average power consumption are 0.193% and 0.175% for *I-mode* and *S-mode*, respectively.

To characterize quantitatively the power consumption, we define the power gain as

$$\rho = \frac{E_{\text{def}} - E_{\text{tot}}}{E_{\text{def}}}$$

where E_{def} and E_{tot} are the average power consumption of *I-mode* or *S-mode* for default MAC and proposed scheme, respectively. The closer ρ to 1, the better the power efficiency. Figure 3.7(c) shows that the power gain increases as traffic regime increases (as η decreases). This improvement is higher for *S-mode* than *I-mode*, e.g., $\rho \approx 0.57$ for *S-mode* with $R_{\min} = 0.95, D_{\max} = 100$. Although there is a strong dependence of the power gain on the traffic regime, our proposed algorithm gives a

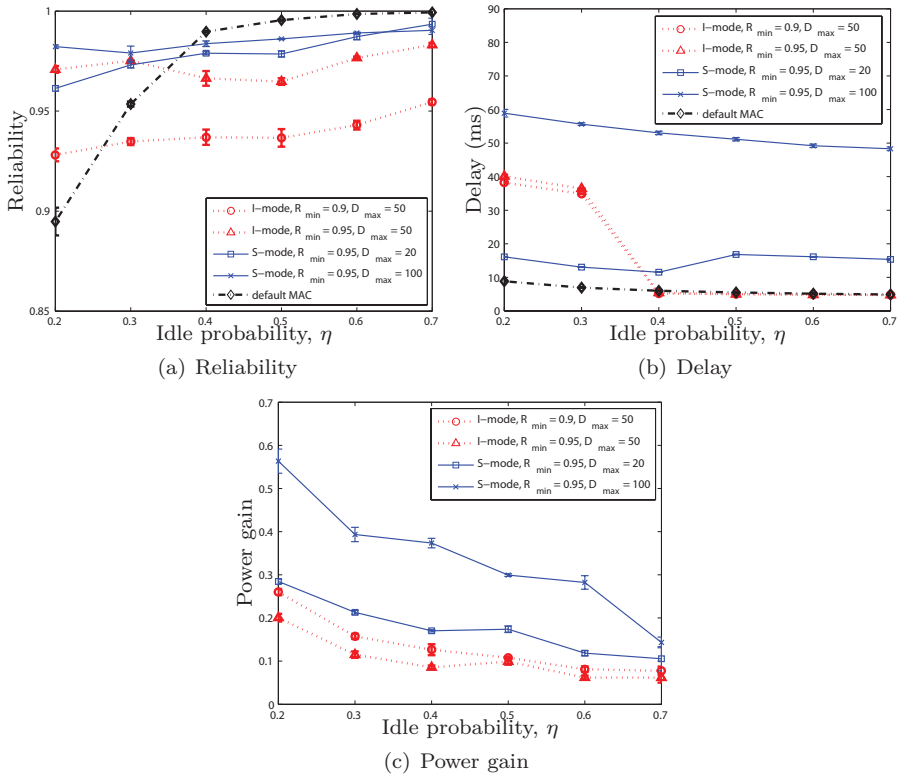

(a) Reliability (b) Delay

(c) Power gain

Figure 3.7: Reliability, delay, and power gain of the *I-mode*, *S-mode* of the proposed scheme and IEEE 802.15.4 with default parameters ($m_0 = 3$, $m_b = 5$, $m = 4$, $n = 3$) as a function of the idle probability $\eta = 0.2, \ldots, 0.7$, the reliability requirement $R_{\min} = 0.9, 0.95$ and delay requirement $D_{\max} = 20, 50, 100$ ms for $L = 5$ and $N = 10$. Note that "default MAC" refers to IEEE 802.15.4 with default parameters. The vertical bars indicate the standard deviation as obtained out of 5 experimental runs of 5×10^5 time slots each.

better energy efficiency than the default MAC. Therefore, the experimental results show the effectiveness of our adaptive IEEE 802.15.4 protocol while guaranteeing the constraints.

We observe a tradeoff between the power consumption, reliability and delay constraints by using the Monte Carlo simulations. Figure 3.8 shows the dependence of the power consumption in *S-mode* with reliability and delay constraints for a given traffic load, length of packets, and number of devices. Observe that as the delay constraint becomes strict the power consumption increases. In other words, the reliability constraint of *S-mode* is less critical than delay constraint. A more extended set of experimental results, which includes transient conditions, robustness

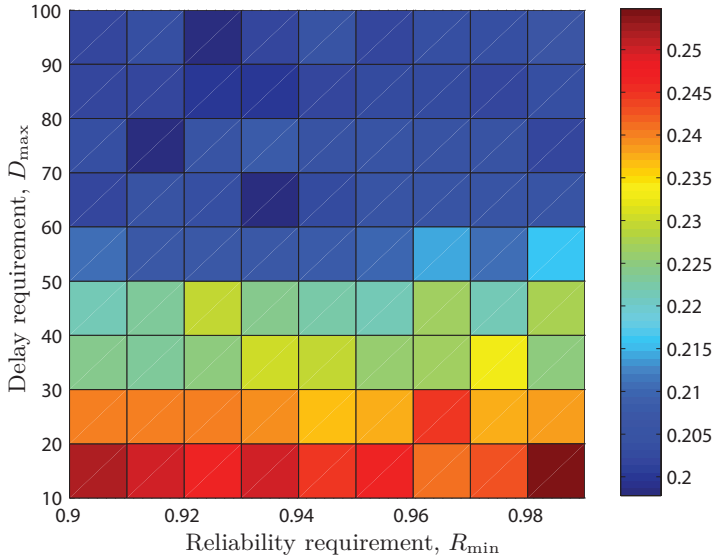

Figure 3.8: Power consumption of *S-mode* as a function of reliability constraint $R_{\min} = 0.9, \ldots, 0.99$ and delay requirement $D_{\max} = 10, \ldots, 100$ ms for $\eta = 0.5$, $L = 3$ and $N = 10$.

and sensitivity analysis is reported in [21]. The objective of the set of results presented here is to show the importance of behavioral models for the adaptation of the protocol to requirements of networked control applications.

3.6 Summary

In this chapter, we reviewed Markov chain models for contention-based MACs and presented a generalized approach to characterize the performance of the slotted CSMA/CA mechanism in the IEEE 802.15.4 standard. Our model considers retry limits, the ACKs, and unsaturated traffic, which are important components of most wireless sensor network applications. We derived expressions of the reliability, delay, and energy consumption offered by the slotted IEEE 802.15.4 MAC by both an accurate and computationally demanding approach, and an approximate and simple approach. We showed that the approximate analysis is effective for low traffic. Furthermore, unlike 802.11, we observed that the delay distribution of IEEE 802.15.4 depends mainly on the MAC parameters and the collision probability. Eventually, we illustrated an adaptive MAC algorithm for minimizing the power consumption while fulfilling reliability and delay requirements of networked control applications. In the following chapter, we extend the model to include the characteristics of multi-hop networks.

Chapter 4

Modeling the MAC and Routing Interactions

Routing information over multi-hop paths is an important networking service for many applications in industrial and environmental monitoring, urban mobility, building automation, etc. [12]. To understand the fundamental performance limitations of IEEE 802.15.4 networks and suggest appropriate routing strategies, an accurate analytical model of the MAC and routing interactions in multi-hop topologies is instrumental.

In this chapter, we propose an analytical study that considers jointly MAC and routing, and we highlight the interdependence between routing decisions and end-to-end performance indicators. Recalling the general flow diagram in Figure 4.1, we consider the loop between MAC and routing, with no explicit dependance on the wireless channel conditions. We provide an accurate model for small-scale networks and an approximate model that yields effective analysis of the performance for large-scale networks. As a major extension of the model presented in Chapter 3, we consider a model of the MAC with heterogeneous traffic conditions and presence of hidden terminals. This is critical in at least three important situations:

1. In single-hop networks, nodes may have different traffic generation rates as a result of different services they provide, such as control applications with varying sampling rates.

2. In multi-hop networks, the traffic load varies according to the routing along the paths. Some nodes may experience a heavier cross traffic, thus transmitting more packets, than nodes that are traversed by fewer routing paths. It follows that the traffic is not homogeneous, regardless that nodes generate their own packets at the same rate.

3. In networks with hidden terminals, the traffic sensed by the nodes is different from node to node, even when every node generates the same traffic. This is due to that some nodes may not perceive the ongoing transmissions of other nodes.

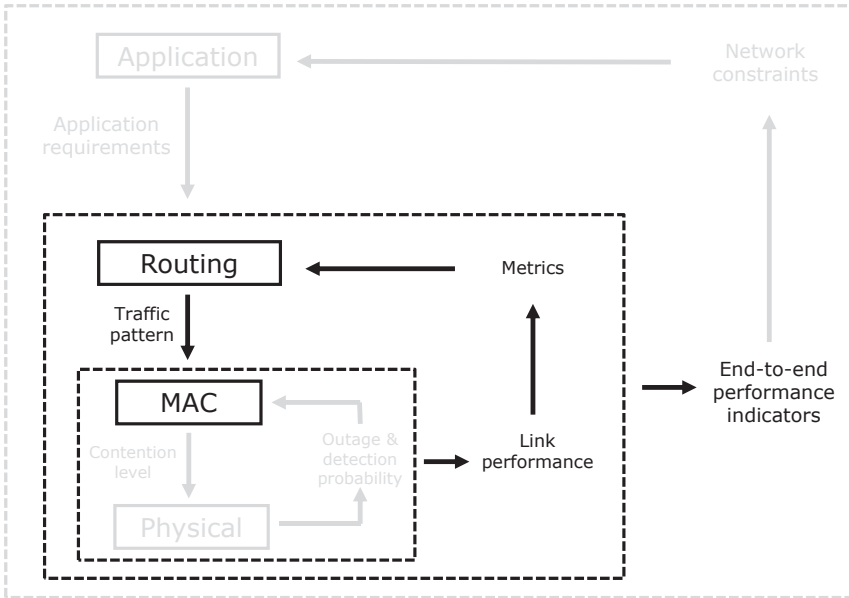

Figure 4.1: Interaction of layers for modeling and design: MAC and routing layers.

In the situations mentioned above, previous analytical studies of the IEEE 802.15.4 MAC are not adequate.

In the following, we attempt to propose a comprehensive analysis that explores the aforementioned aspects. We show how the IEEE 802.15.4 MAC can influence remarkably the routing alternatives. Then, we study different performance indicators of IEEE 802.15.4 MAC over multi-hop networks, namely end-to-end reliability, end-to-end delay, and energy consumption. We include the routing specifications of the IETF RPL [12]. A metric that guides the interaction between MAC and routing is proposed and compared to existing metrics. Moreover, a protocol selection mechanism is implemented to optimally select the routing metric and MAC parameters given specific performance requirements.

The remainder of the chapter is organized as follows. In Section 4.1, the related work and the original contribution are summarized. In Section 4.2, we introduce the system model. In Section 4.3, we derive the analytical model of IEEE 802.15.4 MAC for multi-hop networks with heterogeneous traffic and hidden terminals. Section 4.4 illustrates the integration between MAC and routing models. Simulation results and experiments are shown in Section 4.5. A brief summary concludes the chapter. The limitations of the Markov chain model are discussed in Appendix C. A list of symbols and acronyms is reported in Appendix F.

4.1 Related Work

There have been recent efforts to cover some of the aspects of multi-hop heterogeneous networks for IEEE 802.11 and IEEE 802.15.4 networks. Studies for single-hop networks with heterogenous traffic can be found in [114] – [116], where traffic classes are considered, but no hidden terminals. The effects of hidden terminals in homogeneous single-hop networks have been studied in [117, 118]. In [119], multi-hop communication is modeled for IEEE 802.11 networks under single traffic flow. In [120], the work of [119] has been extended to multiple non-saturated flows. In [121] a model for saturated traffic flows in IEEE 802.11 networks is presented. However, we note that these models cannot be directly applied to IEEE 802.15.4 networks due to the different access mechanism of IEEE 802.11 MAC. In [122], a Markov chain model is presented for multi-hop IEEE 802.15.4 networks, but the model is limited to nodes that communicate to the coordinator through an intermediate relay node, which is assumed as not generating traffic and not competing for channel access.

On the routing side, an experimental performance evaluation of RPL that uses the hop count metric and the ETX metric is presented in [123]. However, the study does not consider explicitly the combined effect of a contention-based MAC protocol and the routing metrics. The importance of considering MAC costs in the routing decisions was raised in [124]. A study on the interaction of RPL with the MAC layer is presented in [125], where the authors investigate the use of a receiver-initiated MAC protocol in enhancing the performance of RPL. However, it is not immediate to derive similar analysis for the IEEE 802.15.4 standard.

4.2 System Model

Consider a network of N nodes, $V_0, ..., V_N$, that use the unslotted IEEE 802.15.4 MAC. We focus on this MAC modality because it is common and relevant for the RPL standardization [12][1]. In the following, we illustrate the system model by considering three topologies, as reported in Figure 4.2. However, the analytical results that we derive are general and not limited to a specific topology.

The topology in Figure 4.2(a) refers to a single-hop (star) network where nodes forward their packets with single-hop communication to the root node V_0. In star networks, we denote by l the link between V_l and V_0, $l = 1, \ldots, N$. The topologies in Figures 4.2(b) and 4.2(c) are examples of multi-hop networks in which nodes forward traffic according to the uplink routing policy to V_0. In multi-hop networks, we label by l, $l = 1, \ldots, G$ the link between a pair of communicating nodes, where G is the number of such pairs.

For every node V_i, we define a *neighborhood* set Ω_i, which contains all the nodes in the carrier sensing range of V_i (delimited by dash-dotted lines in the examples

[1]The model derivation for the slotted mechanism follows similar steps as those presented in this chapter, without a significant increase of complexity.

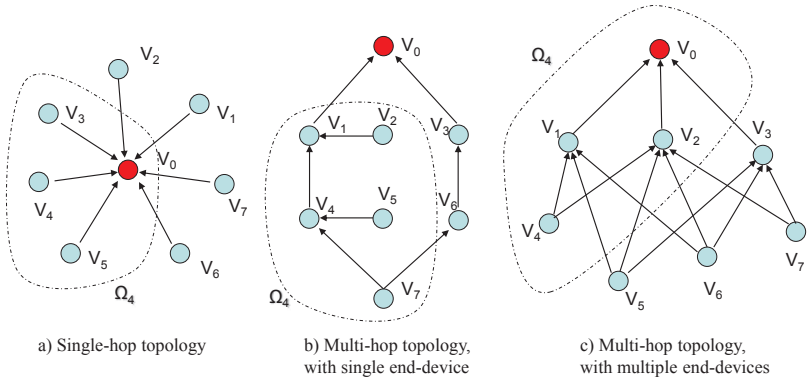

Figure 4.2: Examples of (a) a single-hop topology, (b) a multi-hop topology with single end-device, and (c) a multi-hop topology with multiple end-devices, for IEEE 802.15.4 networks. The dash-dotted area Ω_4 delimits the carrier sensing range of node V_4, i.e., the largest set of nodes that can be heard by V_4 while doing the CCA. The shape of Ω_4 is irregular, because the carrier sensing range can always be not isotropic. Our analysis incorporates any shape.

in Figure 4.2). The carrier sensing range is the set of nodes that can be heard by a node while performing the IEEE 802.15.4 clear channel assessment (CCA), which we describe later on. We denote by $|\Omega_i|$ the cardinality of Ω_i. Note that the carrier sensing radius is not necessarily isotropic. We assume that the channel is symmetric, so that if $V_k \in \Omega_i$, then $V_i \in \Omega_k$, which is natural when transmitting and receiving over similar frequencies. For each link (V_i, V_j), we define $\Omega_{j\setminus i} = \Omega_j - \Omega_i$, the hidden node set of V_i with respect to V_j, namely all nodes that are in the carrier sensing range of the receiver V_j, but that do not belong to the carrier sensing range of the transmitter V_i.

As a reference routing protocol, we consider the specifications of IETF RPL [12], illustrated in Section 2.3.4. We recall that RPL is based on destination-oriented directed acyclic graphs (DODAGs), where all edges are oriented such that no cycles exist. Directional routes in the network are indicated by arrows in Figure 4.2. We define a *parent* set $\Gamma_i \subset \Omega_i$, which contains all nodes that can be next-hop nodes of V_i, and a *children* set $\Delta_i \subset \Omega_i$, which contains all nodes that have V_i as next-hop node. The knowledge of the topological sets Ω_i and Γ_i is then specified by IETF RPL.

We consider two multi-hop topologies in Figure 4.2(b) and Figure 4.2(c) to illustrate our analysis. In Figure 4.2(b) there is one end-device V_7 and two main paths to the destination. Node V_7 can decide to route its packets either through nodes V_4 or V_1, which forward traffic also from nodes V_2 and V_5, or through V_6 and V_3. Note that route V_6–V_3 is less loaded in terms of traffic forwarding. In addition, we study

the more complex routing graph in Figure 4.2(c), where multiple end-devices (V_4, V_5, V_6, and V_7) can decide to route their packets either through nodes V_1, V_2, or V_3 to the destination V_0. Coherently with the RPL specifications, we assume homogeneous link quality between a node and each one of its selected parents, because typically the parent set includes only nodes that can be reached with a guaranteed link quality. The actual forwarding decision is then based on routing metrics such as maximum end-to-end reliability or minimum end-to-end delay, which depend on the link performance at MAC layer. As we show in Section 4.5, the interaction between MAC layer and routing decisions varies substantially between the routing paths, according to the carrier sensing ranges.

In the following section, we introduce the general model for multi-hop unslotted IEEE 802.15.4 MAC and we derive the basic relations with the routing policy.

4.3 Model of the IEEE 802.15.4 MAC for Multi-hop Networks

In this section, a generalized model of a heterogeneous unslotted IEEE 802.15.4 network is proposed. The analysis aims at deriving the network performance indicators, namely the reliability as probability of successful packet reception, the delay for successfully received packets, and the average node energy consumption.

4.3.1 Markov Chain Model of the Unslotted IEEE 802.15.4 MAC

Here, we illustrate the extended Markov chain describing the behavior of the unslotted CSMA/CA mechanism. Let $s_l(t), c_l(t)$ and $r_l(t)$ be the stochastic processes representing the backoff stage, the state of the backoff counter and the state of retransmission counter, respectively, that node V_l experiences at time t. Then, the triple $(s_l(t), c_l(t), r_l(t))$ is the three-dimensional per-link Markov chain in Figure 4.3, where we use (i, k, j) to denote a particular state.

The Markov chain consists of four main parts corresponding to the idle state, backoff states, CCA states, and packet transmission states. The *idle* state corresponds to the idle-queue state when the node is waiting for the next packet generation time. The states from $(i, W_m - 1, j)$ to $(i, W_0 - 1, j)$ represent the backoff states. The states $(i, 0, j)$ represent the CCA. The states $(-1, k, j)$ and $(-2, k, j)$ correspond to the successful transmission and packet collision, respectively.

Differently with respect to the model in Chapter 3, we use a traffic model that includes stochastic packet generation and queueing probability, which is suitable for multi-hop scenarios. The generation of unsaturated traffic at node V_l is modeled by a packet generation probability in idle state q_l, namely the probability of generating a new packet in each time unit when the node is in idle state. Moreover, to include queueing effects of node buffers, we consider the probabilities of having a packet ready to be transmitted after the node has successfully sent a packet $q_{\text{succ},l}$, after

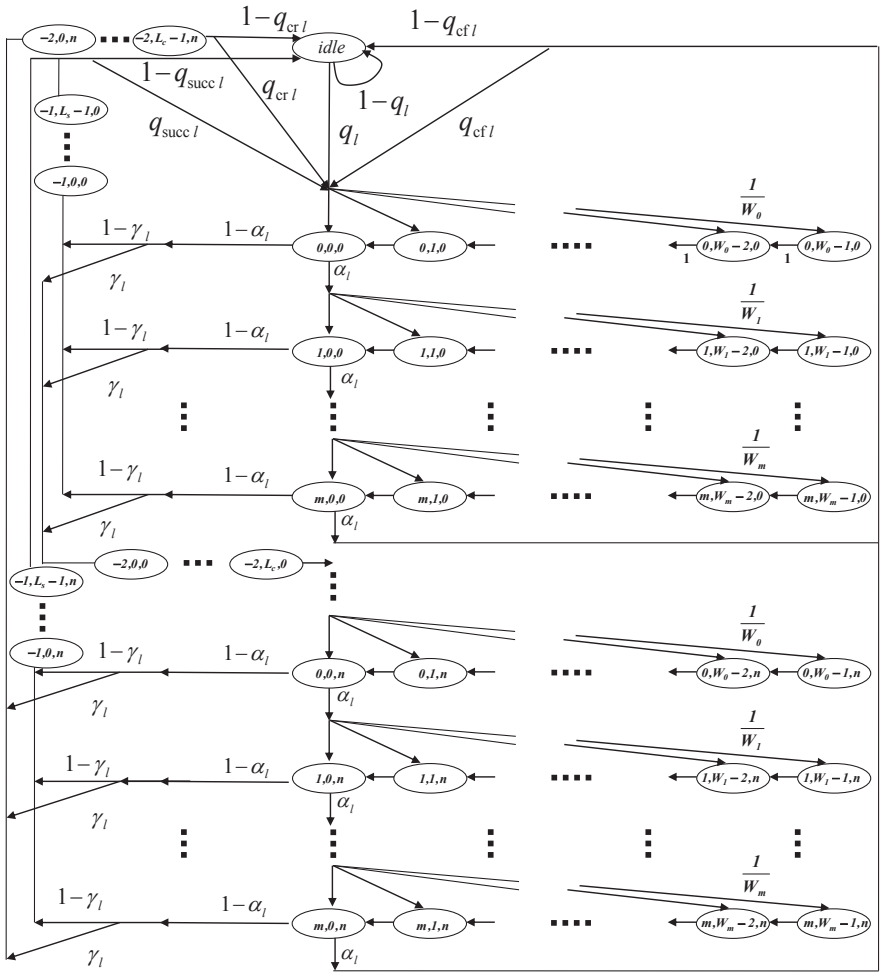

Figure 4.3: Markov chain model of the CSMA/CA algorithm of the transmitting node in link l for unslotted IEEE 802.15.4 MAC.

a packet has been discarded due to channel access failure $q_{cf,l}$, or due to retry limit $q_{cr,l}$. The expressions of the packet generation probabilities are derived in Appendix B.1.

In the unslotted version of IEEE 802.15.4, time units are not synchronized among nodes. In the proposed Markov chain, S_b is the unit time for all state transitions and corresponds to the transmission time of 20 symbols [7]. When performing CCA, a node is listening in RX mode for a duration of 8 symbols. Then the nodes takes a time of 12 symbols ($aTurnaroundTime$) to turn around from RX

mode to TX mode before starting the transmission of the packet, which makes a total time of 20 symbols (S_b) for a successful CCA. The length of the packet L and of the acknowledgement L_{ack} are given as multiplies of S_b. Therefore, it is possible to conclude that S_b is accurate enough to capture the main characteristics of the unslotted mechanism for a transmitting node.

By finding the stationary probabilities for each chain, we can derive the probability τ_l that node V_l attempts CCA. Then, we couple all the per-link Markov chains to obtain a set of equations giving the network operating point, namely the busy channel probabilities α_l, and the collision probabilities γ_l, for $l = 1, \ldots, N$.

We define $b^{(l)}_{i,k,j} = \lim_{t\to\infty} \Pr[s_l(t) = i, c_l(t) = k, r_l(t) = j], i \in (-2, m), k \in (0, \max(W_i - 1, L_s - 1, L_c - 1)), j \in (0, n)$ as the stationary distribution of the Markov chain of Figure 4.3. We remark that these probabilities are related to each link l. Then, we have the following result:

Proposition 4.3.1. *Suppose that the probability to start sensing for every node is independent of the number of retransmissions suffered. Let α_l be the probability that CCA is busy and let γ_l be the probability that a transmitted packet encounters a collision, for $l = 1, \ldots, N$. Then, the probability τ_l that a node V_l attempts CCA in a randomly chosen time unit is*

$$\tau_l = \left(\frac{1-\alpha_l^{m+1}}{1-\alpha_l}\right)\left(\frac{1-y_l^{n+1}}{1-y_l}\right) b^{(l)}_{0,0,0}\,, \tag{4.1}$$

where,

$$b^{(l)}_{0,0,0} = \begin{cases} \Big[\frac{1}{2}\left(\frac{1-(2\alpha_l)^{m+1}}{1-2\alpha_l}W_0 + \frac{1-\alpha_l^{m+1}}{1-\alpha_l}\right)\frac{1-y_l^{n+1}}{1-y_l} \\ +(L_s(1-\gamma_l)+L_c\gamma_l)(1-\alpha^{m+1})\frac{1-y_l^{n+1}}{1-y_l} \\ +\frac{1-q_{cf,l}}{q_l}\frac{\alpha_l^{m+1}(1-y_l^{n+1})}{1-y_l} + \frac{1-q_{cr,l}}{q_l}y_l^{n+1} \\ +\frac{1-q_{\text{succ},l}}{q_l}(1-\gamma_l)\frac{(1-\alpha_l^{m+1})(1-y_l^{n+1})}{1-y_l}\Big]^{-1}, \\ \quad \text{if } m \le \bar{m} = m_b - m_0\,, \\ \\ \Big[\frac{1}{2}\left(\frac{1-(2\alpha_l)^{\bar{m}+1}}{1-2\alpha_l}W_0 + \frac{1-\alpha_l^{\bar{m}+1}}{1-\alpha_l} + (2^{m_b}+1)\alpha_l^{\bar{m}+1}\right. \\ \left.\frac{1-\alpha_l^{m-\bar{m}}}{1-\alpha_l}\right)\frac{1-y_l^{n+1}}{1-y_l} + (L_s(1-\gamma_l)+L_c\gamma_l) \\ (1-\alpha^{m+1})\frac{1-y_l^{n+1}}{1-y_l} + \frac{1-q_{cf,l}}{q_l}\frac{\alpha_l^{m+1}(1-y_l^{n+1})}{1-y_l} \\ +\frac{1-q_{cr,l}}{q_l}y_l^{n+1} + \frac{1-q_{\text{succ},l}}{q_l}(1-\gamma_l) \\ \frac{(1-\alpha_l^{m+1})(1-y_l^{n+1})}{1-y_l}\Big]^{-1}, \\ \quad \text{otherwise,} \end{cases} \tag{4.2}$$

and $y_l = \gamma_l(1-\alpha_l^{m+1})$.

Proof. The proof follows similar steps of the slotted model developed in Section 3.2. The complete derivation is reported in Appendix B.2. □

The probability τ_l given by the previous proposition depends on the probability α_l that CCA is busy and the probability γ_l that a transmitted packet encounters a collision. We study these two probabilities next.

We derive the busy channel probability as follows:

$$\alpha_l = \alpha_{\text{pkt},l} + \alpha_{\text{ack},l}\,, \tag{4.3}$$

where $\alpha_{\text{pkt},l}$ is the probability that node V_l senses the channel and finds it occupied by a packet transmission in the neighborhood Ω_l, whereas $\alpha_{\text{ack},l}$ is the probability of finding the channel busy due to ACK transmissions.

The probability that node V_l finds the channel busy due to a packet transmission is the combination of two events: (i) at least one node accesses the channel in one of the previous L time units; (ii) at least one of the nodes that accessed the channel found it clear. We would like to remark here a major difference with the Markov chain model proposed in Chapter 3. In homogeneous networks with full sensing range, the busy channel probability is network information; it is the same for all the nodes. In heterogeneous networks, it depends on the access and busy channel probabilities of every node in the neighborhood. This introduces substantial analytical challenges.

Denote by $\mathscr{S}_l$ the event that node V_l is sensing, and by $\mathscr{T}_l$ the event that node V_l is transmitting. Denote also by $\mathscr{F}_l$ the event that there is at least one transmission in Ω_l. Then,

$$\alpha_{\text{pkt},l} = \Pr[\mathscr{F}_l|\mathscr{S}_l] = \sum_{i=1}^{|\Omega_l|}\sum_{j=1}^{C_{l,i}} \Pr\left[\bigcup_{k=1}^{i} \mathscr{T}_{k_j}|\mathscr{S}_l\right]\,, \tag{4.4}$$

where

$$C_{l,i} = \binom{|\Omega_l|}{i}\,.$$

The index k accounts for the events of simultaneous transmissions in the channel and the index j enumerates the combinations of events in which a number i of channel accesses are performed in the network simultaneously. Therefore, the index k_j refers to the node in the k-th position in the j-th combination of i elements out of Ω_l, so that

$$\Pr\left[\bigcup_{k=1}^{i} \mathscr{T}_{k_j}|\mathscr{S}_l\right] = L\prod_{k=1}^{i}\tau_{k_j}\left(1-\prod_{k=1}^{i}\alpha_{k_j}\right)\prod_{h=i+1}^{|\Omega_l|}(1-\tau_{h_j})\,.$$

To illustrate Equation (4.4), we consider Figure 4.2(a) and assume that there are two contending nodes in the neighborhood of V_4, $\Omega_4 = \{V_0, V_3, V_5\}$. Note that V_0 does not generate packets. Then, the event of busy channel for node V_4, is given by the sum of three contributions:

1. Only node V_3 accessed the channel and found it clear. The probability of this event is $L\tau_3(1-\tau_5)(1-\alpha_3)$.

2. Only node V_5 accessed the channel and found it clear. Similarly to the previous case, the probability is $L\tau_5(1-\tau_3)(1-\alpha_5)$.

3. Both nodes accessed the channel and at least one node found it clear. Note that V_5 may not belong to Ω_3 in this case. This probability is upper bounded by $L\tau_3\tau_5(1-\alpha_3\alpha_5)$.

Equation (4.4) follows as a generalization of this example.

The computation of the correlation among the busy channel probabilities is not an easy task. We use the upper bound $\left(1-\prod_{k=1}^{i}\alpha_{k_j}\right)$ because it represents a worst case model scenario for the busy channel probability (uncorrelated busy channel events). As we show in Section 4.5, this upper bound provides a good approximation also in the case of perfect sensing (maximum correlation). The reason is that this assumption affects only events in which two or more nodes are listening to the channel in the same time unit. However, in the case of homogeneous networks with full sensing range, the term $\left(1-\prod_{k=1}^{i}\alpha_{k_j}\right)$ can be replaced by the accurate expression $(1-\alpha)$.

In single-hop networks, the busy channel assessment due to ACKs depends on the probability of successful packet reception in Ω_0. Let R_h be the reliability of link h. It follows that

$$\alpha_{\mathrm{ack},l} = L_{\mathrm{ack}} \sum_{h\in\Omega_0, h\neq l} q_h R_h \,, \tag{4.5}$$

where L_{ack} is the length of the ACK and q_h is the packet generation rate of V_h.

In multi-hop networks, ACKs might be sent from any node in the network, according to the distribution of the traffic. In the derivation of the busy channel probability due to ACK transmission $\alpha^{\mathrm{mh}}_{\mathrm{ack},l}$, we replace Equation (4.5) by

$$\alpha_{\mathrm{ack},l} = L_{\mathrm{ack}} \sum_{j\in\Omega_l} \sum_{h\in\Delta_j} q_h T_{l,j} \,, \tag{4.6}$$

which includes the effect of limited carrier sensing range at the destination and the traffic distribution matrix $\mathbf{T}$. We provide a characterization of the traffic distribution matrix $\mathbf{T}$ in Section 4.4. Recall that Δ_j is the set of children nodes of V_j. By summing up Equations (4.4) and (4.6), we can compute α_l in Equation (4.3).

We now turn our attention to the collision probability γ_l, namely the probability that the packet transmission from node V_l to node V_j encounters one or more simultaneous packet transmissions. Note that these transmissions may fully or partially overlap due to the limited size of the packets.

There are two main reasons of packet collisions for V_l:

1. Collision due to turnaround time: at least one node in Ω_l senses the channel idle while V_l is in its turnaround after CCA, or at least one node in Ω_l is in its turnaround after CCA while V_l senses the channel idle.

2. Collision due to hidden nodes: at least one node in $\Omega_{j\setminus l}$ (hidden node) has started a packet transmission in one of the previous L time units, or before V_l ends its transmission.

We define by $\mathscr{A}_l$ the event of collision due to turnaround time in Ω_l, and by $\mathscr{B}_l$, the event of collision due to hidden nodes in $\Omega_{j\setminus l}$. Therefore, the collision probability γ_l is given by

$$\gamma_l = \Pr[\mathscr{A}_l] + \Pr[\mathscr{B}_l] - \Pr[\mathscr{A}_l]\Pr[\mathscr{B}_l]\,. \tag{4.7}$$

Here, the probability of event $\mathscr{A}_l$ is given by the probability that at least one node in Ω_l accesses the channel and finds it free in the same time unit (i.e., $2aTurnaroundTime \approx S_b$), namely

$$\Pr[\mathscr{A}_l] = \sum_{i=0}^{|\Omega_l|}\sum_{j=1}^{C_{l,i}}\prod_{k=1}^{i}\tau_{k_j}\left(1-\prod_{k=1}^{i}\alpha_{k_j}\right)\prod_{h=i+1}^{|\Omega_l|}(1-\tau_{h_j})\,.$$

Similarly, the probability of event $\mathscr{B}_l$ is given by

$$\Pr[\mathscr{B}_l] = 2L\sum_{i=0}^{|\Omega_{j\setminus l}|}\sum_{j=1}^{C_{l,i}}\prod_{k=1}^{i}\tau_{k_j}\left(1-\prod_{k=1}^{i}\alpha_{k_j}\right)\prod_{h=i+1}^{|\Omega_{j\setminus l}|}(1-\tau_{h_j}).$$

In the presence of multi-hop communications, there are also other factors in the collision probability γ_l. In particular, a packet from node V_i might collide with an ACK from a node in the hidden node set. In the simplest situation, this event involves four nodes. There is a collision due to a hidden node ACK if a packet from V_i is transmitted to V_j, while $V_k \notin \{\Omega_i + \Omega_j\}$ successfully transmits a packet to $V_h \in \Omega_{j\setminus i}$. Then the ACK from V_h leads to a collision with the packet from V_i at the receiver V_j. The derivation of the probability of these events is not trivial and computationally demanding. In our model, we assume for simplicity that ACKs from hidden nodes do not prevent the destination node successfully receiving a packet. This hypothesis is supported by the fact that the time in which ACKs and packets can overlap is short with respect to the packet transmission time (i.e., $L_{\text{ack}} \ll L$).

Moreover, in the presence of limited buffer size B, the collision probability includes also the blocking probability $p_{\text{blk},l}$, namely the probability that the packet is discarded at the receiver because the queue is full. For the M/G/1/K queueing model [126], we get

$$p_{\text{blk},l} = 1 - \frac{1}{p_{l,0} + q_l\mathbb{E}\{D_l^s\}} \tag{4.8}$$

where $\mathbb{E}\{D_l^s\}$ is the average service time, and $p_{l,0}$ is derived in Appendix B.1.

In the next subsections, we use these results to derive the expressions of the reliability, the delay for successfully received packets, and the energy consumption.

4.3.2 Reliability

We evaluate the reliability as the successful reception probability. Following similar steps to Section 3.3.1, we derive

$$R_l = 1 - \frac{\alpha_l^{m+1}(1-(\gamma_l(1-\alpha_l^{m+1}))^{n+1})}{1-\gamma_l(1-\alpha_l^{m+1})} - (\gamma_l(1-\alpha_l^{m+1}))^{n+1}\,. \tag{4.9}$$

Due to the inter-dependance between the reliability in Equation (4.9), and the busy channel probability due to ACK transmissions in Equation (4.5), the link reliability is the solution of a system of non-linear equations formed by the expressions of the carrier sensing probability τ_l in Equation (4.1), the busy channel probability α_l in Equation (4.3), and the reliability R_l in Equation (4.9), for $l = 1, \ldots, N$. The system can be solved through numerical methods [109]. We derive then the end-to-end reliability of V_l by the product of each link reliability in the path to V_0.

4.3.3 Delay

The total delay experienced in a successful packet transmission for node V_l can be derived as $D_l = D_l^s + D_l^q$, where D_l^s is the service time for a successfully received packet and D_l^q is the queueing delay.

The service time D_l^s is defined as the time interval from the instant the packet is ready to be transmitted, until an ACK for such a packet is received. If a packet is dropped due to either the limited number of backoffs m or the finite retry limit n, its delay is not included into the derivation.

Let $D_{l,j}^s$ be the delay for a node that sends a packet successfully after j unsuccessful attempts. From the Markov chain of Figure 4.3, we derive the expected value of the delay D_l^s,

$$\mathbb{E}[D_l^s] = \sum_{j=0}^{n} \Pr[\mathscr{C}_j|\mathscr{C}] \left(T_s + j\,T_c + \sum_{h=0}^{j} \mathbb{E}[t_h] \right), \tag{4.10}$$

where

$$\mathbb{E}[t_h] = t_{sc} + \sum_{i=0}^{m} \Pr[\mathscr{D}_i|\mathscr{D}] \left(i\,t_{sc} + \sum_{k=0}^{i} \frac{W_k - 1}{2}\, S_b \right), \tag{4.11}$$

t_h is the backoff stage delay, $T_s = L_s S_b$ and $T_c = L_c S_b$ are the time periods for successful packet transmission and collided packet transmission in Equation (3.1). We recall that γ_l is the collision probability and $1 - \alpha_l^{m+1}$ is the probability of

successful channel access within the maximum number of m backoff stages. We use $\mathscr{C}_j$ as the event of a successful transmission at time $j+1$ after j events of unsuccessful transmission, and $\mathscr{C}$ as the event of successful transmission within the total attempts n. Therefore,

$$\Pr[\mathscr{C}_j|\mathscr{C}] = \frac{\left(1-\gamma_l(1-\alpha_l^{m+1})\right)\gamma_l^j(1-\alpha_l^{m+1})^j}{1-\left(\gamma_l(1-\alpha_l^{m+1})\right)^{n+1}}. \tag{4.12}$$

The event $\mathscr{D}_i$ denotes the occurrence of a busy channel for i-th times, and then of idle channel at the $i+1$th time. By considering all the possibilities of busy channel during one CCA, the probability of $\mathscr{D}_i$ is conditioned on the successful sensing event within m attempts $\mathscr{D}$, given that the node senses an idle channel in CCA. It follows that

$$\Pr[\mathscr{D}_i|\mathscr{D}] = \frac{\alpha_l^i}{\sum_{k=0}^{m}\alpha_l^k} = \frac{\alpha_l^i(1-\alpha_l)}{1-\alpha_l^{m+1}}.$$

Similarly, we compute the average service time for a packet that is discarded due to channel access failure $\mathbb{E}[D_l^m]$ as

$$\mathbb{E}[D_l^m] = \sum_{j=0}^{n}\Pr[\mathscr{C}_j|\mathscr{C}]\,\mathbb{E}[D_{l,j}^m], \tag{4.13}$$

where

$$\mathbb{E}[D_{l,j}^m] = \sum_{h=0}^{j}\mathbb{E}[t_h] + (m+1)t_{sc} + \sum_{k=0}^{m}\frac{W_k-1}{2}S_b. \tag{4.14}$$

The average service time for a packet that is discarded due to the retry limit $\mathbb{E}\{D_l^n\}$ is given by

$$\mathbb{E}[D_l^n] = T_c + \sum_{h=0}^{n}\mathbb{E}[t_h]. \tag{4.15}$$

The expressions of the service time for successful transmission, channel access failure, and failure due to retry limit are used in Appendix B.1 to compute the idle probabilities $q_{\text{succ},l}$, $q_{cf,l}$, and $q_{cr,l}$, respectively.

Next, we focus on the queueing delay D_l^q of node V_l. We consider a limited buffer size B and describe the system as a $M/G/1/K$ queueing model [126]. Under these assumptions, the average queueing delay is

$$\mathbb{E}[D_l^q] = \frac{1}{q_l}\left(\sum_{n=1}^{B-1}np_{l,k} + B(p_{l,0}+q_l\mathbb{E}[D_l^s]-1)\right) - \mathbb{E}[D_l^s], \tag{4.16}$$

where the probabilities $p_{l,k}$, are derived in Appendix B.1.

Finally, we derive then the end-to-end delay as the sum of the delays in the path from transmitter V_l to the root node V_0.

4.3.4 Energy Consumption

Here we develop the expression of the energy consumption. Differently with respect to the single-hop homogeneous case formulated with Equation 3.36, for each relay node, we should include the cost for receiving packets and transmitting ACKs. Moreover, nodes are in idle-listen state during the idle-queue stage in the Markov chain.

By considering the Markov chain model in Figure 4.3, the average energy consumption of node V_l is given by

$$\begin{aligned} E_{\text{tot,l}} =& P_i \sum_{i=0}^{m} \sum_{k=1}^{W_i-1} \sum_{j=0}^{n} b_{i,k,j}^{(l)} + P_{sc} \sum_{i=0}^{m} \sum_{j=0}^{n} b_{i,0,j}^{(l)} + P_t \sum_{j=0}^{n} \sum_{k=0}^{L-1} (b_{-1,k,j}^{(l)} + b_{-2,k,j}^{(l)}) \\ &+ P_i \sum_{j=0}^{n} (b_{-1,L,j}^{(l)} + b_{-2,L,j}^{(l)}) + \sum_{j=0}^{n} \sum_{k=L+1}^{L+L_{\text{ack}}+1} (P_r\, b_{-1,k,j}^{(l)} + P_i\, b_{-2,k,j}^{(l)}) + (P_r L \\ &+ P_i + P_t L_{\text{ack}}) + \sum_{h \in \Delta_i} q_h T_{h,j} b_{\text{idle}}^{(l)} + P_i (1 - (L + L_{\text{ack}} + 1) \sum_{h \in \Delta_i} q_h T_{h,j}) b_{\text{idle}}^{(l)}, \end{aligned} \tag{4.17}$$

where P_i, P_{sc}, P_t, P_r and P_{sp} are the average energy consumptions in idle-listening, channel sensing, transmitting, receiving, and idle-queueing states, respectively. By following the computation of the terms $b_{i,k,j}^{(l)}$ into Equation (4.17), we obtain the average energy consumption in closed form.

4.3.5 Approximate Model for Large-Scale Networks

In the previous sections, we derived closed form expressions of the performance indicators in single-hop and multi-hop IEEE 802.15.4 networks. However, the computation time of the Markov chain parameters $\alpha_{\text{pkt},l}$ and γ_l in Equations (4.4) and (4.7) increases exponentially with the number of neighboring nodes $|\Omega_l|$ and the number of hidden nodes $|\Omega_{j \setminus l}|$. Therefore, the computation of these parameters becomes unpractical when any of these numbers becomes greater than 15–20.

In this section, we propose approximate expressions of α_i and γ_l, which are linear with the number of neighboring and hidden nodes and can be used to derive the performance indicators for large-scale networks. In particular, we consider the event $\mathscr{U}_l$ that the channel is busy in Ω_l for a given time unit. The probability of this event can be approximated by multiplying the probabilities that at least one node in Ω_l accesses the channel and the average probability of idle channel during CCA in Ω_l, i.e.,

$$\Pr(\mathscr{U}_l) = \frac{1}{|\Omega_l| - 1} \left(1 - \prod_{n \in \Omega_l} (1 - \tau_n)\right) \sum_{k \in \Omega_l} (1 - \alpha_k)\,. \tag{4.18}$$

The busy channel probability due to packet transmission $\alpha_{\text{pkt},l}$ and the collision probability γ_l can be then written as

$$\alpha_{\text{pkt},l} = L \Pr(\mathscr{U}_l)\,, \tag{4.19}$$

$$\gamma_l = \Pr(\mathscr{U}_l) + (1 - \Pr(\mathscr{U}_l)) \Pr(\mathscr{U}_{j\setminus l})\,. \tag{4.20}$$

When the number of nodes in Ω_l is small, the previous equations can lead to inaccurate estimation of the parameters due to the averaging operation. However, this model becomes more accurate as the size of the set increases, because the variance of the distribution of busy channel probabilities reduces. The approximate model is validated through simulations in Section 4.5.

4.4 Integrated MAC and Routing Model

In a generic DODAG, the total number of links G is not equal to the number of nodes N. Recall that we associate to every link l a pair transmitter–receiver (V_i, V_j). The proposed Markov chain model is solved for each link of the network, by considering that the generic node V_j forwards an aggregate traffic Q_j.

Let $\lambda = [0, \lambda_1, ..., \lambda_N]$ be a vector of node traffic generation rates, where each component is associated with a node. In addition to λ_i, node V_i has to forward traffic generated by nodes in its children set Δ_i. We measure the total average aggregate traffic in link l as $Q_l = q_l/S_b$ pkt/s, where q_l is the probability of having a packet to transmit in each time unit (see Figure 4.3) and S_b is the duration of the basic time unit in IEEE 802.15.4.

The aim of the following analysis is to investigate the total traffic load Q_l, which we associate to the probability q_l in the per-link Markov chain. To do so, we must characterize the traffic distribution in the network according to a routing policy.

Define $\pi_{i,j}$ as the metric associated with link (V_i, V_j) to build the routing graph, as specified by RPL. In a practical example, $\pi_{i,j}$ can be the end-to-end reliability or delay from node V_i to V_0, by choosing node V_j as next-hop node. At the routing layer, metrics are chosen to be static if the network is stationary. However, due to the dynamic nature of wireless connectivity, link attributes including reliability and delay can change over time and the routing metrics are updated accordingly. We can represent this dynamical behavior using a statistical analysis. The effect of routing can be described by a matrix $\mathbf{M} \in \mathbb{R}^{(N+1)\times(N+1)}$, in which element $M_{i,j}$ corresponds to the probability that the metric in link $l = (V_i, V_j)$ is the highest among the set of candidate receivers Γ_i, i.e.,

$$M_{i,j} = \Pr\left[\pi_{i,j} = \max_{V_h \in \Gamma_i} \pi_{i,h}\right]\,.$$

The distribution of the traffic flows along the network can be modeled by the matrix $\mathbf{M}$, and by scaling it by the probability of successful reception in each link (only successfully received packets are forwarded). Therefore, we define a matrix

$\mathbf{T}$ such that $T_{i,j} = M_{i,j}R_l$ where R_l is the reliability in the link $l = (V_i, V_j)$, as derived in Section 4.3.2. The aggregate traffic vector $Q = [0, Q_1, \ldots, Q_N]$ is the sum of generated traffic and forwarded traffic from children nodes, which gives the system of flow balance equations $Q = \lambda + Q\,\mathbf{T}$. In steady state, we have

$$Q = \lambda \left[\mathbf{I} - \mathbf{T}\right]^{-1}, \tag{4.21}$$

where $\mathbf{I} \in \mathbb{R}^{(N+1)\times(N+1)}$ is the identity matrix. Since the routing graph is assumed to be acyclic, the matrix $\mathbf{T}$ has spectral radius less than one. Therefore, it is easy to show that the inverse matrix $[\mathbf{I} - \mathbf{T}]^{-1}$ always exists.

Equation (4.21) gives the relation between the idle packet generation probability q_l, the effect of routing (through the matrix $\mathbf{M}$) and the performance at MAC layer (through the link reliability R_l). To obtain the integrated model, we couple Equation (4.21) with the expressions for τ_l, α_l and R_l, as obtained by Equations (4.1), (4.3), and (4.9).

The set of candidate receivers Γ_i is composed by the set of nodes that can guarantee a progress toward the destination V_0, according to RPL specifications. However, the choice of the forwarding node in the set is driven by the specific metrics $\pi_{i,j}$. We consider here two metrics that are simple and practical to implement in the standards and are based on the link performance at MAC layer:

- *R-metric*, defines the path for which the end-to-end reliability is maximized. It extends the ETX metric at MAC layer, by considering packet losses due to the MAC contention mechanism.

- *Q-metric*, which distributes the forwarded traffic to guarantee load balancing. In particular, the metric computes $\min_{j\in\Gamma_i} \bar{Q}_j$, where $\bar{Q}_j = c_r Q_j - \lambda_j$.

The constant $c_r = (P_t + P_r)/P_t$ accounts for the extra cost in terms of energy consumption in reception P_r that a node experiences for traffic forwarding with respect to traffic generated by the same node.

We recall that the packet generation follows a Poisson distribution. In the derivation of the total aggregate traffic Q, we assume that the forwarded traffic also follows a Poisson distribution. This assumption holds if the distribution of the number of received packets at node V_j can be approximated by a Poisson distribution. To validate this approximation, in Figure 4.4 we show the probability density function (PDF) of the number of received packets in a time interval of 10 seconds, in a single-hop network with $N = 14$ nodes and traffic generation rates $\lambda_i = 5$ pkt/s, using Monte Carlo simulations. Details of the simulation environment are given in Section 4.5. We observe that a Poisson distribution with arrival rate $Q_j - \lambda_j$ predicts well the PDF of the number of received data packets. We validate the analysis in Section 4.5.

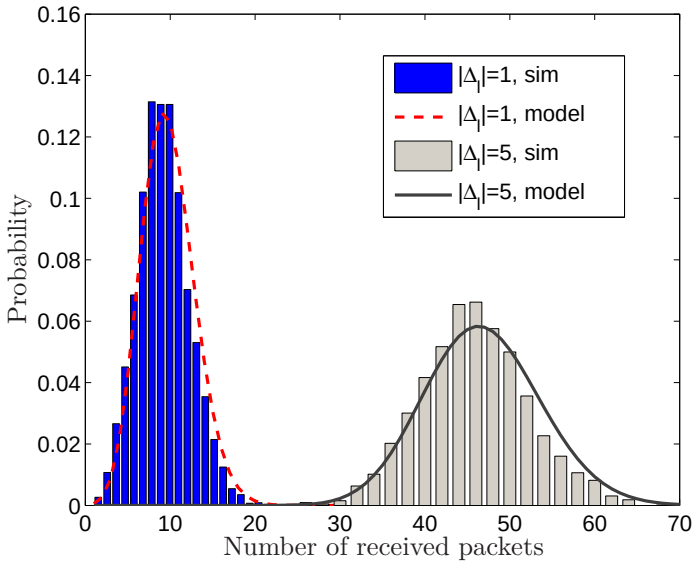

Figure 4.4: Probability density function of the number of received packets in a period $T = 10$ s, for a destination node V_l, by varying the number of children nodes in Δ_l. The network is composed of $N = 14$ nodes, with traffic rate $\lambda_l = 5$ pkt/s, for $l = 1, \ldots, N$.

Table 4.5: Carrier sensing range in the network scenarios in Figure 4.2.

	Figure 4.2(a) reduced sensing	Figure 4.2(b) non-interfering	Figure 4.2(b) interfering	Figure 4.2(c) non-interfering	Figure 4.2(c) interfering
V_1	V_0, V_2, V_7	V_0, V_2, V_3, V_4, V_5	$\{V_i\},\ i \neq 1, 3$	$\{V_i\},\ i \neq 1, 7$	$\{V_i\},\ i \neq 1$
V_2	V_0, V_1, V_3	V_0, V_1, V_4, V_5	$\{V_i\},\ i \neq 2$	$\{V_i\},\ i \neq 2$	$\{V_i\},\ i \neq 2$
V_3	V_0, V_2, V_4	V_0, V_1, V_6	$\{V_i\},\ i \neq 1, 3$	$\{V_i\},\ i \neq 3, 4$	$\{V_i\},\ i \neq 3$
V_4	V_0, V_3, V_5	V_1, V_2, V_5, V_7	$\{V_i\},\ i \neq 4$	V_0, V_1, V_2	$\{V_i\},\ i \neq 4$
V_5	V_0, V_4, V_6	V_1, V_2, V_4, V_7	$\{V_i\},\ i \neq 5$	V_0, V_1, V_2, V_3	$\{V_i\},\ i \neq 5$
V_6	V_0, V_5, V_7	V_3, V_7	$\{V_i\},\ i \neq 6$	V_0, V_1, V_2, V_3	$\{V_i\},\ i \neq 6$
V_7	V_0, V_1, V_6	V_4, V_5, V_6	$\{V_i\},\ i \neq 0, 7$	V_0, V_2, V_3	$\{V_i\},\ i \neq 7$

4.5 Performance Results

In this section, we present extensive Monte Carlo simulations to validate our analysis and experimental results to assess the performance of the routing metrics. The simulations are based on the specifications of the IEEE 802.15.4 [7] with several values of the traffic pattern and node sensing range. In our implementation, time is slotted and synchronized respect to a simulation clock $S_b = 320\mu s$. However, in each iteration we keep into account the asynchronous behavior of the nodes during

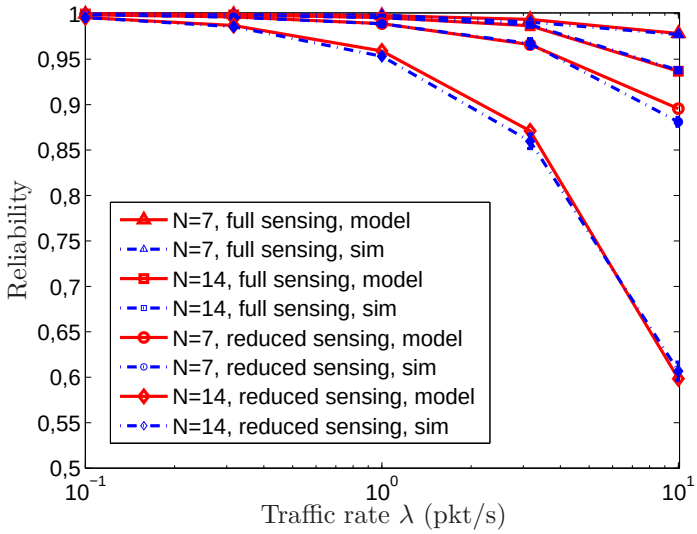

Figure 4.6: Reliability vs. traffic rate λ for the single-hop topology in Figure 4.2(a). Full sensing and reduced sensing correspond to $|\Omega_l| = N$ and $|\Omega_l| = 3$, respectively. The vertical bars indicate the standard deviation as obtained out of 5 simulation runs with 10^4 generated packets.

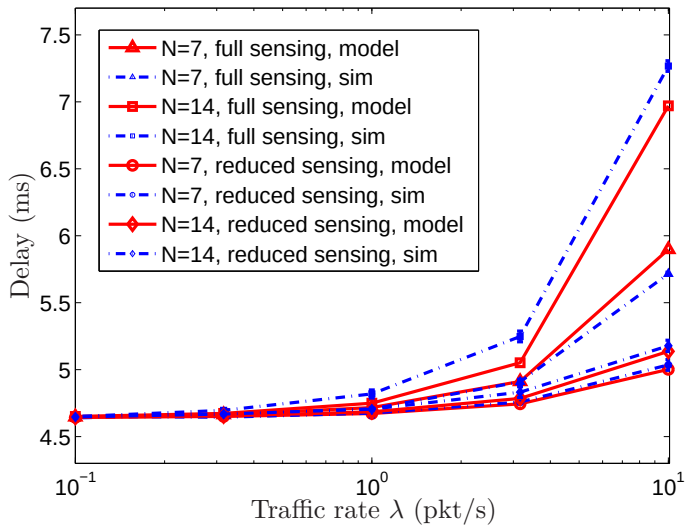

Figure 4.7: Delay vs. traffic rate λ for the single-hop topology in Figure 4.2(a). Full sensing and reduced sensing correspond to $|\Omega_l| = N$ and $|\Omega_l| = 3$, respectively. The vertical bars indicate the standard deviation as obtained out of 5 simulation runs with 10^4 generated packets.

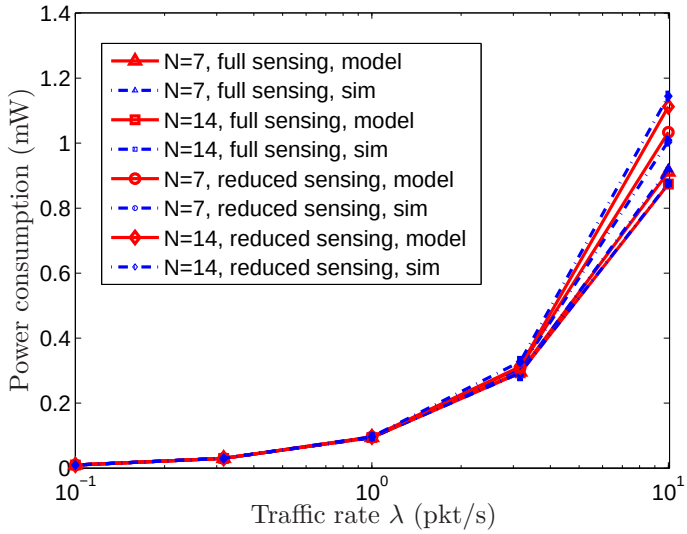

Figure 4.8: Energy consumption vs. traffic rate λ for the single-hop topology in Figure 4.2(a). Full sensing and reduced sensing correspond to $|\Omega_l| = N$ and $|\Omega_l| = 3$, respectively. The vertical bars indicate the standard deviation as obtained out of 5 simulation runs with 10^4 generated packets.

CCA and packet transmission by dividing the slot into sub-slots of $16\mu s$, which corresponds to the symbol period in the standard.

According to the IETF RPL specifications [12], typical applications of interest in urban, industrial, or home environments operate with packet generation rates of the order of few packets per minute. However, to validate our model in more critical situations, we consider also traffic rates of the order of packets per second. We set the MAC parameters to $m_0 = 3$, $m = 4$, $m_b = 7$, $n = [0\,,\,1]$, $L = 7$, $L_{\text{ack}} = 2$. Other settings give results similar to those discussed next. First, we consider single-hop and then multi-hop networks.

4.5.1 Model Validation for Single-hop Networks

In the first set of simulation results, we validate the model proposed in Section 4.3.1 for a single-hop topology, see Figure 4.2(a).

To study the impact of hidden terminals, we consider two basic scenarios, namely $|\Omega_l| = N$, which is denoted by *full sensing* capability, and $|\Omega_l| = 3$ that represents *reduced sensing* capability (the neighborhood is composed by the root node V_0 and two adjacent nodes). The list of nodes in the reduced carrier sensing range of each node is reported in Table 4.5.

Figure 4.6 shows the average reliability computed over all the links for a single-hop network with homogeneous traffic. On the x-axis the node packet generation rate is reported. Results are shown for different sizes of the network ($N = 7$, $N = 14$), and by considering both full and reduced sensing capabilities. A good agreement between simulations and analytical results is observed. By reducing the carrier sensing capabilities, the model proposed in this chapter allows us to observe a negative impact on the reliability.

In Figure 4.7 we present the average delay over all the links for a single-hop network with homogeneous traffic by varying the node packet generation rate. As for the reliability, results are shown for different sizes of the network ($N = 7$, $N = 14$), and by considering both full and reduced sensing capabilities. There is a good matching between the simulations and our analytical model. The small gap when the traffic rate increases is due to the assumption of independent busy channel probabilities. This effect depends on the size of packets, as we discuss in Appendix C.3. We notice here that nodes with reduced sensing capability have a positive effect on the delay performance. This is in contrast with the effect on the reliability in Figure 4.6. The reason is that the average delay is evaluated only for successfully received packets: reduced sensing capabilities decrease the number of competitor nodes for the free channel assessment, thus the busy channel probability is reduced, which in turn decreases the average delay.

In Figure 4.8, the analysis of the node energy consumption is reported. We show the results for default MAC parameters with $n = 1$. The energy consumption is dominated by the actual traffic for every node, because the cost for transmitting and receiving packets is much higher than the other cost components. For this reason, reduced sensing capabilities, which influence the number of collisions, have a stronger impact on the energy consumption with respect to an increase of the size of the network from $N = 7$ to $N = 14$ nodes. Furthermore, with $N = 14$, the number of transmissions reduces with respect to $N = 7$ due to the higher probability that a packet is discarded because of channel access failures.

Let us consider now the interaction between heterogeneous traffic and the reduced sensing capability of the single-hop topology of Figure 4.2(a). In Figure 4.9, we report the link reliability related to every node. We plot analytical results and simulation of the reliability for a single-hop network with $N = 7$ nodes. In the *homogeneous* case, every node generates the same traffic $\lambda_l = 5$ pkt/s, $l = 1, \ldots, N$. In the *heterogeneous* case, node V_4 generates a traffic $\lambda_4 = 20$ pkt/s, while the rest of the network has nodes with $\lambda_l = 5$ pkt/s. The effect of an increased traffic of V_4 leads to a decreasing of the reliability in the rest of the network, whereas the reliability of V_4 is only marginally affected. This effect is more significant when there are reduced sensing capabilities.

In Figure 4.10, we report the delay related to every node. With full sensing capabilities, the effect of an increased traffic in V_4 is an increase of the delay in the rest of the network, whereas the delay of V_4 is not affected. With reduced sensing capabilities, it is interesting to notice that the delay increases only for nodes that are in the sensing range of V_4 (i.e., V_3 and V_5).

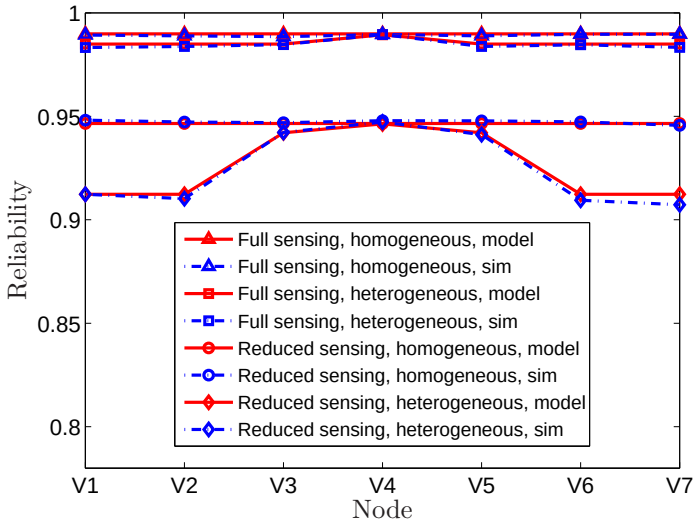

Figure 4.9: Reliability of every node for the single-hop topology in Figure 4.2(a). Full sensing and reduced sensing correspond to $|\Omega_l| = N$ and $|\Omega_l| = 3$, respectively. In homogeneous case, $\lambda_l = 5$ pkt/s, for $l = 1, \ldots, N$. In heterogeneous case, $\lambda_4 = 20$ pkt/s, $\lambda_l = 5$ pkt/s, for $l \neq 4$.

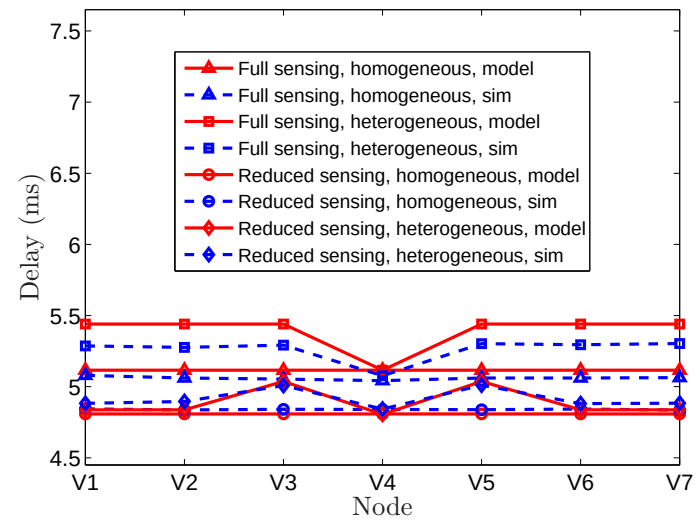

Figure 4.10: Average node delay for the single-hop topology in Figure 4.2(a). Full sensing and reduced sensing correspond to $|\Omega_l| = N$ and $|\Omega_l| = 3$, respectively. In homogeneous case, $\lambda_l = 5$ pkt/s, for $l = 1, \ldots, N$. In heterogeneous case, $\lambda_4 = 20$ pkt/s, $\lambda_l = 5$ pkt/s, for $l \neq 4$.

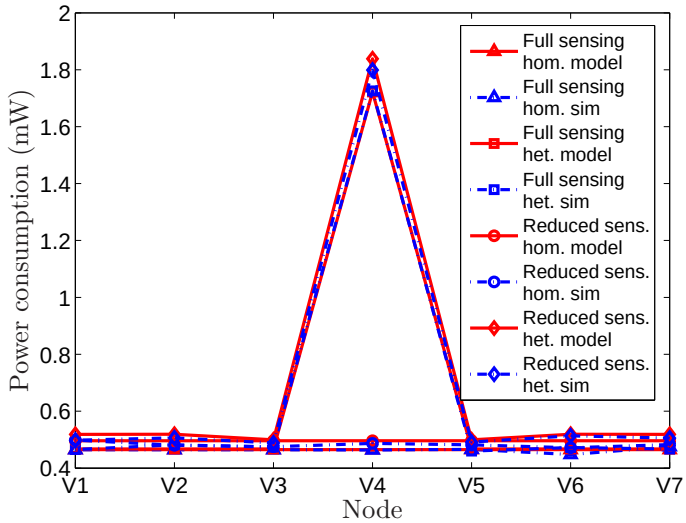

Figure 4.11: Node energy consumption for the single-hop topology in Figure 4.2(a). Full sensing and reduced sensing correspond to $|\Omega_l| = N$ and $|\Omega_l| = 3$, respectively. In homogeneous case, $\lambda_l = 5$ pkt/s, for $l = 1, \ldots, N$. In heterogeneous case, $\lambda_4 = 20$ pkt/s, $\lambda_l = 5$ pkt/s, for $l \neq 4$.

In Figure 4.11, we show the energy consumption for every node. The increasing traffic on V_4 in the heterogeneous condition affects significantly its own energy consumption in both full and reduced sensing capabilities, and in a lower extent, it increases the energy consumption of nodes outside its sensing range. Nodes V_3 and V_5, which are in the sensing range, are not noticeably influenced.

To show the effectiveness of the analytical model for high-traffic networks, we consider saturated conditions were packets are generated back-to-back at each node. In saturated conditions, performance are typically measured in terms of normalized throughput. In Figure 4.12, we report the normalized throughput by varying the packet size L, for a network with $N = 7$ and $N = 14$ in saturated conditions, for full and reduced sensing capabilities. Full sensing and reduced sensing correspond to $|\Omega_l| = N$ and $|\Omega_l| = N/2$, respectively. The analytical model follows quite well the simulation. The throughput tends to increase with the packet size and the gap between $N = 7$ and $N = 14$ is not significant for full sensing capabilities. In the case of reduced sensing capabilities, by increasing the packet size, the number of collisions due to hidden nodes increases and for large L the throughput decreases. This effect is more evident as the number of nodes increases to $N = 14$ due to the higher number of hidden nodes.

We now consider large-scale networks and validate the approximate model pre-

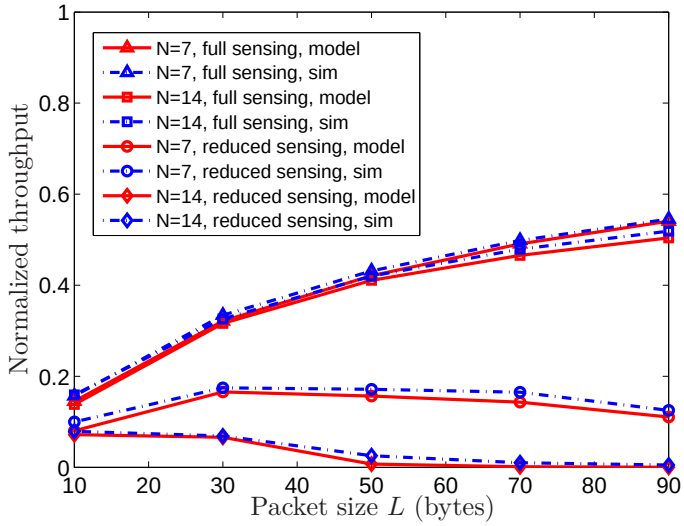

Figure 4.12: Normalized throughput vs. packet size L for the single-hop topology in Figure 4.2(a), under saturated traffic conditions. Full sensing and reduced sensing correspond to $|\Omega_l| = N$ and $|\Omega_l| = N/2$, respectively.

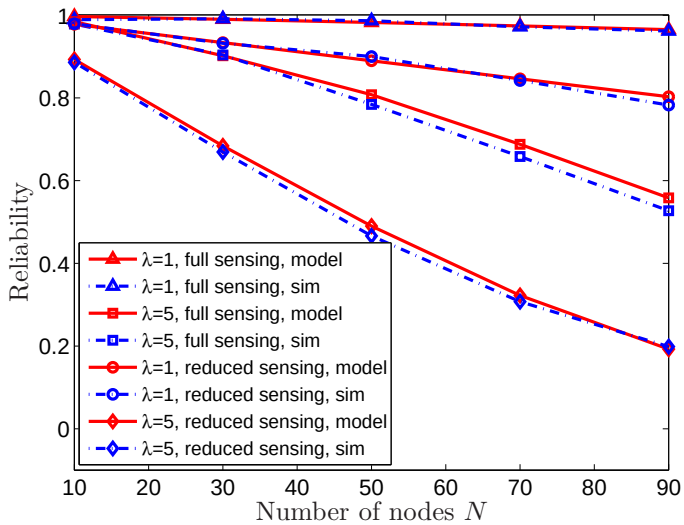

Figure 4.13: Reliability vs. number of nodes N for the single-hop topology in Figure 4.2(a). Full sensing and reduced sensing correspond to $|\Omega_l| = N$ and $|\Omega_l| = N/2$, respectively. The traffic rate λ is expressed in pkt/s.

sented in Section 4.3.5. In Figure 4.13, we show the average reliability for a single-hop network by varying the number of nodes N. We plot analytical results and simulation of the reliability by considering $\lambda_l = [1, 5]$ pkt/s, with full and reduced carrier sensing capabilities. There is a good agreement between the approximate model and the simulations. As the traffic increases, the performance degrades significantly with the number of nodes.

We conclude that heterogeneous traffic conditions and hidden terminals have significant and complex effects on each one of the performance indicators (reliability, delay, and energy consumption), and the effects are well predicted by our model both for small-scale and large-scale networks. In particular, dominant nodes, namely nodes with heavy forwarded traffic load, affect negatively the performance of the other nodes of the network. In the next section, we show how routing decisions are influenced by traffic, carrier sensing range and performance indicators in multi-hop networks.

4.5.2 MAC Performance over Multi-hop Networks

In this section, we validate the analysis for multi-hop networks. First, we consider the topology of Figure 4.2(b). Without loss of generality, we assume that every node generates the same traffic, but the forwarded traffic from every node varies as a consequence of the multi-hop routing. We focus on two cases, which we denote by *Path 1* and *Path 2*. In Path 1, we analyze the end-to-end reliability when node V_7 routes all its packets along the path V_4–V_1 to the root node V_0. In Path 2, V_7 forwards its packets along the path V_6–V_3. We also distinguish between non-interfering and interfering paths. In the former case, nodes along the two paths (Path 1 and Path 2) do not sense each other, with exception of the last hop to V_0. In the latter case, interference among path is determined by letting the carrier sensing range of nodes in a path include nodes in the other path, with exception of the last hop to V_0. The list of nodes in the carrier sensing range of each node for the two cases is reported in Table 4.5.

In Figure 4.14, we report the end-to-end reliability from node V_7 to the root node V_0, and the average end-to-end reliability of the whole network, by varying the node packet generation rate, when the two paths are non-interfering. From both analytical results and simulations, Path 2 outperforms Path 1 in terms of reliability, both from a single node and a network perspective, and the difference increases as the traffic increases. For $\lambda = 10$ pkt/s the gap between the two paths is 7–10%. In fact, Path 2 has lower forwarded traffic load than Path 1.

Figure 4.15 shows the end-to-end reliability of node V_7, and the average network reliability for analytical model and simulations when Path 1 and Path 2 are interfering. Compared to Figure 4.14, the result is different and the best performance in terms of reliability is now on Path 1, both from a node and a network perspective. The gap increases with the traffic and for $\lambda = 10$ pkt/s Path 1 outperforms Path 2 of 7–10%. Nodes in Path 1 result to be dominant in terms of traffic load and affect negatively the performance of nodes in Path 2. The reason is that the reliability

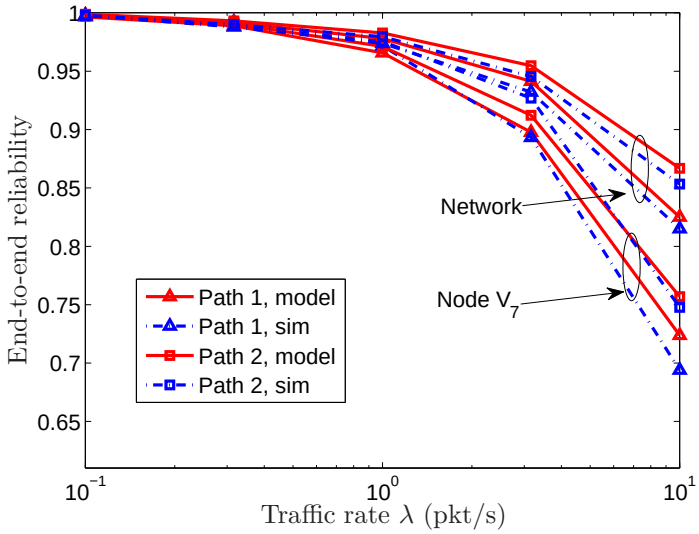

Figure 4.14: End-to-end reliability for non-interfering paths in the multi-hop topology in Figure 4.2(b). Path 1 is V_7-V_4-V_1-V_0, when the link V_7-V_6 is disabled. Path 2 is V_7-V_6-V_3-V_0, when the link V_7-V_4 is disabled. Notice the different scale on the y axis compared to the link reliability in Figures 4.6 and 4.9.

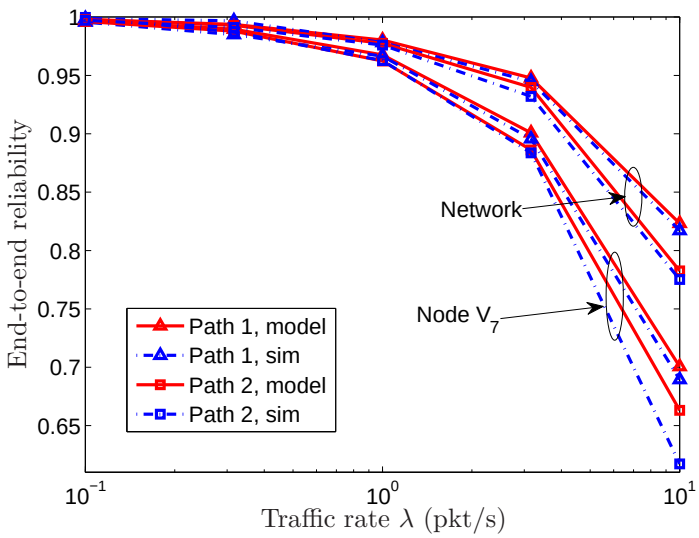

Figure 4.15: End-to-end reliability for interfering paths in the multi-hop topology in Figure 4.2(b). Path 1 is V_7-V_4-V_1-V_0, when the link V_7-V_6 is disabled. Path 2 is V_7-V_6-V_3-V_0, when the link V_7-V_4 is disabled.

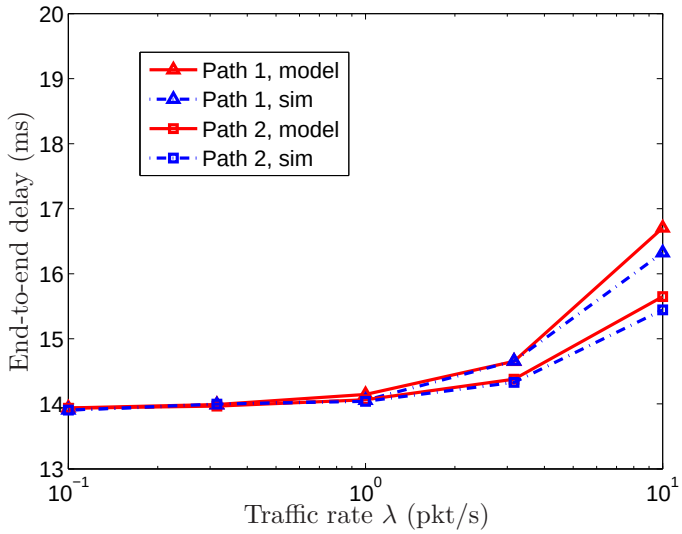

Figure 4.16: End-to-end delay for non-interfering paths in the multi-hop topology in Figure 4.2(b). Path 1 is V_7-V_4-V_1-V_0, when the link V_7-V_6 is disabled. Path 2 is V_7-V_6-V_3-V_0, when the link V_7-V_4 is disabled.

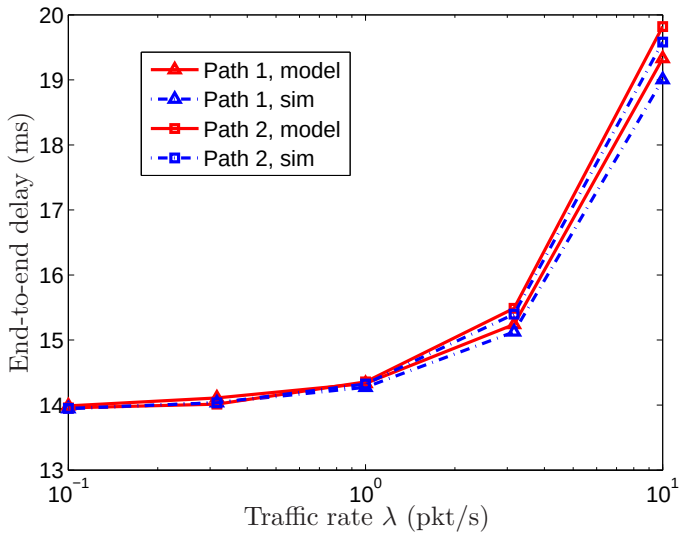

Figure 4.17: End-to-end delay for interfering paths in the multi-hop topology in Figure 4.2(b). Path 1 is V_7-V_4-V_1-V_0, when the link V_7-V_6 is disabled. Path 2 is V_7-V_6-V_3-V_0, when the link V_7-V_4 is disabled.

of a contention access scheme increases as the average number of contenders and hidden terminals in each time unit reduce. Consider a routing metric based only on on the maximization of the end-to-end reliability. If there is a strong interference in the network, the routing decision leads to unbalanced distribution of traffic load, because the routing layer forces the forwarded traffic flow to more dominant nodes, so that the average number of contenders in each time unit is lower. If not taken into account, this phenomenon can be catastrophic for the network and cause stability issues when considering limited node buffer size and energy constraints. On the other side, when stability and load balancing are not critical, dominant paths can be used to improve the end-to-end performance.

In Figure 4.16 and 4.17, the end-to-end delay from node V_7 to the root node V_0 is shown for non-interfering paths and interfering paths, respectively. Path 2 outperforms Path 1 when there is no interference among paths. For $\lambda = 10$ pkt/s, the gap between the two paths is 5–7%. Path 1 has a lower delay when the two paths are interfering. For $\lambda = 10$ pkt/s, the gap between the two paths is 3–5%. Similarly to the reliability analysis, if the routing metric is based only on the minimization of the end-to-end delay, and there is path interference, the result is an unbalanced traffic distribution towards dominant nodes. Once again, if not correctly taken into account, this could lead to negative effects on the network.

In the following, we show simulation results for the multi-hop topology in Figure 4.2(c). We consider multiple end-devices (V_4, V_5, V_6, and V_7) that can decide to route their packets either through nodes V_1, V_2, or V_3 to the destination V_0. The routing decision is based on the end-to-end reliability. We consider a dominant node V_2 that generates $\lambda_2 = 20$ pkt/s, whereas the rest of the network operates with traffic generation rate $\lambda_i = 5$ pkt/s. Similarly to the previous configuration, we distinguish between non-interfering and interfering paths. In the former case, the carrier sensing range of end-devices includes only the candidate parents. In the latter case, interference among path is determined by letting the carrier sensing range of all end-devices include all the other nodes in the network. The list of nodes in the carrier sensing range of each node for the two cases is reported in Table 4.5. In Figure 4.18, we show the resulting time evolution of the parent selection for each end-device in the network for non-interfering paths. The end-devices start from a random initial condition and explore the various routing paths to determine the next-hop node that guarantees the highest end-to-end reliability. Nodes use sliding windows to average the reliability in each iteration. In the case of non-interfering paths, nodes tend to distribute the traffic towards node V_1 and V_3, avoiding the dominant node V_2. In Figure 4.19, we show the time evolution of the parent selection when paths are interfering. In this situation nodes tend to concentrate the traffic towards the dominant node V_2. This result is consistent with the previous analysis for single end-device. The time evolution of the average end-to-end reliability is shown in Figure 4.20 both for non-interfering and interfering paths, where as a reference, the end-to-end reliability computed by the analytical model is reported.

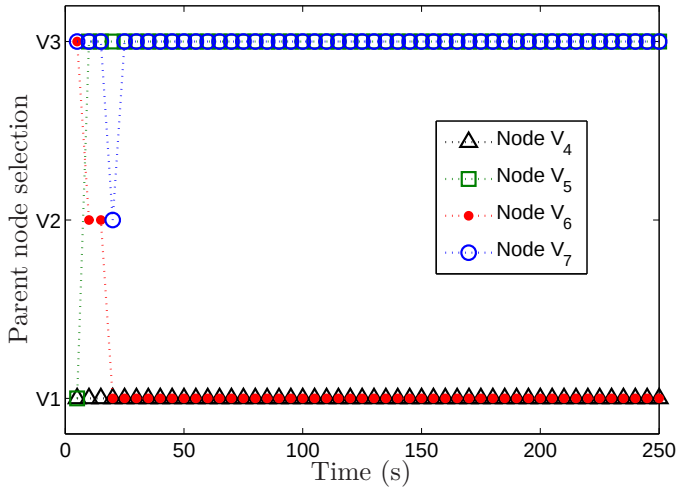

Figure 4.18: Parent node selection vs. time for non-interfering paths in the multi-hop topology in Figure 4.2(c).

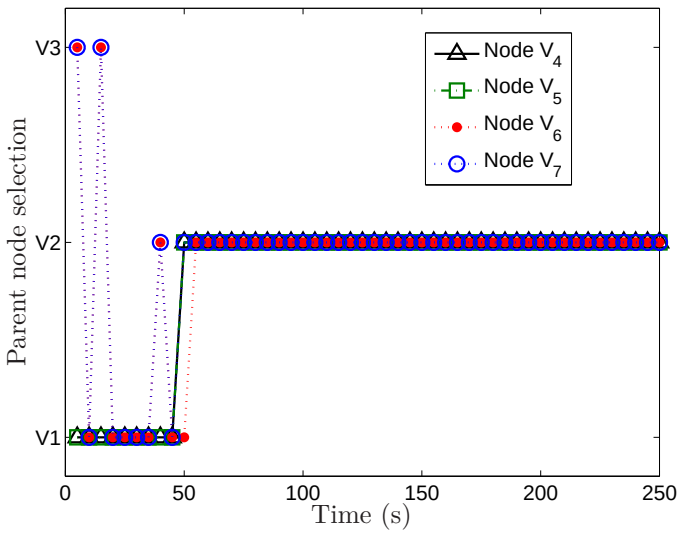

Figure 4.19: Parent node selection vs. time for interfering paths in the multi-hop topology in Figure 4.2(c).

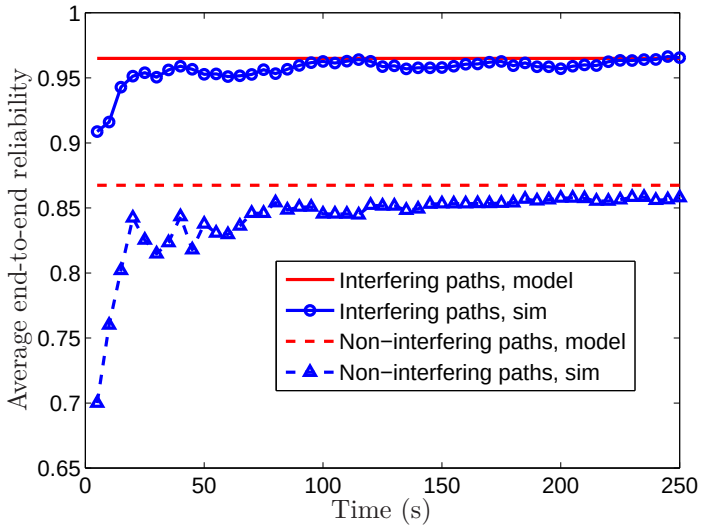

Figure 4.20: Average end-to-end reliability of V_4, V_5, V_6, and V_7 vs. time, for interfering and non-interfering paths in the multi-hop topology in Figure 4.2(c).

4.5.3 Effects of the Routing Metrics

In this section, we present experimental results related to the performance of the IETF RPL over the IEEE 802.15.4 MAC with the proposed metrics. The main target of our experimental evaluation study is to realistically prove that the proposed approach can greatly enhance the behavior of standard protocols.

The IEEE 802.15.4 protocol is implemented on a test-bed using the TelosB platform [111] running the Contiki OS [112], based on the specifications of the IEEE 802.15.4. IEEE 802.15.4 defines one backoff as 20 symbols that correspond to 320 μs for 2.45 GHz. Since the hardware timer available for TelosB is based on a 32768 Hz clock, we use a backoff with duration of 305 μs instead of 320 μs.

We assume that nodes are deployed and connected to form a DODAG as depicted in Figure 4.2(c), with full sensing (interfering paths). Each node generates the same traffic with rate $\lambda = [0.1 - 10]$ pkt/s, except V_2 that generates traffic with rate $\lambda_2 = 20$ pkt/s.

Figure 4.21 shows the end-to-end reliability as obtained by the mathematical model and the experiments when our proposed R-metric and Q-metrics are used. We depict the average reliability among nodes V_4–V_7 and the minimum path reliability achieved in the network. We observe that the experimental results are very close to the analytical results. When using the R-metric, nodes V_4–V_7 tend to forward their traffic through the dominant node V_2, which generates traffic $\lambda_2 = 20$ pkt/s, thus reducing the level of contention at the MAC layer. The level of con-

tention is measured as the probability that the channel is occupied by concurrent transmissions at the same time. Therefore, by concentrating the forwarded traffic to a single node, the level of contention reduces. When using our proposed Q-metric, nodes V_4–V_7 tend to distribute the traffic uniformly in the set of candidate receivers V_1–V_3 thus increasing the level of contention at MAC layer. The average end-to-end reliability of the network is then higher for the R-metric. However, by reducing the level of contention at the dominant nodes, the R-metric increases the level of contention for the communication paths that do not include the dominant nodes. Therefore, if the dominant node V_2 is not in the parent set of one of the nodes, its end-to-end reliability is affected significantly. In Figure 4.21, the minimum reliability for the R-metric is achieved for the path that includes V_4 and V_1. The reliability with the Q-metric does not vary significantly in the paths and the minimum reliability is only slightly lower than the average reliability and it is greater than the minimum reliability for the R-metric. In our experimental evaluation, the gap in the minimum reliability is around 5% for $\lambda = 10$ pkt/s and it increases as the traffic rate increases. We notice that, even though the R-metric achieves the best average performance from a network perspective, the Q-metric is preferable if a guaranteed reliability is required for all paths in the network (which is typically desired in networked control system applications).

In Figure 4.22, the end-to-end delay as obtained by the mathematical model and the experiments with R-metric and Q-metrics is presented. We visualize the average delay achieved for nodes V_4–V_7 and the maximum path delay in the network. By reducing the level of contention at the MAC layer, the average delay is lower when the R-metric is used. In the range of traffic rates analyzed, which is of interest for RPL applications [12], the queueing delay does not influence the performance significantly. Therefore, by concentrating the forwarded traffic to V_2, thus reducing the average level of contention in the network, the R-metric guarantees also a minimization of the average delay. However, the maximum delay, which is again achieved for the path that includes V_4 and V_1, is lower with the Q-metric. If there are delay deadlines for all nodes, as in the proposed network scenario, the Q-metric is preferable. The gain with the Q-metric is about 4% respect to the R-metric for $\lambda = 10$ pkt/s.

In Figure 4.23, we show the average power consumption of each node, by fixing $\lambda_i = 5$ pkt/s for $i \neq 2$ and $\lambda_2 = 20$ pkt/s. By choosing the dominant node V_2 as forwarder, the R-metric determines an unbalanced energy consumption. Node V_2 has a power consumption above 6 mW, while the rest of the network operates with 0.5 mW. With the Q-metric, the power consumption is more balanced among nodes and the maximum consumption, which is determinant for the network lifetime, decreases of at least a factor 2 respect to the R-metric.

4.5.4 MAC and Routing Protocol Selection

Now we turn our attention to show how complicated and inefficient the selection of the MAC parameters or routing metrics can be without considering the mutual

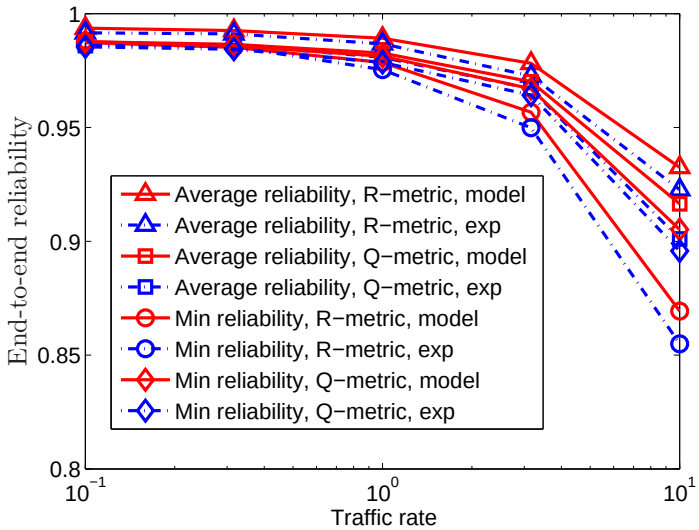

Figure 4.21: End-to-end reliability for the multi-hop topology in Figure 4.2(c). Average reliability is evaluated among nodes V_4–V_7. Minimum reliability is the average reliability of the worst case path.

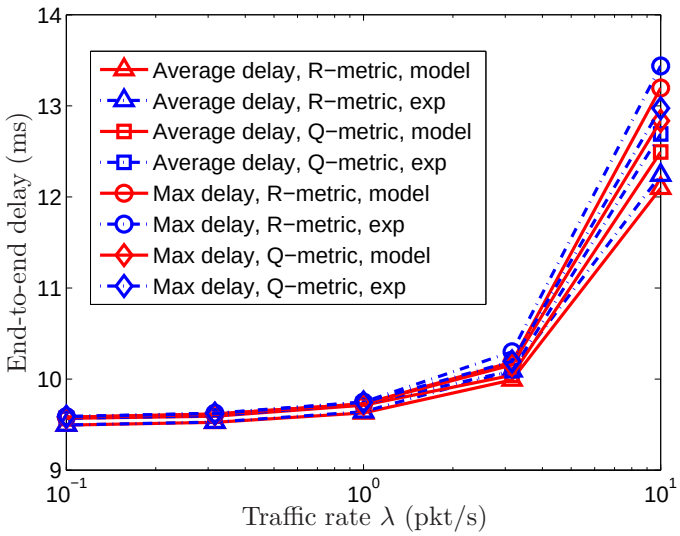

Figure 4.22: End-to-end delay for the multi-hop topology in Figure 4.2(c). Average delay is evaluated among nodes V_4–V_7. Maximum delay is the average delay of the worst case path.

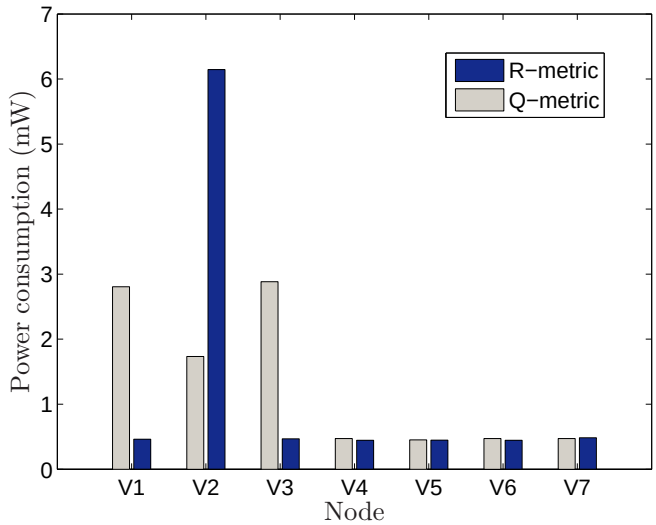

Figure 4.23: Average node power consumption for the multi-hop topology in Figure 4.2(c), by fixing $\lambda_i = 5$ pkt/s for $i \neq 2$ and $\lambda_2 = 20$ pkt/s.

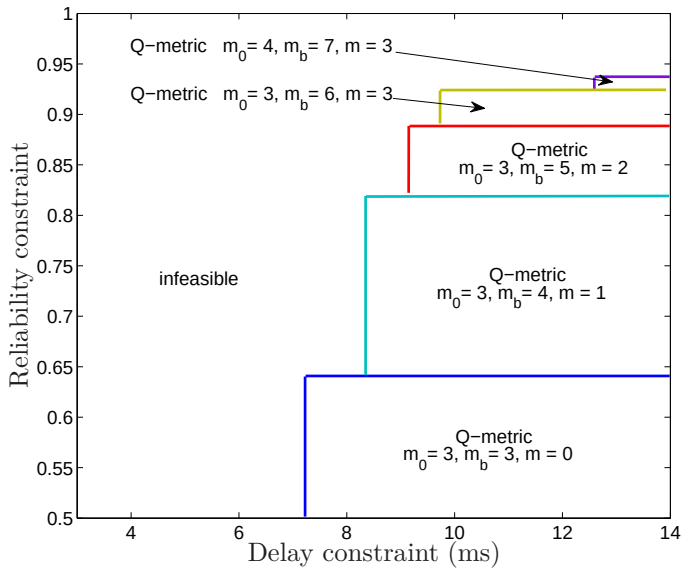

Figure 4.24: IEEE 802.15.4 MAC and RPL protocol parameters selection for the multi-hop network in Figure 4.2(c) by fixing $\lambda_i = 5$ pkt/s for $i \neq 2$ and $\lambda_2 = 20$ pkt/s.

interactions. In Figure 4.24, we report a protocol parameters selection for the multi-hop topology in Figure 4.2. The traffic rate is $\lambda_i = 5$ pkt/s for $i \neq 2$ and $\lambda_2 = 20$ pkt/s. We consider the unslotted IEEE 802.15.4 MAC and we let the protocol choose the initial backoff exponent $m_0 = [3 - 8]$, the maximum backoff exponent $m_b = [m_0 - 8]$, and the maximum number of backoffs $m = [0 - 4]$. Moreover, we apply RPL and we let the protocol choose between R-metric and Q-metric. The optimal protocol is defined as the one that maximizes the lifetime for certain reliability and delay constraints imposed by the application to all nodes, as reported on the x and y axis of the figure. The Q-metric is always preferred to the R-metric, whenever the solution is feasible. This is compliant with the analysis and experiments presented in the previous sections, since the constraints are for all nodes, and the objective is the minimization of the energy consumption of the dominant node. In general, an increase of the MAC parameters determines an increase in the energy consumption and in the delay. However, also the reliability increases. For a reliability constraint smaller than 65%, and delay constraint greater than 7.5 ms, the optimal MAC parameters are $m_0 = 3$, $m_b = 3$, and $m = 0$. However, the optimal parameters increase as the reliability constraint become stricter, as the solutions become unfeasible. For a reliability constraint above 90%, the feasible optimal solution is obtained by increasing both the number of backoffs m and the backoff windows m_0 and m_b. The node energy consumption related to $m_0 = 3$, $m_b = 3$, and $m = 0$ is about 20% lower than the consumption with default parameters $m_0 = 3$, $m_b = 8$, and $m = 4$. In addition, as we showed in Figure 4.23, the maximum energy consumption is halved as we choose the Q-metric over the R-metric. Therefore, by optimally selecting routing metric and MAC parameters according to the reliability and delay constraints, it is possible to obtain a significant impact on the performance.

4.6 Summary

In this chapter, we proposed a novel analysis of single-hop and multi-hop networks using the unslotted IEEE 802.15.4 MAC protocol. We introduced an accurate analytical model that includes heterogeneous traffic distribution, hidden terminal nodes, and queue length. An approximate model is also introduced and it is validated for large networks. We showed mutual influence between routing decisions and MAC performance in terms of reliability, delay and load balancing. We integrated the existing ETX metric in the reliability metric (R-metric) at the MAC layer. The R-metric achieves high average link reliability, but is not able to provide balanced reliability in the network. Considering that a minimum reliability or a maximum delay is required for all the nodes in the network, or the main objective is to minimize the lifetime of the network, we propose the Q-metric. The Q-metric achieves a fair distribution of the traffic and level of contention in the network, and outperforms the R-metric. To support our analysis we provide realistic experimental results. In the next chapter, we include channel models in the analysis.

Chapter 5

Modeling the Effects of Fading in Multi-hop Networks

The physical environment is critical for the performances of wireless networks. When sensors and actuators are immersed in the physical world, potential mobility of nodes, multi-hop networking, obstacles to the communication, and fading of the wireless channel must be carefully addressed to offer reliable services. Wireless interfaces can be bottlenecks as they do not provide solid links.

In this chapter, we propose a model of the cross-layer interactions of multi-hop IEEE 802.15.4 networks over wireless fading channels. Recalling the general flow diagram in Figure 4.1, we develop the inner loop between physical and MAC layers. The main original contributions are the following:

- We propose a generalized approach for the characterization of the MAC with heterogeneous traffic conditions and a composite Nakagami lognormal channel.
- Based on the new model, we determine the impact of fading conditions on the MAC performance under various settings for traffic, node distances, carrier sensing range, and signal-to-(interference plus noise)-ratio (SINR).
- We present situations in which a certain severity of the fading is beneficial for the performance with respect to the case of ideal channel. Based on the new model, it is then possible to optimize the overall network performance, by leveraging on the physical-MAC-routing layers interaction.

To determine the network operating point and the performance indicators in terms of reliability, packet delay, and energy consumption a moment matching approximation for the linear combination of lognormal random variables based on [127, 128] is adopted in combination with a Markov chain model of the MAC mechanism.

The challenging part of the new analytical setup in this chapter is to properly model the rather complex interaction between the MAC protocol and the wireless

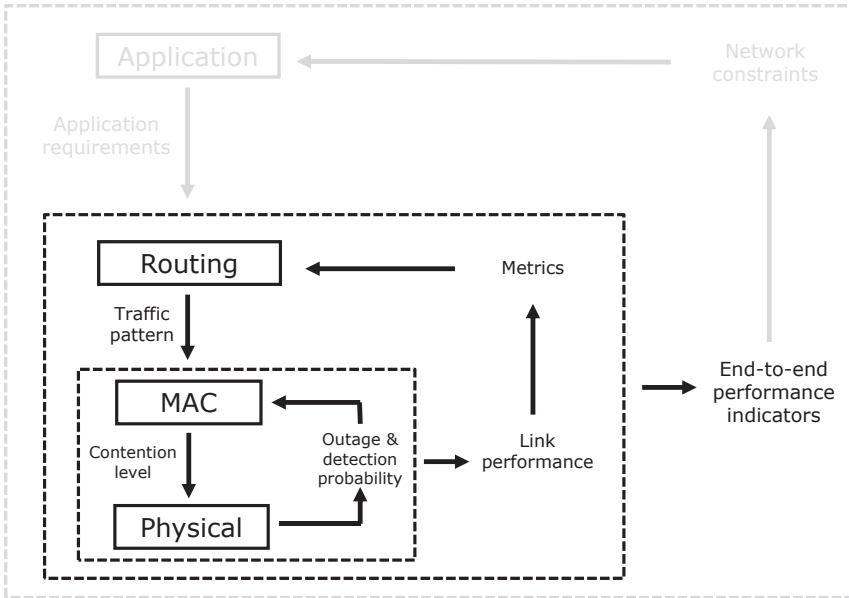

Figure 5.1: Interaction of layers for modeling and design: physical, MAC, and routing layers.

channel with explicit description of the dependence on several topological parameters and network dynamics. For example, we include failures of the channel sensing mechanism and the presence of hidden terminals. Whether two wireless nodes can communicate with each other depends on the relative distance, the transmission power, the wireless propagation characteristics and interference caused by concurrent transmissions on the same frequency: the higher the SINR, the higher the probability that packets can be successfully received. The number of concurrent transmissions depend on the traffic and the MAC parameters. We aim at describing how to account for statistical fluctuations of the SINR in the Markov chain model of the MAC of IEEE 802.15.4 networks.

The remainder of the chapter is organized as follows. In Section 5.1 we introduce the related work. In Section 5.2, we illustrate the system model. In Section 5.3, we derive model equations for IEEE 802.15.4 multi-hop networks over fading channels. The accuracy of the overall model is evaluated by Monte Carlo simulations in Section 5.4. A summary concludes the chapter. A list of symbols and acronyms is reported in Appendix F.

5.1 Related Work

Recent studies have investigated the presence of channel losses in IEEE 802.11 and IEEE 802.15.4 networks. In [129, 130], the optimal carrier sensing range is derived to maximize the throughput of IEEE 802.11 networks, however, statistical modeling of wireless fading has not been considered. In particular, a two-ray ground radio propagation model is used in [129], and only path-loss is considered in [129]. A cross-layer approach for the physical and MAC layers of IEEE 802.15.4 is proposed in [131]. Link quality indicators are used to tune the backoff strategy. In [132], packet losses due to fading channels have been introduced into the homogeneous Markov chain model of IEEE 802.15.4 MAC presented in [22]. However, fading is included only for single packet transmissions, the effect of contention and multiple access interference is neglected, and the analysis is validated neither by simulations nor by experiments. Recent studies have investigated the performance of multiple access networks in terms of multiple access interference and capture effect [133]. However, in [133] the model of the MAC mechanism is limited to homogeneous (same wireless channel for all nodes) single-hop networks with uniform random deployment, which is not a general case. Moreover, the fading caused by multi-path propagation and the presence of obstacles has not been considered, while it is known that it has a crucial impact on the performance of IEEE 802.15.4 [134].

5.2 System Model

We illustrate the system model by considering the three topologies reported in Figure 5.2. However, the analytical results that we derive are general and applicable to any topology.

The topology in Figure 5.2(a) refers to a single-hop (star) network where node i is deployed at distance $r_{i,0}$ from the root node at the center, and where nodes forward their packets with single-hop communication. The topology in Figure 5.2(b) is a multi-hop linear topology, where every node generates and forwards traffic to the root node by multi-hop communication. The distance between two adjacent nodes is denoted as $r_{i,j}$. In Figure 5.2(c), we depict a multi-hop topology with multiple end-devices that generate and forward traffic according to an uplink routing policy to the root.

We assume a natural inverse power model of the attenuation. Consider node i that is transmitting a packet with transmission power $P_{\mathrm{tx},i}$. The received power at node j, which is located at a distance $r_{i,j}$, is

$$P_{\mathrm{rx},i,j} = \frac{c_0 P_{\mathrm{tx},i}}{r_{i,j}^k} f_i \exp(y_i)\,. \tag{5.1}$$

The constant c_0 represents the attenuation at the reference distance 1 m, and it depends on factors such as carrier frequency and antennas. In the operating conditions for IEEE 802.15.4 networks, c_0 is determined in the range $40-60$ dB [7].

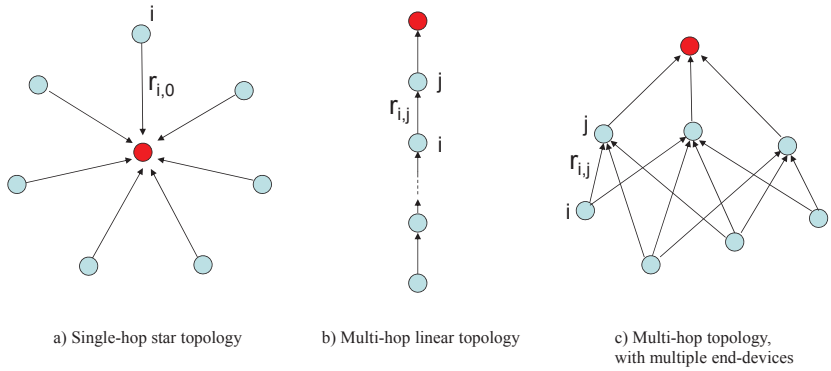

Figure 5.2: Example of topologies: single-hop star topology (on the left), multi-hop linear topology (in the center) and multi-hop topology with multiple end-devices (on the right)

The factor k is called path-loss exponent, and varies according to the propagation environment in the range $2-4$. The component f_i models the power attenuation due to multi-path propagation, which we assume to follow a Nakagami distribution with parameter $\kappa \geq 0.5$ and PDF

$$p_{f_i}(z) = \kappa^{\kappa} \frac{(z)^{\kappa-1}}{\Gamma(\kappa)} \exp(-\kappa z),$$

where $\Gamma(\kappa)$ is the standard Gamma function $\Gamma(\kappa) = \int_0^{\infty} \exp(-x)x^{\kappa-1}dx$. Recall that the Nakagami distribution is the most general because it models Rayleigh and Rice fadings. A random lognormal component models the shadow effect of obstacles, with $y_i = \mathcal{N}(0, \sigma_i^2)$. The standard deviation σ_i is called spread factor of the shadowing. This model is accurate for home or urban environments, in which nodes may not be in line of sight.

5.3 Model of IEEE 802.15.4 Multi-hop Networks with Fading Channels

In this section, we propose an extension of the Markov chain model in Chapter 4 to include the effects of multiple access interference due to the presence of multi-path propagation and shadow fading channels.

5.3.1 Markov Chain Model Equations

Consider the Markov chain in Figure 4.3, which describes the CSMA/CA algorithm for a transmitting node using the unslotted IEEE 802.15.4 MAC. In the following, we show how the state transition probabilities are affected by the presence of fading. For the link (i, j), we aim at deriving the probability α_i of sensing the channel busy during a CCA, and the probability $\gamma_{i,j}$ that a packet is lost due to combined effects of fading and the presence of concurrent transmissions.

We recall that the busy channel probability is obtained as the sum of two contributions

$$\alpha_i = \alpha_{\mathrm{pkt},i} + \alpha_{\mathrm{ack},i}, \tag{5.2}$$

where $\alpha_{\mathrm{pkt},i}$ is the probability that node i senses the channel and finds it occupied by an ongoing packet transmission, whereas $\alpha_{\mathrm{ack},i}$ is the probability of finding the channel busy due to ACK transmission.

The busy channel probability due to packet transmissions evaluated for node i is the combination of three events:

- at least one node accessed the channel in one of the previous L units of time;
- at least one of the nodes that accessed the channel found it idle and started a transmission;
- the total received power in node i is greater than a threshold a, so that the ongoing transmission is detected by node i.

The combinations of all busy channel events yields

$$\alpha_{\mathrm{pkt},i} = L\,\mathcal{H}_i\left(p_i^{\mathrm{det}}\right)\,, \tag{5.3}$$

where

$$\mathcal{H}_i(\chi) = \sum_{l=0}^{N-1}\sum_{j=1}^{C_{N,l}}\prod_{k=1}^{l+1}\tau_{k_j}\prod_{h=l+2}^{N}(1-\tau_{h_j})\sum_{m=0}^{k-1}\sum_{n=1}^{C_{k,l}}\prod_{q=1}^{m+1}(1-\alpha_{q_n})\,\chi\prod_{r=m+2}^{k}\alpha_{r_n}\,, \tag{5.4}$$

and

$$C_{k,l} = \binom{k-1}{l+1}.$$

The index k accounts for events of simultaneous accesses to the channel and the index j enumerates the combinations of events in which a number l of channel accesses are performed in the network simultaneously. Therefore, the index k_j refers to the node in the k-th position in the j-th combination of l out of $N-1$ elements (V_i is not included). The index q_n accounts for the combinations of events

in which one or more nodes find the channel idle simultaneously. Each term is weighted by the detection probability

$$p_i^{\text{det}} = \Pr\left[\sum_{q=1}^{m+1} P_{\text{rx},q_n,i} > a\right] . \tag{5.5}$$

The busy channel probability due to an ACK transmission follows by a similar derivation. However, an ACK is sent only after a successful packet transmission:

$$\alpha_{\text{ack},i} = L_{\text{ack}} \mathcal{H}_i \left((1 - \gamma_{q_n,w}) p_i^{\text{det}}\right) , \tag{5.6}$$

where L_{ack} is the length of the ACK. The index w denotes the destination node of q_n in the expression of $\mathcal{H}_i$. The detection probability p_i^{det} is evaluated with respect to the set of destination nodes. By summing up Equations (5.3) and (5.6), we compute α_i in Equation (5.2).

We derive an expression for the packet loss probability $\gamma_{i,j}$, namely the probability that a transmitted packet from node i is not correctly detected in reception by node j, by using similar arguments as above.

A packet transmission is not detected in reception if there is at least one interfering node that starts the transmission at the same time and the signal-to-interference-and-noise-ratio (SINR) between the received power from the transmitter and the total interfering power plus the noise level N_0 is lower than a threshold b (outage). In the event of no active interferers, which occurs with probability 1-$\mathcal{H}_i(1)$, the packet loss probability is the probability that the signal-to-noise ratio (SNR) between the received power and the noise level is lower than b. Hence,

$$\gamma_{i,j} = (1 - \mathcal{H}_i(1))\, p_{i,j}^{\text{fad}} + \mathcal{H}_i \left(p_{i,j}^{\text{out}}\right) + (2\,L - 1)\, \mathcal{H}_i \left(\left(1 - p_i^{\text{det}}\right) p_{i,j}^{\text{out}}\right) , \tag{5.7}$$

where $p_{i,j}^{\text{fad}}$ is the outage probability due to channel fading (with no interferers),

$$p_{i,j}^{\text{fad}} = \Pr\left[\frac{P_{\text{rx},i,j}}{N_0} < b\right] , \tag{5.8}$$

and $p_{i,j}^{\text{out}}$ is the outage probability in the presence of interferers,

$$p_{i,j}^{\text{out}} = \Pr\left[\frac{P_{\text{rx},i,j}}{\sum_{q=1}^{m+1} P_{\text{rx},q_n,j} + N_0} < b\right] . \tag{5.9}$$

We derive these probabilities next.

5.3.2 Model of Aggregate Multi-path Shadowed Signals

In this section, we approach the problem of computing the sum of multi-path shadowed signals that appears in the detection and the outage probabilities.

Consider node i performing a CCA. Let us focus our attention on the detection probability in transmission $\Pr\left[\sum_{n=1}^{x} P_{\mathrm{rx},n,i} > a\right]$, where x is the current number of active nodes in transmission. By recalling the power attenuation model in Equation (5.1), we define the random variable

$$Y_i = \ln\left(\sum_{n=1}^{x} A_{i,n}\exp(y_n)\right),$$

where

$$A_{i,n} = c_0 \frac{P_{\mathrm{tx},n}}{r_{n,i}^k} f_n,$$

and $y_n \sim \mathcal{N}(0,\sigma_n^2)$. Since a closed form expression of the probability distribution function of Y_i does not exist, we resort to a useful approximation instead. In order to characterize Y_i, we apply the Moment Matching (MMA) method, which approximates the statistics of linear combination of lognormal components to a lognormal random variable, such that $Y_i \sim \mathcal{N}(\eta_{Y_i}, \sigma_{Y_i}^2)$.

According to the MMA method, η_{Y_i} and σ_{Y_i} can be obtained by matching the first two moments of $\exp(Y_i)$ with the first two moments of $\sum_{n=1}^{x} A_{i,n}\exp(y_n)$, i.e.,

$$M_1 \triangleq \exp\left(-\eta_{Y_i} + \frac{1}{2}\sigma_{Y_i}\right) = \sum_{n=1}^{x} E\{A_{i,n}\}\exp\left(\eta_{y_n} + \frac{1}{2}\sigma_{y_n}\right), \tag{5.10}$$

$$\begin{aligned} M_2 \triangleq \exp\left(-2\eta_{Y_i} + 2\sigma_{Y_i}\right) &= \sum_{m=1}^{x}\sum_{n=1}^{x} E\{A_{i,m}A_{i,n}\} \\ &\times \exp\left(\eta_{y_m} + \eta_{y_n} + \left(\frac{\sigma_{y_m}^2}{2} + \frac{\sigma_{y_n}^2}{2} + \rho_{y_m,y_n}\sigma_{y_m}\sigma_{y_n}\right)\right). \end{aligned} \tag{5.11}$$

Solving Equations (5.10) and (5.11) for η_{Y_i} and σ_{Y_i} yields $\eta_{Y_i} = 0.5\ln(M_2) - 2\ln(M_1)$, and $\sigma_{Y_i}^2 = \ln(M_2) - 2\ln(M_1)$. It follows that

$$p_i^{\mathrm{det}} = \Pr\left[\sum_{n=1}^{x} P_{\mathrm{rx},n,i} > a\right] = \Pr\left[\exp(Y_i) > a\right] \approx Q\left(\frac{\ln(a) - \eta_{Y_i}}{\sigma_{Y_i}}\right), \tag{5.12}$$

where

$$Q(z) = \frac{1}{\sqrt{2\pi}}\int_z^{\infty} \exp\left(-\frac{\nu^2}{2}\right) d\nu.$$

Similar derivations follow for the outage probability in reception:

$$\Pr\left[\frac{P_{\mathrm{rx},i,j}}{\sum_{q=1}^{x} P_{\mathrm{rx},q_n,j} + N_0} < b\right]$$

$$= \Pr\left[f_i \left(\sum_{n=1}^{x} \frac{P_{\mathrm{tx},n} r_{i,j}^k}{P_{\mathrm{tx},i} r_{n,j}^k} f_n \exp(y_n - y_i) + \frac{N_0 r_{i,j}^k}{P_{\mathrm{tx},i}} f_n \exp(-y_i) \right)^{-1} < b \right].$$

We define the random variable

$$\tilde{Y}_{i,j} = -\ln\left(\sum_{n=1}^{x+1} B_{i,j,n} \exp(\tilde{y}_n) \right),$$

where

$$B_{i,j,n} = \begin{cases} \frac{P_{\mathrm{tx},n} r_{i,j}^k}{P_{\mathrm{tx},i} r_{n,j}^k} f_n & \text{for} \quad n = 1, ..., x \\ \frac{N_0 r_{i,j}^k}{P_{\mathrm{tx},i}} f_n & \text{for} \quad n = x+1 \end{cases},$$

and

$$\tilde{y} = \begin{cases} y_n - y_i & \text{for} \quad n = 1, ..., x \\ -y_i & \text{for} \quad n = x+1 \end{cases}.$$

According to the MMA method, we approximate $\tilde{Y}_i \sim \mathcal{N}(\eta_{Y_i}, \sigma_{Y_i}^2)$, where $\eta_{\tilde{Y}_{i,j}}$ and $\sigma_{\tilde{Y}_{i,j}}$ can be obtained by matching the first two moments of $\exp(\tilde{Y}_i)$ with the first two moments of $\sum_{n=1}^{N} B_{i,j,n} \exp(\tilde{y}_n)$, i.e.,

$$\tilde{M}_1 \triangleq \exp\left(-\eta_{\tilde{Y}_{i,j}} + \frac{1}{2}\sigma_{\tilde{Y}_{i,j}} \right) = \sum_{n=1}^{x+1} E\{B_{i,j,n}\} \exp\left(\eta_{\tilde{y}_n} + \frac{1}{2}\sigma_{\tilde{y}_n} \right),$$

$$\tilde{M}_2 \triangleq \exp\left(-2\eta_{\tilde{Y}_{i,j}} + 2\sigma_{\tilde{Y}_{i,j}} \right) = \sum_{m=1}^{x+1} \sum_{n=1}^{x+1} E\{B_{i,j,m} B_{i,j,n}\}$$
$$\times \exp\left(\eta_{\tilde{y}_m} + \eta_{\tilde{y}_n} + \left(\frac{\sigma_{\tilde{y}_m}^2}{2} + \frac{\sigma_{\tilde{y}_n}^2}{2} + \rho_{\tilde{y}_m, \tilde{y}_n} \sigma_{\tilde{y}_m} \sigma_{\tilde{y}_n} \right) \right),$$

which yields $\eta_{\tilde{Y}_{i,j}} = 0.5 \ln(\tilde{M}_2) - 2\ln(\tilde{M}_1)$, $\sigma_{\tilde{Y}_{i,j}}^2 = \ln(\tilde{M}_2) - 2\ln(\tilde{M}_1)$. Therefore,

$$p_{i,j}^{\mathrm{out}} = \Pr\left[f_i \exp(\tilde{Y}_{i,j}) < b \right] = \int_0^b \int_0^\infty p_f(z|w) p_{\exp(\tilde{Y}_{i,j})}(w) dw\, dz$$
$$= \int_0^b \int_0^\infty p_f(z|w) \frac{1}{\sqrt{2\pi}\sigma_{\tilde{Y}_{i,j}} w} \exp\left(-\frac{(\ln(w) - \eta_{\tilde{Y}_i})^2}{2\sigma_{\tilde{Y}_i}^2} \right) dw\, dz\,. \qquad (5.13)$$

The analysis above holds for a generic weighted composition of lognormal fading. In the case of Lognormal channel, where only shadow fading components are considered, (i.e., $f_i = 1$), the outage probability becomes

$$p_{i,j}^{\mathrm{out}} = \Pr\left[\exp(\tilde{Y}_{i,j}) < b \right] \approx 1 - Q\left(\frac{\ln(b) - \eta_{\tilde{Y}_{i,j}}}{\sigma_{\tilde{Y}_{i,j}}} \right).$$

For a Nakagami-lognormal channel, the outage probability becomes

$$p_{i,j}^{\text{out}} = \int_0^b \int_0^\infty \kappa^\kappa \frac{(zw)^{\kappa-1}}{\Gamma(\kappa)} \exp(-\kappa z w) \frac{1}{\sqrt{2\pi}\sigma_{\tilde{Y}_{i,j}} w} \exp\left(-\frac{(\ln(w)-\eta_{\tilde{Y}_i})^2}{2\sigma_{\tilde{Y}_i}^2}\right) dw\, dz$$
$$= \int_0^\infty \frac{1}{\sqrt{2\pi}\sigma_{\tilde{Y}_{i,j}} w} \exp\left(-\frac{(\ln(w)-\eta_{\tilde{Y}_i})^2}{2\sigma_{\tilde{Y}_i}^2}\right) \int_0^b \kappa^\kappa \frac{(zw)^{\kappa-1}}{\Gamma(\kappa)} \exp(-\kappa z w) dz\, dw\,.$$

For integer values of m, the integration in z yields

$$p_{i,j}^{\text{out}} = 1 - \int_0^\infty \frac{1}{\sqrt{2\pi}\sigma_{\tilde{Y}_{i,j}} w} \exp\left(-\frac{(\ln(w)-\eta_{\tilde{Y}_i})^2}{2\sigma_{\tilde{Y}_i}^2}\right) \sum_{i=0}^{\kappa-1} \frac{(\kappa\, b\, w)^i}{\Gamma(i+1)} \exp(-\kappa\, b\, w) dw\,.$$

The mean and standard deviation of Y_i and $\tilde{Y}_{i,j}$ can be obtained by inserting the moments of f_i in the moments of $A_{i,n}$ and $B_{i,j,n}$. For Gamma distributed components f_i, it results $E\{f_i\} = 1$ and $E\{f_i^2\} = \frac{\kappa+1}{\kappa}$.

5.3.3 Integrated Physical, MAC, and Routing Model

We illustrate the integrated model of physical, MAC, and routing layer by referring to the block diagram in Figure 5.1. The routing layer determines the distribution of the traffic in the network by Equation (4.21). The traffic distribution is associated with the packet generation probability in each link q_l, which affects directly the channel access probability τ_i in Equation (4.1) at the MAC layer. The MAC layer generates a certain level of contention in the channel described by the busy channel probability α_i in Equation (4.3) and the packet loss probability $\gamma_{i,j}$ in Equation (5.7). The effects of the channel are included in the analysis by considering the detection probability p_i^{det} in Equation (5.12) and the outage probability $p_{i,j}^{\text{out}}$ in Equation (5.13). We obtain a system of non-linear equations that can be solved through iterative numerical methods [109].

We remark here that the evaluation of p_i^{det}, and $p_{i,j}^{\text{out}}$ can be carried out off-line, with respect to the solution of the system of non-linear equations to derive τ_l α_i and $\gamma_{i,j}$. Therefore, the proposed model can be implemented with a slight increase of complexity with respect to the analytical model presented in Chapter 4 and the computation time is not affected significantly (see Appendix C).

Finally, the expressions of the reliability, the delay, and the energy consumption can be derived by Equations (4.9), (4.10), and (4.17), respectively.

5.4 Performance Results

In this section, we present numerical results that have been obtained for various settings for network topology and operations by the developed model. Moreover, we illustrate extensive Monte Carlo simulations to validate the accuracy of the approximations that we have introduced in the model. The settings are based on

the specifications of the IEEE 802.15.4 standard [7]. We perform simulations both for single-hop and multi-hop topologies.

5.4.1 Single-hop Topologies

In this set of performance results, we consider a single-hop star topology as in Figure 5.2(a). We set the number of nodes $N = 7$, the MAC parameters $m_0 = 3$, $m = 4$, $m_b = 7$, $n = 0$, $L = 7$, $L_{\text{ack}} = 2$, and the physical layer parameters $P_{\text{tx},i} = 0$ dBm and $k = 2$. We validate our model and evaluate the performance of the network by varying the traffic rate $\lambda_i = \lambda$, $i = 1, ..., N$, in the range $[0.1 - 10]$ pkt/s, the radius $r_{i,0} = r$, $i = 1, ..., N$, in the range $[0.1 - 10]$ m, the spread of the shadow fading $\sigma_i = \sigma$, $i = 1, ..., N$, in the range $[0 - 6]$, and the Nakagami parameter κ in the range $[1 - 3]$. Moreover, we show results for different values of the carrier sensing threshold $a = -[76, 66, 56]$ dBm, and outage threshold $b = [6, 10, 14]$ dB.

In Figure 5.3, we report the average reliability over all the links by varying the node traffic rate λ. The results are shown for different values of the spread σ in absence of multi-path ($f_i = 1$). There is a good matching between the simulations and the analytical model. The reliability decreases as the traffic increases. An increase of the traffic generates an increase of the contention level at MAC layer. However, the impact of the shadow fading is dominant with respect to variations of traffic. In Figure 5.4, the average delay over all the links is reported. The simulation results follow well the predicted results from the model. An increase of traffic leads to an increase of the average delay due to the greater number of channel contentions and consequently number of backoffs. The spread of the fading does not impact on the delay significantly, particularly for low traffic, because lost packets due to fading are not accounted in the computation of the delay. When the traffic increases, we note that fading is actually beneficial for the delay. In fact, the delay of successfully received packets reduces by increasing σ. This is because the occurrence of a deep fading reduces the probability of successful transmission. However, since this holds for all nodes, the average number of contending nodes for the CCA reduces, thus reducing the average delay of successfully received packets. It is not possible to capture this network behavior by using separate models of MAC and physical layers as in the previous literature, since this effect depends on a cross-layer interaction. In Figure 5.5, the average power consumption over all the links is presented and compared to the analytical expression in Equation (4.17). The number of packet transmissions and ACK receptions is the major source of energy expenditure in the network. Therefore, an increase of the traffic leads to an increase of the power consumption, while performance are marginally affected by the spread of the fading. However, the power consumption is slightly reduced when the spread is $\sigma = 6$, due to the lower number of received ACKs.

In Figure 5.6, the average reliability is reported as a function of the radius r for different values of the spread σ. Again, in this case the analytical results are in good agreement with those provided by simulations. For the ideal channel case (i.e., $\sigma = 0$) the size of the network does not affect the reliability in the range

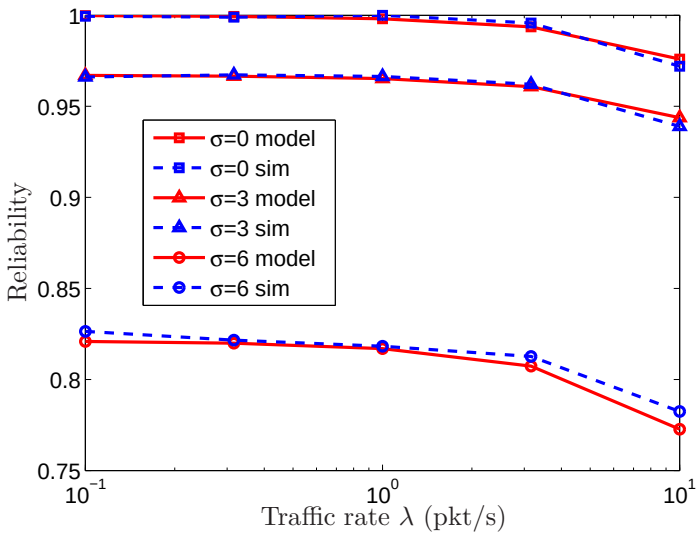

Figure 5.3: Reliability vs. traffic rate λ for the star network in Figure 5.2(a) with $N = 7$ nodes, $r = 1$ m, $a = -76$ dBm, $b = 6$ dB.

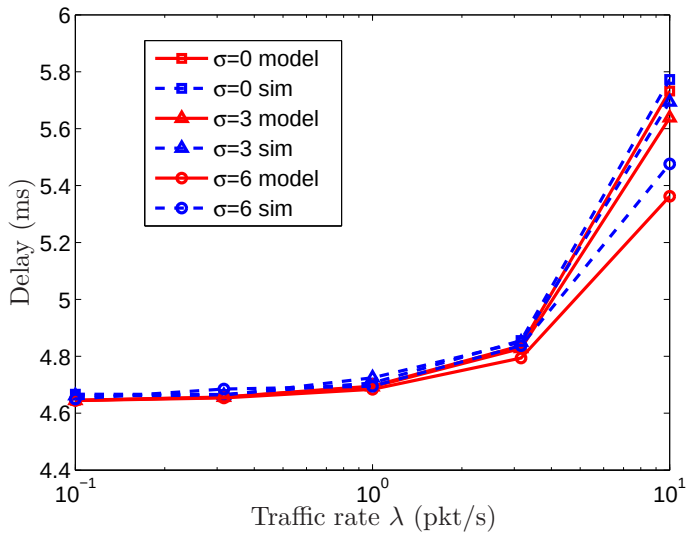

Figure 5.4: Delay vs. traffic rate λ for the star network in Figure 5.2(a) with $N = 7$ nodes, $r = 1$ m, $a = -76$ dBm, $b = 6$ dB.

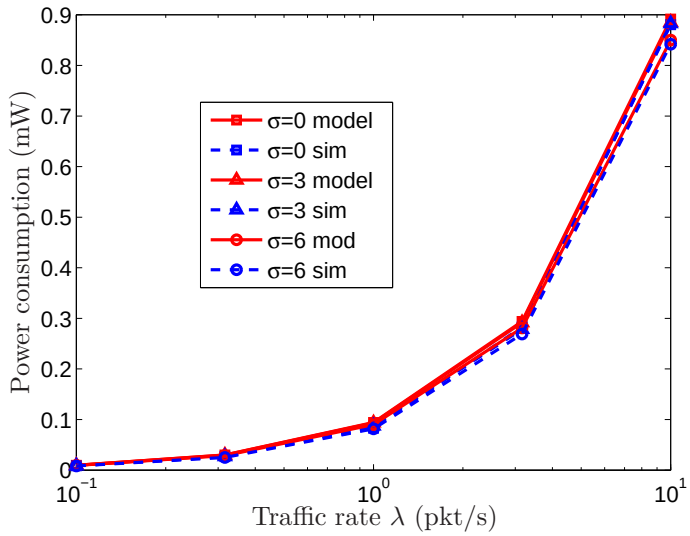

Figure 5.5: Power consumption vs. traffic rate λ for the star network in Figure 5.2(a) with $N = 7$ nodes, $r = 1$ m, $a = -76$ dBm, $b = 6$ dB.

$r = [0.1 - 10]$ m. For $\sigma = 6$, the performance degrades significantly as the radius increases. An intermediate behavior is obtained for $\sigma = 3$, where the reliability is comparable to the ideal channel case for a small size network but reduces for $r > 1$ m. The effect is the combination of an increase of the outage probability with the radius (due to the path-loss component), and hidden terminals that are not detected by the CCA. In Figure 5.7, we report the average delay by varying the radius r for different values of the spread σ. The fading affects the delay positively and the effect is more significant for large size networks. When nodes are more distant to each others, the average number of contending nodes for the free channel assessment reduces, thus the busy channel probability reduces, which in turn decreases the average delay of successfully received packets. In Figure 5.8, the average power consumption by varying r is presented. We notice a similar behavior as for the delay. The power consumption reduces with the fading and the increasing size of the network. Nodes spend less time in the backoff and channel sensing procedure due to reduced number of contenders, and the number of ACKs also reduces.

Figure 5.9 shows the average reliability as a function of the spread σ of the shadow fading. The results are plotted for different values of the carrier sense threshold a. The reliability decreases when the threshold a becomes larger. The impact of the variation of the threshold a is maximum for $\sigma = 0$, and the gap in the reliability reduces when the spread σ increases. In Figure 5.10, the average

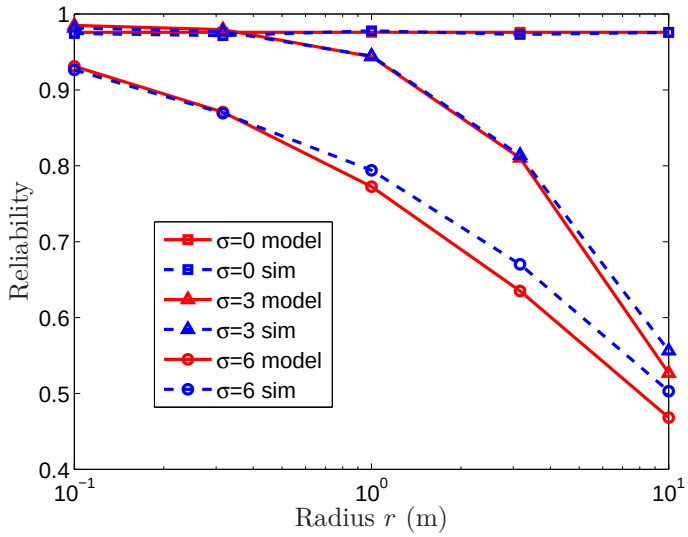

Figure 5.6: Reliability vs. radius r for the star network in Figure 5.2(a) with $N = 7$ nodes, $\lambda = 10$ pkt/s, $a = -76$ dBm, $b = 6$ dB.

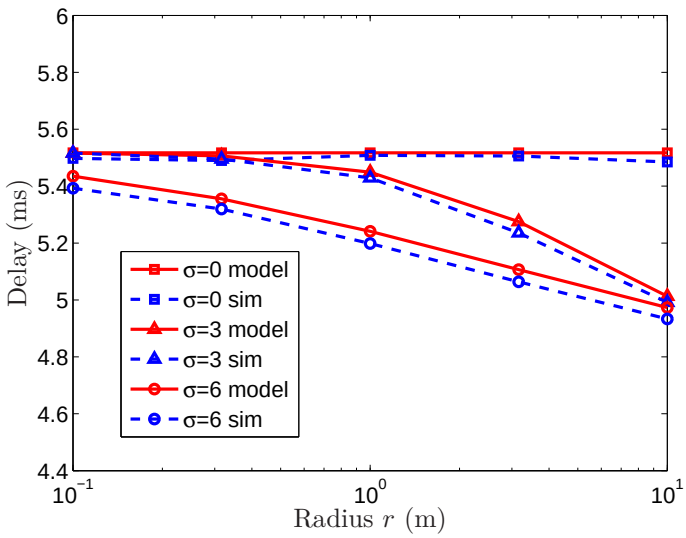

Figure 5.7: Delay vs. radius r for the star network in Figure 5.2(a) with $N = 7$ nodes, $\lambda = 10$ pkt/s, $a = -76$ dBm, $b = 6$ dB.

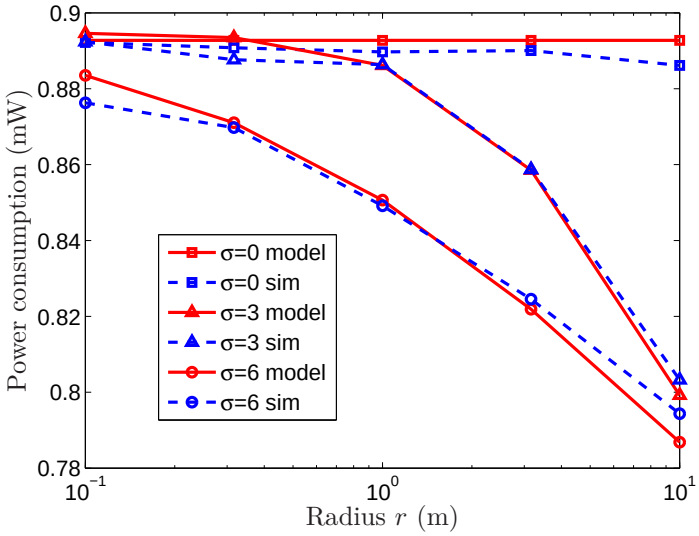

Figure 5.8: Power consumption vs. radius r for the star network in Figure 5.2(a) with $N = 7$ nodes, $\lambda = 10$ pkt/s, $a = -76$ dBm, $b = 6$ dB.

delay by varying the spread σ is reported. Depending on the threshold a, the delay shows a different behavior when increasing σ, it increases for $a = -76$ dBm, and it decreases for $a = -66$ dBm and $a = -56$ dBm. As we discussed above, the spread σ influences positively the delay. However, when the threshold is high, the average number of contenders is less influenced by the fading and does not decrease significantly, while the busy channel probability becomes dominant and the number of backoffs increases, so that the delay increases as well. Figure 5.11 reports the average power consumption by varying the spread σ. The power consumption reduces by increasing the threshold a as a consequence of the smaller number of ACK transmissions.

In Figure 5.12, we plot the average reliability as a function of the spread σ for different values of the outage threshold b. A different threshold b does not affect the performance noticeably for $\sigma = 0$ while the gap on the reliability increases with σ. Note that for high threshold the reliability tends to increase for small values of σ, and it decreases for high spread. In our setup, the maximum reliability is obtained for $\sigma \approx 2$.

In Figure 5.13, we report the combined effects of shadow fading and multi-path on the reliability. We show the reliability as a function of the spread σ of the shadow fading for different values of the Nakagami parameter κ. We recall that $\kappa = 1$ corresponds to a Rayleigh distribution of the fading. There is a good matching between the simulations and the analytical model. The effect of the

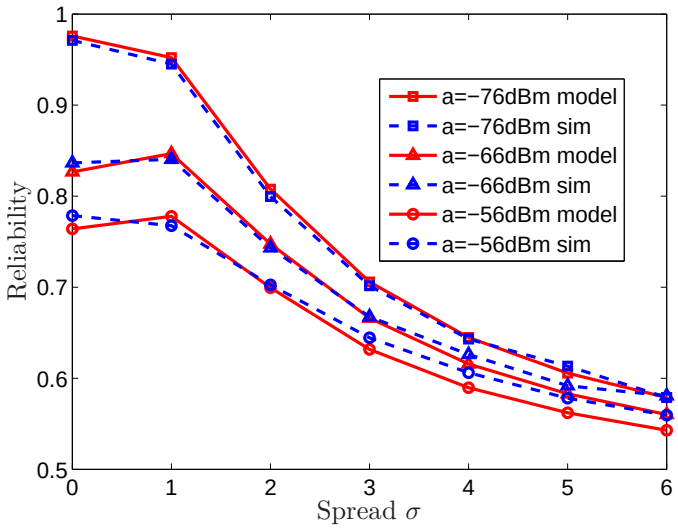

Figure 5.9: Reliability vs. σ for the star network in Figure 5.2(a) with $N = 7$ nodes, $r = 5$ m, $\lambda = 10$ pkt/s, $b = 6$ dB.

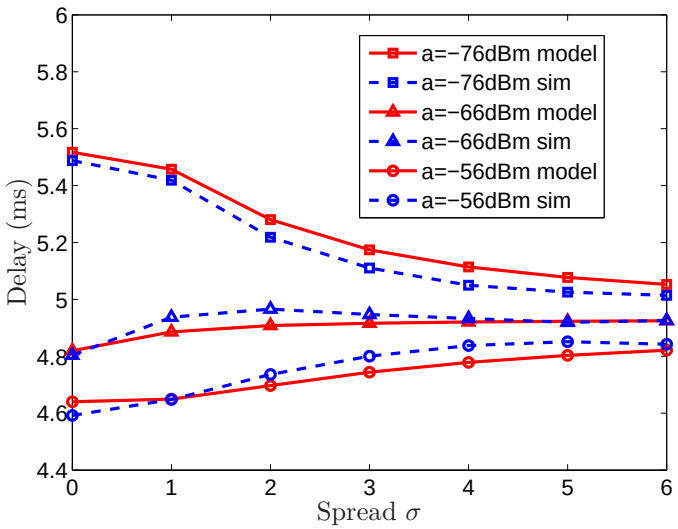

Figure 5.10: Delay vs. σ for the star network in Figure 5.2(a) with $N = 7$ nodes, $r = 5$ m, $\lambda = 10$ pkt/s, $b = 6$ dB.

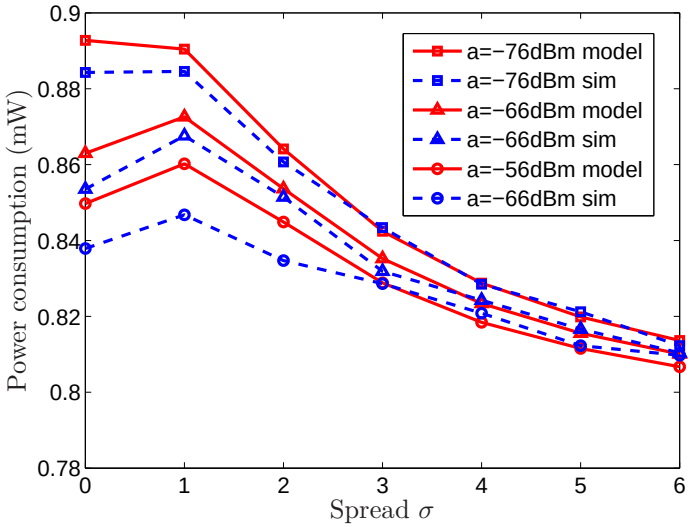

Figure 5.11: Power consumption vs. σ for the star network in Figure 5.2(a) with $N = 7$ nodes, $r = 1$ m, $\lambda = 10$ pkt/s, $b = 6$ dB.

multi-path is a degradation of the reliability. However, the impact reduces as the Nakagami parameter κ increases. In fact, for $\kappa \gg 1$, the effect of multi-path becomes negligible.

5.4.2 Multi-hop Linear Topologies

In this set of performance results, we consider a multi-hop linear topology as in Figure 5.2(b). We set the number of nodes and hops $N = 5$, with same MAC and physical layer parameters as in the single-hop case. We validate our model and study the performance of the network as a function of the hop distance $r_{i,j}$ in the range $r = [0.1 - 10]$ m, and the spread of the shadow fading in the range $\sigma = [0 - 6]$. We show results for each hop, and for different values of the carrier sensing threshold $a = -[76, 66, 56]$ dBm, and outage threshold $b = [6, 10, 14]$ dB.

In Figure 5.14, the end-to-end reliability is reported from each node to the destination node for different values of the spread σ. The analytical model follows well the simulation results. The end-to-end reliability decreases with the hop number and this effect is amplified by the presence of the fading. Figure 5.15 shows the end-to-end reliability from the farthest node to the destination by varying the distance r between two adjacent nodes for different values of the spread σ. The reliability is very sensitive to an increase of hop distance due to fading and hidden nodes. In Figure 5.16, we show the end-to-end reliability by varying the spread σ

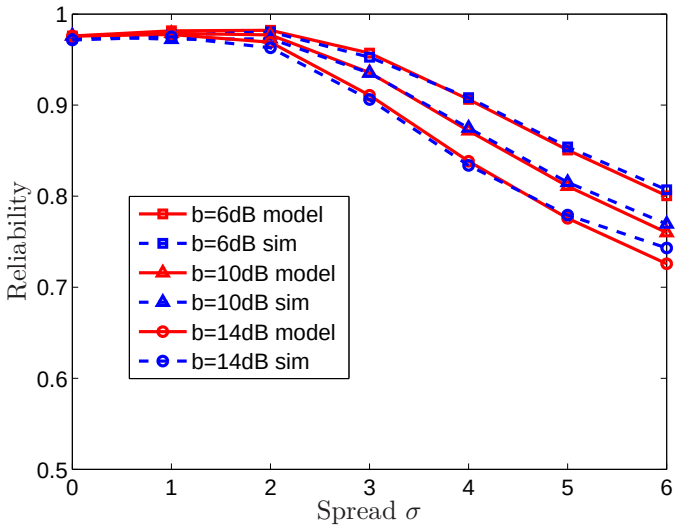

Figure 5.12: Reliability vs. σ for the star network in Figure 5.2(a) with $N = 7$ nodes, $r = 1$ m, $\lambda = 10$ pkt/s, $a = -76$ dB.

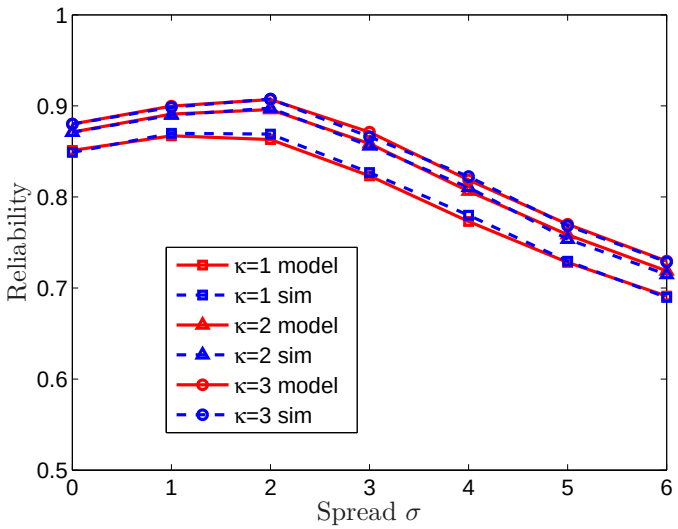

Figure 5.13: Reliability vs. σ for the star network in Figure 5.2(a) with $N = 7$ nodes, $r = 1$ m, $\lambda = 5$ pkt/s, $a = -56$ dB, $b = 6$ dB.

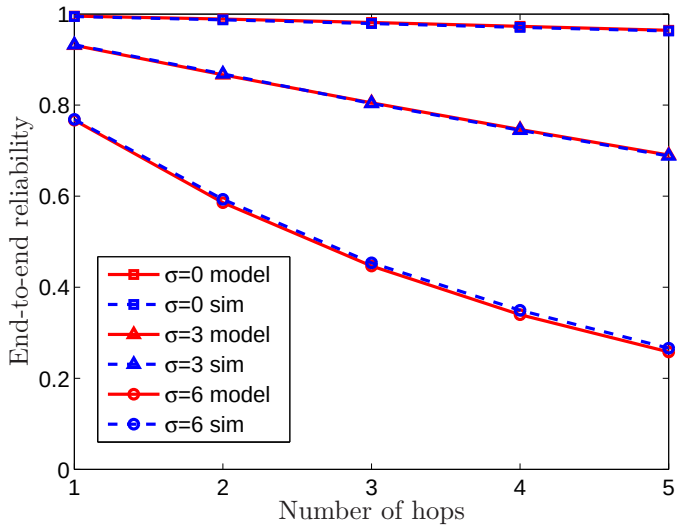

Figure 5.14: End-to-end reliability vs. number of hops for the linear topology in Figure 5.2(b) with $N = 5$ nodes, $r = 1$ m, $\lambda = 2$ pkt/s, $a = -76$ dBm, $b = 6$ dB.

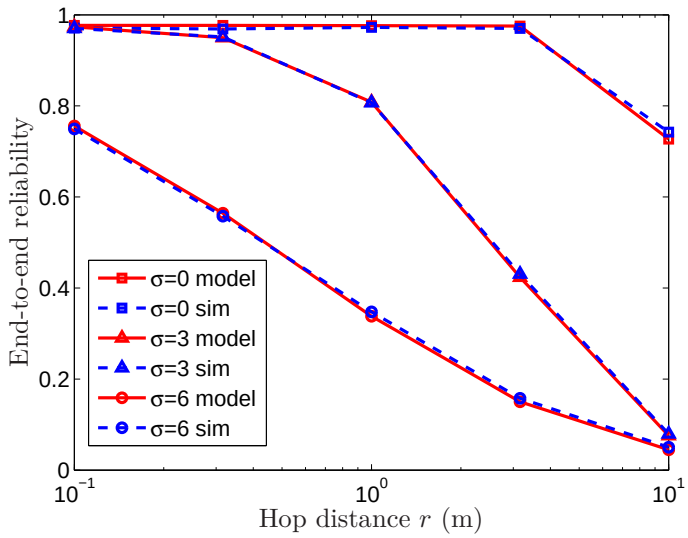

Figure 5.15: End-to-end reliability vs. hop distance r for the linear topology in Figure 5.2(b) with $N = 5$ nodes, $\lambda = 2$ pkt/s, $a = -76$ dBm, $b = 6$ dB.

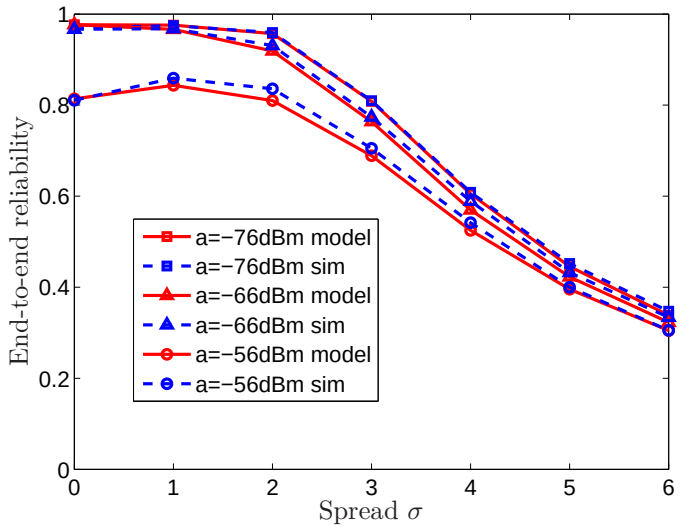

Figure 5.16: End-to-end reliability vs. σ for the linear topology in Figure 5.2(b) with $N = 5$ nodes, $r = 1$ m, $\lambda = 2$ pkt/s, $b = 6$ dB.

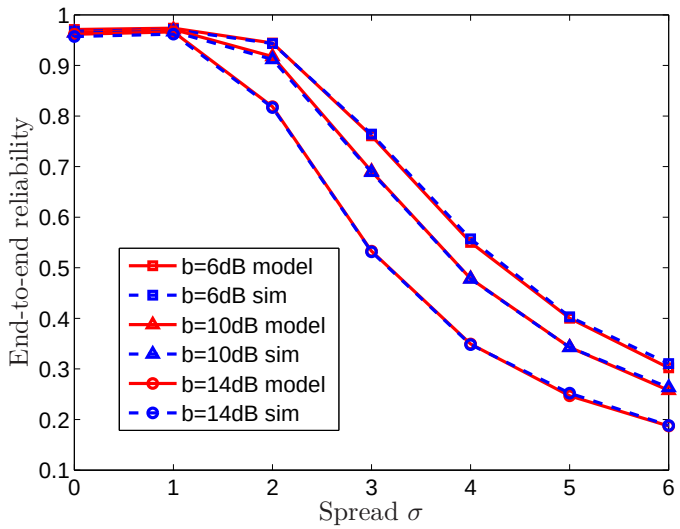

Figure 5.17: End-to-end reliability vs. σ for the linear topology in Figure 5.2(b) with $r = 1$ m, $\lambda = 2$ pkt/s, $a = -76$ dBm.

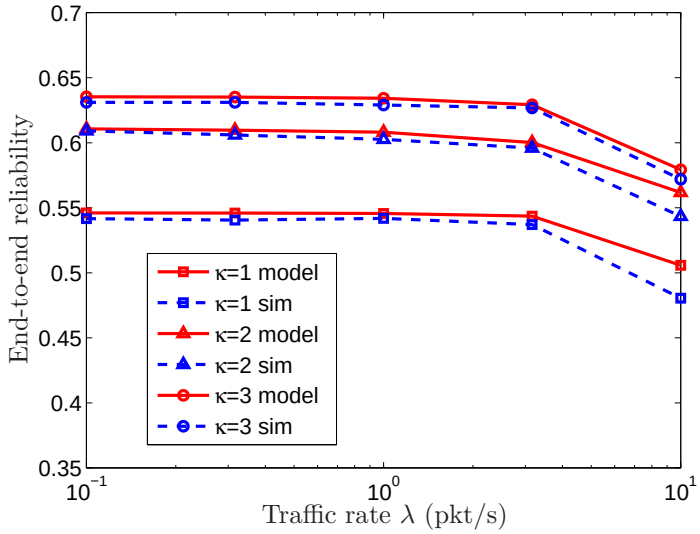

Figure 5.18: End-to-end reliability vs. traffic rate λ for the multi-hop topology in Figure 5.2(c) with $a = -76$ dB, $b = 6$ dB, $\sigma = 6$.

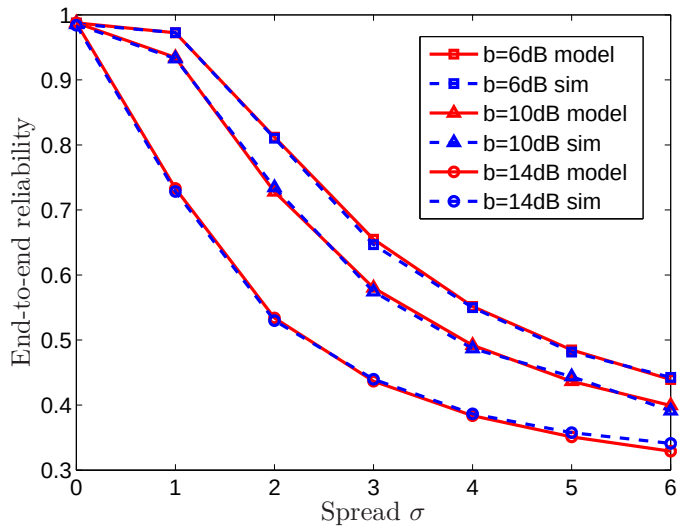

Figure 5.19: End-to-end reliability vs. σ for the multi-hop topology in Figure 5.2(c) with $\lambda = 2$ pkt/s, $a = -76$ dB.

of the shadow fading. Results are shown for different values of the carrier sense threshold a. In Figure 5.17, we plot the end-to-end reliability for different values of b. Similar considerations as for the single-hop case applies here. However, for the linear topology, the reduction of the carrier sensing range from $a = -76$ dBm to $a = -66$ dBm impacts less on the reliability since hidden nodes are often out of the communication range of the receiver (next-hop node), therefore the channel detection failure may not lead to collisions.

5.4.3 Multi-hop Topologies with Multiple End-devices

We consider a multi-hop topology as in Figure 5.2(c). We set the same MAC and physical layer parameters as in the single-hop case. We consider the end-to-end reliability as the routing metric and we study the performance of the network as a function of the traffic $\lambda_i = \lambda$, $i = 1, ..., N$, in the range $[0.1 - 10]$ pkt/s, the spread of the shadow fading in the range $\sigma = [0 - 6]$. Moreover, we show results for different values of the Nakagami parameter $\kappa = [1 - 3]$ and threshold $b = [6, 10, 14]$ dB.

In Figure 5.18, we report the average end-to-end reliability over all the end-devices by varying the node traffic rate. The results are shown for different values Nakagami parameter κ for spread of the shadow fading $\sigma = 6$. The impact of the Nakagami parameter κ is dominant with respect to a variation of traffic. Figure 5.19 shows the end-to-end reliability by varying the spread σ for different values of b. Differently respect to the single-hop and linear cases, a variation of the outage threshold b has a strong impact on the reliability also for small value of the spread. In fact, due to the geometry of the topology with variable distance between each source-destination pair, fading and outage probabilities affect the network noticeably. However, this effect is well predicted by the analytical model.

5.5 Summary

In this chapter, we proposed an integrated model of physical, MAC, and routing layers for unslotted IEEE 802.15.4 networks, by considering explicit effects of multi-path shadow fading channels. We studied the impact of the fading statistics on the MAC performance in terms of reliability, delay, and power consumption, by varying traffic, distances, carrier sensing range, and SINR threshold. We observed that the severity of the fading and the physical layer thresholds have significant and complex effects on every performance indicator at MAC layer, and they are well predicted by our model. In particular, the fading has a relevant negative impact on the reliability. The effect is more evident as traffic and distance between nodes increase. However, depending on the carrier sensing and SINR thresholds, a fading with small spread can improve the reliability with respect to the ideal case. The delay for successfully received packets and the power consumption are instead positively affected by the fading and the performance can be again optimized by tuning the thresholds. In the next chapter, we introduce a cross-layer design that takes into consideration physical, MAC and routing layers.

Chapter 6

Cross-layer Communication Protocol Design

In this chapter, we study the design of energy efficient protocols for control and actuation applications. We consider a multi-hop low-power network that is deployed to measure state information in specific regions needed to a remote controller for real-time actions. Recalling the general flow diagram in Figure 6.1, we consider the communication loops (physical, MAC, and routing) and include in the protocol design the influence of tunable performance requirements from the control application. In agreement with the fundamental approach followed in this thesis, we consider the reliability and the delay as performance indicators. The objective is to minimize the total energy consumption of the network, while satisfying performance requirements. In particular, we are interested in implementation-oriented solutions, in which energy efficient, reliable, and low delay operations are designed for a specific control application to offer:

- A simple algorithm: protocol operations must be simple and computationally light to be embedded in resource constrained network nodes.
- Dynamic adaptation: the protocol should consider and adapt to the time-varying traffic and channel conditions.

We consider all the aforementioned features and develop TREnD[1], a cross-layer protocol for energy efficient wireless networks for industrial control. TREnD is designed by addressing the routing specifications of ROLL [12], and in compliance with IEEE 802.15.4 [7] standard.

This chapter starts by introducing related communication protocols for industrial control in Section 6.1. The system model is then introduced in Section 6.2, followed by a description of the protocol stack in Section 6.3. The optimization problem is then described in Section 6.4 and the protocol operation is illustrated in Section 6.5. After this, we describe the fundamental limitations of the protocol in Section 6.6. Finally, experimental results are presented and discussed in Section 6.7.

[1]The acronym aims to remark the four significant characteristics of the protocol, namely, timeliness, reliability, energy efficiency, and dynamic adaptivity.

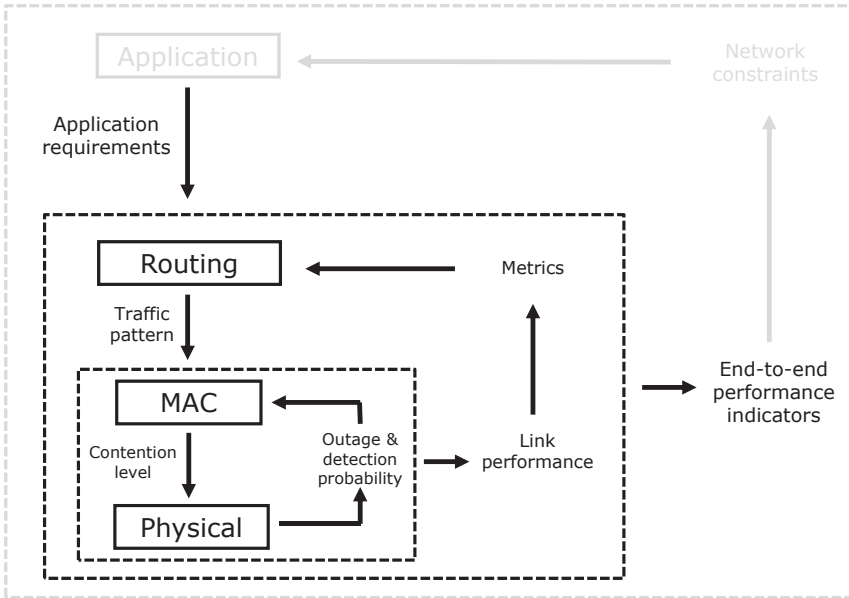

Figure 6.1: Interaction of layers for modeling and design: TREnD protocol for control applications.

The chapter concludes with a brief summary. A list of symbols and acronyms is reported in Appendix F.

6.1 Related Work

In Section 2.3, we summarized relevant protocols for industrial applications. Here, we focus on protocols that support dynamic adaptation to changes of the application requirements, to highlight the original characteristics of TREnD.

MMSPEED [68], SERAN [53], and Breath [74] are protocols that explicitly support application requirements. The MMSPEED routing protocol proposes simultaneous optimization of reliability and delay, but no energy consumption is considered. The protocol satisfies the high reliability constraint by using the duplicated packets of multi-path. However, these duplicated packets will increase the traffic load with negative effect on the stability and energy efficiency. In SERAN [53] and Breath [74] a relevant system-level design methodology has been presented for control application over WSNs. However, SERAN does not support average-high traffic regimes and tunable reliability requirements, which limits the applicability. Furthermore, load balancing and fair duty cycling are not taken into account in SERAN. On the other hand, Breath is limited to scenarios with line topologies and

source nodes at the edge of the network. We conclude that, to the best of our knowledge, there is no protocol from the literature suitable for control applications over WSNs, that is able to embrace all the techniques that concur to the energy efficiency (radio power control, MAC, routing, duty-cycling, and load balancing) and, at the same time, able to guarantee reliability and delay constraints over multi-hop communication.

In contrast to SERAN and Breath, we adopt a novel MAC solution based on sleeping discipline and a beacon mechanism, that offers high reliability and energy efficiency, and we assume a uniform distribution of sensing nodes throughout the network. Finally, TREnD is completely implemented on Tmote Sky sensors [135] by using TinyOS [136]. The experimental results allow us to assess the theoretical analysis and the protocol performance.

6.2 System Model

TREnD considers a general scenario for an industrial control application: the state of a plant must be monitored at locations where cabling is not available or cannot be extended. Information taken by nodes, which are uniformly distributed in clusters, is sent to the sink node by multi-hop communication. The clustered topology is motivated by the energy efficiency, since transmitting data directly to the sink can consume more than routing through relays. The cluster formation is conducted according to the DODAG formation of RPL (see Section 2.3.4). Specifically, nodes with same rank at routing layer are grouped into clusters.

In Figure 6.2, the system model is reported. Nodes are deployed in an indoor environment with rooms. Each dotted curve defines a cluster of nodes. To simplify the analysis, we assume that nodes of a cluster are allowed to send packets only to the nodes of next cluster toward the root node (no intra-cluster communications among siblings), which is reasonable for loop prevention. The root node is directly connected to the controller, which takes appropriate actions upon the timely and reliable reception of source information.

We assume that the controller knows cluster locations and the average number of nodes in each cluster, and nodes know to which cluster they belong (through the rank computation). We assume that the neighborhood set of each node includes all nodes in the same cluster and nodes in the parent and children cluster, so that the hidden terminal problem is avoided. The controller estimates the amount of data generated by each cluster, which is used to adapt the protocol to the traffic regime. These assumptions are reasonable in industrial environments [2].

6.3 TREnD Protocol Stack

In this section, we introduce the protocol stack of TREnD.

Similarly to SERAN [53], the routing algorithm of TREnD is hierarchically subdivided into two parts: a static route at inter clusters level and a dynamical

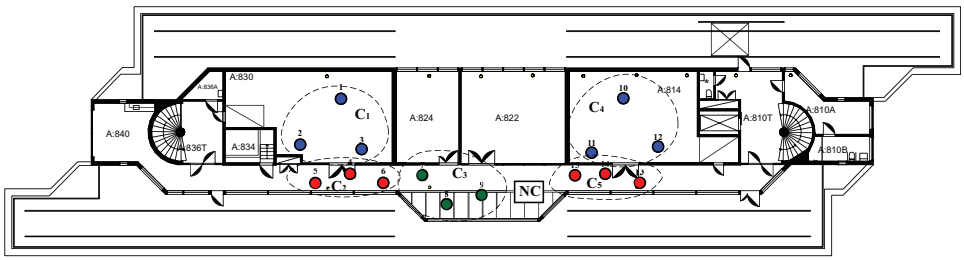

Figure 6.2: System model scenario: a test-bed of 15 nodes is deployed in the Automatic Control laboratory at KTH.

routing algorithm at node level. This is supported at the MAC layer by an hybrid TDMA/CSMA solution.

The static schedule establishes which one is the next cluster to which nodes of a given cluster must send packets, by using the rank information. Alternatively, if the number of clusters is large, the static routing schedule is pre-computed off-line for a set of cluster topologies and stored in the sink node in a look-up array.

The static routing algorithm is supported at MAC level by a weighted TDMA scheme that regulates channel accesses among clusters. Nodes are awake to transmit and receive only during the TDMA-slot associated with the cluster for transmission and reception, respectively, thus achieving consistent energy savings. The organization of the TDMA frame must consider the different traffic regimes depending on the cluster location. Since clusters closer to the sink may experience higher traffic intensity, more than one transmitting TDMA-slot is assigned to them. It is natural to first forward packets of clusters close to the controller, since this minimizes the storage requirement in the network. To minimize the global forwarding time, the evacuation of packets of a cluster is scheduled path-by-path. By following these rules, the controller is able to generate an appropriate TDMA scheduling table.

The dynamic routing is implemented by forwarding the packets to a node within the next-hop cluster in the path chosen at random, as proposed in [65, 71]. In such an operation, no cluster-head node is needed within clusters, and nodes need to be aware only of the next-hop cluster connectivity. The procedure for random selection of next-hop node is performed by considering a duty cycling in the receiving cluster combined with beacon transmissions.

The communication stage between nodes during a TDMA-slot is managed at MAC layer by a receiver-initiated p-persistent CSMA/CA scheme, to offer flexibility for the introduction of new nodes, robustness to node failures, and support for the random selection of next-hop node. As we will see in Section 6.7, in hybrid TDMA/CSMA solutions our receiver-initiated p-persistent MAC gives better performance than the standard BEB mechanism used by IEEE 802.15.4, which we illustrated in Section 2.3.3. However, TREnD is implemented to support the BEB mechanism in the dynamic MAC, in order to be compliant with the standard.

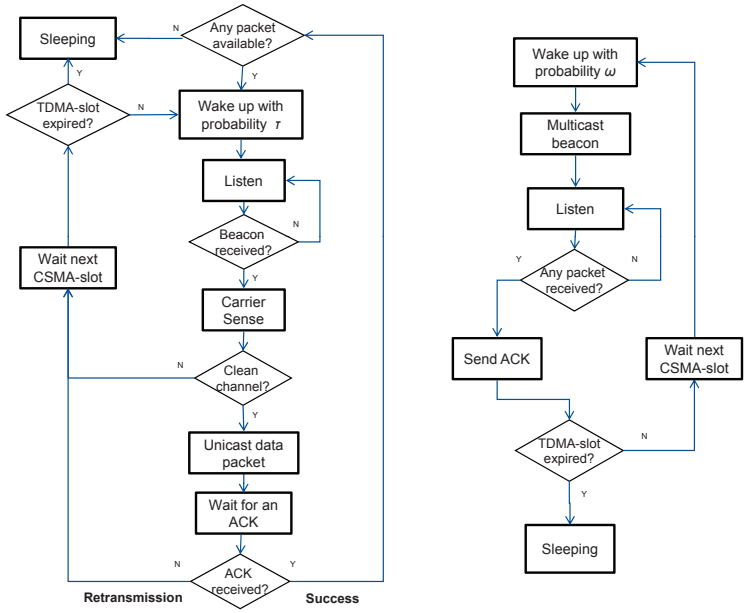

Figure 6.3: MAC operations of TREnD in transmission and reception.

MAC operations of nodes are illustrated in Figure 6.3 and described in the following. Each node in the transmitter cluster having a packet to be sent wakes up in CSMA-slots with probability τ and enters in listening state. At the receiver cluster, each node wakes up with probability ω and multicasts a small length of beacon message to the nodes in the transmitter cluster. An awake node that correctly receives the beacon at the transmitter side, senses the channel and, if clean, tries to unicast its packet to the beacon sender. An ACK can conclude the communication if a retransmission mechanism is implemented. If no beacon is sent or there is a collision, the awake nodes in the transmitter cluster keep on listening in the following CSMA-slot with probability τ or go to sleep with probability $1 - \tau$.

To compare TREnD and SERAN [53], we recall that SERAN communication is initiated by the transmitter. The drawback of SERAN is that nodes in the receiver cluster have to be listening for the overall TDMA-slot duration, due to a contention-based transmission of the ACKs. In TREnD, the selection of the forwarding nodes follows a random policy regulated by ω. The main advantage of this novel solution is the absence of delays between packets exchange during a CSMA-slot. This allows TREnD to work with a much higher traffic regime when compared to SERAN.

TREnD offers the option of data aggregation to fairly distribute the traffic load and energy consumption among clusters. The aggregation has the advantage of reducing the number of TDMA-slots per cluster and of the traffic for clusters closer

to the sink. However, packet aggregation gives significant advantages only when the traffic is sufficiently high, as we will see in Section 6.7, because nodes have to idle-listen longer to catch more than one packet per time and perform the aggregation, and idle-listening is energy inefficient.

6.4 Protocol Optimization

In this section, we pose and solve an optimization problem to select the TREnD protocol parameters by minimizing the overall energy consumption of the network given reliability and delay constraints:

$$\underset{S,\tau,\omega}{\text{minimize}} \quad E_{\text{tot}}(S,\tau,\omega) \tag{6.1}$$

$$\text{subject to} \quad R(S,\tau,\omega) \geq R_{\min} \tag{6.2}$$

$$\Pr[D(S,\tau,\omega) \leq D_{\max}] \geq \delta\,. \tag{6.3}$$

In this problem, $E_{\text{tot}}(S,\tau,\omega)$ is the total energy consumption of the network, $R(S,\tau,\omega)$ is the reliability constraint, and $R_{\min}$ is the minimum desired reliability imposed by the control application. We denote by $D(S,\tau,\omega)$ the random variable describing the distribution of the delay, by $D_{\max}$ the maximum delay desired by the control application, and by δ the minimum probability with which such a maximum delay should be achieved. The parameters $R_{\min}$, $D_{\max}$, and δ are the requirements of the control application. The decision variables of the optimization problem are the TREnD parameters, namely the TDMA-slot duration S, the wake-up probability in transmission τ, and the wake-up probability in reception ω. In the following, we develop the expressions needed in the optimization problem, and derive the solution. Since such a solution must be implemented by a computationally affordable algorithm solved at the sink node of the network, thus the expressions are derived by doing simplifications and approximation without giving up to the accuracy, as we show later.

6.4.1 Reliability Constraint

In this section, we study the reliability constraint in Equation (6.2). Considering a single CSMA-slot, in which p-persistent CSMA and duty cycling in reception are used, we have the following result:

Claim 6.4.1. *Let k be the number of packets awaiting to be forwarded in the cluster. Then, the probability of successful transmission is*

$$p_k = (1-\gamma)\, p_{\text{bc}}\, (1-(1-\tau)^k)\, (1-p_f)^{\tau(k-1)}\,, \tag{6.4}$$

where $p_{\text{bc}} = (1-\gamma)N\omega\,(1-\omega)^{N-1}$ is the successful beacon probability and p_f is the probability of an erroneous sensing of a node, when it competes with another node.

Proof. A proof is provided in Appendix D. □

In TREnD, a radio power control is implemented, so that the attenuation of the wireless channel is compensated by the radio power, which ensures a desired packet loss probability, as proposed in [74] and [137]. As a consequence of the power control, the channel is abstracted by a random variable with bad channel probability γ. Such a modeling has been adopted also in other related works (e.g., [53], [82]). Considering the collision probability p_{cl}, we observe that for design purposes an upper bound suffices. Experimental results, presented later, show that a good upper bound is $p_f = 0.2$.

By using Claim 6.4.1, we derive the following result:

Claim 6.4.2. *Let $V(n) = \{1 - p_n, 1 - p_{n+1}, ..., 1 - p_k\}$, where p_n is given in Equation (6.4) and let $A(n) = [a_{i,j}]_{M_c}^{S-k+n}$ be a matrix containing all the M_c combinations with repetition of the elements in $V(n)$, taken in groups of $S - k + n$ elements. Let $h_{\max}$ be the maximum number of hops in the network. Then, the reliability of TREnD is*

$$R(S, \tau, \omega) = \left[\sum_{n=0}^{k} \frac{k-n}{k} \prod_{l=n+1}^{k} p_l \left(\sum_{i=1}^{M_c} \prod_{j=1}^{S-k+n} a_{i,j} \right) \right]^{h_{\max}} . \tag{6.5}$$

Proof. A proof is provided in Appendix D. □

When packet aggregation is enabled, the following result holds:

Claim 6.4.3. *Let h_i be the number of hops in the path i. Let R_z be the reliability in a single hop when z packets are aggregated. The reliability of a packet that experiences j hops to the controller is*

$$R_j^{\text{ag}}(S, \tau, \omega) = R_{j-1}^{\text{ag}} \, r_{h_i - j + 1} \, , \tag{6.6}$$

where $r_j = \sum_{i=1}^{j} (1 - r_{i-1}) \prod_{z=1}^{j-i+1} R_z$, with $r_0 = 0$.

Proof. A proof is provided in Appendix D. □

If the data aggregation is disabled or the size of aggregated packets does not change significantly, then we simplify Equation (6.6) and obtain the relation in Equation (6.5). The previous claims are verified by experiments in Section 6.7.1.

6.4.2 Delay Constraint

Here we develop the expression of the constraint in Equation (6.3). The furthest cluster from the controller is the one experiencing the highest delay. Therefore, the delay of packets coming from such a cluster must be less than or equal to a given value $D_{\max}$ with a probability δ.

Recalling that the maximum number of hops in the network is $h_{\max}$, an upper bound on the TDMA-slot duration S is

$$S_{\max} = \frac{D_{\max}}{h_{\max}} \, . \tag{6.7}$$

The random variable describing the delay is modeled by

$$D(S,\tau,\omega) = (h_{\max}-1)S + T_e\,,$$

where T_e is a random variable describing the time to evacuate k packets. Then, we provide the following result:

Claim 6.4.4. *The delay constraint in Equation* (6.3) *is well approximated by*

$$\Pr[D(S,\tau,\omega) \le D_{\max}] \approx 1 - \frac{1}{2}\mathrm{erfc}\left(\frac{A-\mu}{\sigma}\right), \tag{6.8}$$

$$\text{where} \quad A = \begin{cases} S & \text{if} \quad S \le \frac{D_{\max}}{h_{\max}} \\ D_{\max} - (h_{\max}-1)S & \text{if} \quad S > \frac{D_{\max}}{h_{\max}} \end{cases}$$

$\mu = \sum_{j=1}^{k} 1/p_j$, *and* $\sigma^2 = \sum_{j=1}^{k}(1-p_j)/p_j^2$.

Explanation. Details of the approximation are provided in Appendix D. □

The previous claim is verified by experiments in Section 6.7.1.

6.4.3 Energy Consumption

The total energy consumed by the network over a period of time is given by the combination of three components: idle-listening, transmission, and reception cost[2].

Listening for a time t gives an energy consumption that is the sum of a fixed wake-up cost E_w and a time dependent cost $P_{\mathrm{i}}t$. The energy consumption in transmission and reception are given by four components: beacon cost E_{bc}, CCA cost E_{cca}, packet cost E_{pkt}, and ACK cost E_{ack}.

Consider a general topology with N nodes and maximum number of hops $h_{\max}$. Let us define W the number of listening TDMA-slots in a TDMA frame and the TDMA frame duration $T_f = SM_s$ where M_s is the number of TDMA-slots in a TDMA frame. We have the following result:

Claim 6.4.5. *For a given packet generation rate* λ*, the total energy consumed in the network in a period* T_{tot} *is*

$$\begin{aligned} E_{\mathrm{tot}}(S,\tau,\omega) =& \frac{T_{\mathrm{tot}}}{(1-\gamma)\,S}\sum_{j=1}^{\lambda T_f} j\tau\omega\,E_{\mathrm{cca}} + T_{\mathrm{tot}}M_s\lambda\,(E_{\mathrm{pkt}}+E_{\mathrm{ack}}) \\ &+ \omega\,\frac{N\,W\,T_{\mathrm{tot}}}{M_s}\left(\frac{E_{\mathrm{bc}}}{d} + \frac{E_w}{S} + P_i\right). \end{aligned} \tag{6.9}$$

Proof. A proof is provided in Appendix D. □

[2]Note that the costs for the initialization of the network are negligible in the energy balance

6.4.4 Protocol Optimization

In the previous sections, we have established the expressions of the energy consumption in Equation (6.9), the reliability in Equation (6.6), and the delay constraint in Equation (6.8). We observe that all these expressions are highly non-linear in the decision variables. Sensor nodes are not equipped with a high processing capacity to use these equations, therefore, we provide a computationally affordable sub-optimal solution to the optimization problem. In the following, we show that such a strategy still gives satisfactorily results.

First, we determine the wake-up probability in transmission τ and wake-up probability in reception ω, for a given TDMA-slot duration S. Since the main component of the energy consumption in a TDMA-slot is given by the number of channel accesses, the parameters are selected such that the channel utilization is optimized or, equivalently, the reliability is maximized. The following claim provides empirical results on τ and ω.

Claim 6.4.6. *The wake-up probability in transmission τ^* and in reception ω^* that maximize the reliability in Equation* (6.5) *depend on S according to the following relations:*

$$\tau^* = \frac{c_1}{\lambda\, S\, M_s + c_2}\,, \tag{6.10}$$

$$\omega^* = \frac{1}{N}\,, \tag{6.11}$$

with coefficients $c_1 = 2.17$, $c_2 = 1.81$. We recall that λ is the cluster traffic rate, M_s is the number of TDMA-slots in a TDMA frame, and N is the number of nodes.

Proof. A proof is provided in Appendix D. □

We note here that such choices are sub-optimal because are limited to strategies with constant wake-up probabilities per each node.

By using Equation (6.10) for the wake-up probability in transmission and wake-up probability in reception, and by assuming S as a real-valued variable, we notice that E_{tot}, given in Equation (6.9), and the reliability R in Equation (6.6) are monotonically decreasing functions of S, while the delay D in Equation (6.8) is a monotonically increasing function of S. It follows that a simple solution for the TDMA-slot duration, S^*, is given by the maximum integer value of S that satisfies the two constraints in problem (6.1). The search of the optimal S is done by a simple additive increasing multiplicative decreasing algorithm, which we initialize at $S^* = S_{\max}$. Indeed, as shown in Section 6.4.2, the delay requirement $D_{\max}$ provides an upper bound for S, given by $S_{\max} = D_{\max}/h_{\max}$.

6.5 Protocol Operation

Suppose that the network user deploys a WSN of nodes implementing the TREnD protocol, and sets the desired control application requirements $R_{\min}, D_{\max}$, and

δ. During an initial phase of operation the sink node retrieves the traffic and the cluster topology by the received packets. After computing or reading from a look-up array the static routing schedule and TDMA frame, the sink computes the optimal parameters as described in Section 6.4.4. Then, the sink communicates these values to the nodes of the network by DIO messages. Such a message passing procedure ensures synchronization among nodes and allows for initializing and self configuring of the nodes to the optimal working point of the protocol. The DIO messages are then forwarded by the nodes closer to the sink to other nodes of the clusters far away by using the ACK mechanism described in [53]. Such messages need also to be updated so that our protocol adapts dynamically to new nodes added in the clusters, variations in the source traffic, control application requirements, and time drift of the clocks. We experienced that a 20 TDMA frames period for the refreshing procedure gives satisfactory performance to maintain an optimal network operation with negligible extra energy consumption.

6.6 Fundamental Limits

The analysis of the fundamental limits of TREnD is critical for the appropriate application of the protocol. In this section, we investigate the minimum reliability and delay requirement, and the minimum number of nodes needed to support the protocol operation.

First, we characterize the minimum CSMA-slot duration d, that the application can set. It holds that

$$d \geq t_b + t_m + t_p + t_a \,,$$

where we consider the packet transmission time t_m, the processing time t_p, the ACK transmission time t_a, and the beacon transmission time t_b. Numerically, we derive that the minimum affordable CSMA-slot size of TREnD is 10 ms, which is compliant with the slotted solution adopted by WirelessHART [5]. This is a strong improvement with respect to SERAN MAC solution where the minimum sustainable CSMA-slot size is 100 ms [53]. Given the limit on d, the range of feasibility for the reliability and delay constraints depends on the traffic rate λ.

From Equation (6.6), the feasible zone of reliability requirement is

$$R_{\min} \leq R(\lambda, d) \,.$$

In addition, from Equation (6.7) we derive a lower bound for the delay constraint,

$$D_{\max} \geq \frac{h_{\max} d}{\lambda M_S} \,.$$

Given a maximum storage capacity B in number of packets for each node, a lower bound to the number of nodes in a cluster is

$$N \geq \left\lceil \frac{\lambda S M_s}{B} \right\rceil \,,$$

where $\lceil x \rceil$ is the ceiling value of x.

6.7 Experimental Implementation and Validation

In this section, we present an implementation of TREnD by using TinyOS 2.x [136] and Tmote Sky nodes [135]. To benchmark our protocol, we implemented also SERAN [53] and the BEB mechanism of the IEEE 802.15.4 MAC [7]. We used the default MAC parameters of IEEE 802.15.4 so that the protocol fits in the higher level TDMA structure and routing algorithm of SERAN and TREnD, for a fair comparison. We denote it in the following as clustered IEEE 802.15.4.

We reproduced the reference test-bed topology reported in Figure 6.2, where clusters are placed in an indoor environment. Each cluster is composed by 3 sensors, deployed at random within a circle with one meter radius. We analyze different scenarios with various sets of traffic rate λ and control application requirements ($R_{\min}$, $D_{\max}$, and δ), which we report in Table 6.7. For each scenario, Table 6.7 shows also the optimal TDMA-slot duration and wake-up probabilities as obtained by the optimization in Section 6.4.4. We measured the duty-cycle of nodes as indicator of the energy efficiency.

6.7.1 Protocol Validation

To validate our analysis, we conducted an experimental measurement campaign to capture the sensitivity of the reliability and delay requirements to variations of the decision variables. Figure 6.4 shows the reliability of TREnD by varying TDMA-slot duration S for $k = 3$ packets in the cluster. The results achieved by experiments follows well the theoretical analysis.

In Figure 6.5, we report the delay analysis by comparing experimental and analytical results. In this case we fixed a large S, and determine average and variance of the evacuation time of a cluster, by varying the number of packets k (i.e., by tuning the wake-up probability in transmission τ, according to Equation (6.10)), for a fixed wake-up probability in reception in Equation (6.11). The analytical model matches well with the experimental results. In Figure 6.6, we report the delay distribution for cluster C_1 and C_2 (located at 3 and 2 hops), respectively. The furthest cluster presents a larger variance, due to the multi-hop. From the figures, we observe that the Gaussian distribution we have adopted is a fair approximation.

6.7.2 Performance Comparison

In the first set of experiments, we show the performance improvements in TREnD, when compared to SERAN. In Figure 6.8, the reliability is reported as a function of the traffic rate λ, by fixing $R_{\min} = \delta = 95\%$, and $D_{\max} = [3\,, 9]$ s. TREnD has high reliability for all traffic rate conditions and SERAN is significantly outperformed. In particular with $D_{\max} = 3$ s, as traffic rate increases over $\lambda = 0.3$ pkt/s, the reliability of SERAN significantly decreases.

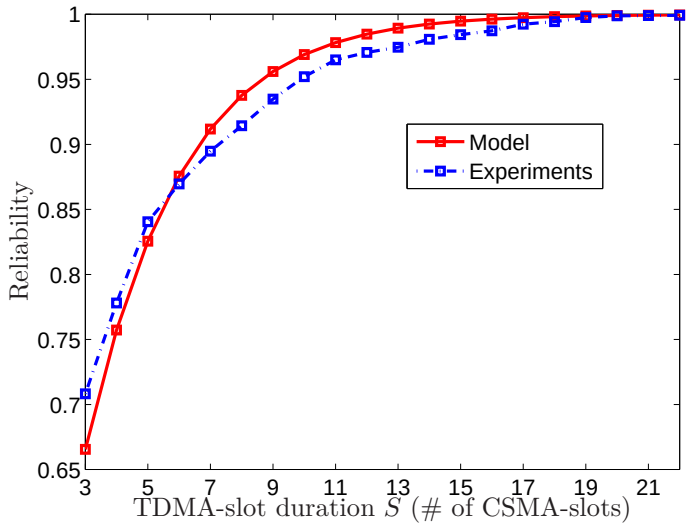

Figure 6.4: Reliability vs. TDMA-slot duration S, for $k = 3$ packets in the cluster and $S \geq k + 1$.

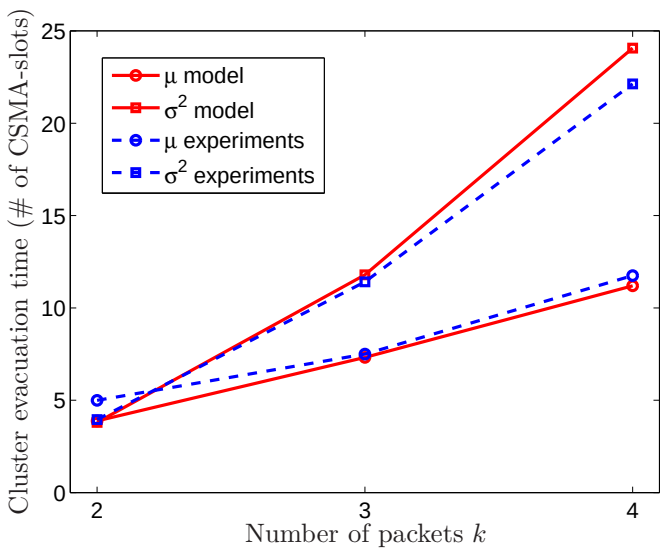

Figure 6.5: Average and variance of the cluster evacuation time T_e vs. the number of packets k in the cluster.

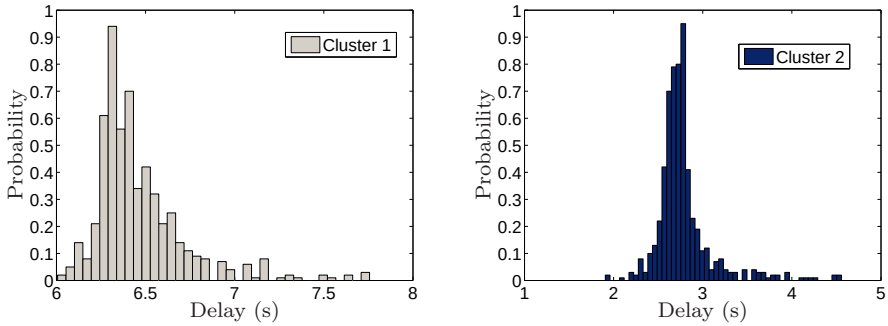

Figure 6.6: Delay distribution for clusters C_1 and C_2.

Table 6.7: Application requirements and experimental results.

Scenario	λ	$D_{\max}$	δ	$R_{\min}$	S^*	τ^*	ω^*
$\mathcal{L}$	0.1 pkt/s	9 s	95%	95%	3.3 s	0.41	0.33
$\mathcal{H}$	0.3 pkt/s	3 s	95%	95%	1.2 s	0.43	0.33

In Figure 6.9 we compare the energy consumption of the two protocols, showing the average duty-cycle of each node, for fixed $R_{\min} = \delta = 95\%$, $D_{\max} = 3$ s and $\lambda = 0.3$ pkt/s. As discussed above, in this operative condition both SERAN and TREnD meet the reliability and delay constraints. By implementing TREnD with data aggregation, we observe a more balanced duty-cycle among clusters, particularly for the last hop clusters. However, the price to pay for having a better load balancing is a slight increasing of the average duty-cycle. In fact, TREnD presents a slightly higher duty-cycle for most of the nodes, but it reduces of about 30% the energy consumption for nodes 7, 8, and 9 (cluster C_3), which are critical for the network operation since they also forward information from clusters C_1 and C_2. This suggests that packet aggregation is a viable choice only for the clusters supporting high traffic, as those next to the sink. In conclusion, TREnD ensures higher reliability, load balancing, and a longer network lifetime than SERAN, without any significant difference in the complexity of the scheme.

Given these results, in the following performance evaluation of TREnD we disregard SERAN and consider the clustered IEEE 802.15.4. We present two sets of experimental results, evaluated for scenarios $\mathcal{L}$ and $\mathcal{H}$ as specified in Table 6.7. Figure 6.10 reports the average values of reliability, delay, and duty-cycle as achieved by the experiments for TREnD and the clustered IEEE 802.15.4. Data of clusters belonging to the same paths are joined by lines. We see that TREnD always ensures the satisfaction of the reliability and delay constraints specified in Table 6.7. TREnD guarantees much better reliability, in particular for cluster C_1 (3 hops). In fact in C_1, the clustered IEEE 802.15.4 does not fulfill the requirement. The aver-

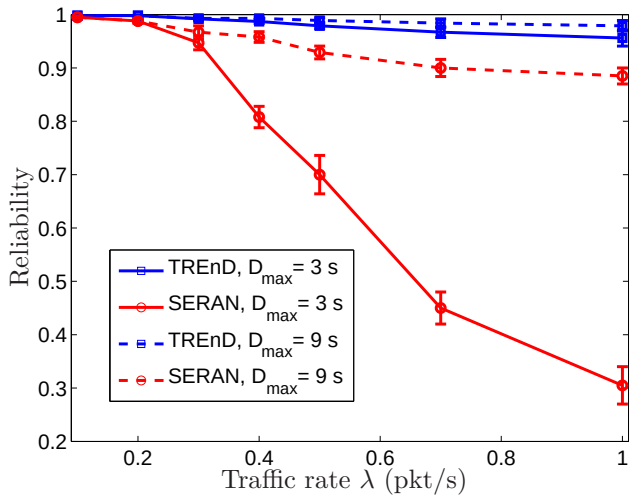

Figure 6.8: TREnD and SERAN: reliability vs. traffic rate λ, for $R_{\min} = \delta = 95\%$.

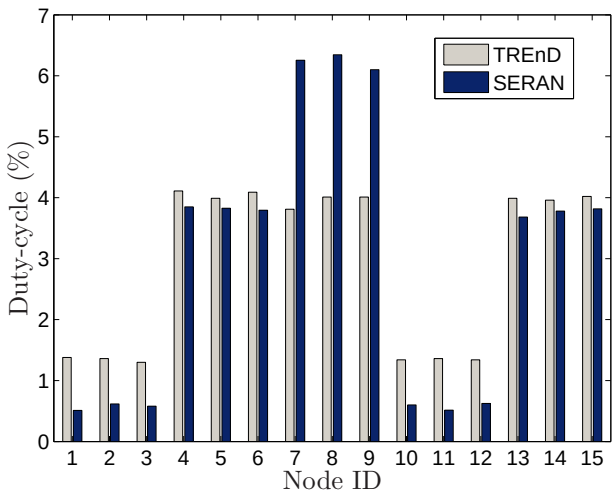

Figure 6.9: TREnD and SERAN: duty-cycle distribution among nodes for $\lambda = 0.3$ pkt/s, $R_{\min} = \delta = 95\%$.

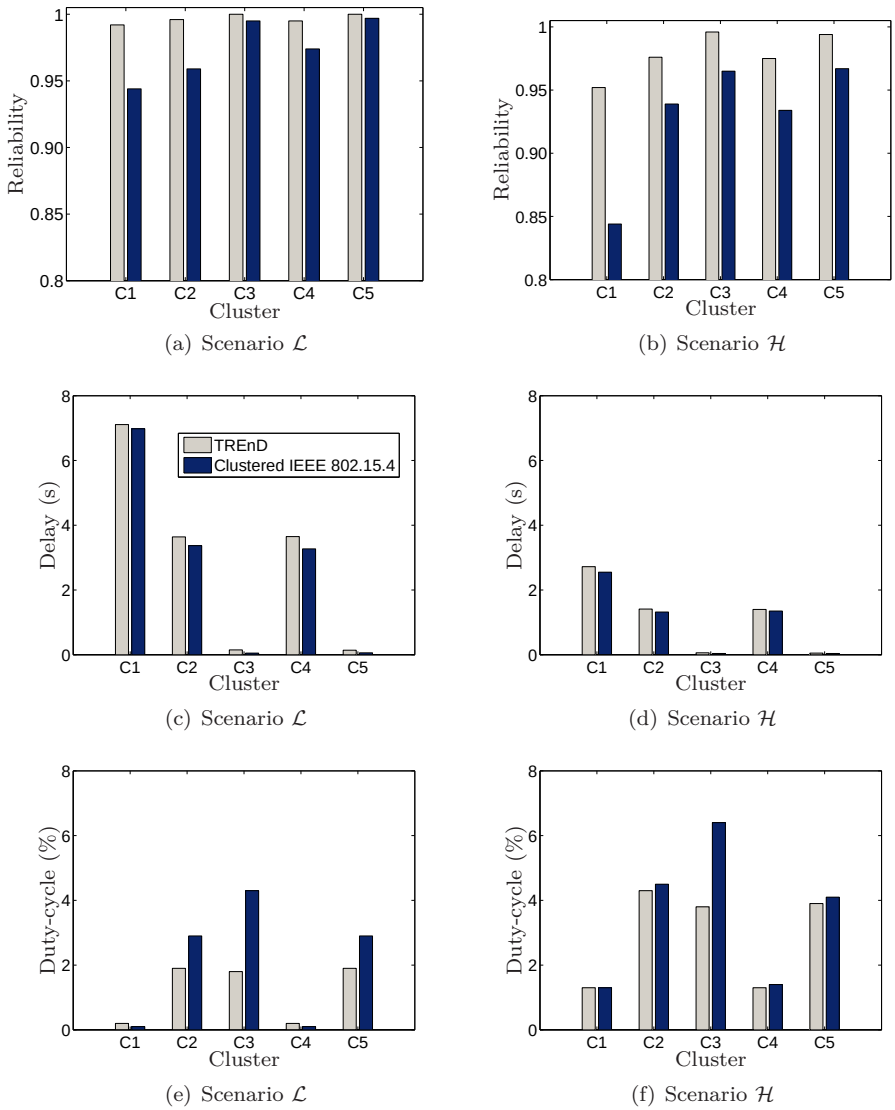

Figure 6.10: TREnD and clustered IEEE 802.15.4: average reliability, delay, and duty-cycle in each cluster in the network.

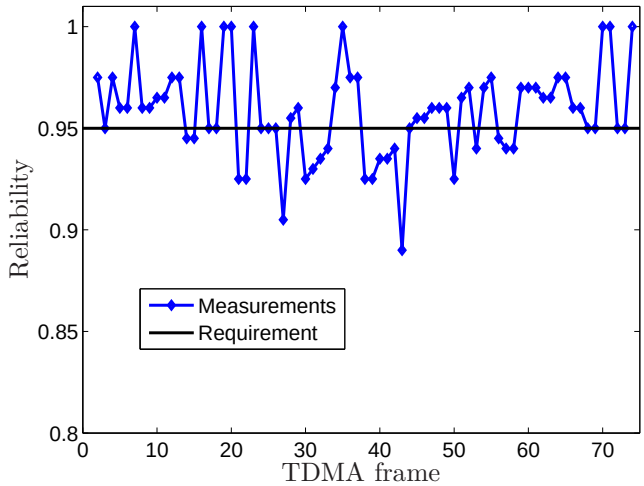

Figure 6.11: TREnD: reliability trace given by the experiments.

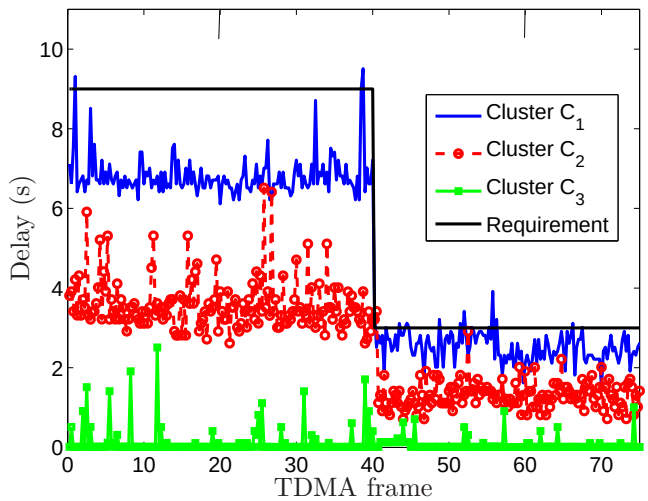

Figure 6.12: TREnD: delay trace given by the experiments for clusters C_1, C_2, and C_3.

age delay of IEEE 802.15.4 is slightly lower than TREnD, but note that the delay of IEEE 802.15.4 is computed only for packets arriving successfully at the sink. We observe similar behavior also for other scenarios. Finally, we present some results about the duty-cycle. According to the traffic load supported by the clusters and their allotted TDMA-slots, we notice that the duty-cycle depends on the number of times a cluster wakes up for the forwarding procedure. The duty-cycle is the same for the clusters far away from the sink (C_1 and C_4, see Figure 6.2), but for all other clusters TREnD gives a consistent duty-cycle reduction with respect to the clustered IEEE 802.15.4.

We remark here that the duty-cycle strongly depends on the traffic load in the network. In Dozer [72], an average duty-cycle 0.2% is achieved for a network of 40 nodes with a packet generation period of 120 s each (total traffic load $\simeq 0.3$ pkt/s). TREnD gives an average duty-cycle 2.5%, but the total traffic rate is much higher ($\simeq 5$ pkt/s) than Dozer.

6.7.3 Dynamic Adaptation

In the previous section, we used a static network topology where each node is placed at fixed position and the application requirements do not change with time. In this section, we show the dynamical behavior of the protocol.

We present the experimental results of dynamic changes between two scenarios ($\mathcal{L}$ and $\mathcal{H}$ in Table 6.7) in static and time-varying channel conditions. A Rayleigh fading channel is obtained by moving the nodes around their initial position and also by placing metal obstacles in front of the source nodes so that the line-of-sight with the sink is lost. The network starts with scenario $\mathcal{L}$ and static channel, then after 20 TDMA frames we introduce a Rayleigh fading channel which persists until the TDMA frame 60. At TDMA frame 40, the application requirements change to scenario $\mathcal{H}$.

Figures 6.11 and 6.12 report the resulting snapshot of the experiment in terms of reliability and delay. The reliability is measured at the sink node as average on each TDMA frame, while the delay is measured for each successfully received packet. In Figure 6.11, we observe that TREnD guarantees the reliability requirement for both static and Rayleigh fading conditions, continuously adapting to the severe fading. The protocol is also robust to the change of scenario at TDMA frame 40. In Figure 6.12 a snapshot of the delay is reported for clusters at different hops to the controller. We observe that the peaks of delay are limited due to the TDMA structure, the average and dynamics of the delay are slightly increasing in the time-varying stage but the delay constraint is fulfilled. Moreover, the protocol adapts well to the change of scenario at TDMA frame 40.

6.8 Summary

We proposed TREnD, a cross-layer protocol for control applications over energy efficient multi-hop wireless networks. The protocol is based on guaranteeing the

respect of control requirements on reliability and delay while minimizing energy consumption. Duty-cycle, routing, data link, and physical layers were considered all together to maximize the network lifetime by taking into account the tradeoff between energy consumption and application requirements for control applications in compliance with RPL and IEEE 802.15.4 standard. The design approach was based on optimization problems to select the protocol parameters by simple algorithms that can run on resource constrained nodes.

We provided a complete test-bed implementation of the protocols that we designed on the base of the method proposed in this chapter. An experimental campaign was conducted to test the validity of TREnD in an indoor environment. Experimental results showed that the protocol achieves the reliability and delay requirements, while minimizing the energy consumption. TREnD outperformed a clustered IEEE 802.15.4 implementation in terms of both energy efficiency and reliability. In addition, the protocols showed good load balancing performance, and it is scalable with the number of nodes.

In the next chapter, we develop a methodology in which the effects of communication constraints on the control application are included in the design.

Chapter 7

Wireless Networked Control Systems Design

In this chapter, we show an example of contract-based methodology applied to a heterogeneous wireless networked control system design. We focus on heating, ventilation, and air conditioning (HVAC) control in intelligent buildings, which is a challenging automation problem with objectives that comprise several research areas of current interest, such as wireless automation and control of complex interconnected subsystems. The complexity arises from the different physical properties and associated dynamics of the subsystems. Therefore, we believe that a successful design, in which costly and time consuming re-design cycles are avoided, can be achieved by using a contract-based methodology that allows for component reuse and for evaluation of requirements at the early stages of the design flow.

We aim at studying control strategies that are robust enough to cope with variations and disturbances due to Markovian processes, nonlinearities in the system model, and delays and losses in a heterogeneous wireless network. The H_∞ control approach has been selected due to its intrinsic emphasis on robustness, the existence of a well established systematic design procedure, and its efficiency in a wide range of applications, in particular with time delays as illustrated in [138]. In Figure 7.1, we visualize the analysis performed in this chapter with respect to the problem formulation in Section 1.3. A loop is closed between application and underlying layers, so that the performance indicators from the communication level are considered explicitly in the controller. A mixed sensitivity H_∞ synthesis is compared with two approaches that explicitly take contracts on the communications into account.

This chapter is outlined as follows. First, we introduce related works in Section 7.1, then we present our case study in Section 7.2. We describe the contract-based design flow in Section 7.3. The model of the system is presented in Section 7.4. We derive contracts for the communication network in Section 7.5, and for the controller synthesis in Section 7.6. Eventually, implementation examples are presented in Section 7.7 and the chapter is concluded with a short summary. A list of symbols and acronyms is reported in Appendix F.

7.1 Related Work

There is an increasing interest in model-based design approaches for the design of control systems. In [139], a model-based approach for the design of control algorithms for HVAC systems is introduced and validated. Challenges in the design of embedded controllers using contracts are discussed in [140]. In [38], contracts are introduced for the design of embedded controllers where the plant, sensors and actuators are described by hybrid systems. The validity of the composition is verified using the assumptions and guarantees of the plant, sensors, actuators, and controller. The contract composition for a simple control system described by linearized equations is illustrated in [141]. In [40], a platform-based design methodology that uses assumption/guarantee analog contracts is proposed to develop reliable abstractions and design-independent interfaces for analog and mixed-signal integrated circuit design. The effectiveness of the methodology is demonstrated on the design of an ultra-wide band receiver used in an intelligent tire system, an on-vehicle wireless sensor network for active safety applications. However, to the best of our knowledge, the concept of contract has not yet been applied to the design of wireless protocols, and there is no systematic methodology proposed for the design of networked control systems.

For the controller design, we are interested in strategies that are able to cope with the stochastic behavior of the underlying wireless network. In [142]–[144], methods for the stability analysis of sampled data systems with delays are provided. Robust control strategies, based on the multi-objective H_∞ design approach [145], [146] are suitable for our purpose, since they provide guarantees on the performance under uncertainties.

7.2 System Architecture

We consider a control system for building automation over a heterogeneous wireless network. The application scenario is an under floor air distribution (UFAD) regulation system [147]. An indoor climate regulation process is set with the injection of a fresh airflow from the floor and an exhaust located at the ceiling level, as depicted in Figure 7.2. The considered system is composed of ventilated rooms, fans, and plena. Note that we consider the specific case where a common plenum is used at both the underfloor and ceiling levels. Feedback regulation is a key element for an optimized system operation and it can be achieved thanks to actuated diffusers and distributed measurements provided by a sensor network deployed in the ventilated area.

The heterogeneous network infrastructure is visualized in Figure 7.3. N_e wireless sensor nodes are deployed to sense temperature, humidity, and carbon dioxide level from the rooms and report to a sink node. We consider also that N_t wireless sensor nodes are deployed in the same environment to monitor the electricity consumption of the appliances.

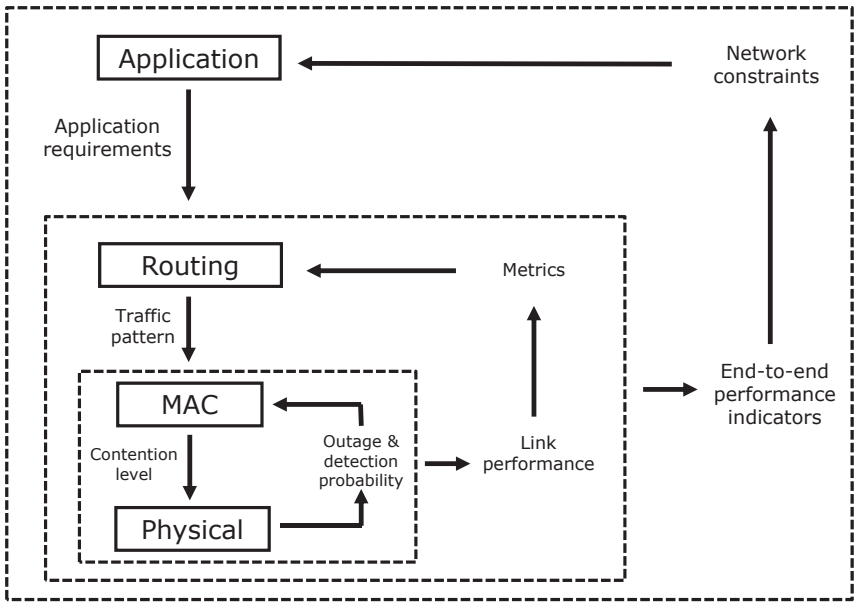

Figure 7.1: Interaction of layers for modeling and design: Control synthesis over heterogeneous wireless networks.

HVAC and lighting control systems are typically based on event-triggered operations. Temperature, humidity, and carbon dioxide levels are sensed continuously but the information is sent to the controller sporadically, either due to threshold crossing or for periodic report. Other sensors are used to report occupancy levels in each room. Events are sporadic and the traffic generation is usually low. We assume that the contention-based medium access mechanism of the IEEE 802.15.4 protocol is used for communication, since there is no need to allocate resources permanently and events are usually localized, therefore, a single event does not generate a high level of contention in the network. A certain reliability in terms of delivery ratio and certain delay constraints are required, for comfort (temperature and lighting control) and security reasons (intrusion detection).

Energy monitoring applications are instead examples of time-triggered operation. Wireless sensors can be installed in specific appliances to report periodically the instantaneous electricity consumption. Depending on the specific appliance, the generated traffic could be high but predictable. Therefore, a schedule-based medium access mechanism (TDMA) is preferable for communication. Delivery ratio and communication delay are not critical but requirements can be imposed to guarantee a correct interpretation of the information for modeling or feedback control.

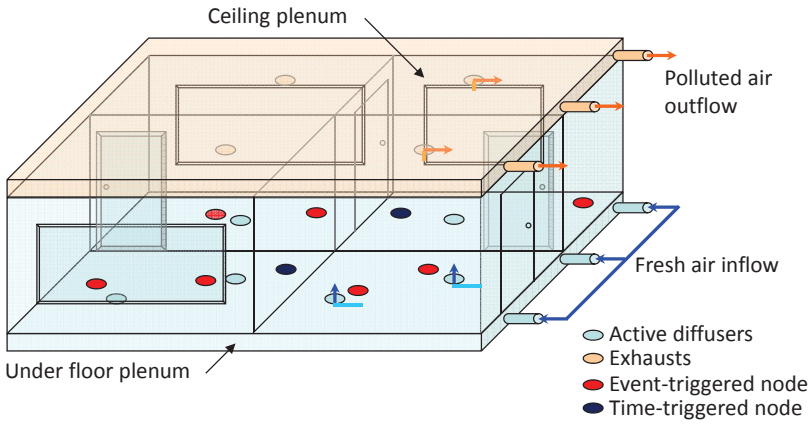

Figure 7.2: UFAD system overview.

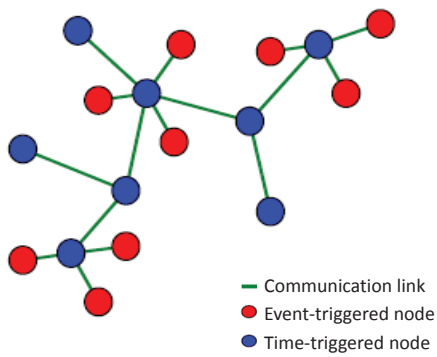

Figure 7.3: Graph topology for the communication among event-triggered and time-triggered nodes.

In current design flows, the two applications and the two networks are designed and optimized separately over different communication infrastructures. In practice, it is convenient that the two sensing applications share the same infrastructure, with communication platforms that relay information for both applications [148]. However, the complexity of the design of the wireless network increases, and the performance of the applications can be affected. In particular, when the requirements provided with the applications are different, the composition of the two applications over the same infrastructure could not be a feasible solution.

7.3 Contract-based Design Flow

In this section, we illustrate the contract-based design flow for communications and controls with reference to the considered building automation system.

7.3.1 Subsystems

Instrumental to the deployment of the contract-based design flow is the development of a component-based library of models that are hierarchically organized to represent the system at different levels of abstraction. At each abstraction level, the models are capable of exposing different, complimentary views of a component. Components are organized into subsystems, each one defined by:

- a set of input variables $u \in \mathcal{U}$, a set of output variables $y \in \mathcal{Y}$, a set of internal variables $x \in \mathcal{X}$ (including state variables), a set of configuration parameters $\kappa \in \mathcal{K}$, a set of interface parameters $\iota \in \mathcal{I}$, for connections with other components or the environment;
- a *behavioral model*, which implicitly represents the behavior of the component; in its most general form, it is a set of integro-differential or difference equations uniquely determining y and x given u, κ and ι;
- a *performance model* that computes the performance indicators P corresponding to particular values of u, κ and ι by solving the behavioral model (performance mapping).
- a set of *assumptions*, which is a set of constraints on the variables and parameters of the component for which behavioral and performance models are guaranteed to be *valid* within a set of tolerable margins $\epsilon \in \mathcal{D}$. A design implementation is valid when all its assumptions are satisfied, which guarantees the model outputs correspond to the actual outputs and performance within a tolerance ϵ.

In our scenario, a high level subsystem categorization is the following:

- UFAD system
- IEEE 802.15.4 cluster
- TDMA infrastructure
- Robust controller

7.3.2 Requirements

The first step of the contract-based design methodology consists in identifying requirements for the systems.

The requirements are related to the different components of the system, i.e., subsystems. Responsibilities in the requirements, i.e., which actor is supposed to guarantee that the requirements are met and which actor impacts and is impacted by the requirement, allows identifying some implicit assumptions that can become a source of faulty design.

The system requirements of a control application are typically given in terms of stability, performance, and robustness, such as

- The feedback control system is asymptotically stable.
- The sensitivity to low frequency disturbances is bounded.
- High frequency measurement noise is attenuated.
- The control signal is bounded.
- The system is robust to model errors.

Such application requirements need to be satisfied under some assumptions on the communication infrastructure, which translate into requirements for the network design. Top-level communication network requirements are the following:

- N_e nodes are required to report sensed information periodically every T seconds (time-triggered nodes).
- N_t nodes are needed to monitor events with average occurrence rate λ (event-triggered nodes).
- The end-to-end delay should not be higher than d.
- The successful packet reception rate should not be lower than p.

Depending on the specific protocol implemented, the set of requirements can be enriched with assumptions, such as

- IEEE 802.15.4 sensor nodes communicates with single-hop transmissions to a coordinator node.
- IEEE 802.15.4 coordinators can be connected with sensor nodes and other coordinators.
- 15 non-overlapping channels can be used for data transmission in the 2,4 GHz band.

7.3.3 Design Procedure

The proposed contract-based design flow is developed into refinement steps:

1. Identification of responsibilities: we allocate requirements to each subsystem, collecting the requirements for which the subsystem is responsible. These requirements constitute the set of guarantees that the subsystem has to provide. The requirements that affect the subsystem but are not under its responsibility constitute the assumptions under which the subsystem must operate. Vertical $top - down$ contracts are thus inferred for each subsystem. For example, the robust controller will assume a certain reliability and delay from the communications and provide guarantees in terms of stability, sensitivity, and robustness.

2. Independent implementation: the design of each subsystem is verified with respect to its set of assumptions and physical constraints derived from the implementation space. Vertical $bottom - up$ contracts on each subsystem are utilized. In our example, the design algorithm verifies if the TDMA infrastructure can schedule at least its own generated traffic within the deadlines, and the event-triggered nodes should be able to guarantee the minimum reliability in each IEEE 802.15.4 cluster. Moreover, the controllers should be able to guarantee stability and the desired performance, considering the physical model of the UFAD system, without packet delay and losses from communication.

3. Composition: the models of subsystems at the same level of abstraction are composed to refine the contracts on individual subsystems. Refinement amounts to checking that the guarantees offered by the composition are stronger than or equal to the guarantees required by the subsystems, under a weaker set of assumptions. Horizontal contracts between subsystems define the composition. As an example, the composition of TDMA infrastructure and IEEE 802.15.4 clusters removes constraints on the environment by taking the intersection of the feasible solutions of the equations that model their interface. The composition of TDMA infrastructure and IEEE 802.15.4 clusters constitute a new subsystem, with a set of assumptions and guarantees that can be composed then with the controller.

4. Optimization: among all feasible compositions, an optimization tool is used to explore the component library to find the design that minimizes a specific cost.

If the contracts are consistent with respect to the provided system requirements and the composition is compatible, the obtained design is guaranteed to be correct-by-construction. However, checking consistency and compatibility can be computationally expensive during the optimization. In this case, heuristics are adopted to prune the exploration space [40]. In our study, we are interested in showing how contracts can be used to determine a valid composition with respect to the set of requirements, and the optimization phase is not addressed. In the next sections, we study models and derive examples of contract for each subsystem and for the composition of subsystems.

7.4 UFAD System Model

In this section, we describe the UFAD model. In order to use a model-based control approach, we exploit the thermodynamics properties of the ventilation process with a control volume approach. This approach allows for a reduced-order, easily reconfigurable system description that includes nonlinearities and discrete events (doors, internal power sources, etc.). Such events are handled specifically with a Markovian approach and the resulting system is described as a hybrid state-space model. We aim at defining the controlled system as:

- A set of inputs (controlled input u, exogenous input w), output y, and state variable x;
- A *behavioral* model represented by the state dynamics.

In the case of UFAD, the controlled input is expressed in terms of injected mass flow rates from the plenum, $u = [\dot{m}_{pl_1} \dots \dot{m}_{pl_{N_r}}]^T$, where N_r is the number of rooms. Exogenous inputs are the underfloor temperature $w_1 = T_{pl}$ and the outside temperature $w_2 = T_{\text{out}}$. The state and the output are expressed as a vector of room temperatures $y = x = [T_1 \dots T_n]^T$. The UFAD interfaces directly with the controller through the input u, and with the IEEE 802.15.4 clusters through its output y.

7.4.1 Behavioral Model

We describe the behavioral model of the UFAD system by the following state dynamics

$$\frac{dx_i(t)}{dt} = F_i(t) + D_i(t)\,. \tag{7.1}$$

where we distinguish between continuous dynamics $F_i(t)$ and discrete events $D_i(t)$.

Continuous Dynamics

The continuous dynamics of the model is set by the walls, ceiling, and plenum. Consider a 0-D model based on the mass and energy conservation. Each room is interconnected with the other building elements, as depicted in Figure 7.4. The interconnections are defined by the mass flow rate and heat transport. A model of an UFAD system is derived next.

Contract 7.4.1. *Assume that*

- *the air flow is incompressible;*
- *the control volume (CV) remains constant relative to the coordinate frame;*
- *the state of mass within the CV is uniform at any time;*

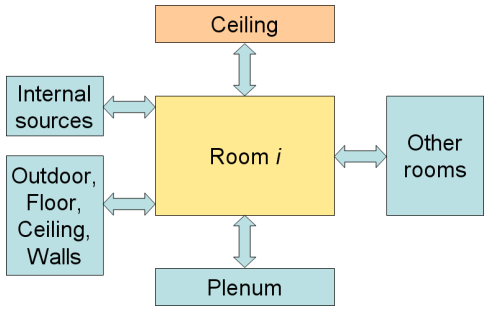

Figure 7.4: UFAD block diagram model.

- *the state of the mass crossing the CV is constant with time but the mass flow rates may vary;*
- *the kinetic and potential energy of the gas within the room are neglected;*
- *the doors are closed and that there is no power source within the room.*

Then, the temperature dynamics for room i is given as:

$$F_i(t) = \frac{1}{\rho_{\text{air}} V_i C_v} \left[-(\Theta_i + C_p \dot{m}_{pl_i}) T_i + \sum_{l=1}^{N_{iw}} \alpha_{iw_l} T_l + \sum_{l=1}^{N_{ow}} (\alpha_{ow_l} + \alpha_{gl_l}) T_{\text{out}} + (C_p \dot{m}_{pl_i} + \alpha_{pl_i}) T_{pl} \right] , \tag{7.2}$$

where

$$\Theta_i = \sum_{l=1}^{N_{iw}} \alpha_{iw_l} + \sum_{l=1}^{N_{ow}} \left(\alpha_{ow_l} + \alpha_{\text{glass}_l} \right) + \alpha_{pl_i} ,$$

ρ_{air} id the air density, V_i is the volume of the room, C_v is the constant volume specific heat, C_p is the constant pressure specific heat, N_{iw} is the number of connected inside walls, N_{ow} is the number of outside walls. For each component x, i.e., plenum (pl), inside wall (iw), outside wall (ow), and windows glass (gl), we have $\alpha_x = k_x A_x / \Delta x_x$, where k_x is the conductivity, A_x is the exchange surface area, and Δx_x is the thickness.

Derivation: A thermodynamical model of the continuous state dynamics of the UFAD system is discussed in details in Appendix E, and the state equations are derived under the proposed assumptions. □

By recalling the state as the vector of room temperatures $x = [T_1 \dots T_n]^T$, the controlled input as $u = [\dot{m}_{pl_1} \dots \dot{m}_{pl_n}]^T$ and the exogenous input as $w = [T_{pl}\ T_{\text{out}}]^T$, where n is the number of rooms, the system dynamics is given by

$$\dot{x} = (A_1 + A_2(u))x + B_u u + B_w w , \tag{7.3}$$

where the state matrices A_1 and A_2, and the input matrices B_u and B_w are computed according to Equation (7.2).

Moreover, we can rewrite the system dynamics with a change of variables to remove the known exogenous inputs and set the feedback on the tracking error. Defining the steady-state variables x_{ss}, u_{ss} and introducing the variations $\tilde{x}(t) \doteq x(t) - x_{ss}$ and $\tilde{u}(t) \doteq u(t) - u_{ss}$, the regulated dynamics are obtained from Equation (7.3) as

$$\begin{aligned}\dot{\tilde{x}} &= (A_1 + A_2 \operatorname{diag}(u_{ss} + \tilde{u}))(x_{ss} + \tilde{x}) + B_u(u_{ss} + \tilde{u}) + B_w w \\ &\approx (A_1 + A_2 \operatorname{diag}(u_{ss}))\tilde{x} + (A_2 \operatorname{diag}(x_{ss}) + B_u)\tilde{u}\,. \end{aligned} \tag{7.4}$$

Note that this model is fully determined by the building architecture and constant physical variables.

Discrete Dynamics

The discrete events are induced by the presence of power sources and the doors.

Contract 7.4.2. *Assume that*

- *there are N_q power sources in each room;*
- *there is a door connecting every adjacent rooms, but only one door can be open in a room at a given time;*
- *there is no return from the plenum due to power sources and door opening.*

Then, the temperature dynamics in room i is given by

$$D_i(t) = \frac{\sum_{k=0}^{N_q} \delta_{q,ik} \dot{Q}_{s,ik}}{\rho_{\text{air}} V_i C_v} + \begin{cases} 0, & \text{if } T_i > T_j \\ \delta_{d,ij} \frac{C_p \sqrt{2(C_p - C_v)}}{\rho_{\text{air}} V_i C_v} (T_j - T_i)^{3/2}, & \text{if } T_i < T_j \end{cases}$$

where $\dot{Q}_{s,ik}$ is the energy associated with the source k in the room i, N_q is the number of power sources, and $\delta_{q,ik}$ and $\delta_{d,ij}$ are introduced to denote the on/off operation of power sources and doors opening in room i.

Derivation: A thermodynamical model of the discrete state dynamics of the UFAD system is discussed in details in Appendix E, and the state equations are derived under the proposed assumptions. □

The discrete transitions are set by Markovian independent processes, constrained by the maximum and minimum periods during which a given event can occur. Further details are available in [149].

7.5 Wireless Network Design

In this section, we illustrate how contracts can be used in the compositional design of heterogeneous wireless networks with reference to the system architecture described in Section 7.2. Vertical contracts can be defined between different abstraction layers of the same subsystem, and between communication layers and application layer, whereas horizontal contracts can be defined for the composition of different subsystems at the same abstraction layer.

First, we identify subsystems composed by homogeneous protocol components, namely the IEEE 802.15.4 cluster, and the TDMA infrastructure. We construct an example of horizontal contracts at a high level of abstraction and give indication on how to build vertical contracts by using various model refinements such as the ones proposed in this thesis.

7.5.1 Subsystem: IEEE 802.15.4 Cluster

The IEEE 802.15.4 cluster j is composed of coordinator and a set of event-triggered nodes $i = 1, ..., N_{e,j} \leq N_e$.

The subsystem is defined at the MAC layer abstraction by:

- A set of inputs (number of nodes $N_{e,j}$, packet generation rate λ), output (delivered traffic Q_j), and internal parameters (number of backoffs m, initial backoff window m_0, maximum backoff window m_b, retry limits n, and packet length L);
- A *behavioral* model represented by a Markov chain and a system of non-linear equation to obtain the operating point.
- A $per formance$ model in terms of equations describing the reliability, delay, and energy consumption of the cluster.

This subsystem is responsible for the event-triggered application since it determines the guarantees. Moreover, the IEEE 802.15.4 cluster is involved in the time-triggered operation since it provides some of the assumptions.

Behavioral and Performance Models of the IEEE 802.15.4 Cluster

The behavior of an IEEE 802.15.4 cluster has been described under different levels of abstraction, throughout the previous chapters. Each model can be used in the design at different steps of refinement. For each step, it is necessary to define appropriate contracts. In the following, we introduce a contract at the MAC layer abstraction of the IEEE 802.15.4 cluster, which is based on the Markov chain analysis developed in Chapter 3, adapted to the unslotted mechanism.

Contract 7.5.1. *Given the following assumptions:*

- *There are $N_{e,j}$ nodes in the same contention range generating independent Poisson traffic with rate λ (packets per unit time), and packet length L (unit times).*
- *The detection probability at the receiver is higher than p_j.*
- *The unslotted IEEE 802.15.4 MAC yields m backoffs, no acknowledgments, and no retransmissions ($n = 0$).*

Then, the average probability of successful reception is at least

$$R_j = p_j \frac{1-(L+1)(N_{e,j}-1)\lambda}{1-L(N_{e,j}-1)\lambda}(1-(L(N_{e,j}-1)\lambda)^{m+1}),$$

and the delay for successfully received packets is at most

$$D_j = \frac{2^{m_0}}{1-2L(N_{e,j}-1)\lambda}\,.$$

Derivation: An upper bound for the busy channel probability is obtained as

$$\alpha = L(1-(1-\tau)^{N_{e,j}-1})(1-\alpha) < L(N_{e,j}-1)\tau(1-\alpha)\,,$$
$$\tau = \sum_{i=0}^{m}\alpha^i\lambda = \frac{1-\alpha^{m+1}}{1-\alpha}\lambda < \frac{\lambda}{1-\alpha}\,.$$

We obtain a simple equation for α,

$$\alpha < L(N_{e,j}-1)\lambda\,.$$

The collision probability is

$$\gamma = (1-(1-\tau)^{N_{e,j}-1}) < \frac{(N_{e,j}-1)\lambda}{1-L(N_{e,j}-1)\lambda}\,.$$

A lower bound on the successful packet reception probability at MAC layer is then

$$R_j = p_j(1-\alpha^{m+1})(1-\gamma) > \frac{1-(L+1)(N_{e,j}-1)\lambda}{1-L(N_{e,j}-1)\lambda}(1-(L(N_{e,j}-1)\lambda)^{m+1})\,,$$

An upper bound for the service time delay for successfully received packets is

$$D_j < \sum_{i=0}^{m}\alpha^i 2^{i+m_0} < \frac{2^{m_0}}{1-2L(N_{e,j}-1)\lambda}\,.$$

□

The previous contract determines guaranteed performance of the IEEE 802.15.4 MAC layer and provides a sufficient condition for the amount of traffic $N_{e,j}\lambda$ generated in the cluster to guarantee reliability and delay requirements imposed by the application layer. The input-output relation of the IEEE 802.15.4 cluster is then given by

$$Q_j = R_j N_{e,j} \lambda \,. \tag{7.5}$$

Contracts at different levels of abstraction can be defined by using the models equations developed in Chapters 4, and 5.

7.5.2 Subsystem: TDMA Infrastructure

The TDMA infrastructure is composed by the set of nodes $j \in \mathcal{T}$, where $|\mathcal{T}| = N_t$. The system is defined by:

- A set of inputs (number of nodes N_t, packet generation period T_j), output (scheduled traffic Q_s), and internal parameters (slot duration S, frame size T_f);
- A *behavioral* model represented by a routing matrix and a scheduling table.
- A *performance* model in terms of equations describing the reliability, delay, and energy consumption of the nodes.

This subsystem is responsible for the time-triggered application since it determines the guarantees. Moreover, the TDMA infrastructure is involved in the event-triggered application since it uses some of the guarantees.

Behavioral and Performance Models of the TDMA Infrastructure

We consider a static centralized TDMA scheme. Each node generates and forward traffic via multi-hop communications to a sink (data collection). Time is divided into slots of fixed duration S, and scheduled in periodic frames of length T_f. Considering that for each packet of node j, at least h_j slots need to be allocated, where h_j is the number of hops to the sink, therefore

$$T_f = \sum_{j=1}^{N_t} h_j n_j S \,, \tag{7.6}$$

where $n_j \in \mathbb{Z}^+$ is the number of slots per frame allocated for packets generated at node j.

A feasibility condition for the TDMA infrastructure is given by the length of the scheduling frame. At least one slot per frame must be allocated to each node

$$T_f > \sum_{j=1}^{N_t} \frac{h_j}{S} \,.$$

However the previous condition does not guarantee schedulability of the periodic frame. In fact, to guarantee that all the traffic is schedulable, the number of slots in each frame allotted to each node must be sufficient to allocate the generated and forwarded traffic in that frame. If a TDMA frame is schedulable, then the following relation holds

$$T_f > \sum_{j=1}^{N_t} \frac{h_j T_f}{T_j} S \,,$$

and, therefore,

$$\sum_{j=1}^{N_t} \frac{h_j}{T_j} T < 1 \,.$$

The maximum delay of node i for a generic scheduling algorithm in a schedulable TDMA frame of duration T_f is then

$$D_{\max,j} = T_f + h_j S = S \left(\sum_{i=1}^{N_t} h_i n_i + h_j \right) .$$

An example of a scheduling frame can be constructed by assigning to node j at least one slot in each period T_j, by following an earliest deadline first (EDF) approach [150].

In the following, we introduce a contract at the MAC layer abstraction of the TDMA infrastructure:

Contract 7.5.2. *Given the following assumptions:*

- *No packets are lost due to channel fading and interference.*
- *There are N_t nodes, each one described by the hop distance to the sink h_j, generating independent periodic traffic with periods T_j and slot duration S such that*

$$\sum_{j=1}^{N_t} \frac{h_j}{T_j} S < 1.$$

- *Only one packet can be scheduled in each time slot (no reuse).*
- *Consecutive slots are allocated to links in the same path to the sink.*

Then, there exists a scheduling that guarantees that the packet delay is at most

$$D_j = \min\{2T_j, T_f\} + h_j S \,.$$

Derivation: For an EDF scheduling algorithm, each node has a slot scheduled at least once in its generation period T_j. Therefore, the maximum distance between two allocated slots is $2T_j$. For asynchronous periodic packet arrival, the worst case delay is obtained when the packet arrives right after the allocated slot in the current period is occurred. However, for sporadic traffic, it is ensured that a node has at least one allocated slot in each TDMA frame T_f. The last assumption ensures that the delay for the forwarding procedure is $h_j S$. □

The minimum size of the TDMA frame T_f for the EDF scheduling can be found by solving the following combinatorial optimization problem

$$\min_{n_i \in \mathbb{Z}^+} \quad \sum_{i=1}^{N_t} n_i$$
$$\text{s. t.} \quad n_j T_j - \sum_{i=1}^{N_t} n_i \geq 0 \qquad j = 1, ..., N_t \, .$$

where we obtain $T_f = \sum_{i=1}^{N_t} n_i$. For a feasible schedule, an upper bound for the minimum EDF scheduling is given by the least common multiple (LCM) of the packet generation periods, i.e., $T_f <$LCM(T_i). The problem can be solved iteratively in polynomial time with the following algorithm:

1. set $T_f =$LCM(T_i) and choose $n_i = \lceil T_f / T_i \rceil$,
2. if $\sum_i n_i = T_f$, then $T_f^* = T_f$,
3. if $T_f > \sum_{i=1}^{N_t} h_j$ set $T_f = T_f - 1$ and go to step 1.

7.5.3 Protocol Composition

Characterizing the interface between subsystems is important. In particular, the input T_j for the TDMA infrastructure is dependent on the output Q_j of the IEEE 802.15.4 cluster, according to the following relation:

$$T_j = \bar{T}_j + \frac{1}{Q_j}, \tag{7.7}$$

where $\bar{T}_j$ is the traffic generation period by the node $j \in \mathcal{T}$, and Q_j is the forwarded traffic of the IEEE 802.15.4 cluster as derived in Equation (7.5).

Independent IEEE 802.15.4 clusters and TDMA infrastructure are obtained by choosing different channels among the available transmission frequencies. However, IEEE 802.15.4 devices contain only a single radio chip. When a coordinator node is scheduled for transmission or reception in the TDMA infrastructure, packets from the corresponding IEEE 802.15.4 cluster cannot be correctly detected. The detection probability at the receiver p_j in Contract 7.5.1 abstracts the physical layer

with the probability of channel fading p_j^{fad}. However, it includes the probability that the coordinator is active, either transmitting or receiving packets over the TDMA infrastructure p_j^{act}, according to

$$p_j = (1 - p_j^{\text{act}})(1 - p_j^{\text{fad}}). \tag{7.8}$$

Given $n_{tx,j}$ and $n_{rx,j}$ slots allocated to coordinator j in the TDMA infrastructure in transmission and reception, respectively, the probability that coordinator j is active in the TDMA infrastructure is

$$p_j^{\text{act}} = \frac{(n_{tx,j} + n_{rx,j})S}{T_j}. \tag{7.9}$$

By solving the system of Equations (7.7), (7.8), and (7.9), the composition of the IEEE 802.15.4 and TDMA infrastructure is characterized.

7.6 Robust Controller Synthesis

The aim of this section is to present the control design procedure for the problem presented above. Considering the discrete perturbations induced by the doors and power sources along with the communication constraints, the robustness issue appears as critical. We propose various multi-objectives H_∞ design strategies with tunable performance, input signal and sensitivity to disturbance.

The system is defined by:

- A set of inputs (reference signal x_{ref}, received state measurement x, exogenous input w), outputs (control signal u), and internal parameters (performance weight W_p, input weight W_u, disturbance weight W_d);
- A *behavioral* model represented by the regulated dynamics.
- A *performance* model in terms of temperature regulation and control effort.

We introduce these models next.

7.6.1 Behavioral and Performance Models

The standard H_∞ optimal control problem is to find a stabilizing controller $K(s)$ that minimizes $\|F(s)\|_\infty$, where $F(s)$ is the transfer function between the exogenous input w and the error signal e_f respect to the specified control objectives.

A first idea is to introduce the application requirements for the control system (i.e., performance, input boundary, and robustness) as weights on the sensitivity functions of the system. The approach is called mixed-sensitivity H_∞ synthesis (see [145] for more details). Denoting the system sensitivity function as $S(s)$ and

the complementary sensitivity as $T(s)$, the controller $K(s)$ is then designed to minimize

$$\left\| \begin{bmatrix} W_p(s)S(s) \\ W_u(s)K(s)S(s) \\ W_d(s)T(s) \end{bmatrix} \right\|_\infty .$$

We consider N_r inputs, corresponding to N_r rooms. The performance weight is tuned to guarantee performance with respect to the sensitivity bound as

$$W_p(s) = \text{diag}\left\{ \frac{s/M + \omega^*_{Bi}}{s + \omega^*_{Bi}A} \right\}, \quad i = 1 \dots N_r ,$$

where $A = 10^{-4}$ ensures an approximate integral action, $M = 2$, and ω^*_{Bi} different for each output (a large value yields a faster response for the corresponding output). The input weight is tuned to guarantee the input boundary as

$$W_u(s) = \text{diag}\left\{ \frac{s}{s + \omega_u} \right\},$$

where ω_u is approximately the closed-loop bandwidth. The robustness weight is introduced to reduce the impact of discrete events and measurements noise as

$$W_d(s) = \text{diag}\left\{ \frac{s + \omega^*_{Ti}/M}{As + \omega^*_{Ti}} \right\}, \quad i = 1 \dots N_r .$$

The desired closed-loop response is obtained thanks to an appropriate tuning of ω^*_{Bi}, ω_u, and ω^*_{Ti}. The parameters are set as

$$\omega^*_{Bi} = \alpha_p \frac{\text{mean}_i\{\rho_{\text{air}} V_i C_v\}}{\rho_{\text{air}} V_i C_v}, \quad \omega_u = \alpha_u \text{mean}_i\{\omega^*_{Bi}\}, \quad \omega^*_{Ti} = \alpha_t \omega^*_{Bi},$$

to take into account the fact that faster control can be achieved in rooms with faster time constants (smaller volume). The design problem is reduced to the choice of three scalar parameters α_p, α_u, and α_t. Simulation results for the mixed-sensitivity H_∞ synthesis applied to our UFAD model are discussed in Section 7.7.

The previous approach, does not consider the presence of communication constraints in the control system. An alternative approach is to insert the weights in the system dynamics by defining $e_f = W_p(s)(x_{\text{ref}} - x)$, $u_f = W_u(s)u$, and $w_f = W_d(s)w$. and consider the extended system dynamics

$$\begin{aligned} \dot{\mathbf{x}}_e &= A_g \mathbf{x}_e + B_g u + E_g \begin{bmatrix} w_f \\ x_{\text{ref}} \end{bmatrix} \\ \begin{bmatrix} e_f \\ u_f \end{bmatrix} &= C_g \mathbf{x}_e + D_g u + F_g \begin{bmatrix} w_f \\ x_{\text{ref}} \end{bmatrix} . \end{aligned} \tag{7.10}$$

The control problem is to find a stabilizing controller $K(s)$ that minimizes $\|F_e(s)\|_\infty$, with respect to the specified control objectives, where $F_e(s)$ is the transfer function between $\begin{bmatrix} w_f \\ x_{\text{ref}} \end{bmatrix}$ and $\begin{bmatrix} e_f \\ u_f \end{bmatrix}$. The considered controller is a state-feedback controller of the form:

$$u(t) = K_1 x(t) + K_2 x_e(t) + K_3 x_u(t)\,, \tag{7.11}$$

where the gains K_i have to be determined.

A first contract can be constructed by inserting the maximum admissible delay $D_{\max}$ in the set of assumptions for the controller synthesis.

Contract 7.6.1. *Given the following assumptions:*

- *The transmission delay is lower than $D_{\max}$.*
- *There exist matrices $P = P^T \succ 0$, $S = S^T \succ 0$, $R = R^T \succ 0$ and N_e of appropriate dimensions such that the following linear matrix inequalities hold:*

$$\Pi_1 + D\Pi_2 \prec 0, \quad \begin{bmatrix} \Pi_1 & D_{\max} N \\ \star & -D_{\max} R \end{bmatrix} \prec 0,$$

with

$$\begin{aligned} \Pi_1 &= M_1^T P M_3 + M_3^T P M_1 - M_2^T S M_2 - N M_2 - M_2^T N^T\,, \\ \Pi_2 &= M_2^T S M_3 + M_3^T S M_2 + M_3^T S M_3\,, \end{aligned}$$

and $M_1 = \begin{bmatrix} I & 0 \end{bmatrix}$, $M_2 = \begin{bmatrix} I & -I \end{bmatrix}$, and $M_3 = \begin{bmatrix} A_g & B_g K \end{bmatrix}$.

Then, the system (7.10) *is asymptotically stable.*

Derivation: The result is obtained from Theorem 1 in [144]. □

A second approach is obtained from [151].

Contract 7.6.2. *Given the following assumptions:*

- *The transmission delay is lower than $D_{\max}$.*
- *There exist $\nu > 0$, and matrices $P = P^T \succ 0$ and Y of appropriate dimensions such that the linear matrix inequality*

$$\begin{bmatrix} A_g P + P A_g^T + B_g Y + Y^T B_g^T & E_g & P C_g^T + Y^T D_g^T \\ \star & -\nu I & F_g^T \\ \star & \star & -\nu I \end{bmatrix} \prec 0$$

is fulfilled.[1]

[1] *Here, the $\star$ denotes blocks that are inferred by symmetry.*

Then, there exists a control low (7.11) *with gains*

$$\begin{bmatrix} K_1 & K_2 & K_3 \end{bmatrix} = Y P^{-1},$$

such that:

- *The system* (7.10) *is asymptotically stable.*
- *The* H_∞ *bound on the transfer function* $(w, x_{ref}) \to (e_f, u_f)$ *is lower than* ν.

Derivation: The result is a direct application of the Real Bounded Lemma [151]. In order to characterize the stability of the closed-loop system with delays and losses, we assume that the controller maintains the last measurement on its inputs until a new measurement is available. We also suppose that the same delay acts simultaneously on all the measurement. This is equivalent to a system output sampled at a time-varying sampling period. Hence, it is possible to use stability analysis of systems with time-varying sampling period to analyze the system stability under communication constraints. A bisection approach on the time-varying sampling period allows one to compute the relation between ν and the maximal admissible delay $D_{\max}$. □

In the following section, we show implementation results and performance comparisons for the proposed synthesis approaches.

7.7 Implementation Examples

We perform a simple design space exploration by considering the test case in Figure 7.5. We set the desired room temperature as $T_d = 273.15 + [18 \;\; 21 \;\; 19 \;\; 23]^T$ K.

First, we test the achievable performance of the control system without delays and losses due to the network. We consider the controller based on the mixed-sensitivity H_∞ synthesis.

Figure 7.6 shows the temperature tracking error $|T_{d,i} - T_i|$ when the controller parameters are set as

$$\alpha_p = 1000, \quad \alpha_u = 10, \quad \alpha_t = 1.$$

The high values of the parameters imply that all the desired bandwidth is available for control purposes, as the aim of this first test case is to get the best achievable performance without communication constraints. The higher sensitivity to door actuation observed in rooms 1 and 3 is due to the fact that these rooms have a lower temperature than the adjacent ones, combined with the limitation to single-direction flows induced by the 0-D model (see Appendix E).

The communication constraints are introduced thanks to the communication network model described in Section 7.5. Sampling, delay, and packet losses are

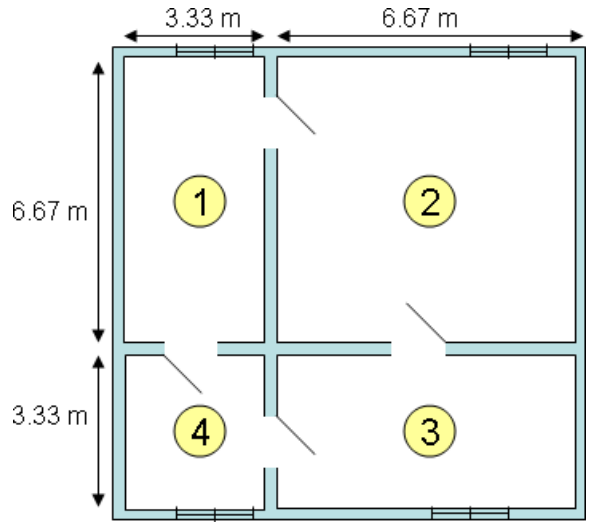

Figure 7.5: Flat architecture for the test case.

introduced between the measurements and the controller. The four dimensions of the state vector require a communication network of at least four event-triggered nodes. Moreover, consistently with the time dynamics of the UFAD behavioral model, an asynchronous traffic generation rate $\lambda = 5$ pkt/s for each node is assumed.

Given the physical dimensions of the rooms reported in Figure 7.5, we consider a distance $r < 10\,m$ between the nodes and the IEEE 802.15.4 coordinator. Based on the analysis developed in Chapter 5, for default MAC parameters ($m_0 = 3$, $m_B = 5$, $m = 4$, and $n = 0$), physical layer parameters ($P_{\text{tx}} = 0$ dBm, $a = -76$ dBm, and $b = 6$ dB), and a composite Nakagami-lognormal channel with $\sigma < 2$, the packet loss probability due to fading is guaranteed to be $p^{\text{fad}} < 0.01$. By applying Contract 7.5.1 without considering the TDMA infrastructure, the resulting IEEE 802.15.4 cluster guarantees a delay $D < 6$ ms with probability of reception $R > 0.99$.

The TDMA infrastructure needs to allocate at least four slots in a period $1/Q = 0.202$ s to the IEEE 802.15.4 coordinator, to forward traffic from the cluster. By assuming a packet generation period $\bar{T} = 1$ s, and a TDMA frame duration $T_f = 0.2$ s, the horizontal composition of IEEE 802.15.4 and TDMA infrastructure illustrated in Section 7.5.3 guarantees a delay $D < 0.2$ s with probability of reception $R > 0.95$.

We consider again the mixed-sensitivity H_∞ controller without including assumptions on the communication performance. When using the same parameters $\alpha_p = 1000$, $\alpha_u = 10$, and $\alpha_t = 1$, the system is unstable. In order to ensure the closed-loop stability and give satisfying performances, the control parameters are tuned to fulfill the new environment assumptions. The obtained parameters

are $\alpha_p = 0.1$, $\alpha_u = 1$, and $\alpha_t = 10$. The resulting temperature tracking error is presented in Figure 7.7. Note that the peak values of the error ($\approx 2.5°$ C) are considerably higher with respect to the ideal case in Figure 7.6. Indeed, the value of the performance weight α_p is limited by the closed loop stability requirement.

The controllers obtained from the Contracts 7.6.1 and 7.6.2 are tested as follows. We choose the weights

$$W_u(s) = \frac{s}{(s+\omega_1)}, \qquad W_p(s) = \frac{(s/M+\omega_b)}{(s+A\omega_b)}, \qquad W_d(s) = \alpha_t,$$

with $\omega_1 = 10$, $M = 2$, $\omega_b = 0.5$, $A = 10^{-4}$, and $\alpha_t = 10$.

First, Contract 7.6.1 is used for the synthesis with the simplifications $S = \varepsilon_s P$, $\varepsilon_s = 67$, $R = \varepsilon_r P$, $\varepsilon_r = 34$, and $D_{\max} = 0.2\,s$. The temperature tracking error for the resulting controller is shown in Figure 7.8. We can see that the maximal error values and the time needed to compensate a perturbation are significantly larger when the delay is included in the controller synthesis by using Contract 7.6.1. This is related to the inherent conservatism related to such a method.

By using Contract 7.6.2, with $\omega_1 = 10$, $M = 2$, $\omega_b = 0.5$, $A = 10^{-4}$, and $\alpha_t = 10$, we obtain $\nu = 0.93294$. However, such a small performance criterion is related to large values for eigenvalues and thus is responsible for a high sensitivity to delays. In order to reduce this sensitivity, we set $\nu = 10$ and get the following gains:

$$K_1 = \begin{bmatrix} 2.1921 & 0.0093 & 0.0009 & 0.0029 \\ 0.0065 & 2.5798 & 0.0060 & 0.0003 \\ 0.0010 & 0.0092 & 2.1173 & 0.0029 \\ 0.0072 & 0.0013 & 0.0067 & 1.3593 \end{bmatrix},$$

$$K_2 = \begin{bmatrix} -1.1461 & -0.0009 & -0.0004 & 0.0002 \\ -0.0011 & -1.1673 & -0.0008 & -0.0002 \\ -0.0004 & -0.0011 & -1.1516 & 0.0001 \\ -0.0016 & -0.0005 & -0.0014 & -1.1115 \end{bmatrix},$$

$$K_3 = \begin{bmatrix} 7.3908 & -0.0042 & -0.0011 & -0.0056 \\ -0.0054 & 7.6000 & -0.0054 & -0.0011 \\ -0.0010 & -0.0040 & 7.2683 & -0.0054 \\ -0.0029 & -0.0008 & -0.0029 & 5.4823 \end{bmatrix}.$$

The corresponding maximum admissible value of the delay is $D_{\max} = 0.2426$ s, which is sufficient for our application as the communication network guarantees a mean peak value for the delay of 0.2 s with 95% probability. The temperature tracking error for such a controller is shown in Figure 7.9. A significant improvement is obtained with respect to the previous approaches.

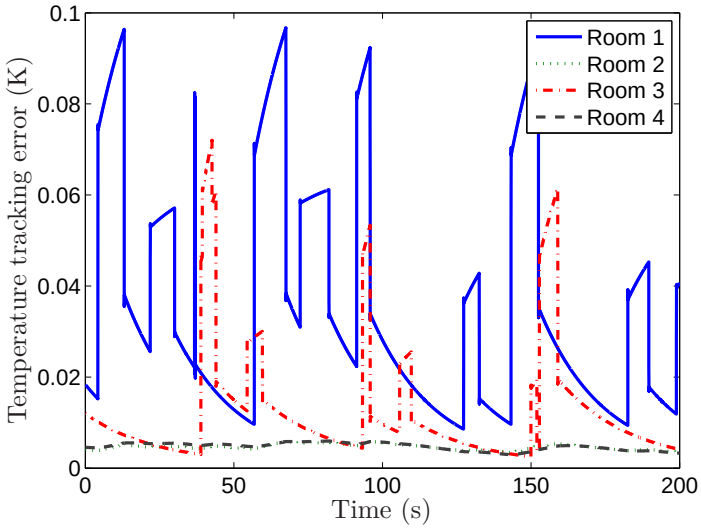

Figure 7.6: Temperature tracking error for the flat architecture in Figure 7.5. Mixed-sensitivity H_∞ controller without the presence of the network.

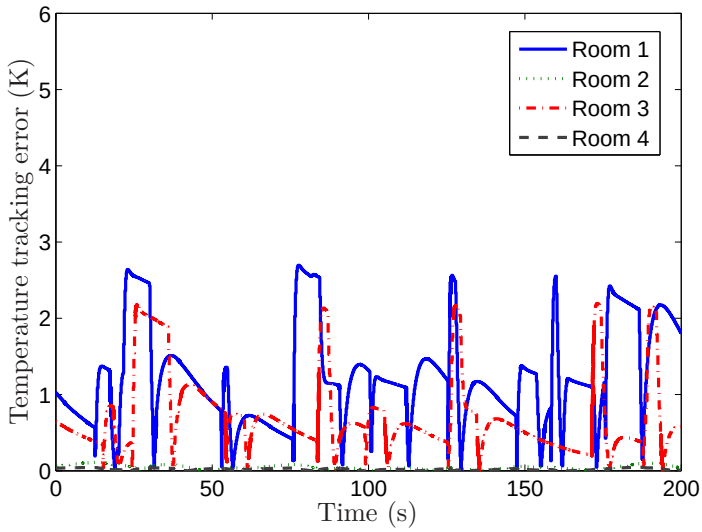

Figure 7.7: Temperature tracking error for the flat architecture in Figure 7.5. Mixed-sensitivity H_∞ controller over wireless network. Notice the different y-axis scale with respect to Figure 7.6.

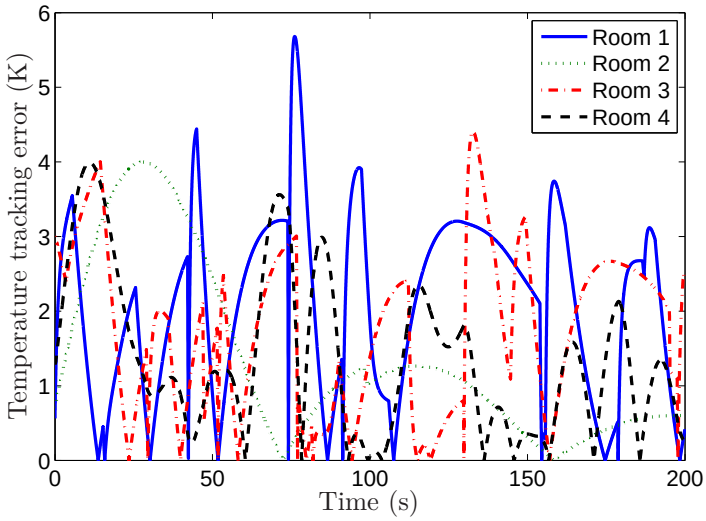

Figure 7.8: Temperature tracking error for the flat architecture in Figure 7.5. The controller is obtained from Contract 7.6.1, where the communication constraints are inserted *a-priori* in the controller synthesis.

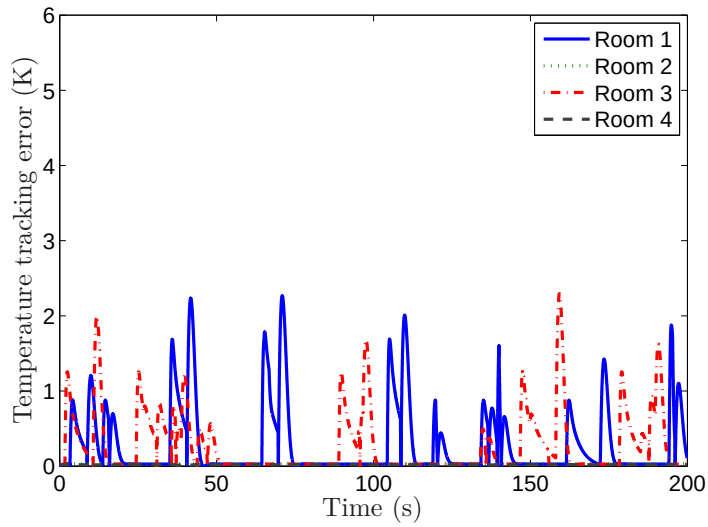

Figure 7.9: Temperature tracking error for the flat architecture in Figure 7.5. The controller is obtained from Contract 7.6.2, where parameters are tuned to fulfill the contract with the communication protocol.

7.8 Summary

In this chapter, we considered the problem of temperature regulation in intelligent buildings as the real-time control of an actuated UFAD process over a heterogeneous wireless network. Assume/guarantee reasoning was introduced in the compositional design of communication and control.

First, we presented a behavioral model of the UFAD system based on the thermodynamic properties of the room control volume. Discrete events such as doors openings, presence of people, and the use of appliances were introduced as Markovian processes, which resulted in a hybrid nonlinear state-space description of the complete interconnected system.

We defined contracts for a communication infrastructure composed of event-triggered and time triggered nodes, by considering the contention-based IEEE 802.15.4 MAC and the contention free TDMA. Sufficient condition for the composition of protocols were derived in terms of traffic and performance indicators (reliability and delay), and used in the UFAD system design.

We discussed the interaction between communication and control by considering various MIMO H_∞ controllers synthesized based on linearized model dynamics and compared in terms of temperature regulation performance. It was shown that the communication infrastructure has a strong impact on the closed-loop stability and the achievable performance. An alternative controller was designed by considering the assumption of a maximum communication delay directly in the gain synthesis. However, the resulting closed-loop performances appeared to be worse than the other design strategies, with a larger error and longer response time. This is probably related to the conservatism induced by the method. Moreover, we proposed a controller based on the bounded-real lemma. An appropriate choice of the norm allowed for tuning the sensitivity to communication delays. The maximum admissible delay was computed a posteriori and tuned with the guarantees from the communication. This controller appeared to be the most efficient, in terms of temperature regulation (maximum peaks and response time).

The results illustrated how contracts can be inserted in the design flow and suggested that a careful analysis of the requirements in the composition of subsystems is essential for the efficient operation of the networked control system.

Chapter 8

Conclusions

In this thesis, we proposed an analytical framework to model and design communication protocols for application such as industrial control, intelligent transportation systems, and building automation. In the following, we summarize the main results and propose ideas and directions for our future work.

8.1 Summary of Results

The main contributions of the thesis were presented in five steps.

First, we investigated a generalized approach to characterize the performance of the slotted CSMA/CA mechanism in the IEEE 802.15.4 standard. The approach is based on a Markov chain that considers retry limits, the acknowledgement mechanism, and unsaturated traffic, which are important components of wireless networks for control applications. We derived expressions of the reliability, delay, and energy consumption of the slotted IEEE 802.15.4 MAC by an accurate model and approximate equations. We analyzed experimentally the impact of MAC parameters on reliability, delay, and energy consumption. We showed that the approximated analysis is very effective for low traffic. Furthermore, we observed that the delay distribution of IEEE 802.15.4 depends on the MAC parameters and the collision probability. In addition, we illustrated an adaptive MAC algorithm for minimizing the power consumption while guaranteeing reliability and delay constraints of networked control systems.

As a second contribution, we studied the mutual influence between routing decisions and MAC performance in terms of reliability, delay, and load balancing, by considering the RPL routing specifications over the unslotted IEEE 802.15.4 MAC. We introduced an analytical model that includes the important features of multihop networks, such as heterogeneous distribution of the traffic and hidden terminal nodes. We showed that the distribution of traffic load in the network influences the performance in terms of reliability, delay, and energy consumption. The effect depends strongly on the carrier sensing range of nodes in the network. Furthermore, we derived conditions in which routing decisions based on packet loss probability

or delay can lead to an unbalanced distribution of the traffic load across paths with potentially dangerous effects on the energy consumption. We proposed metrics that take this interaction into account and validated the performance experimentally.

In the third contribution, we introduced a composite Nakagami-lognormal fading model in the analysis of MAC and routing performance. We studied the impact of the fading statistics on the end-to-end performance in terms of reliability, delay, and power consumption, by varying traffic, distances, carrier sensing range, and SINR threshold. We observed that the severity of the fading and the physical layer thresholds have significant and complex effects on every performance indicator, and the effects are well predicted by our model. In particular, the fading has a relevant negative impact on the reliability. The effect is more evident as traffic and distance between nodes increase. However, depending on the carrier sensing and SINR thresholds, a fading with small spread can improve the reliability with respect to the ideal case. The delay for successfully received packets and the power consumption are instead positively affected by the fading and the performance can be again optimized by acting on the thresholds.

Then, we extended our perspective by including the effect of the requirements from the application in the design of a communication protocol stack compliant with ROLL and IEEE 802.15.4, as we developed TREnD, a novel cross-layer solution for control applications over wireless networks, which satisfies application requirements on reliability and delay while minimizing energy consumption. We posed and solved an optimization problem to select the protocol parameters. We presented a testbed implementation of the protocol that we designed with TinyOS and Tmote sensors. An experimental campaign was conducted to validate the protocol in an indoor environment. Experimental results showed that the protocol achieves the reliability and delay requirements in practice as well, while minimizing the energy consumption. In addition, the protocol showed good load balancing performance and scalability.

As a final contribution, we closed the loop between communication and control applications, introducing the effects of communication constraints into the design of a real-time control of an actuated under-floor air distribution process. Contracts on reliability and delay were defined to design the composition of an IEEE 802.15.4 network and a TDMA infrastructure, and the integration of the resulting constraints in the synthesis of a robust controller. Three MIMO H_∞ controllers were synthesized based on a linearized model of the system and compared in temperature regulation performance. An appropriate choice of the norm allowed for tuning the sensitivity to the communication constraints and giving satisfactory performance.

8.2 Future Work

The contract-based methodology can potentially have a great impact in the design of wireless networked control systems. However, some additional aspects of the overall design procedure are yet to be defined. The main challenge is to automate

the design in a correct-by-construction fashion. The methodology should count on a vast library of components, namely protocols and their analytical models. We provided a proof-of-concepts analysis, following the block diagram presented in Figure 1.6, and provided models only for some reference components. For the communication layers, we focused on basic mechanisms (CSMA and TDMA MAC), standard solutions (slotted and unslotted IEEE 802.15.4, IETF RPL), and the cross-layer protocols TREnD. From a control perspective, we considered mixed-sensitivity H_∞ approaches. Besides the contribution presented in this thesis, there are various aspects of the problem that are under development and contain ideas for future studies. Here, we describe various directions of research.

The MAC layer analysis can be extended by considering evolutions of the standards, as the IEEE 802.15.4e [152]. TDMA and frequency hopping are included in the MAC layer specifications. Scheduling algorithms have been recently proposed and analyzed for the new MAC modality [153]. Simple bounds on the delay are derived. Results can be extended to determine reliability, delay, and energy consumption of the IEEE 802.15.4e.

At the network level, an important issue is the dynamic behavior and stability of routing protocols. We considered reliability, delay, and energy metrics, but the interaction between MAC and routing has been developed for stationary conditions. As described in Chapter 2, nodes perform global and local maintenance through DIO messages. A slow update of the routing information reduces the energy consumption, but it makes the routing sensitive to channel variabilities and thereby degrades performance. Conversely, a fast update causes continuous routing topology changes and generates instability in the network. A tradeoff can be exploited to offer energy efficiency and stable routing. For real-time control applications, the standard mechanism implemented in RPL may be not efficient. We are currently working on the evaluation of different strategies for re-routing, and their effects on the performance of a control application over multi-hop networks.

The analysis of fading channel conditions can be extended to include space and time correlations among nodes in the network. Models for the sum of space-correlated lognormal components are available in [127]. Preliminary analysis and simulations show that the effect of space correlation is not significant for the packet loss probability in our setup, with respect to the variability of each fading component. Time correlation may have strong effects on the performance, especially considering the short time between consecutive backoffs in the IEEE 802.15.4 MAC.

The work on TREnD can be extended by including a more general model of the hybrid TDMA/CSMA.The problem is formulated as follows: each node has a buffer of packets that have been generated during the sleeping time (inactive TDMA-slots). N nodes contend for the medium by using p-persistent MAC or the CSMA/CA mechanism, and need to deliver their packets within a deadline given by the TDMA-slot duration. When the buffer is empty, the node goes to sleep. The Markov chain in Figure D.1 can be extended to a two-dimensional chain, in which the two states represent the number of packets to deliver and the number of contending nodes. A tradeoff between accuracy and tractability of the equations is

important for a practical implementation of the protocol.

The work proposed above can provide new insights on the interaction among protocol layers, and new components for our library of protocols. The results can be used to formalize more contracts and guide the compositional design of communication and control. Although the results have been validated in test-beds, an implementation of the full design in a real building automation system or industrial site would be useful to validate the methodology.

Appendix A

Proof for Chapter 3

A.1 Derivation of Approximation 3.3.1

The expression of the state probability $b_{0,0,0}$ is the main responsible for the non-linear equations that give α, β, and τ. Therefore, we approximate $b_{0,0,0}$. Let the approximation be $\widetilde{b}_{0,0,0}$. Given $z \geq 0$, we use

$$\frac{1-z^{m+1}}{1-z} \approx 1+z\,, \qquad \text{if} \quad z \ll 1\,. \tag{A.1}$$

By using this approximation, Equation (3.15) is approximated as

$$\sum_{i=0}^{m}\sum_{k=0}^{W_i-1}\sum_{j=0}^{n} b_{i,k,j} \approx \frac{b_{0,0,0}}{2}\left[(1+2x)W_0+1+x\right](1+y)\,. \tag{A.2}$$

Similarly, Equation (3.16) is approximated by

$$\sum_{i=0}^{m}\sum_{j=0}^{n} b_{i,-1,j} \approx b_{0,0,0}(1-\alpha)(1+x)(1+y) \approx 0\,. \tag{A.3}$$

Equation (3.17) is approximated by

$$\sum_{j=0}^{n}\left(\sum_{k=0}^{L_s-1} b_{-1,k,j} + \sum_{k=0}^{L_c-1} b_{-2,k,j}\right) \approx b_{0,0,0}L_s(1-x^{m+1})(1+y), \tag{A.4}$$

where we assume that the packet collision time is approximated to the packet successful transmission time, namely $L_s \approx L_c$. Using $K_0 = L_0\eta/(1-\eta)$, the approximate idle-queue stage probability of Equation (3.18) is

$$\sum_{l=0}^{L_0-1} Q_l \approx b_{0,0,0}K_0\left(1+y+\gamma(1-x^{m+1})(y^n-y-1)\right). \tag{A.5}$$

Finally, the approximated packet copying stage probability of Equation (3.19) is

$$\sum_{l=0}^{L_1-1} H_l \approx b_{0,0,0} L_1 \left(1 + y + \gamma(1 - x^{m+1})(y^n - y - 1)\right). \tag{A.6}$$

By summing up together Equations (A.2)–(A.6) and applying the approximation of Equation (A.1), the state probability is

$$\widetilde{b}_{0,0,0} \approx \frac{2}{W_0 r_1 + 2 r_2} \tag{A.7}$$

where

$$\begin{aligned} r_1 &= (1 + 2x)(1 + \hat{y}), \\ r_2 &= L_s(1 - x^2)(1 + \hat{y}) + (K_0 + L_1)(1 + \hat{y}^2 + \hat{y}^{n+1}), \\ \hat{y} &= (1 - (1 - \tau)^{N-1})(1 - x^2). \end{aligned}$$

Now, we insert $\widetilde{b}_{0,0,0}$ into Equation (6.2) to obtain the approximated reliability:

$$\widetilde{R} = 1 - x^{m+1}(1 + \widetilde{y}) - \widetilde{y}^{n+1},$$

where $\widetilde{y} = (1 - (1 - \widetilde{\tau})^{N-1})(1 - x^2)$ and $\widetilde{\tau}$ is the approximated carrier sensing probability $\widetilde{\tau} = (1 + x)(1 + \hat{y})\widetilde{b}_{0,0,0}$.

A.2 Proof of Proposition 3.3.2

The PGFs of the delay is obtained from the generalized state transition diagram of the Markov chain in Figure 3.2. The Markov chain is enriched by including the transition time in each stage, namely the time for each state transition to take place, as an exponent of a Z variable. The state transition probability together with the transition time on each branch indicates that the state transition happens with that probability and, if it does, it takes that transition time [154].

Whenever the node succeeds two CCAs, a transmission commences. According to the probability γ of a collision seen by a packet being transmitted on the medium, the node has a probability $1-\gamma$ to finish the transmission within a time Z^{L_s}, and a probability γ to initialize the backoff procedure until the maximum retransmission limit is reached after Z^{L_c}. Since a packet is transmitted after successful channel access during two CCAs, the probability for successful channel access is $1-(\alpha+(1-\alpha)\beta)^{m+1}$. The PGF of the random backoff process $H_i(Z)$ is given by the product of the i stages in Figure 3.2 as

$$H_i(Z) = \prod_{k=0}^{i} W_k(Z), \tag{A.8}$$

where $W_i(Z)$ is the PGF of the backoff time at the i-th stage:

$$W_i(Z) = \begin{cases} \sum_{l=0}^{2^i W_0 - 1} \frac{M_d(Z)^l}{2^i W_0} = \frac{1 - Z^{2^i W_0}}{2^i W_0 (1-Z)} & \text{if } i \leq m_b - m_0 \\ \sum_{l=0}^{2^{m_b} - 1} \frac{M_d(Z)^l}{2^{m_b}} = \frac{1 - Z^{2^{m_b}}}{2^{m_b}(1-Z)} & \text{otherwise} \end{cases}$$

where we considered $M_d(Z) = Z$, because the decrement of backoff counter happens with probability 1. Then we can evaluate the transfer function of the event of i sensing fails due to the busy channel condition $G_i(Z)$ as follows. During the backoff process, the backoff timer at i-th stage decreases by one unit time regardless of the channel state. When the random backoff time of node is equal to zero the node goes to sensing state. If the medium is idle (with probability $1 - \alpha$) at CCA_1 then the node goes to CCA_2. If an ongoing transmission (with probability α) is detected, the backoff exponent is increased by one and a random backoff time is generated until the maximum number of stages is reached. The node repeats the same mechanism during the second sensing in Figure 3.2. The total number of combinations for i elements is equal to 2^i and are collected in the set $C_{\alpha\beta}(i)$. $C^k_{\alpha\beta}(i)$ is one of the combinations out of 2^i events. The function $2N^k_\beta(i)$ gives the sensing fails at the second sensing state. Therefore we obtain

$$G_i(Z) = \sum_{k=1}^{2^i} C^k_{\alpha\beta}(i) S_c(Z)^{N^k_\alpha(i) + 2N^k_\beta(i)} \tag{A.9}$$

where $S_c(Z) = Z$ is the sensing time, $C^k_{\alpha\beta}(i)$ returns the k-th combination of $C_{\alpha\beta}(i)$, and $N^k_\alpha(i)$, $N^k_\beta(i)$ returns the number of α and $(1-\alpha)\beta$ in the combination, respectively. Note that $H_{m+1}(Z), G_{m+1}(Z)$ consider the random backoff process and sensing delay for discarded packets due to channel sensing fails, respectively. By considering the normalized probability of successful transmission after j collisions obtained in Equation (3.28), the PGF of packet delay for successfully received packets follows after simple passages.

A.3 Derivation of Approximation 3.3.3

By considering the busy channel during two CCAs, the probability of the event $\mathscr{D}_i$ given $\mathscr{D}$ is approximated by

$$\widetilde{\Pr}(\mathscr{D}_i | \mathscr{D}) = \frac{\xi^i}{\sum_{k=0}^{m} \xi^k}, \tag{A.10}$$

where $\xi = \max(\alpha, (1-\alpha)\beta)$. Note that the approximation is based on the worst case of the busy channel probabilities. The approximation of the average backoff

period is

$$\begin{aligned}\mathbb{E}[\widetilde{t}_h] =& \sum_{i=0}^{m} \widetilde{\Pr}(\mathscr{D}_i|\mathscr{D})\, \mathbb{E}[\widetilde{t}_{h,i}] \\ =& 2t_{sc} + \sum_{i=0}^{m} \widetilde{\Pr}(\mathscr{D}_i|\mathscr{D}) \sum_{k=0}^{i} \left(\frac{2^k W_0 - 1}{2} S_b + 2t_{sc}\, k \right)\end{aligned} \tag{A.11}$$

where the approximated sensing time $\mathbb{E}[\widetilde{t}_{h,i}]$ considers the worst case, i.e., a failure of CCA_2, which implies that $t_{sc} = S_b$ and that each sensing failure takes $2t_{sc}$. Therefore, the expected value of the approximated backoff delay is

$$\begin{aligned}\mathbb{E}[\widetilde{t}_h] =& 2S_b \left(1 + \frac{1}{4} \left(\frac{1-\xi}{1-\xi^{m+1}} \left(2W_0 \frac{1-(2\xi)^{m+1}}{1-2\xi} \right.\right.\right. \\ & \left.\left.\left. - \frac{3(m+1)\xi^{m+1}}{1-\xi} \right) + \frac{3\xi}{1-\xi} - (W_0+1) \right) \right) ,\end{aligned} \tag{A.12}$$

where $\xi = \max(\alpha, (1-\alpha)\beta)$. By inserting Equation (A.12) into Equation (3.30), we derive the approximate delay in Equation (3.35)

A.4 Derivation of Approximation 3.3.4

By considering Equation 3.36, the average power consumption of *I-mode* can be represented as

$$\widetilde{E}_{\mathrm{tot},i} = E_{b,i} + E_{sc} + E_t + E_q + E_h + E_{w,i}\,.$$

In the following, we derive these terms. The idle backoff power consumption is

$$E_{b,i} = P_i \sum_{i=0}^{m} \sum_{k=1}^{W_i - 1} \sum_{j=0}^{n} b_{i,k,j} = \frac{P_i \tau}{2} \left[\frac{(1-x)(1-(2x)^{m+1})}{(1-2x)(1-x^{m+1})} W_0 - 1 \right] , \tag{A.13}$$

where the carrier sensing probability τ is measured by each device and P_i is the average power consumption in idle-listen. By putting together Equations. (3.15), (3.16) and (3.21), the average power consumption of the sensing state is

$$E_{sc} = P_{sc} \sum_{i=0}^{m} \sum_{j=0}^{n} (b_{i,0,j} + b_{i,-1,j}) = P_{sc}(2-\alpha)\tau\,, \tag{A.14}$$

where P_{sc} is the average power consumption in channel sensing. Similarly, by substituting Equation (3.17) and Equation (3.21), the average power consumption for packet transmission including both successful transmission and packet collision

E_t is

$$\begin{aligned} E_t =& P_t \sum_{i=-2}^{-1} \sum_{k=0}^{L-1} \sum_{j=0}^{n} b_{i,k,j} + P_i \sum_{i=-2}^{-1} \sum_{j=0}^{n} b_{i,L,j} \\ &+ \sum_{j=0}^{n} \sum_{k=L+1}^{L+L_{\text{ack}}+1} (P_r\, b_{-1,k,j} + P_i\, b_{-2,k,j}) \\ =& (1-x)\tau \left(P_t L + P_i + L_{\text{ack}} \left(P_r(1-\gamma) + P_i\gamma\right)\right), \end{aligned} \tag{A.15}$$

where P_t and P_r are the average power consumption in transmitting and receiving states, respectively. Analogously, E_q is the power consumption of idle stage without packet generation:

$$E_q = P_{sp} \sum_{l=0}^{L_0-1} Q_l \approx 0\,, \tag{A.16}$$

where P_{sp} is the average power consumption in sleep states, which we assume negligible, and E_h is the power consumption of packet copying stage:

$$E_h = P_{sp} \sum_{l=0}^{L_1-1} H_l \approx 0\,, \tag{A.17}$$

which we assume negligible. Since a device wakes up only after copying packet, the wake-up power consumption is

$$\begin{aligned} E_{w,i} =& P_w H_{L_1-1} = P_w \frac{1-\eta}{\eta} Q_0 \\ =& P_w \left(x^{m+1}(1+y) + \left(\gamma y^n + (1-\gamma)(1+y)\right)(1-x^2)\right) \widetilde{b}_{0,0,0}\,, \end{aligned} \tag{A.18}$$

where P_w is the average power consumption in wake-up state and the state probability $\widetilde{b}_{0,0,0}$ is given in Equation (A.7). By summing Equations (A.13)–(A.18), we obtain the average power consumption of *I-mode* in closed form.

The average power consumption of *S-mode* can be derived by following an similar approach to the *I-mode* where the sleep backoff power consumption is

$$E_{b,s} = P_{sp} \sum_{i=0}^{m} \sum_{k=1}^{W_i-1} \sum_{j=0}^{n} b_{i,k,j} \approx 0\,,$$

the wake-up power consumption is

$$E_{w,s} = P_w \sum_{i=0}^{m} \sum_{j=0}^{n} b_{i,1,j} \approx P_w \left(\tau - \frac{\widetilde{b}_{0,0,0}}{W_0} \frac{1-(0.5x)^{m+1}}{1-0.5x} \frac{1-y^{n+1}}{1-y}\right),$$

and E_{sc}, E_t, E_q, E_h is given in Equations (A.14), (A.15), (A.16), and (A.17), respectively. Since the radio is set in sleep mode during backoff period, device wakes up for each CCA_1 state.

Appendix B

Proof for Chapter 4

B.1 Queueing Model for the Markov Chain in Figure 4.3

In this section, we derive the probabilities of having a new packet to send in the different stages of the Markov chain. We consider four different situations: (i) probability of generation of a new packet after an idle unit time q_l; (ii) probability that the node queue is not empty after a packet has been successfully sent $q_{\text{succ},l} = 1 - p^s_{l,0}$; (iii) probability that the node queue is not empty after a packet has been discarded due to channel access failure $q_{cf,l} = 1 - p^m_{l,0}$; (iv) probability that the node queue is not empty after a packet has been discarded due to the retry limit $q_{cr,l} = 1 - p^n_{l,0}$. By assuming generation of packets with Poisson distribution at rate λ_l, the probability of generation of a new packet after an idle unit time can be easily derived as $q_l = 1 - \exp(-\lambda_l / S_b)$. The other terms are derived in the following.

If we assume limited buffer size B, the packet queue in the device buffer can be modeled as a $M/G/1/K$ queueing system. Denoting a_k as the probability to have k packets arrivals into the buffer of a node during the service time, its probability-generating function (PGF) can be expressed as a function of the PGF of the service time $\mathcal{T}_l(z)$ as [126]

$$a_k = \frac{1}{k!} \frac{d^k \mathcal{T}_l(1 - q_l + q_l z)}{dz^k} \bigg|_{z=0} . \tag{B.1}$$

The steady state probability $p_{l,k}$ that there are k packets in the buffer of node V_l after a packet transmission attempt is given by solving the following system in a recursive manner [94].

$$\begin{cases} p_{l,k} = p_{l,0} a_k + \sum_{j=1}^{k+1} p_{l,j} a_{k-j+1} & 0 \le k \le B-2 \,, \\ p_{l,B-1} = p_{l,0} \sum_{k=B-1}^{\infty} a_k + \sum_{j=1}^{B-1} p_{l,j} \sum_{k=B-1}^{\infty} a_k \,. \end{cases} \tag{B.2}$$

By inserting the expression of the PGF of the service time for successful transmission $\mathcal{T}_{tx,l}$, failure due to maximum number of backoffs $\mathcal{T}_{cf,l}$, and failure due to retry limit $\mathcal{T}_{cr,l}$ into Equation (B.1), it is possible to derive the probabilities of empty queue $p^s_{l,0}$, $p^m_{l,0}$, and $p^n_{l,0}$, respectively.

The delay distribution of IEEE 802.15.4 MAC with ACK and retransmission is derived for the slotted mechanism in Section 3.3.2. The derivation for the Markov chain in Figure 4.3 follows similar steps. However, the derivation of the PGFs for each node is unpractical and computationally expensive. In case the average queue length is lower than the buffer size B, a good approximation of the empty queue probability can be obtained by using a $M/G/1$ model [114]. For Poisson arrivals with rate λ_l, we obtain

$$p^s_{l,0} = 1 - \lambda_l \mathbb{E}\{D^s_l\}\,, \tag{B.3}$$

where the average service time is computed in Section 4.3.3 for all the situations mentioned here.

B.2 Proof of Proposition 4.3.1

First, we compute the stationary distribution of the Markov chain in Figure 4.3. The transition probabilities of the chain are

$$\Pr[i,k,j|i,k+1,j] = 1, \qquad \text{for } k \geq 0\,, \tag{B.4}$$

$$\Pr[i,k,j|i-1,0,j] = \frac{\alpha_l}{W_i}, \qquad \text{for } i \leq m\,, \tag{B.5}$$

$$\Pr[0,k,j|i,0,j-1] = \frac{(1-\alpha_l)P_{\text{coll},l}}{W_0}, \qquad \text{for } j \leq n\,, \tag{B.6}$$

$$\Pr[\text{idle}|i,0,j] = (1-q_{\text{succ},l})\,(1-\gamma_l)\,\alpha_l, \qquad \text{for } i < m\,,\ j < n\,, \tag{B.7}$$

$$\Pr[\text{idle}|m,0,j] = (1-q_{cf,l})\,\alpha_l, \qquad \text{for } j < n\,, \tag{B.8}$$

$$\Pr[\text{idle}|i,0,n] = (1-q_{cr,l})(1-\alpha_l), \qquad \text{for } i < m\,, \tag{B.9}$$

$$\Pr[\text{idle}|m,0,n] = (1-q_{cr,l})(1-\alpha_l) + (1-q_{cf,l})\alpha_l\,, \tag{B.10}$$

$$\Pr[0,k,0|\text{idle}] = \frac{q_l}{W_0}, \qquad \text{for } k \leq W_0 - 1\,. \tag{B.11}$$

Equation (B.4) is the decrement of backoff counter, which happens with probability 1. Equation (B.5) represents the probability of finding busy channel in CCA and of choosing a state uniformly in the next backoff stage. Equation (B.6) gives the probability of unsuccessful transmission after finding a clear channel, where a node selects uniformly a state in the next retransmission. Equations (B.7)–(B.9) represent the probability of going back to the idle stage due to success, channel access failure and retry limit, respectively. Equation (B.10) is the probability of going back to the idle stage at backoff counter m and retransmission stage n. Equation (B.11) models the probability of going back to the first backoff stage from the idle stage.

Owing to the chain regularities and Equations (B.4)–(B.11), we have

$$b_{i,k,j}^{(l)} = \frac{W_i - k}{W_i} b_{i,0,j}^{(l)}\,, \tag{B.12}$$

where $W_i = \begin{cases} 2^i W_0 & i \le m_b - m_0 \\ 2^{m_b - m_0} W_0 & i > m_b - m_0\,. \end{cases}$

From Equation (B.5), for $i \le m$ we obtain

$$b_{i,0,j}^{(l)} = \alpha_l^i b_{0,0,j}^{(l)}. \tag{B.13}$$

From Equation (B.6), $b_{0,0,j}^{(l)}$ is rewritten as follows,

$$b_{0,0,j}^{(l)} = \left((1-\alpha_l)\gamma_l \sum_{i=0}^{m} \alpha_l^i\right)^j b_{0,0,0}^{(l)}\,. \tag{B.14}$$

By the normalization condition, we know that

$$\sum_{i=0}^{m}\sum_{k=0}^{W_i-1}\sum_{j=0}^{n} b_{i,k,j}^{(l)} + \sum_{j=0}^{n}\left(\sum_{k=0}^{L_s-1} b_{-1,k,j}^{(l)} + \sum_{k=0}^{L_c-1} b_{-2,k,j}^{(l)}\right) + b_{\text{idle}}^{(l)} = 1. \tag{B.15}$$

We next derive the expressions of each term in Equation (B.15). From Equations (B.12), (B.13), (B.14), we have

$$\sum_{i=0}^{m}\sum_{k=0}^{W_i-1}\sum_{j=0}^{n} b_{i,k,j}^{(l)} = \sum_{i=0}^{m}\sum_{j=0}^{n} \frac{W_i+1}{2}\alpha_l^i\, b_{0,0,j}^{(l)} \tag{B.16}$$

$$= \begin{cases} \frac{b_{0,0,0}^{(l)}}{2}\left(\frac{1-(2\alpha_l)^{m+1}}{1-2\alpha_l}W_0 + \frac{1-\alpha_l^{m+1}}{1-\alpha_l}\right)\frac{1-y_l^{n+1}}{1-y_l} \\ \qquad\qquad \text{if } m \le \bar{m} = m_b - m_0, \\ \frac{b_{0,0,0}^{(l)}}{2}\left(\frac{1-(2\alpha_l)^{\bar{m}+1}}{1-2\alpha_l}W_0 + \frac{1-\alpha_l^{\bar{m}+1}}{1-\alpha_l}\right. \\ \left. + (2^{m_b}+1)\alpha_l^{\bar{m}+1}\frac{1-\alpha_l^{m-\bar{m}}}{1-\alpha_l}\right)\frac{1-y_l^{n+1}}{1-y_l} \qquad \text{otherwise,} \end{cases}$$

where $y_l = \gamma_l(1-\alpha_l^{m+1})$.
Similarly,

$$\sum_{j=0}^{n}\left(\sum_{k=0}^{L_s-1} b_{-1,k,j}^{(l)} + \sum_{k=0}^{L_c-1} b_{-2,k,j}^{(l)}\right) = (L_s(1-\gamma_l) + L_c\gamma_l)(1-\alpha_l^{m+1})\frac{1-y_l^{n+1}}{1-y_l}\, b_{0,0,0}^{(l)}\,. \tag{B.17}$$

By considering that the successful transmission and the failure events are due to the limited number of backoff stages m and the retry limit n, the idle state probability

is

$$
\begin{aligned}
b_{\text{idle}}^{(l)} =& (1-q_l) b_{\text{idle}}^{(l)} + (1-q_{cf,l}) \sum_{j=0}^{n} \alpha_l \, b_{m,0,j}^{(l)} \\
&+ (1-q_{cr,l}) \sum_{i=0}^{m} \gamma_l (1-\alpha_l) \, b_{i,0,n}^{(l)} \\
&+ (1-q_{\text{succ},l}) \sum_{i=0}^{m} \sum_{j=0}^{n} (1-\gamma_l)(1-\alpha_l) \, b_{i,0,j}^{(l)} \qquad \text{(B.18)} \\
=& \frac{1}{q_l} \left[(1-q_{cf,l}) \frac{\alpha_l^{m+1}(1-y_l^{n+1})}{1-y_l} + (1-q_{cr,l}) y_l^{n+1} \right. \\
&\left. + (1-q_{\text{succ},l})(1-\gamma_l) \frac{(1-\alpha_l^{m+1})(1-y_l^{n+1})}{1-y_l} \right] b_{0,0,0}^{(l)}.
\end{aligned}
$$

Note that Equations (B.16)–(B.18) give the state values $b_{i,k,j}^{(l)}$ as a function of $b_{0,0,0}^{(l)}$. By replacing Equations (B.16)–(B.18) in the normalization condition given by Equation (B.15), we obtain $b_{0,0,0}^{(l)}$ in Equation (4.2). As a last step, we can derive τ_l by summing up the probabilities of being in the generic sensing stage $b_{i,0,j}^{(l)}$,

$$
\tau_l = \sum_{i=0}^{m} \sum_{j=0}^{n} b_{i,0,j}^{(l)} = \left(\frac{1-\alpha_l^{m+1}}{1-\alpha_l} \right) \left(\frac{1-y_l^{n+1}}{1-y_l} \right) b_{0,0,0}^{(l)} \, .
$$

Appendix C

Markov Chain Model Limitations

Here, we discuss the fundamental limitations of the Markov chain models of the IEEE 802.5.4 MAC developed in Chapters 3, 4, and 5.

C.1 Computation Complexity

The accurate Markov chain models presented in Chapters 3, 4, and 5 require the solution of systems of non-linear equations to derive performance indicators. For the use of the models for sensor network applications, the computation complexity is a critical factor since the typical micro-controller does not support well a heavy computing. Typical sensors use 8MHz TI MSP 430 micro-controller [111].

For this reason, in Chapter 3, we have introduced approximated model equations for the slotted IEEE 802.15.4 MAC in homogeneous single-hop networks. Fig. C.1 compares the computation time for performance metrics including reliability, average delay, and energy consumption by solving nonlinear equations and using an approximate approach as a function of the number of devices $N = 10, \ldots, 50$, traffic regime $\eta = 0.5, 0.7$. The vertical bars indicate the standard deviation as obtained out of 10 runs with different initial points of α, β, τ between 0 and 0.5. The approximated model enables the computation time savings of 95% compared to the one of solving non-linear equations. The system of non-linear equations is solved using the common trust-region dogleg algorithm [109]. When the traffic regime is high $\eta = 0.5$, the initial point is more critical for the computation time to apply this algorithm. The computation time by solving non-linear equations shows weak dependency with the number of device and the traffic regime.

The heterogeneous model in Chapter 4 requires the solution of a Markov chain for every link in the network. Moreover, the computation complexity to calculate the parameters $\alpha_{\mathrm{pkt},i}$ and γ_i in Equations (5.3) and (4.7) increases exponentially with the number of neighboring nodes $|\Omega_i|$ and the number of hidden nodes $|\Omega_{j\setminus i}|$. Therefore, the computation of these parameters becomes impractical when any of these numbers becomes greater than 15–20. However, also in this case, approximate model equations have been derived in Section 4.3.5.

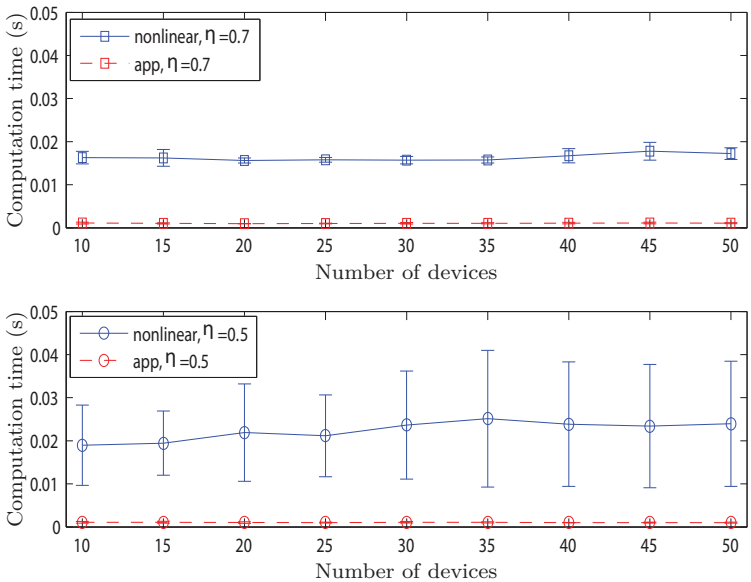

Figure C.1: Computation time for performance metrics by solving nonlinear equations and using an approximate approach as a function of the number of devices $N = 10, \ldots, 50$, traffic regime $\eta = 0.5, 0.7$. The vertical bars of solving nonlinear equations indicate the standard deviation as obtained out of 10 runs with different initial points for α, β, and τ between 0 and 0.5.

Table C.2 compares the computation time of both analytical model and simulations as a function of the number of nodes and traffic rate. The Monte Carlo simulations comprise of 5 runs of 10^4 packets generated. The computation time for the analytical model is significantly reduced with respect to the simulation time. The simulation time increases as the traffic rate decreases (less packets are generated per time unit) and as the number of nodes increases. The accurate analytical model computation time depends significantly on the number of nodes. However, the number of nodes in a one-hop neighborhood is typically up to 10, according to the IETF routing requirements for urban, industrial, and home environments [12]. When the approximate model is used, the computation time remains limited also for large networks.

The physical model in Chapter 5 requires a slight increase in the complexity with respect to the analytical model in Chapter 4, including the evaluation of the terms p_i^{det}, and $p_{i,j}^{\text{out}}$ in Equations (5.12) and (5.13), respectively. However, the computation of these terms can be carried out off-line, with respect to the solution of the system of nonlinear equations to derive τ_l, α_i, and $\gamma_{i,j}$. Therefore, the computation time is not affected significantly.

Table C.2: Computation Time of Analytical Model and Simulations

λ	N	Model	Approx	Simulations
0.1 pkt/s	7	6.8 s	0.4 s	$2.5 \cdot 10^5$ s
	14	1810 s	0.6 s	$4.8 \cdot 10^5$ s
	50	-	9.3 s	$2.6 \cdot 10^6$ s
1 pkt/s	7	7.0 s	0.5 s	$2.5 \cdot 10^4$ s
	14	2262 s	0.6 s	$4.8 \cdot 10^4$ s
	50	-	9.2 s	$2.8 \cdot 10^5$ s
10 pkt/s	7	8.2 s	0.4 s	2530 s
	14	2317 s	0.6 s	4910 s
	50	-	9.5 s	$2.9 \cdot 10^4$ s

C.2 Effects of Imperfect Carrier Sensing

The assumption of perfect carrier sensing plays a critical role to understand the fundamental limitations of the IEEE 802.15.4 protocol. However, in the unslotted mechanism of the IEEE 802.15.4 MAC nodes are not time-synchronized. In this section, we analyze the performance of CSMA/CA algorithm in the presence of carrier sensing errors. We consider the typical two types of carrier sensing errors, i.e., false negative and false positive. Their impact on the system performance is analyzed through simulation results. A false negative failure happens when the carrier sensing incorrectly detects that the medium is idle when it is actually busy. A false positive event occurs when a busy state is reported when the medium is idle. We model carrier sensing failures by independent Bernoulli trials with success probability $1 - p_f$, where $0 \leq p_f \leq 1$. The independence of the trial results is assumed to be over all the links and the attempts.

We consider the single-hop network in Figure 4.2(a) with $N = 7$, with both full and reduced sensing capabilities. In Figure C.3 and C.4, we report the reliability and average packet delay, respectively, as a function of the probabilities of the carrier sensing error. Note that "false negative" and "false negative + false positive" refer to the consideration of the false negative event and the combined event of the false negative and positive failure for the simulation setup, respectively. The false negative and positive failures decrease the system performance in terms of reliability. The effect of the false positive failure on the reliability is more evident as the failure probability increases. The false negative failure slightly decreases the delay of successfully received packets since it reduces the average number of backoffs in the network. The false positive failure affects directly the average number of backoffs and it increases the average delay. For large values of false positive probability, packets start being dropped due to the number of backoffs and the delay starts decreasing. If the carrier sensing failure probability is small ($p_f < 0.2$), the effect of

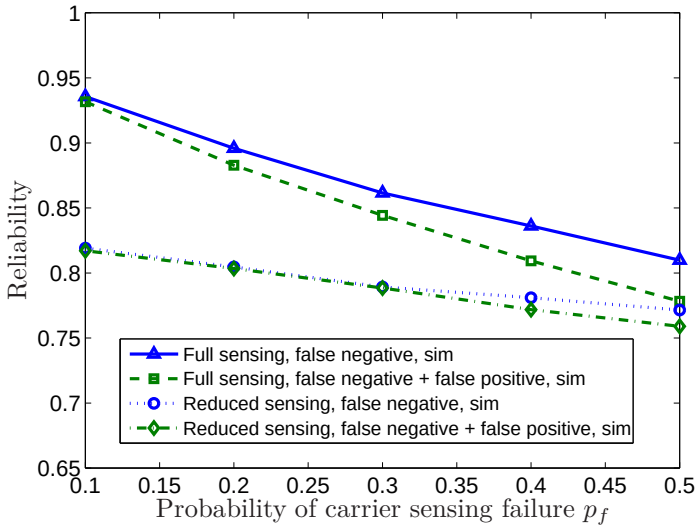

Figure C.3: Reliability vs. probability of carrier sensing failure for the single-hop topology in Figure 4.2(a), with $N = 7$, $\lambda_l = 10$ pkt/s, for $l = 1, \ldots, N$. Full sensing and reduced sensing correspond to $|\Omega_l| = N$ and $|\Omega_l| = 3$, respectively. Note that "false negative" and "false negative + false positive" refer to the consideration of the false negative event and the combined event of the false negative and positive failure for the simulation setup, respectively.

the imperfect carrier sensing is not critical for the reliability and delay. Hence, we argue that our model predicts well the performance of the network for small false negative and false positive probabilities.

C.3 Effects of Finite Packet Size

In this section, we investigate the basic assumption of independent busy channel probability α along the backoff stages of the Markov chain. In practice, this is realistic for many situations, but not for all. In [155], it is shown that this assumption has an impact on the delay and power consumption, mainly for small scale networks. In Figure C.5, we report the average busy channel probability in different backoff stages of the chain (i.e., $i = 0$ $i = 1$, $i = 2$). We consider $N = 7$ nodes with no hidden terminals, MAC parameters $m_0 = 3$, $m = 4$, $m_b = 7$, $n = 0$, traffic rate $\lambda_l = 5$ pkt/s for $l = 1, ..., N$, packet size $L = 7$, ACK size $L_{\text{ack}} = 2$, and we compare results from the analytical model with Monte Carlo simulations. The simulation results are presented for each stage and the average value is reported as a reference. There is a significant increase in the busy channel probability be-

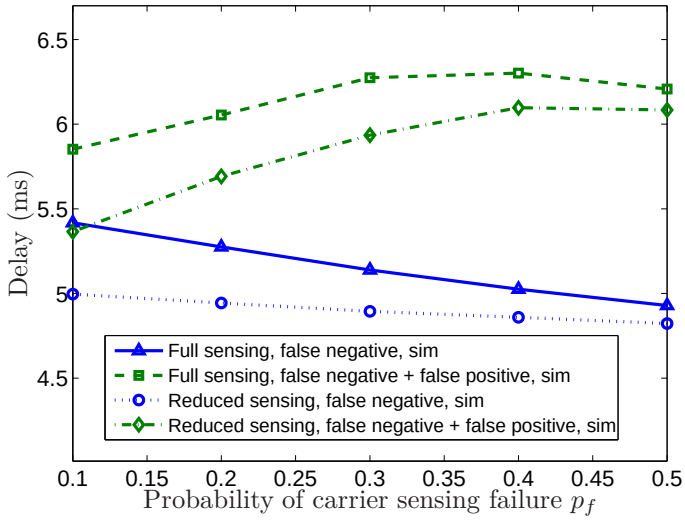

Figure C.4: Delay vs. probability of carrier sensing failure for the single-hop topology in Figure 4.2(a), with $N = 7$, $\lambda_l = 10$ pkt/s, for $l = 1, \ldots, N$.

tween the initial backoff stage ($i = 0$) and the second backoff stage ($i = 1$). Then the probability decreases in the following backoff stages to agree with the analysis. This increase is due to the transmission time (of packets plus ACKs), which is not negligible compared to the backoff time. If the channel is busy after the initial backoff, there is a certain probability that the same transmission is still ongoing after the second backoff. This probability reduces as the backoff increases in the following stages. We consider two assumptions in the model. At *network level*, α is obtained as a network parameter, by using the homogeneous model in Chapter 3. At *node level*, α_l is obtained for each node independently as in Equation (4.4). As we see in Figure C.5, the value predicted at network level well approximates the busy channel probability of the simulation in the initial backoff ($i = 0$), but it underestimates the average busy channel probability. The analytical approach at node level tends to overestimate the busy channel probability in the initial backoff stage but it compensates for the increase in α in the following backoff stages.

In [156], a derivation of the busy channel probability for different backoff stages is introduced. However, the system scenario is different from our model scenario. In fact, the network topology in [156] considers a single-hop star network, in which nodes transmit packets only upon reception of a query from the coordinator. Therefore, the carrier sensing mechanism is synchronized for all nodes and the number of contending nodes at the beginning of the first backoff is supposed known. By contrast, in our system scenario, nodes are allowed to generate traffic with a random

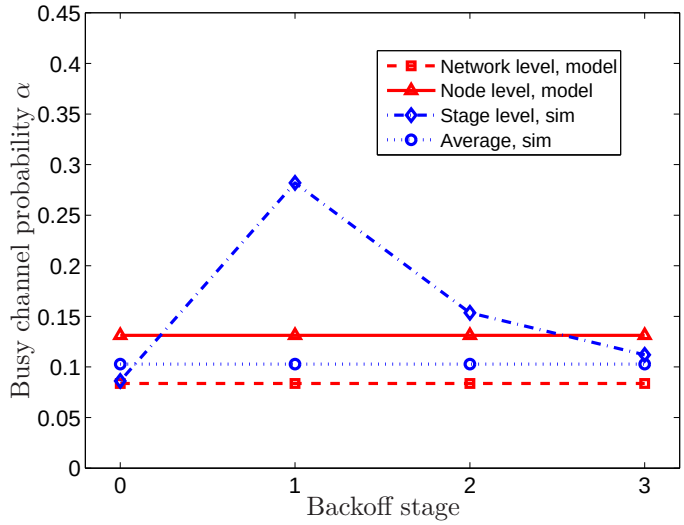

Figure C.5: Busy channel probability vs. backoff stage for the single-hop topology in Figure 4.2(a), with $N = 7$, $\lambda_l = 5$ pkt/s, for $l = 1, \ldots, N$, with full sensing capabilities.

Poisson distribution at different rates, which is more general and greatly complicates the analysis. The number of contending nodes that a transmitting node encounters when it starts the first backoff procedure cannot be determined a priori and those nodes that are contending are not necessarily in their first backoff. Moreover, the presence of re-transmitted packets complicates the analysis. Therefore, we believe that the analytical derivation of the impact of packet size on the busy channel probability in the different backoff stages in our model scenario is a formidable task. However, as shown in previous sections, an approximation by a busy channel probability that is independent of the backoff stage is accurate enough to derive the network reliability, delay, and energy consumption.

Appendix D

Proofs for Chapter 6

D.1 Proof of Claim 6.4.1

Let k be the generic number of packets that a cluster has to evacuate at the beginning of a transmitting TDMA-slot. In the analytical derivations, we consider the worst case scenario for packet collisions, which occurs when k packets are distributed over k different nodes. The cluster behavior is modeled by a discrete time Markov chain, where the state is associated with the number of nodes that have to forward packets (Figure D.1). The state 0 corresponds to the situation where no packets are stored in the cluster. Then, p_k is the probability to go from state k to $k-1$ in the chain. In an ideal CSMA, all nodes are able to sense ongoing transmissions avoiding collisions. By this hypothesis, p_k is the probability to have at least one node attempting to transmit the packet (i.e., $(1-(1-\tau)^k)$), given the probability that a beacon is received p_{bc}. Since all N nodes in the receiving cluster are candidate to send the beacon, $p_{\mathrm{bc}} = (1-\gamma)N\omega\,(1-\omega)^{N-1}$. Packet collisions occur when a simultaneous sensing attempt is done by more than one node (i.e., $p_{\mathrm{cl}}^{\tau(k-1)}$ where $\tau(k-1)$ is the expected number of additional accesses to the channel in the same CSMA-slot by the $k-1$ nodes in the same cluster). By considering all these factors, the successful transmission probability is given in Equation (6.4).

D.2 Proof of Claim 6.4.2

Let $P(n,S,k)$ be the probability to be in the state n after a number S of steps in the Markov chain when there are k packets in the cluster. In other words, $P(n,S,k)$ is the probability of losing n out of k packets in a cluster after a time of S CSMA-slots. In fact, if there are still n packets left after S CSMA-slots, these packets are discarded. Let $p_n^* = 1-p_n$ where p_n is the successful transmission probability given in Equation (6.4). We derive $P(n,S,k)$ recursively, by noting that:

$$P(n,S,k) = P(n+1,S-1,k)\,p_{n+1} + P(n,S-1,k)\,p_n^*\,,$$

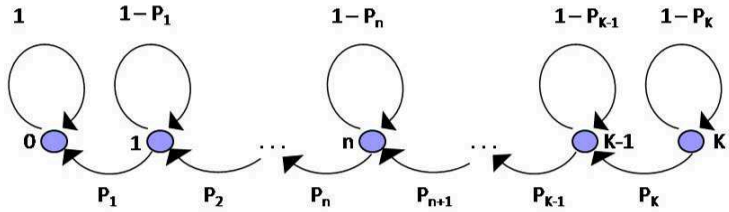

Figure D.1: Markov chain model of TREnD MAC. The state k represents the number of packets in a cluster.

where

$$P(k, S-k+n, k) = (p_n^*)^{S-k+n}\,,$$

$$P(n, k-n, k) = \prod_{l=n+1}^{k} p_l\,.$$

By defining a set $V(n) = \{p_n^*, p_{n+1}^*, ..., p_k^*\}$ and a matrix that contains all the M_c combinations with repetition of the elements in $V(n)$, taken in groups of $S-k+n$: $A(n) = [a_{i,j}]_{M_c}^{S-k+n}$, a closed form expression of $P(n,S,k)$ is

$$P(n,S,k) = \prod_{l=n+1}^{k} p_l \left(\sum_{i=1}^{M_c} \prod_{j=1}^{S-k+n} a_{i,j} \right)\,,$$

for all n, k, S, where $n \leq k \leq S$.

Let us consider a numerical example. Let $k = 3$ and $S = 4$, we determine $P(1,4,3)$, which is given by the sum of the probabilities of all possible paths in the Markov chain in Figure D.1 that start from the state 3 and end in 1 within exactly four steps. It follows that

$$P(1,4,3) = p_2 p_3 [p_1^* p_1^* + p_2^* p_2^* + p_3^* p_3^* + p_1^* p_2^* + p_1^* p_3^* + p_2^* p_3^*]\,.$$

The product $p_2 p_3$ is present in all paths, whereas, within brackets, there are all the combinations with repetition of the elements p_1^*, p_2^*, p_3^*, taken two per time. Then,

$$V(1) = \{p_1^*, p_2^*, p_3^*\}\,,$$

$$A(1) = \begin{bmatrix} p_1^* & p_2^* & p_3^* & p_1^* & p_1^* & p_2^* \\ p_1^* & p_2^* & p_3^* & p_2^* & p_3^* & p_3^* \end{bmatrix}^T\,.$$

The reliability R over $h_{\max}$ hops is:

$$R = \left(\sum_{n=0}^{k} \frac{k-n}{k} P(n,S,k) \right)^{h_{\max}}\,,$$

where Equation (6.5) follows after substitutions.

D.3 Proof of Claim 6.4.3

R_j^{ag} is computed iteratively by considering the dependance on the number of aggregated packets that the hop j has to forward from the hop $j+1$, and R_{j-1}^{ag}. Suppose $h_i = 4$, then

$$\begin{aligned}
R_4^{\text{ag}} &= R_3^{\text{ag}} r_1 = R_3^{\text{ag}} R_1 \,, \\
R_3^{\text{ag}} &= R_2^{\text{ag}}[(1-r_1)r_1 + r_1 r_2] = R_2^{\text{ag}} R_2 \,, \\
R_2^{\text{ag}} &= R_1^{\text{ag}}[(1-R_2)r_1 + (1-r_1)r_1 r_2 + r_1 r_2 r_3] = R_1^{\text{ag}} R_3 \,, \\
R_1^{\text{ag}} &= [(1-R_3)r_1 + (1-r_2)r_1 r_2 + (1-r_1)r_1 r_2 r_3 + r_1 r_2 r_3 r_4] = R_0^{\text{ag}} R_4 \,.
\end{aligned}$$

By defining $r_j = \sum_{i=1}^{j}(1-r_{i-1}) \prod_{z=1}^{j-i+1} R_z$, with $r_0 = 0$, it follows that Equation (6.6) holds for a generic h_i.

D.4 Explanation of Claim 6.4.4

According to the Markov chain in Figure D.1, the required number of CSMA-slots to advance in the chain from state j to $j-1$ follows a Geometric distribution of parameter p_j. By the Central Limit Theorem, the cluster evacuation time T_e is approximated by a normal random variable having mean μ and variance σ^2. These moments are given by the sum of the expected times and variances, respectively, to advance a step in the chain. Consequently, we have that $T_e \sim \mathcal{N}(\mu, \sigma^2)$, where $\mu = \sum_{j=1}^{k} 1/p_j$, and $\sigma^2 = \sum_{j=1}^{k}(1-p_j)/p_j^2$. By considering the properties of the cumulative distribution function of T_e, we derive Equation (6.8).

D.5 Proof of Claim 6.4.5

Let us consider a single TDMA-slot. According to the p-persistent MAC mechanism described in Section 6.3, the number of CCAs performed in a TDMA-slot depends on the average number of packets to be forwarded λT_{cyc} according to the relation:

$$W_{\text{cca}} = \sum_{j=1}^{\lambda T_{\text{cyc}}} j \frac{\tau\omega}{(1-\gamma)} \,,$$

where τ, ω, and $(1-\gamma)$ respectively account for wake-up probability in transmission, wake-up probability in reception and good channel probability. Given a successful CCA, the number of transmitted packets is approximated by $W_{\text{pkt}} \approx \lambda T_{\text{cyc}}$. Similarly, the number of acknowledgements is $W_{\text{ack}} \approx \lambda T_{\text{cyc}}$. The costs for beacon transmission, wake-up, and listening in a TDMA-slot depend on the sleeping discipline in reception by introducing the factor $W_{\text{rx}} = \omega N W / M_s$, which accounts for

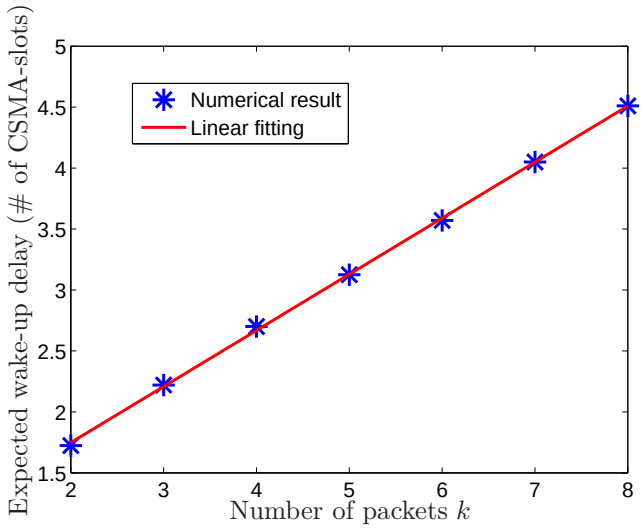

Figure D.2: Empirical evaluation of the optimal wake-up probability in transmission τ^*. A linear fitting is performed on the expected wake-up delay $1/\tau^*$.

the average number of times there is an awake node. Hence, considering a total time T_{tot}, *rovato*

$$E_{\text{tot}} = \frac{T_{\text{tot}}}{S}\left(W_{\text{cca}}E_{\text{cca}} + W_{\text{pkt}}E_{\text{pkt}} + E_{\text{ack}} + W_{\text{rx}}\left(E_{\text{bc}}\frac{S}{\delta} + E_w + P_i S\right)\right).$$

Equation (6.9) follows after substitutions.

D.6 Proof of Claim 6.4.6

For a p-persistent CSMA, it is shown that the access probability optimizing in terms of reliability is $\tau^* = 1/j$, given that there are j packets to be sent during a CSMA-slot [53]. Such a probability, however, depends on the entire cluster state, namely the current number of packets to be forwarded in a cluster, which can be hardly used. In fact, a node does not have knowledge of the number of packets in a cluster at a given CSMA time slot. We derive the optimal empirical constant access probability by evaluating numerically the access probability τ^* that maximizes the reliability in Equation (6.5) as a function of $k = \lambda M_s S$. By a linear fitting of the expected wake-up delay $(1/\tau^*)$ (see Figure D.2), we derive the coefficients: $c_1 = 2.17$, $c_2 = 1.81$. The wake-up probability in reception ω is determined by similar arguments. In reception, the number of contending nodes is constant during a slot and upper bounded by the number of nodes in the cluster N, which is known at the controller. Hence, the sub-optimal wake-up probability is $\omega^* = 1/N$.

Appendix E

Thermodynamical Model for UFAD Systems

We consider the under floor air distribution (UFAD) regulation system introduced in Section 7.2, and we exploit the thermodynamics properties of the ventilation process with a control volume approach.

E.1 Physical Model

The room dynamics is illustrated using the fundamental laws of thermodynamics [157]. The internal state of room i, represented by its density ρ_i and temperature T_i, is determined based on the following hypotheses:

H1. the flow is incompressible: $\rho_i = \rho_{\text{air}}$;

H2. the control volume (CV) remains constant relative to the coordinate frame;

H3. the state of mass within the CV is uniform at any time;

H4. the state of the mass crossing the CV is constant with time but the mass flow rates may vary;

H5. the kinetic and potential energy of the gas within the room are neglected.

Hypothesis (*H1*) is straightforward considering the low speed of the airflow within the rooms. (*H2*)-(*H4*) are classical for uniform-state, uniform-flow processes, i.e., when there is no change in the state of mass (we consider only gas in our case). (*H5*) is related to the fact that the gas moves slowly in the room and that the mass of the gas in the CV does not generate significant potential energy. The CV considered is strictly limited to the inside room volume: it does not include the underfloor and ceiling plenums.

The continuity equation, along with incompressibility (*H1*), implies mass conservation $\sum \dot{m}_{\text{in}_i} = \sum \dot{m}_{\text{out}_i}$, where $\dot{m}_{\text{in}}$ and $\dot{m}_{\text{out}}$ are the input and output mass flow rates, respectively. The first law of thermodynamics with (*H2*)-(*H4*) gives the

energy exchange in the room CV as:

$$\frac{dE_i}{dt} = \dot{Q}_i + \sum \dot{m}_{\text{in}_i} h_{\text{tot,in}_i} - \sum \dot{m}_{\text{out}_i} h_{\text{tot,out}_i} ,$$

where E_i is the room energy, $\dot{Q}_i$ the heat exchange, and h_{tot} the total enthalpy, approximated as $h_{\text{tot}} = C_p T$, at temperature T, with C_p the constant pressure specific heat. Considering (*H5*), the room energy is the internal energy

$$E_i = \rho_{\text{air}} V_i C_v T_i ,$$

where V_i is the room volume and C_v is the constant volume specific heat. For air at 25° C and 1 atm, $C_v = 717\,\text{J/(kg·K)}$, $C_p = 1004\,\text{J/(kg·K)}$ and $\rho_{\text{air}} = 1.169\,\text{kg/m}^3$.

The heat exchange Q_i can be decomposed, depending on the nature of the heat transfers, as:

- conduction (Fourier's law):

$$\dot{Q}_{\text{cond}} = k\,A\,\frac{\Delta T}{\Delta x} ,$$

  where k [W/(m·K)] is the conductivity ($\approx$ 10 for glass, 0.1 for insulation materials) and A the surface area where exchange occurs;

- convection (Newton's law):

$$\dot{Q}_{\text{conv}} = A\,h\,\Delta T ,$$

  where h [W/m^2] is the heat transfer coefficient (typically $5 - 25$ for natural convection and $25 - 250$ for forced convection;

- radiation (electromagnetic waves):

$$\dot{Q}_{\text{rad}} = \epsilon\,\sigma\,A\,T_s^4 ,$$

  where ϵ is the emissivity (0.92 for nonmetallic surfaces), $\sigma = 5.67 \times 10^{-8}$ W/(m$^2 \cdot$ K^4) is the Stephan-Boltzmann constant and T_s is the surface temperature.

Under the previous hypotheses, the mass flow rate $\dot{m}$ going from a high temperature volume T_h to a low temperature volume T_l through a section A is obtained by combining Bernoulli's and the ideal gas equations as:

$$\dot{m} = \rho A \sqrt{2(C_p - C_v)(T_h - T_l)} . \tag{E.1}$$

Supposing that all the doors are closed and that there is no power source within the room, the temperature dynamics for room i is given as:

$$\begin{aligned}\frac{dT_i}{dt} = F_i(t) =& \frac{1}{\rho_{\text{air}} V_i C_v}\left[\dot{Q}_{\text{conv}} + \dot{Q}_{\text{cond}} + \dot{Q}_{\text{rad}} + C_p \dot{m}_{pl_i}(T_{pl} - T_i)\right] \\ =& \frac{1}{\rho_{\text{air}} V_i C_v}\left[-\sum_{l=1}^{N_{iw}} \alpha_{iw_l}(T_i - T_l) - \sum_{l=1}^{N_{ow}} \left(\alpha_{ow_l} + \alpha_{\text{glass}_l}\right)(T_i - T_{\text{out}})\right. \\ & \left. + C_p \dot{m}_{pl_i} T_{pl} - \alpha_{pl_i}(T_i - T_{pl}) - C_p \dot{m}_c T_i\right] \\ =& \frac{1}{\rho_{\text{air}} V_i C_v}[-(\Theta_i + C_p \dot{m}_{pl_i})T_i + \sum_{l=1}^{N_{iw}} \alpha_{iw_l} T_l + \sum_{l=1}^{N_{ow}} \left(\alpha_{ow_l} + \alpha_{\text{glass}_l}\right) T_{\text{out}} \\ & + (C_p \dot{m}_{pl_i} + \alpha_{pl_i})T_{pl}]\,,\end{aligned}$$

where

$$\Theta_i = \sum_{l=1}^{N_{iw}} \alpha_{iw_l} + \sum_{l=1}^{N_{ow}} \left(\alpha_{ow_l} + \alpha_{\text{glass}_l}\right) + \alpha_{pl_i}\,,$$

$\alpha_x = k_x A_x / \Delta x_x$ for component x, N_{iw} is the number of connected inside walls, N_{ow} is the number of outside walls.

E.2 Room Dynamics

Based on the previous description, we obtain the room temperature dynamics:

$$\frac{dT_i}{dt} = \frac{1}{\rho_{\text{air}} V_i C_v}\left[\dot{Q}_{\text{conv}} + \dot{Q}_{\text{cond}} + \dot{Q}_{\text{rad}} + \dot{Q}_{\text{so}} + C_p \sum \dot{m}_{\text{in}_i} T_{\text{in}_i} - C_p \sum \dot{m}_{\text{out}_i} T_i\right],$$

where we introduced the additional source $\dot{Q}_{\text{so}}$ to model the internal heat sources (computers, printers, etc.) and considered the outflow temperature as the room temperature (which is a direct consequence of the 0-D approximation). A simplified classification of the heat sources for room i is proposed in Table E.1, where T_j indicates the temperature in an adjacent room, A_x the exchange surface areas, and Δx_x the thicknesses. Note that the last three components correspond to discrete events while the previous ones have continuous variations. This description is easily refined by introducing additional terms (walls radiation, windows airflow, etc.), depending on the desired level of model accuracy.

The ceiling, plenum, and door mass flow rates are constrained by the conservation of mass (continuity) with (setting $\dot{m} > 0$ when the flow is entering the room):

$$\dot{m}_{c_i} + \sum_{l=1}^{N_{pl}} \dot{m}_{pl_i,l} + \sum_{l=1}^{N_d} \dot{m}_{d_{ij},l} = 0\,,$$

Table E.1: Energy sources in room i.

Component	Associated energy
Inside walls	$\dot{Q}_{iw} = -k_{iw}\, A_{iw}\, \frac{(T_i - T_j)}{\Delta x_{iw}}$
Outside walls	$\dot{Q}_{ow} = -\left(k_{ow}\, \frac{A_{ow}}{\Delta x_{ow}} + k_{\text{glass}}\, \frac{A_{\text{glass}}}{\Delta x_{\text{glass}}}\right)(T_i - T_{\text{out}})$
Plenum	$\dot{Q}_{pl} = C_p\, \dot{m}_{pl}\, T_{pl}$
Floor	$\dot{Q}_f = -k_{pl}\, A_{pl}\, \frac{(T_i - T_{pl})}{\Delta x_{pl}}$
Ceiling	$\dot{Q}_c = -C_p\, \dot{m}_c\, T_i$
People	$\dot{Q}_b = \epsilon\, \sigma\, A_b\, (T_b^4 - T_i^4)$
Inside sources	$\dot{Q}_{\text{so}}$
Doors	$\dot{Q}_d = C_p\, \rho\, A_d \sqrt{2(C_p - C_v)(T_j - T_i)}T_j$, if $T_j > T_i$
	$\dot{Q}_d = C_p\, \rho\, A_d \sqrt{2(C_p - C_v)(T_i - T_j)}T_i$, if $T_i > T_j$

where N_{pl} is the number of diffusers in the room and N_d denotes the number of doors. The door mass flow rate can be computed thanks to Bernoulli's equation (E.1) as $\dot{m}_d = \text{sgn}(T_j - T_i)\, \rho\, A_d \sqrt{2(C_p - C_v)|T_j - T_i|}$, where the sign function is introduced to indicate the flow direction.

Concerning the doors influence, the proposed energy-based model implies that for a given room i and adjacent room j (supposing that there is no return from the upper plenum):

- if $T_i > T_j$ then the flow going out of room i equals the inflow $\dot{m}_{pl_i}$ and the fact that it is leaving through the ceiling or the open door does not change the energy balance;
- if $T_i < T_j$ then an extra term $C_p \dot{m}_d (T_j - T_i)$ has to be introduced, with $\dot{m}_d = \rho A_d \sqrt{2(C_p - C_v)(T_j - T_i)}$.

The room temperature is then obtained as (supposing that only one door is open in room i at a given time, to simplify the notations):

$$\frac{dT_i}{dt} = F_i(t) + \frac{\sum_{k=0}^{N_q} \delta_{q,ik} \dot{Q}_{s,ik}}{\rho_{\text{air}} V_i C_v} + \begin{cases} 0, & \text{if } T_i > T_j \\ \delta_{d,ij} \frac{C_p \sqrt{2(C_p - C_v)}}{\rho_{\text{air}} V_i C_v} (T_j - T_i)^{3/2}, & \text{if } T_i < T_j \end{cases}$$

The temperature regulation is achieved by controlling the mass flow rate from the plenum $\dot{m}_{pl_i,l}(t)$, considering a given underfloor temperature $T_{pl}(t)$ (regulated globally for the whole building).

Finer models, including the height-dependency of the temperature variations, can be derived using the stratified flow theory [158, 159] or buoyancy driven flow dynamics [160]. The WSN measurements can also be set to determine the temperatures distribution shape, along the lines suggested in [161]. The aim of this model is to give the proper directions of the regulated states according to the actuation and disturbances.

Appendix F

Notation

F.1 Symbols

α	busy channel probability during the first CCA
α_p	performance control parameter
α_t	disturbance control parameter
α_u	input control parameter
β	busy channel probability during the second CCA
γ	packet loss probability
δ	outage probability constraint
η	transition probability to idle state
κ	Nakagami parameter
λ	traffic generation rate
π	routing metric
ρ	power gain
ρ_i	density in room i
σ	spread factor of the shadowing
τ	channel sensing probability
ω	wake-up probability in reception
Γ	parent set
Δ	children set
Ω	neighborhood set
$\Omega_{l\setminus j}$	hidden node set
a	detection threshold
b	outage threshold
$b_{i,j,k}$	stationary probability of the Markov chain

d	CSMA-slot duration in TREnD
h	number of hops
$h_{\max}$	maximum number of hops
h_{tot}	total hentalpy
$\dot{m}$	mass flow rate
m	maximum number of backoffs
m_0	initial backoff exponent
m_b	maximum backoff exponent
n	maximum number of retransmissions
p	detection probability at the receiver
p_{bc}	successful beacon transmission probability
p_{blk}	blocking probability
p_{cf}	discarded packet probability due to channel access failure
p_{cr}	discarded packet probability due to retransmission failure
p_f	probability of carrier sensing failure
p_k	successful transmission probability with k packets
$p_{l,k}$	probability of k packets in buffer l
p^{det}	detection probability
p^{fad}	fading probability
p^{out}	outage probability
q	packet generation probability in idle state
q_{cf}	packet generation probability after CCA failure
q_{cr}	packet generation probability after retry limit
q_{succ}	packet generation probability after successful transmission
r	distance
t_{ack}	ACK waiting time
t_b	beacon transmission time
t_h	backoff delay
t_p	processing time
t_{sc}	carrier sensing time
B	buffer size
C_p	constant pressure specific heat
C_v	constant volume specific heat
D	delay
$D_{\max}$	delay constraint
G	number of links in the network

E_{ack}	energy spent for a single ACK transmission
E_{cca}	energy spent for a single CCA
E_{pkt}	energy spent for a single packet transmission
E_{tot}	total energy consumption
E_w	energy spent for a single wake-up
K	control gain
L	packet length
L_{ack}	ACK length
L_c	collision duration
L_s	successful transmission duration
L_0	idle state duration
L_1	packet copying delay
$\mathbf{M}$	routing matrix
M_s	number of CSMA-slots in a TDMA-slot
N	number of nodes in the network
N_d	number of doors in each room
N_e	number of event-triggered nodes in the network
N_{pl}	number of diffusers in each room
N_q	number of power sources in each room
N_t	number of time-triggered nodes in the network
P_i	power consumption in idle-listening state
P_r	power consumption in reception state
P_{rx}	received power level
P_{sc}	power consumption in carrier sensing state
P_{sp}	power consumption in sleeping state
P_t	power consumption in transmission state
P_{tx}	transmission power level
P_w	power consumption in wake-up state
Q	aggregate traffic (generated and forwarded)
$\dot{Q}$	heat exchange
R	reliability
$R_{\min}$	reliability constraint
S	TDMA-slot duration
S_b	backoff unit time
$\mathbf{T}$	traffic distribution matrix

T	sampling time
T_d	desired temperature
T_e	cluster evacuation time
T_f	TDMA frame duration
T_i	temperature in room i
V	volume
W	number of listening TDMA-slots in a TDMA-cycle
W_i	backoff window at stage i
W_p	performance weight
W_t	disturbance weight
W_u	input weight

F.2 Acronyms

ACK	Acknowledgement
BEB	Bynary Exponential Backoff
CAP	Contention Access Period
CFP	Contention Free Period
CSMA/CA	Carrier Sense Multiple Access / Collision Avoidance
DODAG	Destination-Oriented Directed Acyclic Graph
ETX	Expected Transmission Count
GST	Guaranteed Time Slot
HVAC	Heating, Ventilation, and Air Conditioning
IEEE	Institute of Electrical and Electronics Engineers
IETF	Internet Engineering Task Force
MAC	Medium Access Control
MIMO	Multiple Input and Multiple Output
PDF	Probability Density Function
PGF	Probability Generating Function
RPL	Routing Protocol for Low-power Lossy Networks
SINR	Signal-to-(Interference plus Noise)-Ratio
TDMA	Time Division Multiple Access
UFAD	Under-Floor Air Distribution
WSN	Wireless Sensor Network

Bibliography

[1] P. Harrop and R. Das. *Wireless Sensor Networks 2012-2022*. IDTechEx, October 2012.

[2] A. Willig. Recent and emerging topics in wireless industrial communication. *IEEE Transactions on Industrial Informatics*, 4(2):102–124, 2008.

[3] Frost & Sullivan. *Wireless Devices in the Factory Automation - An Overview of Adoption Trends*, 2008. `http://www.frost.com/prod/servlet/frost-home`.

[4] G. Scheible, D. Dzung, J. Endresen, and J. E. Frey. Unplugged but connected, design and implementation of a truly wireless real-time sensor/actuator interface. *IEEE Industrial Electronics Magazine*, 1(2):25–34, 2007.

[5] *WirelessHART Specitications*, 2007. `http://www.hartcomm2.org`.

[6] ISA. *SP-100*, 2008. `http://www.isa.org/isasp100/`.

[7] *IEEE 802.15.4 Wireless Medium Access Control (MAC) and Physical Layer (PHY) Specifications for Low-Rate Wireless Personal Area Networks (WPANs)*, 2006. `http://www.ieee802.org/15/pub/TG4.html`.

[8] Swedish Governmental Agency for Innovation Systems (VINNOVA). *WiComPI project*. `http://www2.teknik.uu.se/wicompi/`.

[9] EU Hydrobionets project. *Autonomous Control of Large-scale Water Treatment Plants based on Self-Organized Wireless BioMEM Sensor and Actuator Networks*. `http://www.hydrobionets.eu/`.

[10] A. Willig, K. Matheus, and A. Wolisz. Wireless technology in industrial networks. *Proceedings of the IEEE*, 93(6):1130–1151, 2005.

[11] W. Lerner. *The Future of Urban Mobility – Towards networked, multimodal cities of 2050*. Arthur D. Little, October 2011.

[12] Internet Engineering Task Force (IETF). *Routing Over Low power and Lossy networks*. `http://www.ietf.org/dyn/wg/charter/roll-charter.html`.

[13] *IEEE 1609 Standard for Wireless Access in Vehicular Environments (WAVE)*, 2010. http://standards.ieee.org/develop/wg/1609_WG.html.

[14] EU Hycon2 project. *Highly-complex and networked control systems.* http://www.hycon2.eu/.

[15] P. Papadimitratos, A. La Fortelle, K. Evenssen, R. Brignolo, and S. Cosenza. Vehicular communication systems: Enabling technologies, applications, and future outlook on intelligent transportation. *IEEE Communications Magazine*, 47(11):84–95, 2009.

[16] Swedish Governmental Agency for Innovation Systems (VINNOVA). *iQFleet Intelligent real-time fleet control and management.* http://www.vinnova.se/.

[17] D. Snoonian. Smart buildings. *IEEE Spectrum*, 40(8):18–23, 2003.

[18] Stockholm City Development Administration. *Stockholm Royal Seaport.* http://www.stockholmroyalseaport.com/.

[19] W. Zhang, M. S. Branicky, and S. M. Phillips. Stability of networked control systems. *IEEE Control Systems Magazine*, 21(1):84–99, 2001.

[20] L. Schenato, B. Sinopoli, M. Franceschetti, K. Poolla, and S. Sastry. Foundations of control and estimation over lossy networks. *Proceedings of the IEEE*, 95(1):163–187, 2007.

[21] P. Park, P. Di Marco, C. Fischione, and K. H. Johansson. Modeling and optimization of the IEEE 802.15.4 protocol for reliable and timely communications. *IEEE Transactions on Parallel and Distributed Systems*, 2012. To appear.

[22] P. Park, P. Di Marco, P. Soldati, C. Fischione, and K. H. Johansson. A generalized Markov chain model for effective analysis of slotted IEEE 802.15.4. In *Proceedings of the 6th IEEE International Conference on Mobile Ad-hoc and Sensor Systems (MASS)*, 2009.

[23] P. Park, P. Di Marco, C. Fischione, and K. H. Johansson. Delay distribution analysis of wireless personal area networks. In *IEEE Conference on Decision and Control (CDC)*, 2012.

[24] P. Di Marco, P. Park, C. Fischione, and K. H. Johansson. Analytical modeling of multi-hop IEEE 802.15.4 networks. *IEEE Transactions on Vehicular Technology*, 61(7):3191–3208, 2012.

[25] P. Di Marco, P. Park, C. Fischione, and K. H. Johansson. Analytical modelling of IEEE 802.15.4 for multi-hop networks with heterogeneous traffic and hidden terminals. In *IEEE GLOBECOM*, 2010.

[26] P. Di Marco, C. Fischione, and G. Athanasiou. MAC and routing interactions in low power and lossy networks. *IEEE SECON*, 2013. Submitted.

[27] P. Di Marco, C. Fischione, F. Santucci, and K. H. Johansson. Modeling IEEE 802.15.4 networks over fading channels. *IEEE Transactions on Vehicular Technology*, 2012. Submitted.

[28] P. Di Marco, C. Fischione, F. Santucci, and K. H. Johansson. Effects of Rayleigh-lognormal fading on IEEE 802.15.4 networks. In *IEEE International Conference on Communications (ICC)*, 2012. Submitted.

[29] P. Di Marco, P. Park, C. Fischione, and K. H. Johansson. Trend: A timely, reliable, energy-efficient and dynamic wsn protocol for control applications. In *IEEE International Conference on Communications (ICC)*, 2010.

[30] P. Di Marco, P. Park, C. Fischione, and K. H. Johansson. A dynamic energy-efficient protocol for reliable and timely communications for wireless sensor networks in control and automation. In *IEEE Communications Society Conference on Sensor, Mesh and Ad Hoc Communications and Networks Workshops, (SECON Workshops)*, 2009.

[31] C. Fischione, P. Park, P. Di Marco, and K. H. Johansson. Design principles of wireless sensor networks protocols for control applications. In Sudip K. Mazumder, editor, *Wireless Networking Based Control*, pages 203–238. Springer New York, 2011.

[32] E. Witrant, P. Di Marco, P. Park, and C. Briat. Limitations and performances of robust control over WSN: UFAD control in intelligent buildings. *IMA Journal of Mathematical Control and Information*, 27(4):527–543, 2010.

[33] C. W. Lin, A. Puggelli, P. Di Marco, and A. Sangiovanni-Vincentelli. VMS communication modeling and architecture. In *MuSyC Workshop: Distributed Sense and Control Systems*, April 2012.

[34] B. Talha, P. Di Marco, and M. Kaveh. Application of an integrated PHY and MAC layer model for half-duplex IEEE 802.15.4 networks to smart grids. In *ACM International Symposium on Applied Sciences in Biomedical and Communication Technologies*, (ISABEL), 2011.

[35] S. Coleri Ergen, P. Di Marco, and C. Fischione. MAC protocol engine for sensor networks. In *IEEE GLOBECOM*, 2009.

[36] P. Di Marco, C. Rinaldi, F. Santucci, K. H. Johansson, and N. Moller. Performance analysis and optimization of TCP over adaptive wireless links. In *IEEE International Symposium on Personal, Indoor and Mobile Radio Communications*, 2006.

[37] W. Pree. *Design patterns for object-oriented software development.* ACM Press Books, Reading, MA: Addison-Wesley, 1994.

[38] L. Benvenuti, A. Ferrari, E. Mazzi, and A. L. Vincentelli. Contract-based design for computation and verification of a closed-loop hybrid system. In *Proceedings of the 11th international workshop on Hybrid Systems: Computation and Control*, 2008.

[39] X. Sun, P. Nuzzo, C. Wu, and A. Sangiovanni-Vincentelli. Contract-based system-level composition of analog circuits. In *ACM/IEEE Design Automation Conference (DAC)*, 2009.

[40] P. Nuzzo, A. Sangiovanni-Vincentelli, X. Sun, and A. Puggelli. Methodology for the design of analog integrated interfaces using contracts. *IEEE Sensors Journal*, 12(12):3329–3345, 2012.

[41] A. Benveniste, W. Damm, A. Sangiovanni-Vincentelli, D. Nickovic, R. Passerone, and P. Reinkemeier. Contracts for the design of embedded systems part i: Methodology and use cases. *Proceeding of the IEEE*, 2012. To appear.

[42] A. Benveniste, W. Damm, A. Sangiovanni-Vincentelli, D. Nickovic, R. Passerone, and P. Reinkemeier. Contracts for the design of embedded systems part ii: Theory. *Proceeding of the IEEE*, 2012. To appear.

[43] K. Keutzer, A. R. Newton, J. M. Rabaey, and A. Sangiovanni-Vincentelli. System-level design: orthogonalization of concerns and platform-based design. *IEEE Transactions on Computer-Aided Design of Integrated Circuits and Systems*, 19(12):1523–1543, 2000.

[44] P. R. Kumar. New technological vistas for systems and control: the example of wireless networks. *Control Systems Magazine, IEEE*, 21(1):24–37, 2001.

[45] K. E. Årzén, A. Robertsson, D. Henriksson, M. Johansson, H. Hjalmarsson, and K. H. Johansson. Conclusions of the ARTIST2 roadmap on control of computing systems. *ACM SIGBED (Special Interest Group on Embedded Systems) Review*, 3(3), 2006.

[46] X. Liu and A. J. Goldsmith. Wireless medium access control in networked control systems. In *ACC*, 2004.

[47] V. Kawadia and P. R. Kumar. A cautionary perspective on cross-layer design. *IEEE Wireless Communications*, 12(1):3–11, 2005.

[48] G. C. Walsh, Y. Hong, and L. G. Bushnell. Stability analysis of networked control systems. *IEEE Transactions on Control Systems Technology*, 10(3):438–446, May 2002.

[49] G. N. Nair, F. Fagnani, S. Zampieri, and R. J. Evans. Feedback control under data rate constraints: An overview. *Proceedings of the IEEE*, 95(1):108–137, 2007.

[50] W. S. Wong and R.W. Brockett. Systems with finite communication bandwidth constraints. ii. stabilization with limited information feedback. *IEEE Transactions on Automatic Control*, 44(5):1049–1053, 1999.

[51] J. Richard. Time-delay systems: an overview of some recent advances and open problems. *Automatica*, 39(10):1667–1694, 2003.

[52] J. P. Hespanha, P. Naghshtabrizi, and Y. Xu. A survey of recent results in networked control systems. *Proceedings of the IEEE*, 95(1):138–162, 2007.

[53] A. Bonivento, C. Fischione, L. Necchi, F. Pianegiani, and A. Sangiovanni-Vincentelli. System level design for clustered wireless sensor networks. *IEEE Transactions on Industrial Informatics*, 3(3):202–214, 2007.

[54] T. Abdelzaher, T. He, and J. Stankovic. Feedback control of data aggregation in sensor networks. In *Proceedings of the IEEE Conference on Decision and Control*, 2004.

[55] P. Park. *Modeling, Analysis, and Design of Wireless Sensor Network Protocols*. PhD thesis, Royal Institute of Technology (KTH), 2011.

[56] J. Polastre, J. Hill, and D. Culler. Versatile low power media access for wireless sensor networks. In *ACM SenSys*, 2004.

[57] M. Buettner, G. Yee, E. Anderson, and R. Han. X-MAC: A short preamble MAC protocol for duty-cycled wireless sensor networks. In *ACM SenSys*, 2006.

[58] Y. Sun, O. Gurewitz, and D. Johnson. RI-MAC: A receiver-initiated asynchronous duty cycle MAC protocol for dynamic traffic loads in wireless sensor networks. In *ACM SenSys*, 2008.

[59] V. Rajendran, K. Obraczka, and J. Garcia-Luna-Aceves. Energy-efficient, collision-free medium access control for wireless sensor networks. In *ACM SenSys*, 2003.

[60] S. C. Ergen and P. Varaiya. PEDAMACS: Power efficient and delay aware medium access protocol for sensor networks. *IEEE Transactions on Mobile Computing*, 5(7):920–930, 2006.

[61] K. Pister and L. Doherty. TSMP: Time synchronized mesh protocol. In *Proceedings of the IASTED International Symposium on Distributed Sensor Networks (DSN)*, 2008.

[62] W. Ye, J. Heidemann, and D. Estrin. Medium access control with coordinated adaptive sleeping for wireless sensor networks. *IEEE/ACM Transactions on Networking*, 12(3):493–506, 2004.

[63] T. van Dam and K. Langendoen. An adaptive energy-efficient MAC protocol for wireless sensor networks. In *ACM SenSys*, 2003.

[64] I. Rhee, A. Warrier, M. Aia, J. Min, and M. L. Sichitiu. Z-MAC: A hybrid MAC for wireless sensor networks. *IEEE/ACM Transactions on Networking*, 16(3):511–524, 2008.

[65] W. Heinzelman, A. Chandrakasan, and H. Balakrishnan. An application-specific protocol architecture for wireless microsensor networks. *IEEE Transactions on Wireless Communications*, 1(4):660–670, 2002.

[66] O. Gnawali, R. Fonseca, K. Jamieson, D. Moss, and P. Levis. Collection tree protocol. In *Proceedings of the 7th ACM Conference on Embedded Networked Sensor Systems*, 2009.

[67] S. Moeller, A. Sridharan, B. Krishnamachari, and O. Gnawali. Routing without routes: the backpressure collection protocol. In *ACM/IEEE IPSN*, 2010.

[68] E. Felemban, C. G. Lee, and E. Eylem. MMSPEED: Multipath multi-speed protocol for QoS guarantee of reliability and timeliness in wireless sensor networks. *IEEE Transactions on Mobile Computing*, 5(6):738–754, 2006.

[69] Y. Xu, J. Heidemann, and D. Estrin. Geography-informed energy conservation for ad-hoc routing. In *ACM MobiCom*, 2001.

[70] B. Chen, K. Jamieson, H. Balakrishnan, and R. Morris. SPAN: An energy-efficient coordination algorithm for topology maintenance in ad hoc wireless networks. In *Proceedings of the Annual International Conference on Mobile Computing and Networking (MobiCom)*, 2001.

[71] M. Zorzi and R. R. Rao. Geographic random forwarding (GeRaF) for ad hoc and sensor networks: energy and latency performance. *IEEE Transactions on Mobile Computing*, 2(4):349–365, 2003.

[72] N. Burri, P. von Rickenbach, and R. Wattenhofer. Dozer: ultra-low power data gathering in sensor networks. In *Proceedings of the IEEE/ACM International Conference on Information Processing in Sensor Networks (IPSN)*, 2007.

[73] M. C. Vuran and I. F. Akyildiz. XLP: A cross-layer protocol for efficient communication in wireless sensor networks. *IEEE Transactions on Mobile Computing*, 9(11):1578–1591, 2010.

[74] P. Park, C. Fischione, A. Bonivento, K. H. Johansson, and A. Sangiovanni-Vincentelli. Breath: an adaptive protocol for industrial control applications using wireless sensor networks. *IEEE Transactions on Mobile Computing*, 10(6):821–838, 2011.

[75] C. Gomez, J. Paradells, and J. Caballero. *Sensors Everywhere (Wireless Network Technologies and solutions)*. i2CAT Fundation and Fundacion Vodafone, 2010.

[76] J. L. Hill and D. Culler. Mica: a wireless platform for deeply embedded networks. *IEEE Micro*, 22(6):12–24, 2002.

[77] E.-Y.A. Lin, J.M. Rabaey, and A. Wolisz. Power-efficient rendez-vous schemes for dense wireless sensor networks. In *IEEE International Conference on Communications (ICC)*, 2004.

[78] K. Jamieson, H. Balakrishnan, and Y. C. Tay. Sift: A MAC protocol for event-driven wireless sensor networks. Technical report, MIT Laboratory for Computer Science, 2003.

[79] IETF. *The internet engineering task force*, 2010. `http://www.ietf.org`.

[80] ZigBee Alliance. *ZigBee Specification*, 2005. `http://www.caba.org/standard/zigbee.html`.

[81] S. Subramanian and S. Shakkottai. Geographic routing with limited information in sensor networks. *IEEE Transactions on Information Theory*, 56(9):4506–4519, 2010.

[82] F. Stann and J. Heidemann. RMST: Reliable data transport in sensor networks. In *Proceedings of the IEEE Workshop on Sensor Network Protocols and Applications*, 2003.

[83] J. Gutiérrez. On the use of IEEE std. 802.15.4 to enable wireless sensor networks in building automation. *International Journal of Wireless Information Networks*, 14(4):295–301, 2007.

[84] G. Bianchi. Performance analysis of the IEEE 802.11 distributed cordination function. *IEEE Journal on Selected Areas in Communications*, 18(3):535–547, 2000.

[85] P. Chatzimisios, A. C. Boucouvalas, and V. Vitsas. IEEE 802.11 packet delay: A finite retry limit analysis. In *IEEE GLOBECOM*, 2003.

[86] P. Chatzimisios, V. Vitsas, and A. C. Boucouvalas. Throughput and delay analysis of IEEE 802.11 protocol. In *IEEE IWNA*, 2002.

[87] Z. Hadzi-Velkov and B. Spasenovski. Saturation throughput-delay analysis of IEEE 802.11 in fading channel. In *IEEE ICC*, 2003.

[88] H. Zhai, Y. Kwon, and Y. Fang. Performance analysis of IEEE 802.11 MAC protocols in wireless LANs. *Wireless Communications and Mobile Computing*, 4(8):917–931, 2004.

[89] O. Tickioo and B. Sikdar. Queueing analysis and delay mitigation in IEEE 802.11 random access MAC based wireless networks. In *IEEE INFOCOM*, 2004.

[90] H. Wu, Y. Peng, K. Long, S. Cheng, and J. Ma. Performance of reliable transport protocol over IEEE 802.11 wireless LAN: Analysis and enhancement. In *IEEE INFOCOM*, 2002.

[91] F. Cali, M. Conti, and E. Gregori. Dynamic tuning of the IEEE 802.11 protocol to achieve a theoretical throughput limit. *IEEE/ACM Transactions on Networking*, 8(6):785–799, 2006.

[92] P. Raptis, A. Banchs, and K. Paparrizos. A simple and effective delay distribution analysis for IEEE 802.11. In *IEEE PIMRC*, 2006.

[93] J. Zheng and M. L. Lee. Will IEEE 802.15.4 make ubiquitous networking a reality?: A discussion on a potential low power, low bit rate standard. *IEEE Communications Magazine*, 42(6):140–146, 2004.

[94] J. Misic, S. Shaf, and V. B. Misic. Performance of a beacon enabled IEEE 802.15.4 cluster with downlink and uplink traffic. *IEEE Transactions Parallel and Distributed Systems*, 17(4):361–376, 2006.

[95] S. Pollin, M. Ergen, S. C. Ergen, B. Bougard, L.V. Perre, I. Moerman, A. Bahai, P. Varaiya, and F. Catthoor. Performance analysis of slotted carrier sense IEEE 802.15.4 medium access layer. *IEEE Transactions on Wireless Communication*, 7(9):3359–3371, 2008.

[96] C. Y. Jung, H. Y. Hwang, D. K. Sung, and G. U. Hwang. Enhanced Markov chain model and throughput analysis of the slotted CSMA/CA for IEEE 802.15.4 under unsaturated traffic conditions. *IEEE Transactions on Vehicular Technology*, 58(1):473–478, 2009.

[97] A. Faridi, M. R. Palattella, A. Lozano, M. Dohler, G. Boggia, L. A. Grieco, and P. Camarda. Comprehensive evaluation of the IEEE 802.15.4 MAC layer performance with retransmissions. *IEEE Transactions on Vehicular Technology*, 59(8):3917–3932, 2010.

[98] C. Buratti. Performance analysis of IEEE 802.15.4 beacon-enabled mode. *IEEE Transactions on Vehicular Technology*, 59(4):2031–2045, 2010.

[99] A. Giridhar and P. R. Kumar. Toward a theory of in-network computation in wireless sensor networks. *IEEE Communication Magazine*, 44(4):98–107, 2006.

[100] F. Cali, M. Conti, and E. Gregori. IEEE 802.11 protocol: design and performance evaluation of an adaptive backoff mechanism. *IEEE Journal on Selected Areas in Communications*, 18(9):1774–1786, 2000.

[101] R. Bruno, M. Conti, and E. Gregori. Optimization of efficiency and energy consumption in p-persistent CSMA-based wireless LANs. *IEEE Transactions on Mobile Computing*, 1(1):10–31, 2002.

[102] K. Yedavalli and B. Krishnamachari. Enhancement of the IEEE 802.15.4 MAC protocol for scalable data collection in dense sensor networks. In *ICST WiOPT*, 2008.

[103] A. Nafaa and A. Ksentini. On sustained qos guarantees in operated IEEE 802.11 wireless lans. *IEEE Transactions on Parallel and Distributed Systems*, 19(8):1020–1033, 2008.

[104] V. Bharghavan, A. J. Demers, S. Shenker, and L. Zhang. MACAW: A media access protocol for wireless LAN's. In *ACM SIGCOMM*, 1994.

[105] B. Bensaou, Y. Wang, and C. C. Ko. Fair medium access in 802.11 based wireless ad-hoc networks. In *ACM MobiHoc*, 2000.

[106] P. Patras, A. Banchs, P. Serrano, and A. Azcorra. A control theoretic approach to distributed optimal configuration of 802.11 WLANs. *IEEE Transactions on Mobile Computing*, 10(6):897–910, 2011.

[107] K. J. Åström and B. Wittenmark. *Computer-Controlled Systems*. Prentice Hall, 1997.

[108] F. Österlind and A. Dunkels. Approaching the maximum 802.15.4 multi-hop throughput. In *ACM HotEmNets*, 2008.

[109] D. P. Bertsekas and J. N. Tsitsiklis. *Parallel and Distributed Computation: Numerical Methods*. Athena Scientific, 1997.

[110] J. A. Storer. Special issue on lossless data compression. *Proceedings of the IEEE*, 88(11):1685–1688, 2000.

[111] Crossbow. *TelosB Device*. `http://www.xbow.com/`.

[112] SICS. *Contiki Operating System*. `http://www.sics.se/contiki/about-contiki.html`.

[113] M. Tabbara and D. Nesic. Input output stability of networked control systems with stochastic protocols and channels. *IEEE Transactions on Automatic Control*, 53(5):1160–1175, 2008.

[114] D. Malone, K. Duffy, and D. Leith. Modeling the 802.11 distributed coordination function in nonsaturated heterogeneous conditions. *IEEE/ACM Transactions on Networking*, 15(1):159–172, 2007.

[115] M. Chen, G. Liu, D. Wu, and G. Zhu. A unified model for performance analysis of 802.11 in heterogeneous traffic and saturation condition. In *Proceedings of the IEEE International Communications Conference (ICC)*, 2008.

[116] E. Ndih, N. Khaled, and G. De Micheli. An analytical model for the contention access period of the slotted IEEE 802.15.4 with service differentiation. In *Proccedings of the IEEE International Communications Conference (ICC)*, 2009.

[117] T. Kim and J.T. Lim. Throughput analysis considering coupling effect in IEEE 802.11 networks with hidden stations. *IEEE Communication Letters*, 13(3):175–177, 2009.

[118] H. Wu, F. Zhu, Q. Zhang, and Z. Niu. Analysis of IEEE 802.11 DCF with hidden terminals. In *Proceedings of the IEEE Global Communications Conference (GLOBECOM)*, 2006.

[119] M. Hira, F. Tobagi, and K. Medepalli. Throughput analysis of a path in an IEEE 802.11 multihop wireless network. In *Proceedings of the IEEE Wireless Communications and Networking Conference (WCNC)*, 2007.

[120] J. Baras, V. Tabatabaee, P. Papageorgiou, and N. Rentz. Modelling and optimization for multi-hop wireless networks using fixed point and automatic differentiation. In *Proceedings of the 6th Intl. Symposium on Modeling and Optimization in Mobile, Ad Hoc, and Wireless Networks (WiOpt)*, 2008.

[121] M. Carvalho and J. Garcia-Luna-Aceves. A scalable model for channel access protocols in multihop ad hoc networks. In *ACM Mobicom*, 2004.

[122] M. Martalò, S. Busanelli, and G. Ferrari. Markov chain-based performance analysis of multihop IEEE 802.15.4 wireless networks. *Elsevier Performance Evaluation*, 66(12):722–741, 2009.

[123] J. Tripathi, J.C. de Oliveira, and J.P. Vasseur. A performance evaluation study of rpl: Routing protocol for low power and lossy networks. In *Proceedings of the 44th Annual Conference onInformation Sciences and Systems (CISS)*, 2010.

[124] M. Rossi and M. Zorzi. Integrated cost-based mac and routing techniques for hop count forwarding in wireless sensor networks. *IEEE Transactions on Mobile Computing*, 6(4):434–448, 2007.

[125] M.R. Akhavan, T. Watteyne, and A.H. Aghvami. Enhancing the performance of rpl using a receiver-based mac protocol in lossy wsns. In *Proceedings of the 18th International Conference onTelecommunications (ICT)*, 2011.

[126] H. Takagi. *Queueing Analysis: Volume 2 Finite Systems*. North-Holland, Amsterdam, The Netherlands, 1993.

[127] M. Pratesi, F. Santucci, and F. Graziosi. Generalized moment matching for the linear combination of lognormal rvs: application to outage analysis in wireless systems. *IEEE Transactions on Wireless Communications*, 5(5):1122 –1132, 2006.

[128] C. Fischione, F. Graziosi, and F. Santucci. Approximation for a sum of on-off lognormal processes with wireless applications. *IEEE Transactions on Communications*, 55(9):1822–1822, 2007.

[129] X. Yang and N. Vaidya. On physical carrier sensing in wireless ad hoc networks. In *Proceedings of the 25th IEEE International Conference on Computer Communications INFOCOM*, 2005.

[130] H. Zhai and Y. Fang. Physical carrier sensing and spatial reuse in multirate and multihop wireless ad hoc networks. In *Proceedings of the 25th IEEE International Conference on Computer Communications INFOCOM*, 2006.

[131] P. Papadimitratos, A. Mishra, and D. Rosenburgh. A cross-layer design approach to enhance 802.15.4. In *Proceedings of the IEEE Military Communications Conference (MILCOM)*, 2005.

[132] M. Zayani, V. Gauthier, and D. Zeghlache. A joint model for IEEE 802.15.4 physical and medium access control layers. In *IEEE IWCMC*, 2011.

[133] C. Gezer, C. Buratti, and R. Verdone. Capture effect in IEEE 802.15.4 networks: Modelling and experimentation. In *IEEE ISWPC*, 2010.

[134] M. Zorzi and F. Borgonovo. Performance of capture-division packet access with slow shadowing and power control. *IEEE Transactions on Vehicular Technology*, 46(3):687–696, 1997.

[135] Moteiv, San Francisco, CA. *Tmote Sky Data Sheet*, 2006. `http://www.moteiv.com/products/docs/tmote-sky-datasheet.pdf`.

[136] D. Gay, P. Levis, and D. Culler. Software Design Patterns for TinyOS. *Proceedings of the ACM Conference on Languages, Compilers and Tools for Embedded Systems*, 2005.

[137] M. Zuniga, B. Krishnamachari. Analyzing the transitional region in low power wireless links. In *Proceedings of the 1st IEEE International Conference on Sensor and Ad hoc Communications and Networks (SECON)*, 2004.

[138] O. Sename and A. Fattouh. Robust H_∞ control of bilateral teleoperation systems under communication time-delay. In *LNCIS Applications of Time Delay Systems*. Springer, 2007.

[139] M. Maasoumy, A. Pinto, and A. Sangiovanni-Vincentelli. Model-based hierarchical optimal control design for HVAC systems. In *ASME Conference Proceedings*, 2011.

[140] M. Torngren. Timing problems and opportunities for embedded control systems; modeling and co-design. Technical report, UC Berkeley, September 2011.

[141] A. Sangiovanni-Vincentelli, W. Damm, and R. Passerone. Taming Dr. Frankenstein: Contract-based design for cyber-physical systems. In *IEEE Conference on Decision and Control (CDC)*, 2011.

[142] E. Fridman, A. Seuret, and J. P. Richard. Robust sampled-data stabilization of linear systems: An input delay approach. *Automatica*, 40(8):1441–1446, 2004.

[143] P. Naghshtabrizi, J. P. Hespanha, and A. R. Teel. Exponential stability of impulsive systems with application to uncertain sampled-data systems. *Systems & Control Letters*, 57(5):378–385, 2008.

[144] A. Seuret. Stability analysis for sampled-data systems with a time-varying period. In *Proceedings of the IEEE Conference on Decision and Control*, 2009.

[145] S. Skogestad and I. Postlethwaite. *Multivariable Feedback Control: analysis and design*. John Wiley & Sons, 2005.

[146] K. Zhou and J. C. Doyle. *Essentials Of Robust Control*. Prentice Hall, 1997.

[147] Center for the Built Environment (CBE). Design guide on underfloor air distribution systems. Technical report, ASHRAE, 2002.

[148] M. Sgroi, A. Wolisz, A. Sangiovanni-Vincentelli, and J.M. Rabaey. A service-based universal application interface for ad-hoc wireless sensor networks. *whitepaper, UC Berkeley*, 2004.

[149] E. Witrant, S. Mocanu, and O. Sename. A hybrid model and MIMO control for intelligent buildings temperature regulation over WSN. In *Proceedings of the IFAC Workshop on Time Delay Systems*, Sinaia, Romania, 2009.

[150] C. L. Liu and James W. Layland. Scheduling algorithms for multiprogramming in a hard-real-time environment. *Journal of the ACM*, 20(1):46–61, January 1973.

[151] R. E. Skelton, T. Iwasaki, and K. M. Grigoriadis. *A Unified Algebraic Approach to Linear Control Design*. Taylor & Francis, 1997.

[152] IEEE. *IEEE 802.15.4e - Low-Rate Wireless Personal Area Networks (LR-WPANs)*, 2012. `http://standards.ieee.org/getieee802/download/802.15.4e-2012.pdf`.

[153] M. Palattella, N. Accettura, M. Dohler, L. Grieco, and G. Boggia. Traffic aware scheduling algorithm for multi-hop IEEE 802.15.4e networks. *IEEE PIMRC*, 2012.

[154] R. Sittler. Systems analysis of discrete Markov processes. *IRE Transactions on Circuit Theory*, 3(4):257–266, 1956.

[155] A. Faridi, M. R. Palattella, M. Dohler, G. Boggia, A. Grieco, P. Camarda, and A. Lozano. Comprehensive evaluation of the IEEE 802.15.4 MAC layer performance with retransmissions. *IEEE Transactions on Vehicular Technology*, 59(8):3917–3932, 2010.

[156] C. Buratti and R. Verdone. Performance analysis of IEEE 802.15.4 non beacon-enabled mode. *IEEE Transactions on Vehicular Technology*, 58(7):3480–3493, 2009.

[157] R. E. Sonntag, C. Borgnakke, and G. J. Van Wylen. *Fundamentals of Thermodynamics*. John Wiley & Sons, 5^{th} edition, 1998.

[158] B. R. Morton. Forced plumes. *Journal of Fluid Mechanics*, 5(1):151–163, 1959.

[159] C. S. Yih. Stratified flows. *Annual Review of Fluid Mechanics*, 1(1):73–110, 1969.

[160] C. Gladstone and A. Woods. On buoyancy-driven natural ventilation of a room with a heated floor. *Journal of Fluid Mechanics*, 441(8):293–314, 2001.

[161] E. Witrant, A. D'Innocenzo, G. Sandou, F. Santucci, M. D. Di Benedetto, A. J. Isaksson, K. H. Johansson, S. I. Niculescu, S. Olaru, E. Serra, S. Tennina, and U. Tiberi. Wireless ventilation control for large-scale systems: the mining industrial case. *International Journal of Robust and Nonlinear Control*, 20(2):226–251, 2010.